UNIVERSIDAD COMPLUTENSE DE MADRID

FACULTAD DE FARMACIA

TESIS DOCTORAL

Estudio de proteínas con dominios TIR humanas y bacterianas, mediante su expresión heteróloga en Saccharomyces cerevisiae.
Study of human and bacterial TIR domain-containing proteins, through their heterologous expression in Saccharomyces cerevisiae

MEMORIA PARA OPTAR AL GRADO DE DOCTOR

PRESENTADA POR

Julia María Coronas Serna

DIRECTORES

María Molina Martín
Víctor Jiménez Cid

UNIVERSIDAD COMPLUTENSE DE MADRID

FACULTAD DE FARMACIA

TESIS DOCTORAL

Estudio de proteínas con dominios TIR humanas y bacterianas, mediante su expresión heteróloga en Saccharomyces cerevisiae.
Study of human and bacterial TIR domain-containing proteins, through their heterologous expression in Saccharomyces cerevisiae.

MEMORIA PARA OPTAR AL GRADO DE DOCTOR

PRESENTADA POR

Julia María Coronas Serna

DIRECTOR

María Molina Martín

Víctor Jiménez Cid

COMPLUTENSE UNIVERSITY OF MADRID

FACULTY OF PHARMACY

DEPARTMENT OF MICROBIOLOGY AND PARASITOLOGY

Study of human and bacterial TIR domain-containing proteins, through their heterologous expression in *Saccharomyces cerevisiae*.

Thesis submitted in fulfillment of the requirements for the Degree of Doctor by

Julia María Coronas Serna

Maria Molina Martin

Firmado digitalmente por Maria Molina Martin
Nombre de reconocimiento (DN): cn=Maria Molina Martin, o=Universidad Complutense de Madrid, ou=Facultad de Farmacia, email=molmifa@ucm.es, c=ES
Fecha: 2020.10.02 19:29:08 +02'00'

Supervisors

María Molina Martín

Víctor Jiménez Cid

JIMENEZ CID VICTOR - DNI 00825507Z

Firmado digitalmente por JIMENEZ CID VICTOR - DNI 00825507Z
Nombre de reconocimiento (DN): c=ES, o=UNIVERSIDAD COMPLUTENSE DE MADRID, ou=CERTIFICADO ELECTRONICO DE EMPLEADO PUBLICO, serialNumber=IDCES-00825507Z, sn=JIMENEZ CID, givenName=VICTOR, cn=JIMENEZ CID VICTOR - DNI 00825507Z
Fecha: 2020.10.02 23:50:15 +02'00'

Madrid, 2020

UNIVERSIDAD COMPLUTENSE DE MADRID

FACULTAD DE FARMACIA

DEPARTAMENTO DE MICROBIOLOGÍA Y PARASITOLOGÍA

Estudio de proteínas con dominio TIR humanas y bacterianas, mediante su expresión heteróloga en *Saccharomyces cerevisiae*.

Memoria presentada para optar al
grado de doctor por

Julia María Coronas Serna

Directores

María Molina Martín

Víctor Jiménez Cid

Maria Molina Martin

Firmado digitalmente por Maria Molina Martin
Nombre de reconocimiento (DN): cn=Maria Molina Martin, o=Universidad Complutense de Madrid, ou=Facultad de Farmacia, email=molmifa@ucm.es, c=ES
Fecha: 2020.10.02 19:29:37 +02'00'

JIMENEZ CID VICTOR - DNI 00825507Z

Firmado digitalmente por JIMENEZ CID VICTOR - DNI 00825507Z
Nombre de reconocimiento (DN): c=ES, o=UNIVERSIDAD COMPLUTENSE DE MADRID, ou=CERTIFICADO ELECTRONICO DE EMPLEADO PUBLICO, serialNumber=IDCES-00825507Z, sn=JIMENEZ CID, givenName=VICTOR, cn=JIMENEZ CID VICTOR - DNI 00825507Z
Fecha: 2020.10.02 23:50:44 +02'00'

Madrid, 2020

Esta tesis doctoral ha sido posible gracias a…

Las ayudas concedidas:

- Ayudas para contratos predoctorales de personal investigador en formación. Convocatoria 2015 CT45/15-CT46/15. Dpto. de Microbiología y Parasitología de la Facultad de Farmacia de la UCM. 2015-2020.

- Ayudas para estancias breves en España y en el extranjero de los beneficiarios del Programa de Formación de Personal Investigador de la UCM. Convocatoria 2019. IBCP-CNRS-Université de Lyon 1. 2019.

- Contrato personal de apoyo a la investigación con cargo a proyectos. Plaza PAII46/20-08/2020-04. Dpto de Microbiología y Parasitología de la Facultad de Farmacia de la UCM. 2020

Las estancias breves en centros de investigación fuera de España.

- Estancia Predoctoral en el laboratorio del Dr. Jonathan C. Kagan, experto en señalización en inmunidad innata. Boston Children's Hospital, Harvard University, 2018.

- Estancia Predoctoral en el laboratorio de la Dra. Suzana P. Salcedo, experta en la interacción patógeno-hospedador de *Brucella*. IBCP-CNRS-Université de Lyon 1, 2019.

Los proyectos concedidos al grupo de investigación:

- InGEMICS-CM: Ingeniería Microbiana, Salud y Calidad de Vida B2017/BMD-3691. Ayudas a grupos para el desarrollo de programas de actividades de I+D en biociencias. Entidad financiadora: Comunidad Autónoma de Madrid. Coordinador: María Molina. Duración: 1-1-2018 al 31-12-2022

- Reprogramación celular por fosforilación dependiente de la MAPK SLT2 e integración de un módulo de señalización por receptores de tipo Toll en *Sacharomyces cerevisiae*. BIO2016-75030-P. Entidad financiadora: Ministerio de Economía y Competitividad. Duración: 30/12/2016 al 29/12/2019

La colaboración de los Centros de Apoyo a la Investigación (CAI) de la UCM:

-CAI de Genómica y Proteómica UCM.
-CAI de Espectrometría de Masas UCM.

Muchísimas gracias…

…A María y a Víctor, que confiasteis en mi desde el primer momento y me habéis dado un proyecto apasionante y una oportunidad maravillosa de crecer en la ciencia y en la vida.

…A las chicas de la U3, pasadas y presentes: perdonad que no os nombre a todas, si no me saldrían dos tomos. Habéis hecho que mi paso por el laboratorio sea una época inolvidable de mi vida. Con especial cariño para Tere, Elba e Isa, que me habéis acompañado mucho más de cerca y con quienes he compartido proyectos. No me olvido de María Rodríguez Escudero, sin tu excelente trabajo previo esta Tesis hubiera sido muy distinta, ni de Víctor Fuentes, el becario de colaboración junto al cual comencé este proyecto. Voglio ricordare alle ragazze torinesi, Grazie mille.

…A todo el departamento, por toda su ayuda y por generar una atmosfera de trabajo en la que es posible sonreír cada día.

…A Nicola y Lucía, mis primeros compañeros de laboratorio, y a Juan González y Carmen Cuéllar que me abrieron las puertas a la investigación en el fascinante mundo de *Anisakis simplex*.

…A mis padres, por creer en mí y porque sin ellos no sería quien soy ahora. A mis hermanos Luis y Javi por su cariño y su apoyo. A mis abuelos y abuelas, sois mi ejemplo a seguir, no os olvidaré nunca. A Antonio, que ha aguantado en pie hasta en las peores tempestades.

…A la gran familia de Triaca Teatro, por darme tablas, y a cada uno de mis profesores de idiomas, porque me han ayudado a llegar hasta aquí. A Jota, por todas las veces que me ha preguntado ¿Qué tal va la tesis?.

Many thanks…

…to Dr. Jonathan Kagan, for hosting me in his lab at Harvard University, and his team, especially to Kat, for her help during the stay.

…to Dr. Suzana Salcedo, for letting me into her lab at the CNRS. Merci beaucoup à tous mes amis à Lyon, spécialement Arthur et Tristan.

General index

General index

General index

List of Tables

List of Tables

List of Figures

List of Figures

List of Figures

Abbreviations

Abbreviations

a.k.a	Also known as
aa	Amino acid
ADPR	ADP ribose
ANK	Ankyrin repeats
AP-1	Activator protein 1
ARM	Heat Armadillo repeat motif
BANK1	B-cell scaffold protein with ankyrin repeats 1
BCAP	B cell adapter for Phosphatidylinositol 3-kinase (a.k.a PI3KAP1)
BCV	*Brucella* containing vacuole
BtpA	*Brucella* TIR-containing protein A (a.k.a Btp1/TcpB)
BtpB	*Brucella* TIR-containing protein B
cADPR	Cyclic ADPR
CD14	Cluster of differentiation 14
CLIP170	Cytoplasmic linker protein 170
C-term	C-terminal
DBB	Dof/BANK/BCAP domain
DC	Dendritic cell
DD	Death Domain
ER	Endoplasmic Reticulum
ERAD	ER-associated degradation
FL	Full-length
G6PDH	Glucose-6-phosphate dehydrogenase
GAP	GTPase activating proteins
GEF	Guanine nucleotide exchange factors
GTPase	Guanosine triphosphate hydrolase
HIN	Hematopoietic expression, interferon-inducible nature, and nuclear localization
IF	Immunofluorescence
IFN	Interferon
Ig-like	Immunoglobulin-like domain
IKK	IκB kinase
IL	Interleukin
IL-1RI	Interleukin 1 receptor I
INT	Intermediate domain
IRAK	Interleukin-1 Receptor-Associated Kinase
IRE1α	Inositol-requiring enzyme 1α
IRF3	Interferon regulator factor 3
IκB	Inhibitor of NF-κB
JNK	c-Jun N-terminal kinase
LAMP-1	Lysosome-associated membrane protein 1
LBP	LPS binding protein
LPS	Lipopolysaccharide
LRR	Leucine-rich repeats
MAPK	Mitogen-activated protein kinase

Abbreviations

MAPKKK	Mitogen-activated protein kinase kinase kinase
MD-2	Myeloid differentiation protein-2
MyD88	Myeloid differentiation primary response gene 88
NAD^+	Nicotinamide adenine dinucleotide
NADase	Nicotinamide adenine dinucleotide consuming enzyme
Nam	Nicotinamide
NAMPT	Nicotinamide phosphoribosyltransferase (a.k.a PBEF)
NBS	Nucleotide-binding site
NEMO	NF-κB essential modulator
NF-κB	Nuclear factor-κB
NLR	NOD(Nucleotide-binding oligomerization domain)-like receptor in animals or NBS (Nucleotide-binding site)-LRR receptor in plants
N-term	N-terminal
ORF	Open reading frame
PAMP	Pathogen Associated Molecular Pattern
PARP	Poly (ADP–ribose) polymerase
PDB	Protein Data Bank
PEST	Pro-Glu-Ser-Thr-rich domain
PH	Pleckstrin Homology
pi	Post-infection
PI3K	Phosphatidylinositol 3-kinase
PM	Plasma membrane
PP2A	Phosphatase 2A
PRR	Pattern Recognition Receptors
$PtdIns(3,4,5)P_3$	Phosphatidylinositol-3,4,5-trisphosphate
$PtdIns(4,5)P_2$	Phosphatidylinositol-4,5-bisphosphate
PTEN	Phosphatase and tensin homolog
PumA	*Pseudomonas aeruginosa* TIR protein
Rab5	Ras related protein rab5
Rab7	Ras related protein rab7
RHIM	RIP homotypic interaction motif
ROS	Reactive Oxigen Species
RT	Room Temperature
RUN1	Resistance to *Uncinula necator* 1
SAM	Sterile α motif
SARM	Sterile α and armadillo-motif containing protein
SD	Synthetic dextrose medium
SDS-PAGE	Sodium dodecyl sulfate-polyacrylamide gel electrophoresis
SG	Synthetic Galactose medium
SGD	*Saccharomyces* Genome Database
SMOC	Supramolecular Organizing Centers
Smurf	Smad ubiquitin regulatory factor 1
SNP	Single nucleotide polymorphism
SR	Synthetic Raffinose medium
T3SS	Type III Secretion System
T4SS	Type IV Secretion System

TAB	TAK1-binding protein
TAK1	Transforming Growth Factor β-Activated Kinase 1
TANK	TRAF family member-associated NF-κB activator
TB	Tuberculosis
TBK1	TANK-binding kinase 1
TcpC	TIR-containing protein C
TGF-β	Transforming growth factor-β
ThsB	Thoeris system B
TIR	Toll/interleukin-1 receptor
TIRAP	TIR-containing adaptor protein (a.k.a Mal)
TirS	Staphylococcal TIR gene
TlpA	TIR-like protein A
TLR	Toll-like receptor
TM	Transmembrane
TNFα	Tumor Necrosis Factor-α
TNL	TIR-NBS-LRR plant receptor
TRAF	TNF receptor–associated factor
TRAM	TIR-domain-containing adaptor molecule (a.k.a TICAM2)
TRIF	TIR-containing adaptor inducing interferon-β (IFN-β) (a.k.a TICAM1)
UPR	Unfolded Protein Response
v-cADPR	Variant of cyclic ADPR
WB	Western blotting
WxxxE	Tryptophan-x-x-x-glutamic acid motif

Summary

Summary

Study of human and bacterial TIR domain-containing proteins, through their heterologous expression in *Saccharomyces cerevisiae*.

Introduction. Living organisms use efficient systems to detect pathogens, such as the Toll-like receptor (TLR) signaling. Upon recognition of a ligand, TLRs amplify the signal via the formation of Supramolecular Organizing Centers (SMOCs) (Kagan *et al.*, 2014), triggering innate immunity responses. These SMOCs are complexes of proteins sharing protein-protein interaction motifs, namely the Toll/interleukin-1 receptor (TIR) domain. Human TLR4 signals from two SMOCs: myddosome and triffosome (Fitzgerald and Kagan, 2020), containing TIRAP and MyD88 or TRAM and TRIF respectively. TIR proteins are widespread along phylogeny and some of their functions remain obscure. Indeed they are not just sticky domains, but some can enzymatically consume NAD^+ (Essuman *et al.*, 2018). They play immunity-related roles in animals and plants, and some pathogenic bacteria produce TIR effectors to subvert host immunity (Spear *et al.*, 2009). Among them, *Brucella*, an intracellular pathogen, bears two TIR effectors called BtpA and BtpB, both secreted by its Type IV Secretion System. BtpA can degrade NAD^+ (Essuman *et al.*, 2018), and together with BtpB, they block mammalian TLR signaling (Salcedo *et al.*, 2013) and stabilize host microtubules (Felix *et al.*, 2014). *Saccharomyces cerevisiae* is an excellent eukaryotic cell model, having highly conserved mechanisms and a myriad of molecular biology tools available (Khurana and Lindquist, 2010). To date, several yeast models of human disease, e.g. the PIK3/PTEN/Akt1 (Coronas-Serna *et al.*, 2020b), or bacterial virulence, e.g. the *Samonella* effector SopB (Rodríguez-Escudero *et al.*, 2006) have been developed by our research group.

Objectives. Reconstructing the human TLR4-associated SMOC through yeast heterologous expression. Understanding the phenotypes derived from *Brucella* BtpA and BtpB expression in *S. cerevisiae*, besides checking the effects of human and bacterial TIR proteins when co-expressed in the yeast model.

Results and discussion. Upon *S. cerevisiae* heterologous expression of the human TIR adaptors MyD88, TIRAP, TRIF, and TRAM, under the control of an inducible strong promoter, none of them altered yeast growth and were localized: (i) MyD88 and TRIF at cytosolic spots, (ii) TIRAP and TRAM forming filaments at the plasma membrane (PM). We also found that TIRAP binds the yeast PM using a polybasic motif, but it does not coincide with the septin ring or a phosphatidylinositol-4,5-*bis*phosphate (PtdIns(4,5)P_2) marker. MyD88 and TIRAP co-localize and co-purify as expected, but, although interacting *in vitro*, TRIF and TRAM did not co-localize in the

yeast cell. However, the TLR4 TIR domain co-purifies with both MyD88-TIRAP and TRIF-TRAM adaptor pairs and recruits TIRAP and TRAM to PM spots. The IRAK4 downstream kinase directly phosphorylate MyD88 in yeast, and 10 phosphorylated residues were identified using a proteomic approach. IRAK1/2 interact with TIRAP WT and a TIRAP mutant on the BB loop, a structural motif involved in TIR-TIR interactions. Indeed, the BB loop mutants of MyD88 and TIRAP no longer co-localize with each other, and mutations on the TRAM BB loop and the acidic residues D91 E92 lead to filament loss.

The *Brucella* effectors BtpA and BtpB inhibit yeast growth through their TIR domains, while non-TIR regions determine their location and modulate their toxicity. Both TIR domains but not the complete proteins form long cytoplasmic filaments, probably driven by self-interactions. Full BtpB and its TIR domain depolarize actin patches, block endocytosis, and impair MAPK signaling. To better understand these phenotypes, we performed an *S. cerevisiae* ORF overexpression screen, from which Dog2, Rbk1, and Inm2 metabolic enzymes were found to suppress BtpB toxicity in yeast cells. Besides, we detected a depletion of yeast cellular NAD^+ and ATP levels upon BtpB and the TIR domains of BtpA/B expression, which would explain the observed phenotypes. Moreover, a mutation on the glutamic acid in the conserved WxxxE motif of BtpA, BtpB, BtpA-TIR, and BtpB-TIR eliminated their effect on yeast growth, MAPK signaling, or, in the case of BtpB, the ATP/NAD^+ levels and the endocytosis blockage. Twelve loss-of-function BtpB mutants were obtained from a random mutagenesis screen. When reproduced into the BtpB TIR construct, some mutations still assemble into filaments, strongly suggesting that growth inhibition and filament formation are features depending on different structural motifs. We eventually co-expressed the human TIR adaptors with the bacterial TIR effectors in yeast, and found out that the adaptors do not prevent BtpA/B toxicity, BtpA interacts with MyD88 and TRIF, and TRAM filaments disappear upon co-expression of BtpA/B TIR wild type, but not that of the inactive mutants.

Conclusions. 1.-The heterologous expression of the human TIR adaptors MyD88, TIRAP, TRIF, TRAM, and the cytosolic side of TLR4 does not alter yeast growth. 2.- TIR-TIR self-interactions are involved in the filament formation of TRAM, TIRAP, and the TIR domains of the *Brucella* effectors BtpA and BtpB upon yeast expression. 3.- MyD88 and TIRAP co-localize in the yeast cell, requiring an intact BB loop, whereas TRIF and TRAM do not co-localize, despite physically interacting. 4.-The yeast model recapitulates the interactions among human adaptors and the TIR domain of TLR4, including the recruitment of TIRAP and TRAM to plasma membrane patches. 5.-Overexpression in *S. cerevisiae* evidenced the ability of IRAK4 to phosphorylate MyD88 on several Ser/Thr residues. 6.- Both IRAK1 and IRAK2 interact with TIRAP, independently of its BB

loop, in the yeast system. 7.-The formation of TRAM filaments at the yeast plasma membrane relies on the BB loop and the acidic residues D91 E92. 8.-The expression of *Brucella* TIR proteins in yeast allowed us to confirm the NADase activity of BtpA and to identify for the first time this activity on BtpB. 9.-The glutamic acid on the WxxxE motif of BtpB and the TIR domains of BtpA and BtpB is essential to deplete cellular NAD^+ and consequently to reduce ATP, impair MAPK signaling, and inhibit yeast growth. 10.-The N-terminal non-TIR extensions of BtpA and BtpB determine their subcellular location and modulate their NADase activity. 11.- BtpA and BtpB TIR domain filament formation and toxicity in yeast rely on distinct structural determinants. 12.-The TIR domains of BtpA and BtpB require their catalytic activity to interfere with TRAM filament formation.

Resumen

Resumen

Estudio de proteínas con dominios TIR humanas y bacterianas, mediante su expresión heteróloga en *Saccharomyces cerevisiae*.

Introducción. Los seres vivos utilizan la señalización por receptores *Toll-like* (TLR) para detectar patógenos. Al reconocer un ligando, los TLRs amplifican la señal formando Centros Organizadores Supramoleculares (SMOCs) (Kagan *et al.*, 2014), e induciendo la respuesta inflamatoria. Los SMOCs contienen proteínas con dominios de interacción, como el dominio *Toll/interleukin-1 receptor* (TIR). El TLR4 señaliza desde dos SMOCs, el myddosoma y el triffosoma (Fitzgerald and Kagan, 2020), que contienen a TIRAP y MyD88 o TRAM y TRIF, respectivamente. Las proteínas TIR están en diversos organismos y ciertas funciones permanecen ocultas. De hecho, no sólo interaccionan, sino que algunos consumen NAD^+ enzimáticamente (Essuman *et al.*, 2018). Son parte de la inmunidad en plantas y animales y algunos patógenos producen factores de virulencia TIR para sabotear la inmunidad del hospedador (Spear *et al.*, 2009). *Brucella* es un patógeno intracelular que tiene dos efectores TIR, BtpA y BtpB, ambos secretados por su sistema de secreción tipo 4. BtpA degrada el NAD^+ (Essuman *et al.*, 2018), y junto a BtpB, bloquean la señalización por TLR (Salcedo *et al.*, 2013) y estabilizan los microtúbulos del hospedador (Felix *et al.*, 2014). *Saccharomyces cerevisiae* es un modelo celular eucariótico, con mecanismos conservados y varias herramientas de laboratorio disponibles (Khurana and Lindquist, 2010). Hasta ahora, varios modelos de enfermedad humana (Coronas-Serna *et al.*, 2020b), o de virulencia bacteriana (Rodríguez-Escudero *et al.*, 2006) han sido desarrollados por nuestro grupo de investigación.

Objetivos. Reconstruir los SMOCs humanos de TLR4 mediante expresión heteróloga en levadura. Descifrar los fenotipos derivados de la expresión de BtpA y BtpB de *Brucella* en *S. cerevisiae*, además de comprender los efectos de las proteínas TIR humanas y bacterianas cuando son co-expresadas en el modelo de levadura.

Resultados y discusión. Ninguna de las proteínas TIR humanas causaron toxicidad en levadura, y se localizaron: (i) MyD88 y TRIF en puntos citosólicos y (ii) TIRAP y TRAM en filamentos en la membrana plasmática (PM). TIRAP se une a la PM mediante un motivo polibásico, pero no coincide con el anillo de septinas ni con un marcador del fosfatidilinositol-4,5-*bis*fosfato ($PtdIns(4,5)P_2$). MyD88 y TIRAP co-localizan, pero, aunque interaccionan *in vitro*, TRIF y TRAM no co-localizan en levadura. Sin embargo, el dominio TIR de TLR4 co-purifica con las dos parejas de adaptadores y redirige a TIRAP y a TRAM a puntos de PM. IRAK4, la quinasa posterior,

fosforila a MyD88 y los residuos fosforilados se identificaron por espectrometría de masas. En levadura, IRAK1/2 interaccionan con TIRAP silvestre y con un mutante de TIRAP en el *BB loop*, un motivo estructural implicado en las interacciones TIR-TIR. De hecho, los mutantes del *BB loop* de MyD88 y TIRAP no co-localizan entre ellos. Las mutaciones de TRAM en el *BB loop* y en D91 E92 no forman filamentos.

BtpA y BtpB inhiben el crecimiento de levadura a través de sus dominios TIR, mientras que las regiones "no-TIR" dirigen la localización y regulan la toxicidad. Ambos TIR forman largos filamentos citoplásmicos que seguramente se deban a interacciones entre sí. BtpB y su TIR despolarizan la actina, bloquean la endocitosis e impiden la señalización por MAPK. Un rastreo por sobreexpresión de genes de levadura mostró que las enzimas metabólicas Dog2, Rbk1 e Inm2 suprimen la toxicidad inducida por BtpB. Además, detectamos una caída de los niveles celulares de NAD^+ y ATP al expresarse BtpB y los TIR de BtpA/B, que podría explicar los fenotipos. Los mutantes en el ácido glutámico del motivo conservado WxxxE, no alteraron ni el crecimiento de la levadura, ni la señalización por MAPK, ni los niveles de NAD^+/ATP. Un rastreo por mutagénesis al azar reveló 12 mutantes de pérdida de función de BtpB. Cuando se reprodujeron en el TIR, algunas todavía formaban filamentos, sugiriendo que la inhibición del crecimiento y la formación de filamentos dependen de distintos motivos estructurales. Por último, hemos expresado las proteínas TIR humanas junto a las bacterianas en levadura y visto que las humanas no influyen en la toxicidad de BtpA/B, BtpA interacciona con MyD88 y TRIF, y que los filamentos de TRAM desaparecen al co-expresar BtpA/B silvestres, pero no los mutantes inactivos.

Conclusiones. 1.-La expresión heteróloga de los adaptadores TIR humanos MyD88, TIRAP, TRIF, TRAM, así como la de la región citosólica de TLR no alteran el crecimiento de la levadura. 2.- Las interacciones TIR-TIR están implicadas en la formación de filamentos de TRAM, TIRAP y los dominios TIR de los efectores de *Brucella* BtpA y BtpB al expresarse en levadura. 3.- MyD88 y TIRAP co-localizan en la célula de levadura, requiriendo el *BB loop* intacto, mientras que TRIF y TRAM no co-localizan, a pesar de interaccionar físicamente. 4.- El modelo de levadura reproduce las interacciones entre los adaptadores humanos y el dominio TIR de TLR4, incluido el reclutamiento de TIRAP y TRAM a acúmulos en la membrana plasmática. 5.- La sobreexpresión en *S. cerevisiae* evidenció la capacidad de IRAK4 de fosforilar MyD88 en varios residuos de Ser/Thr. 6.- Tanto IRAK1 como IRAK2 interaccionan con TIRAP, independientemente de su *BB loop*, en el sistema de levadura. 7.- La formación de los filamentos de TRAM en la membrana plasmática de levadura depende del *BB loop* y de los residuos ácidos D91 E92. 8.- La expresión de las proteínas TIR de *Brucella* en levadura nos ha permitido confirmar la actividad NADasa de BtpA e identificar esta actividad por primera vez en BtpB. 9.- El ácido glutámico del motivo

WxxxE de BtpB y de los dominios TIR de BtpA y BtpB es esencial para la eliminación del NAD^+ celular y en consecuencia la reducción del ATP, el impedimento de la señalización por MAPK y la inhibición del crecimiento en levadura. 10.- La extensión N-terminal “no-TIR” de BtpA y BtpB determina su localización subcelular y modula su actividad NADasa. 11.- La formación de filamentos y la toxicidad de los dominios TIR de BtpA y BtpB en levadura dependen de distintos determinantes estructurales. 12.- Los dominios TIR de BtpA y BtpB requieren su actividad catalítica para interferir con la formación de los filamentos de TRAM.

Introduction

Introduction

1.- Innate immunity and the Toll-like receptor signaling.

Living organisms are constantly exposed to environmental challenges. Different species have co-evolved to develop complex communities, in which multiple ecological interactions occur and a variety of molecular signals are produced and sensed by their members. Higher organisms co-exist with a myriad of microorganisms in different forms of symbiosis. Thus, they have developed efficient systems to discriminate between beneficial members of their microbiota and potentially harmful pathogens. One of those mechanisms will be explored in the present Thesis: the human Toll-like receptor (TLR) signaling, and particularly the interaction among conserved Toll/interleukin-1 receptor (TIR) protein domains. We will also investigate a system developed by pathogens to subvert such host defenses: the bacterial TIR proteins. To gain insight into these pathways, we chose to take advantage of a simple eukaryotic model, the budding yeast *Saccharomyces cerevisiae*.

1.1.- Innate immunity and supramolecular organizing centers.

Multicellular organisms fight against the invasion of microbial pathogens in many ways. Regarding vertebrates, two different types of immunity are identified, namely adaptive and innate immunity. Whereas adaptive requires the previous contact with the pathogen, innate immunity is one of the very first barriers that will set the alarm (Medzhitov and Janeway, 2000).

Pattern Recognition Receptors (PRR) are designed to recognize Pathogen or Damage Associated Molecular Patterns (PAMPs or DAMPs respectively), which indicate the presence of an unwanted visitor or a malfunctioning cell or organ. Innate immunity signaling pathways, unlike classical signaling pathways, rarely rely on secondary messengers. Their signaling mechanism rather depends on the formation of Supramolecular Organizing Centers (SMOCs) (Kagan *et al.*, 2014). For this reason, the system is called Signaling by Cooperative Assembly Formation (SCAF) (Nimma *et al.*, 2017).

In the last thirty years, much research has been done on the understanding of innate immunity signaling, with the identification of five main pathways mediated by TLRs, C-type lectin receptors (CTLs), retinoic acid-inducible gene (RIG)-I-like receptors (RLRs), Nod-like receptor (NLRs), and AIM2-like receptors (ALRs) (Blander and Sander, 2012; Ha *et al.*, 2020; Kagan *et al.*, 2014; Marongiu *et al.*, 2019) (Table 1).

Upon recognition of a very low concentration of the pattern, PRRs oligomerize and amplify the signal via SMOC formation: recruiting adaptor proteins that generate the physical scaffold, and effector enzymes, such as kinases, E3 ubiquitin ligases, and proteases (Kagan *et al.*, 2014; Tan and Kagan, 2019). The signal is conveyed through protein-protein interactions and posttranslational modifications, ending up in nuclear translocation of transcription factors. These are to induce the expression of cytokines and interferon (IFN), which eventually set off typical innate immunity responses (Chuenchor *et al.*, 2014; Guven-Maiorov *et al.*, 2015) (Table 2).

Table 1.- Innate immunity receptor families in *Homo sapiens*.

Family	Members	Ligand	Location	Domains	SMOC	Refs
TLRs	TLR1-10	PAMPs or DAMPs	PM/ endosome	LRR, TIR	Myddosome/ triffosome	(Kagan *et al.*, 2014)
CTLs	Dectin-1/2	fungal β-1,3-glucans	PM	C-type lectin, hemITAM	CARD9 signalosome	(Brubaker *et al.*, 2015; Drouin *et al.*, 2020)
RLRs	RIG-I, MDA5, LGP2	Viral RNA	Cytosol	DExD/H, CARD	RLR complex	(Yoneyama *et al.*, 2005)
NLRs	NLRP1/3, NIAP, NLRC4, NOD1/2	PAMPs	Cytosolic/ Endosome associated	LRR, NOD, PYD, CARD	Inflammasome	(Broz and Dixit, 2016)
ALRs	AIM2	Viral DNA	Cytosolic	PYD, HIN		

Abbreviations: Plasma membrane (PM), Leucine-rich repeats (LRR), Modified immunoreceptor tyrosine-based activation motif (hemITAM), Caspase recruitment domain (CARD), Melanoma differentiation-associated protein 5 (MDA5), Laboratory of genetics and physiology 2 (LGP2), Asp-Glu-x-Asp/His RNA helicase domain (DExD/H), NLR family containing PYD domain (NLRP), NLR family apoptosis inhibitory protein (NIAP), NLR family containing CARD domain (NLRC), Nucleotide-binding oligomerization domain (NOD), Pyrin domain (PYD), Absent in melanoma 2 (AIM2), Hematopoietic expression, interferon-inducible nature, and nuclear localization (HIN).

Table 2.- Example of SMOCs in innate immunity.

SMOC	Location	PRR	Adaptor	Effector	Domains	Function	Ref
Myddosome	PM	TLRs	TIRAP, MyD88	IRAKs, TRAF6	TIR/DD	NF-κB activation	(Brubaker *et al.*, 2015; Kagan *et al.*, 2014; Marongiu *et al.*, 2019)
Triffosome	Endosome	TLRs	TRAM, TRIF	TRAFs	TIR/ TRAF-B, RHIM	IRF3 and NF-κB activation, IFN production	
RLR complex	Mitochondria, peroxisome, and MAMs	RLRs	MAVS	TRAFs	CARD/Pro-rich region, TRAF-B	NF-κB activation and IFN production	(Blander and Sander, 2012; Brubaker *et al.*, 2015; Kagan *et al.*, 2014; Nanson *et al.*, 2019)
Inflammasome	Cytosol, mitochondria	NLRs, ALRs	ASC	Casp-1, GSDM	PYD/ CARD	Cell death by pyroptosis, IL-1β maturation	

Abbreviations: TIR-containing adaptor protein (TIRAP), Myeloid differentiation primary gene 88 (MyDD8), Interleukin-1 Receptor-Associated Kinase (IRAK), TRAF family member-associated NF-κB activator (TRAF),

Death Domain (DD), Nuclear factor-κB (NF-κB), TIR-domain-containing adaptor molecule (TRAM), TIR-containing adaptor inducing interferon-β (TRIF), RIP homotypic interaction motif (RHIM), Interferon regulator factor 3 (IRF3), Mitochondria-associated membranes of the ER (MAM), Mitochondrial antiviral signaling protein (MAVS), Apoptosis-associated speck-like protein containing a CARD (ASC), Caspase-1 (Casp-1), Gasdermin (GSDM), Interleukin (IL).

Nevertheless, more efforts are still required to decipher stoichiometry and regulatory mechanisms. These are of outstanding interest as they represent valuable potential pharmacological targets. Failures in the fine-tuning of any of those SMOC elements would trigger either an autoinflammatory disease, as signaling would be over-activated, or increased susceptibility to otherwise mild pathogens (Chen *et al.*, 2016; Evavold and Kagan, 2018). Thus, the analysis of host adaptor variants or the study of pathogen mechanisms to evade innate immunity, particularly via molecular mimicry, are appealing research fields (Patterson and Werling, 2013).

1.2.- TLR signaling and its associated SMOC.

One of the first innate immunity pathways, identified in the mid- '90s, was the TLR signaling. Researchers in the *Drosophila melanogaster* model identified an antifungal response upon activation of the transmembrane Toll receptor of the Toll-Dorsal signaling pathway (initially established as crucial for embryo development) (Belvin and Anderson, 1996; Lemaitre *et al.*, 1996). Their striking structural and functional similarities led the scientific community to acknowledge an innate immunity signaling pathway evolutionarily conserved throughout vertebrates, insects, and nematodes (Tenor and Aballay, 2008). Thus, TLRs were named after the *Drosophila* Toll receptor (Belvin and Anderson, 1996; Lemaitre *et al.*, 1996; Medzhitov *et al.*, 1997). Furthermore, Bruce A. Beutler and Jules A. Hoffmann were honored with the 2011 Nobel Prize in Physiology or Medicine "for their discoveries concerning the activation of innate immunity" thanks to their research in the *Toll* gene and Toll-like receptors as lipopolysaccharide (LPS) sensors respectively (Nobel-Assembly, 2011).

To date, ten human TLRs have been described (Table 3). These transmembrane receptors bear extracellular Leucine-rich repeats (LRRs) and a conserved TIR-domain on the cytosolic side (Takeda and Akira, 2015), through which convey signals via SCAF. All of them require the key component Myeloid differentiation primary response gene 88 (MyD88), excepting TLR3, which exclusively uses the TIR-containing adaptor inducing interferon-β (IFN-β) (TRIF, a.k.a TICAM-1). TLR4 steers alternative signaling pathways through either MyD88 at the plasma membrane or TRIF at the endosome. The TIR-containing adaptor protein (TIRAP, a.k.a Mal) is an additional

adaptor required for TLR2/1/6, TLR9, and TLR4 at the MyD88-dependent pathway, whereas the TIR-domain-containing adaptor molecule (TRAM, a.k.a TICAM2/TIRP) is essential for TLR4 signaling through the TRIF-mediated route (Kawai and Akira, 2007). Both signaling pathways activate the canonical Nuclear factor κB (NF-κB) transcription factor, triggering the expression of inflammatory cytokines, but also turn on other unique routes that lead to distinct effector functions (Kawai and Akira, 2007).

Table 3.- Human Toll-Like Receptors.

Location	TLR	Main ligand	Origin of ligands	Dimer	Adaptors	Ref
PM/ endosome	TLR4	LPS	Gram-(-) bacteria	TLR4	MyD88, TIRAP, TRIF, TRAM	(Lu *et al.*, 2008; Takeda and Akira, 2015)
PM	TLR2	Peptidoglycan, lipopeptides	Bacteria	TLR1/6	MyD88, TIRAP, TRAM	(Mahita and Sowdhamini, 2018b; Stack *et al.*, 2014)
	TLR1	Triacyl-lipopeptide	Bacteria, mycoplasm	TLR2	MyD88, TIRAP	(Horng *et al.*, 2002; Yamamoto *et al.*, 2002)
	TLR6	Diacyl-lipopeptide	Mycoplasm	TLR2	MyD88, TIRAP	(Takeda and Akira, 2015)
	TLR5	Flagellin	Bacteria	TLR5	MyD88, TRIF	(Luo *et al.*, 2019; Takeda and Akira, 2015)
	TLR9	CpG DNA	Bacteria, virus, parasites	TLR9	MyD88, TIRAP	(Bonham *et al.*, 2014; Ohto *et al.*, 2015)
	TLR10	HIV-1 proteins	Viruses	TLR10 TLR1/2	MyD88	(Hasan *et al.*, 2005; Henrick *et al.*, 2019)
Endosome	TLR3	dsRNA	Viruses	TLR3	TRIF	(Mahita and Sowdhamini, 2018b)
	TLR7	ssRNA		TLR7	MyD88, TRAM	(Shevlin and Miggin, 2014; Takeda and Akira, 2015)
	TLR8			TLR8	MyD88	(Takeda and Akira, 2015)

Abbreviations: Cytosine-phosphate-guanine containing deoxyribonucleic acid (CpG DNA), Human immunodeficiency virus-1 (HIV-1), Double-stranded ribonucleic acid (dsRNA), Single-stranded RNA (ssRNA).

1.2.1.- TLR4 and MyD88-dependent signaling.

It is well established that the plasma membrane (PM) is not a uniform set of phospholipids, but it rather contains discrete microdomains known as lipid rafts. These are usually composed of higher concentrations of cholesterol, sphingolipids, and proteins such as flotillin and glycosylphosphatidylinositol (GPI)-anchored proteins, and defined by their lipid-lipid, lipid-protein, or protein-protein interactions (Płóciennikowska *et al.*, 2015a; Ruysschaert and Lonez, 2015). Lipid rafts play an important role in the initiation of TLR4 signaling (Fessler and Parks, 2011; Ruysschaert and Lonez, 2015). The Cluster of differentiation 14 (CD14), a GPI-linked protein, recognizes LPS captured by the LPS binding protein (LBP) and transfers it to Myeloid differentiation protein 2 (MD-2) and TLR4 (Płóciennikowska *et al.*, 2015a; Ruysschaert and Lonez, 2015). TLR4 is absent from lipid rafts at the resting state, but upon LPS recognition, the TLR4-MD2 complex is driven to CD14 containing PM microdomains and dimerizes (Fig 1) (Park

et al., 2009). Co-adaptors located in the inner leaflet of those areas are ready to encounter activated TLR4. TIRAP has N-terminal lysine residues that bind phosphatidylinositol-4,5-*bis*phosphate (PtdIns(4,5)P_2) within lipid rafts (Kagan and Medzhitov, 2006; Patra and Choi, 2018). Indeed, CD14 is known to boost PtdIns(4,5)P_2 generation upon LPS sensing, which facilitates TIRAP clustering into CD14-containing rafts (Płóciennikowska *et al.*, 2015b).

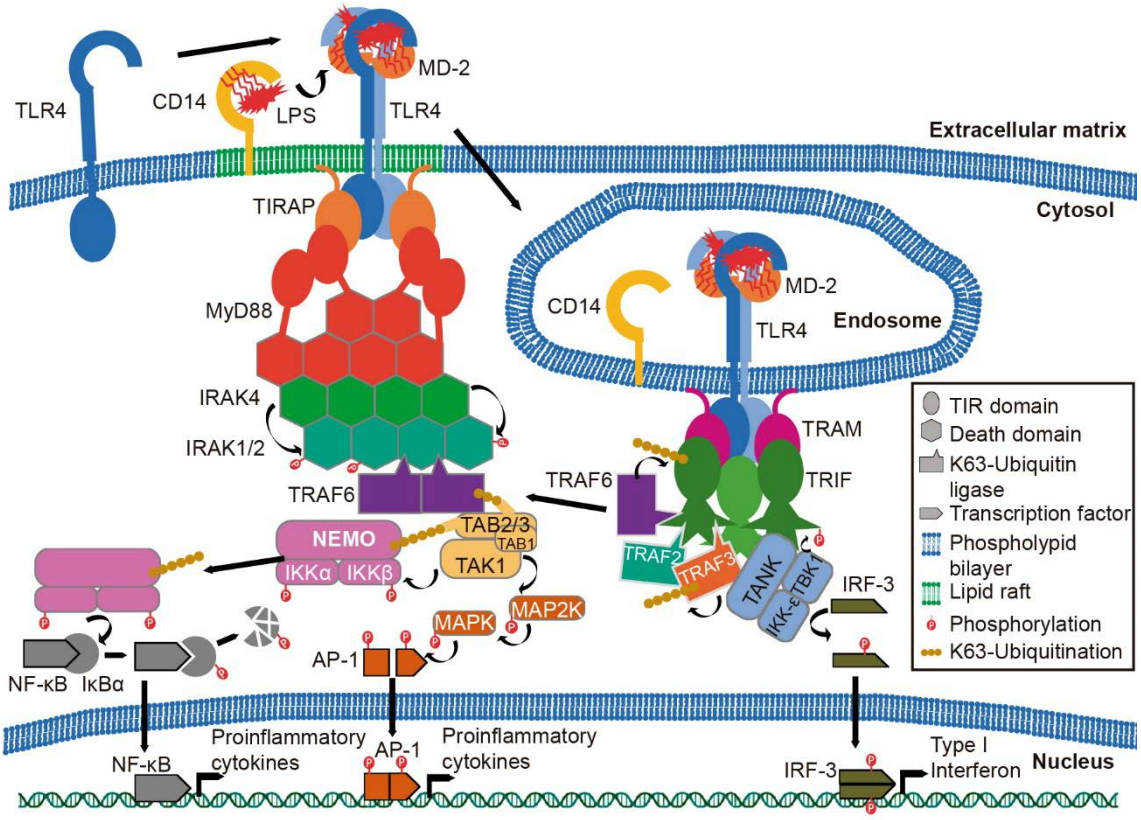

Fig 1.- Schematic view of TLR4 mediated signaling.

The MyD88-dependent pathway (left) and TRIF-mediated signaling (right), see text for more details. The figure does not show the real stoichiometry of the complexes. Figure generated with PowerPoint and Adobe Illustrator, except the DNA drawings, which were created with BioRender.com.

Cytosolic TLR4-TIR dimers bind to TIRAP, which in turn recruits the TIR domain of MyD88 (Fig 1) All these TIR-TIR protein interactions end up in highly ordered hetero-oligomerization forming a left-handed helix (Ve *et al.*, 2017; Vyncke *et al.*, 2016). This results in the assembly of the TIR side of the myddosome, whose stoichiometry is still controversial (Ve *et al.*, 2017; Vyncke *et al.*, 2016). MyD88, the key component of SMOC is composed of a C-terminal TIR and an N-terminal Death Domain (DD). Interleukin-1 Receptor-Associated Kinases1/2/4 (IRAK1/2/4), all displaying an N-terminal DD and a C-terminal Ser/Thr kinase domain (or kinase-like for IRAK2), are recruited by MyD88 via DD-DD connections (Lin *et al.*, 2010). The stoichiometry of this DD-DD complex was resolved ten years ago (Lin *et al.*, 2010), and its assembly has been recently

visualized *in vivo* (Latty *et al.*, 2018). First, six molecules of MyD88-DD are placed in two layers of 2 + 4 items. Then 4 IRAK4-DD units associate with the 4 MyD88 proteins at the second row and finally, another 4 IRAK2 molecules connect with the IRAK4 units to generate the last layer (Fig 1). The alternative IRAK1 would presumably behave as IRAK2 at the complex (Lin *et al.*, 2010). Together they generate a tower-shaped, left-handed helix complex, with a sizable cavity in the inner side between the two MyD88 layers (Lin *et al.*, 2010). Inside the myddosome, IRAK4 subunits are close enough to undergo autophosphorylation and activation, as well as IRAK1/2 phosphorylation (Fitzgerald and Kagan, 2020).

Active IRAK1/2 tether and dimerize the TNF receptor-associated factor 6 (TRAF6) protein (Fig 1). This is an E3-ubiquitin ligase that generates K63-linked linearly polyubiquitinated proteins, a different link to typical K48 ubiquitination, which does not drive to proteasomal degradation, with the collaboration of Ubc-like protein 1A (Uev1A) and ubiquitin-conjugating enzyme 13 (Ubc13) (Brubaker *et al.*, 2015). K63-Ubiquitin tagged proteins at the myddosome, including TRAF6 itself (Zhang *et al.*, 2019b), recruit the Transforming Growth Factor β-Activated Kinase 1 (TAK1, a.k.a. MAP3K7) complex: TAK1 together with TAK1-binding protein 1 (TAB1) and either TAB2 or TAB3 (Fig 1). Redundant TAB2/3 proteins have a C-terminal zinc finger domain that binds specifically K63-ubiquitin chains. Through this interaction, a conformational change activates the TAK1 kinase via autophosphorylation (Aashaq *et al.*, 2019; Cohen and Strickson, 2017; Strickson *et al.*, 2017; Walsh *et al.*, 2015).

The Inhibitor of κB-(IκB) kinase (IKK) complex, formed by IKKα, IKKβ, and NF-κB essential modulator (NEMO, a.k.a IKKγ) is driven to the myddosome. NEMO gets K63-ubiquitinated by TRAF6 and is recognized by TAB2/3 (Walsh *et al.*, 2015). Once close enough, active TAK1 phosphorylates and activates IKKα/β. The active IKK complex then releases the NF-κB transcription factor from its inhibitor IκBα by phosphorylation, which undergoes subsequent proteasomal degradation (Brubaker *et al.*, 2015; Cohen and Strickson, 2017) (Fig 1). NF-κB is a central transcription factor that triggers the expression of proinflammatory cytokines and thus initiates the inflammatory response (Mitchell *et al.*, 2016). Simultaneously, the TRAF6-TAK1 complex is translocated to the cytosol (Brubaker *et al.*, 2015). There, TAK1 turns on mitogen-activated protein kinase (MAPK) signaling cascades, acting as mitogen-activated protein kinase kinase kinase (MAPKKK). This leads to the eventual phosphorylation of MAPKs, such as c-Jun N-terminal kinase (JNK) or p38. They in turn phosphorylate and activate the components of the Activator protein 1 (AP-1) transcription factor complex (cJun-ATF-2) (Shim *et al.*, 2005) (Fig 1). AP-1 and NF-κB induce the expression of proinflammatory cytokines IL-1, and IL-6, and Tumor Necrosis Factor-α (TNFα) (Kawai and Akira, 2007; Luo *et al.*, 2019; Marongiu *et al.*, 2019).

1.2.2.- TLR4 and TRIF-dependent signaling.

Shortly after triggering MyD88-dependent signaling, the TLR4-MD2-LPS complex with CD14 is internalized by endocytosis (Marongiu *et al.*, 2019; Palsson-McDermott *et al.*, 2009; Zanoni *et al.*, 2011). This movement reduces PtdIns(4,5)P_2 membrane content, a fact that disassembles TIRAP and the myddosome (Kagan *et al.*, 2008). Subsequently, TLR4 switches to the TRIF-dependent pathway, using TRAM as its key adaptor (Zanoni *et al.*, 2011). Besides its TIR domain, TRAM has a bipartite sorting region consisting of a myristoylation signal and a polybasic region that targets it to the PM, Golgi, and early endosomes at the resting state (Kagan *et al.*, 2008; Rowe *et al.*, 2006). TRAM binds the TLR4-TIR domain on the inner side of PM and follows its internalization. Once in early endosomes, TRAM tethers TRIF to initiate the formation of the triffosome SMOC (Ullah *et al.*, 2016) (Fig 1).

Homo-oligomerized TRIF is required to activate downstream factors (Funami *et al.*, 2008). TRAF2/6 directly bind TRIF and K63-polyubiquitinate it, while TRAF3 undergoes auto K63-ubiquitination nearby the SMOC (Matsumoto *et al.*, 2013; Sasai *et al.*, 2010). Thus ubiquitinated, TRAF3 positions the TRAF family member-associated NF-κB activator (TANK) into the complex, which in turn recruits TANK-binding kinase 1 (TBK1) and IKK-ε. TBK1 phosphorylates TRIF, which then recruits the interferon regulator factor 3 (IRF-3) transcription factor to the triffosome. IKK-ε and TBK1 phosphorylate and activate IRF-3, which triggers the expression of type I Interferons (IFNs) and TNFα (Liu *et al.*, 2015a; Marongiu *et al.*, 2019; Matsumoto *et al.*, 2013; Sheedy and O'Neill, 2007; Ullah *et al.*, 2016) (Fig 1).

2.- General structural and functional features of the TIR domain.

2.1.- The TIR domain is a universal motif.

The TIR domain signature is found in proteins through bacteria, plants, and animals, but is seldom present in fungi and archaea (Spear *et al.*, 2009; Ve *et al.*, 2015). It was assumed at first that the TIR domain was simply an immunity signaling motif among multicellular eukaryotic organisms. When such domains began to be identified in pathogenic bacteria, it was immediately thought to have evolved as a smart molecular mimicry mechanism to disrupt SMOC formation (Patterson and Werling, 2013; Rana *et al.*, 2013; Spear *et al.*, 2009). Indeed, some bacterial TIR containing proteins have been identified as virulence factors (Cirl *et al.*, 2008; Newman *et al.*, 2006; Salcedo *et al.*, 2013; Salcedo *et al.*, 2008).

The roles for such a widespread and versatile motif found all along the phylogenetical tree, have been intriguing for many years. Although initially related to immunity pathways, there is no particular reason why it should be kept only for host defense (Beutler and Rehli, 2002). Instead, its universality suggests it to be an ancient multipurpose binding domain. While TIR domains gained immunity-related duties in the case of both animals and plants, they seem to have evolved in a convergent pathway (Spear *et al.*, 2009). Furthermore, new evidence makes TIR no longer mere sticky motifs: Essuman and collaborators unraveled their intrinsic Nicotinamide adenine dinucleotide (NAD^+)-consuming enzymatic activity (NADase), not only for human Sterile α and armadillo-motif containing protein (SARM1) (Essuman *et al.*, 2017) but also for some bacterial (Essuman *et al.*, 2018) and plant TIRs (Wan *et al.*, 2019). Table 4 shows some examples of TIR proteins across species.

Table 4.- Examples of TIR proteins across species and their functions.

Clade	Example species	Known roles	Examples of TIR proteins	Comments	Ref
Animalia					
Mammals (Chordata)	*H. sapiens* (Human)	TLR signaling	hTLR4	Best known TLR	(Brubaker *et al.*, 2015)
Avian (Chordata)	*Gallus gallus* (Chicken)		chTLR16	Combines specificity of hTLR1/6	(Keestra *et al.*, 2013)
Amphibians (Chordata)	*Xenopus tropicalis* (African frog)		xtrTLR14.1	Related to zebrafish TLR14	(Ishii *et al.*, 2007)
Fish (Chordata)	*Danio rerio* (Zebrafish)		drTLR22	Fish-specific, for dsRNA	(Zhang *et al.*, 2014)
Insects (Arthropoda)	*Drosophila melanogaster* (Fruit fly)	Embryo polarization, immunity	Toll-1	First TIR protein identified	(Lemaitre *et al.*, 1996)
Nematoda	*Caenorhabditis elegans* (Soil worm)	Development and immunity	TOL-1	Pathway lacking components	(Tenor and Aballay, 2008)

Echinodermata	*Strongylocentro-tus purpuratus* (Sea urchin)	Innate immunity	TLR222	More than 200 TLR identified	(Hibino *et al.*, 2006)
Cnidaria	*Acropora digitifera* (Coral)		adiTLR-1	27 animal and 12 bacterial-like TLRs	(Poole and Weis, 2014)
Plantae					
Dicotyledon (Angiosperms)	*Arabidopsis thaliana*	TNL, immunity	RPS4	NADase activity	(Wan *et al.*, 2019)
Monocotyledon (Angiosperms)	*Brachypodium distachyon* (grass)	TIR-only, immunity	bdTIR		
Other eukaryotes					
Amoeba	*Dictyostelium discoideum* (social amoeba)	Nutrition	TirA	Needed for phagocytosis	(Chen *et al.*, 2007)
Fungi	*Aspergillus niger*	Unknown	An11g08390	-	(Spear *et al.*, 2009)
Bacteria					
Gram-negative bacteria	*Salmonella enterica* serovar Enteritidis	Virulence factor	TlpA	Inhibits NF-κB signaling	(Newman *et al.*, 2006)
	Uropathogenic *Escherichia coli*		TcpC	Macrophage uptake	(Cirl *et al.*, 2008)
	Brucella melitensis		BtpA	T4SS	(Salcedo *et al.*, 2008)
	Pseudomonas aeruginosa		PumA	UBAP1 modulator	(Imbert *et al.*, 2017)
Gram-positive	*Staphylococcus aureus*	Virulence factor	TirS	Linked to drug-resistance genes	(Patot *et al.*, 2017)
	Bacillus cereus	Anti-phage	ThsB	Linked to NAD hydrolisis	(Doron *et al.*, 2018)
Archaea					
Euryarchaeota	*Theionarchaea archaeon*	Unknown	TcpA	NADase activity	(Essuman *et al.*, 2018)

Abbreviations: C. elegans Toll-like (TOL-1), Resistance to *Pseudomonas syringae* 4 (RPS4), *Brachypodium distachyon* TIR (BdTIR), TIR protein A (TirA), TIR-like protein A (TlpA), TIR-containing protein C (TcpC), *Brucella* TIR-containing protein A (BtpA), Type IV secretion system (T4SS), *Pseudomonas aeruginosa TIR protein* (PumA), Ubiquitin-associated protein 1 (UBAP1), Staphylococcal TIR gene (TirS), Thoeris system B (ThsB), TIR-containing protein A (TcpA).

2.2.- Structure of the TIR domain.

TIR domains are general protein-protein interaction modules composed of 125-200 amino acids (aa) in a flavodoxin-like fold (Ve *et al.*, 2015). General features of the tertiary structure are a central 5-stranded parallel β-sheet (βA-βE) surrounded by five α-helices (αA-αE) and their corresponding connecting loops, named after the connecting elements. For example, the functionally relevant BB loop links strand βB with helix αB (Rana *et al.*, 2013; Ve *et al.*, 2015) (Fig 2).

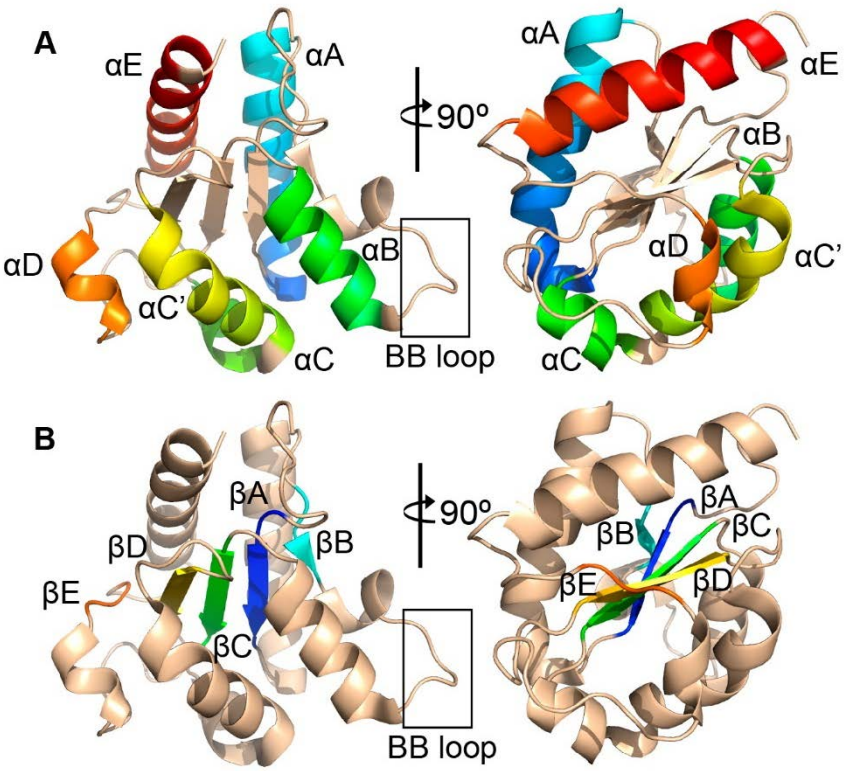

Fig 2.- Secondary structure of a TIR domain.

Representation of TIRAP TIR domain (PDB 5UZB) with the five helixes colored in (A): αA (blue), αB (green), αC (green), αC' (yellow), αD (orange), and αE (red), and the five strands in (B): βA (blue), βB (cyan), βC (green), βD (yellow), and βE (orange). BB loop connecting αB and βB is highlighted. Image generated with PyMOL (Schrödinger, 2020).

Initially, three sequence motifs defined mammalian TIR domains, namely Box 1, Box 2, and Box 3 (Rana *et al.*, 2013; Ve *et al.*, 2015), though boxes 2 and 3 are not universally conserved (Toshchakov and Neuwald, 2020; Ve *et al.*, 2015). Box1 [(F/Y)DAFISY] fits within the inner βA strand, critical for structural stability (Ve *et al.*, 2015). Box2 (GYKLC-RDxϕPG) (x=any, ϕ = hydrophobic) corresponds with the βB strand and the superficial BB loop (Rana *et al.*, 2013; Ve *et al.*, 2015). Box 3 (W surrounded by basic aa) matches the αE helix and is the less conserved Box outside animal TIRs (Toshchakov and Neuwald, 2020; Ve *et al.*, 2015). As an example, Fig 3 shows an alignment of various TIR proteins from diverse organisms, displaying sequence motifs together with typical secondary structure elements. Various available 3D structures of TIR-containing proteins are listed in Table 5.

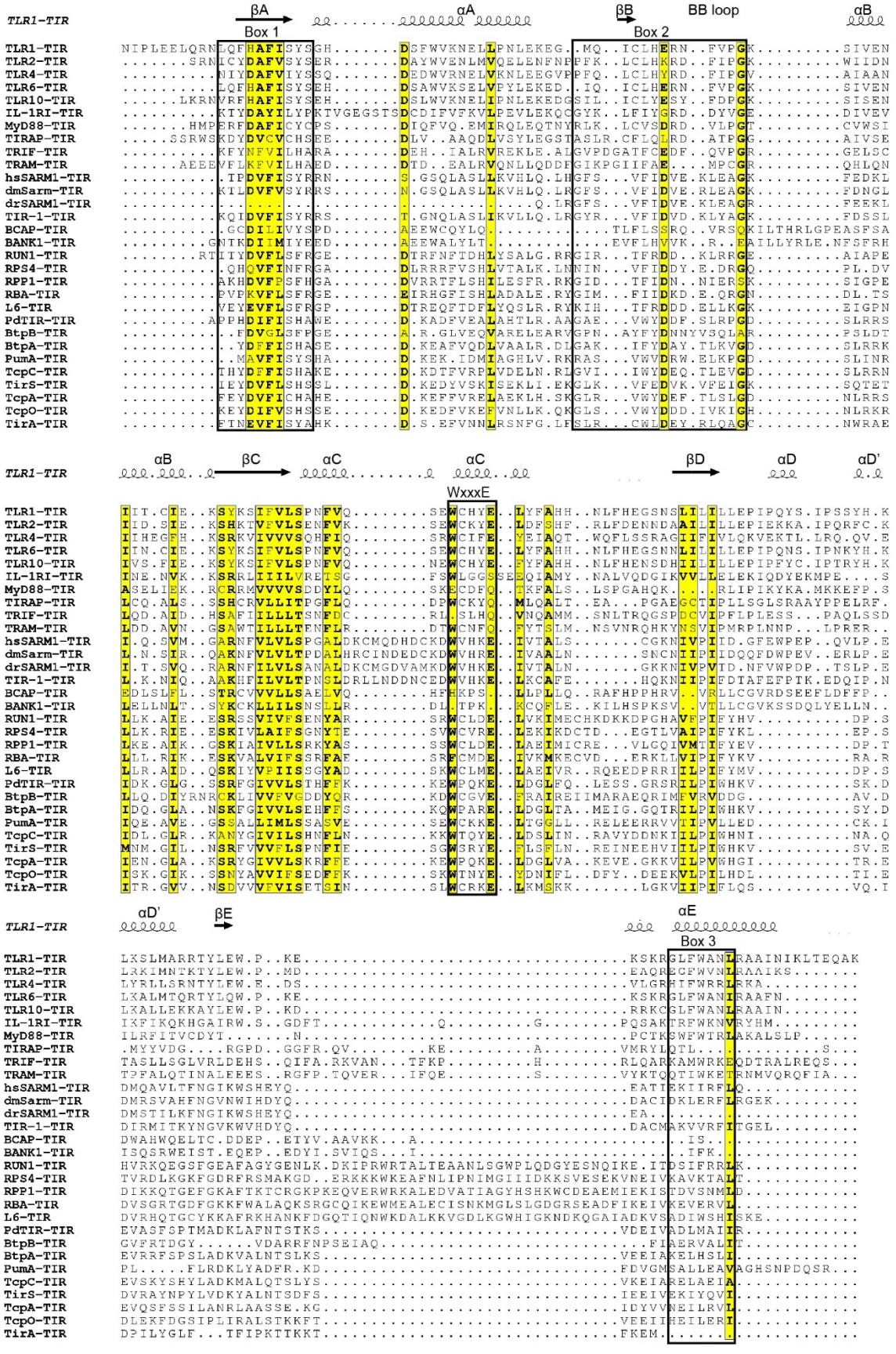

Fig 3.- Alignment of selected TIR domains from different species.

Introduction

Columns are highlighted in yellow if more than 70% of its residues are similar according to physicochemical properties, and similar residues appear in bold. Primary structure motifs Box1/2/3, and the WxxxE motif, key for the enzymatic NADase activity are highlighted inside black boxes. Secondary structure elements correspond to the hTLR1 crystal structure as an example (PDB: 1FYV) (Xu *et al.*, 2000). The alignment was generated with Clustal Omega (Sievers *et al.*, 2011) and formatted together with the structural data using ESPript (Robert and Gouet, 2014). Sequences displayed belong to the TIR domains of (i) *Homo sapiens* innate immunity signaling: TLR1/2/4/6/10, IL-1RI, MyD88, TIRAP, TRIF, TRAM (ii) SARM homologs from *H. sapiens* (hsSARM1), *Drosophila melanogaster* (dmSarm), *Danio rerio* (drSARM), and *Caenorhabditis elegans* (TIR1) (iii) *H. sapiens* BCAP and BANK1; (iv) Plant TIR-NBS-LRR (TNLs) from *Vitis rotundifolia* RUN1, *Arabidopsis thaliana* RPS4 and RPP1, *Linum usitatissimum* L6 and the plant TIR-only protein RBA1 from *A. thaliana* (v) bacterial TIR proteins from *Paracoccus denitrificans* (PdTIR), *Brucella abortus* (BtpA/B), *Pseudomonas aeruginosa* (PumA), *E. coli* (TcpC), *Staphylococcus aureus* (TirS) (vi) archaeal TIR proteins from *Theionarchaea archaeon* (TcpA) and *Methanobrevibacter olleyae* (TcpO) and (vii) the TIR protein from the social amoeba *Dictyostelium discoideum* (TirA).

Table 5.- List of resolved structures from TIR domains and the methods applied.

Species	Method	Protein	PDB number	Ref
Homo sapiens	X-Ray Diffraction	BCAP	5FOR	(Halabi *et al.*, 2017)
		IL-1RAPL	1T3G	(Khan *et al.*, 2004)
		MyD88	4DOM, 4EO7	(Snyder *et al.*, 2013)
		SARM1 (G601P)	6O0V, 6O0B	(Horsefield *et al.*, 2019)
		SARM1 (H685A)	6O0U	
		SARM1 + glycerol	6O0R	
		SARM1 + ribose	6O0Q	
		TIRAP	4LQD, 2Y92, 3UB2	(Lin *et al.*, 2012; Snyder *et al.*, 2014; Valkov *et al.*, 2011)
		TIRAP (D96N)	3UB3	(Lin *et al.*, 2012)
		TIRAP (S180L)	3UB4	
		TLR1	1FYV	(Xu *et al.*, 2000)
		TLR2	1FYW	
		TLR2 (P618H)	1FYX	
		TLR2 (C713S)	1O77	(Tao *et al.*, 2002)
		TLR6	4OM7	(Jang and Park, 2014)
		TLR10 dimer	2J67	(Nyman *et al.*, 2008)
	Solution NMR	MyD88	2Z5V	(Ohnishi *et al.*, 2009)
		TIRAP (C116A)	2NDH	(Hughes *et al.*, 2017)
		TRAM (C117H)	2M1W	(Enokizono *et al.*, 2013)
		TRIF (P434H)	2M1X	
	Cryo-EM	TIRAP	5UZB	(Ve *et al.*, 2017)
Hydra magnipapillata	X-Ray Diffraction	TRR-2	4W8G, 4W8H	Unpublished. PDB released in 2015

Arabidopsis thaliana	X-Ray Diffraction	AtTIR	3JRN	(Chan *et al.*, 2010)
		RPP1	5TEB	(Zhang *et al.*, 2017a)
		RPS4	4C6R, 4C6S	(Williams *et al.*, 2014)
		RPS4 + RRS1	4C6T	
		RRS1 + PopP2	5W3X	(Zhang *et al.*, 2017b)
		SNC1	5H3C, 5TEC	(Hyun *et al.*, 2016; Zhang *et al.*, 2017a)
Linum usitatissimum		L6	3OZI	(Bernoux *et al.*, 2011)
Vitis rotundifolia		RPV1	5KU7	(Williams *et al.*, 2016)
		RUN1	6O0W	(Horsefield *et al.*, 2019)
Brucella melitensis	X-Ray Diffraction	BtpA	4LZP, 4C7M, 4LQC	(Alaidarous *et al.*, 2014; Kaplan-Türköz *et al.*, 2013; Snyder *et al.*, 2014)
Paracoccus denitrificans		PdTIR	3H16	(Chan *et al.*, 2009)
Bacillus cereus		ThsB	6LHY	(Ka *et al.*, 2020)

All structures are available on the Protein Data Bank (PDB) database rcsb.org (Berman *et al.*, 2000), using the corresponding PDB number. Abbreviations: B-cell adaptor for phosphatidylinositol 3-kinase (BCAP), IL-1R accessory protein-like (IL-1RAPL), Sterile α and armadillo-motif containing protein (SARM1), Toll-related Receptor (TRR-2), *A. thaliana* TIR protein (AtTIR), Recognition of *Peronospora parasitica* 1 (RPP1), Resistance to *Ralstonia solanacearum* 1 (RRS1), Effector from *R. solanacearum* (PopP2), Suppressor of npr1-1, constitutive 1 (SNC1), Linum resistance 6 (L6), Resistance to *Plasmopara viticola* 1 (RPV1), Resistance to *Uncinula necator* 1 (RUN1), *Paracoccus denitrificans* TIR (PdTIR).

2.3.- Human TIR proteins.

As stated above, Human TIR-containing proteins are mostly related to TLR and Interleukin signaling. They set the basis of myddosome and triffosome SMOCs, although some display further features on their additional domains (Fig 4).

Looking at their TIR structure, two general interaction interfaces have been proposed for both self-interaction and the association with other TIR proteins. They are called after the main secondary structure elements involved in each one: the BB loop and the αE helix form the BE interface, and helixes αB, αC, and αD, together with the BB loop, generate the BCD interface (Nimma *et al.*, 2017). Fig 5 displays TIRAP self-interacting interfaces as an example since each TIR domain has unique interaction details.

The BE interface constitutes an asymmetrical one-to-one head-to-tail conformation, in which the BB loop (Box2) of one molecule binds to some residues at the αE helix (Box3) in the second molecule (Nimma *et al.*, 2017). αE surface is also composed of surrounding elements such as the

EE loop or βE and βD strands (Ve *et al.*, 2017; Vyncke *et al.*, 2016) (Fig 5). BB loop is a critical region (Rana *et al.*, 2013; Ve *et al.*, 2015). In agreement, an LPS-nonresponsive variant of TLR4 found on a mouse strain bore a mutation in a conserved proline to histidine (P712H) within the BB loop (Poltorak *et al.*, 1998). Corresponding mutations in human TIR proteins [hTLR4 (P714H), MyD88(P200H), TIRAP (P125H), TRIF (P434H) and TRAM (C117H)] impaired signaling (Bovijn *et al.*, 2012; Funami *et al.*, 2008; Horng *et al.*, 2001; Oshiumi *et al.*, 2003; Ve *et al.*, 2017) and human BB loop-derived peptides displayed an inhibitory effect on NF-κB activation (Toshchakov and Javmen, 2020). BE connections may be supported by electrostatic interactions, as BB loop and αE show negative and positive charged surfaces respectively (Vyncke *et al.*, 2016).

The BCD interface sets TIR domains into a symmetrical conformation. In the case of TIRAP (Fig 5), it allows one TIR molecule to bind another two (Ve *et al.*, 2017). They face their αC helixes to each other, assisted by other regions such as the αB/BB loop from one unit and the αD helix from the other (Nimma *et al.*, 2017). The contact is proposed to happen via hydrophobic connections (Vyncke *et al.*, 2016).

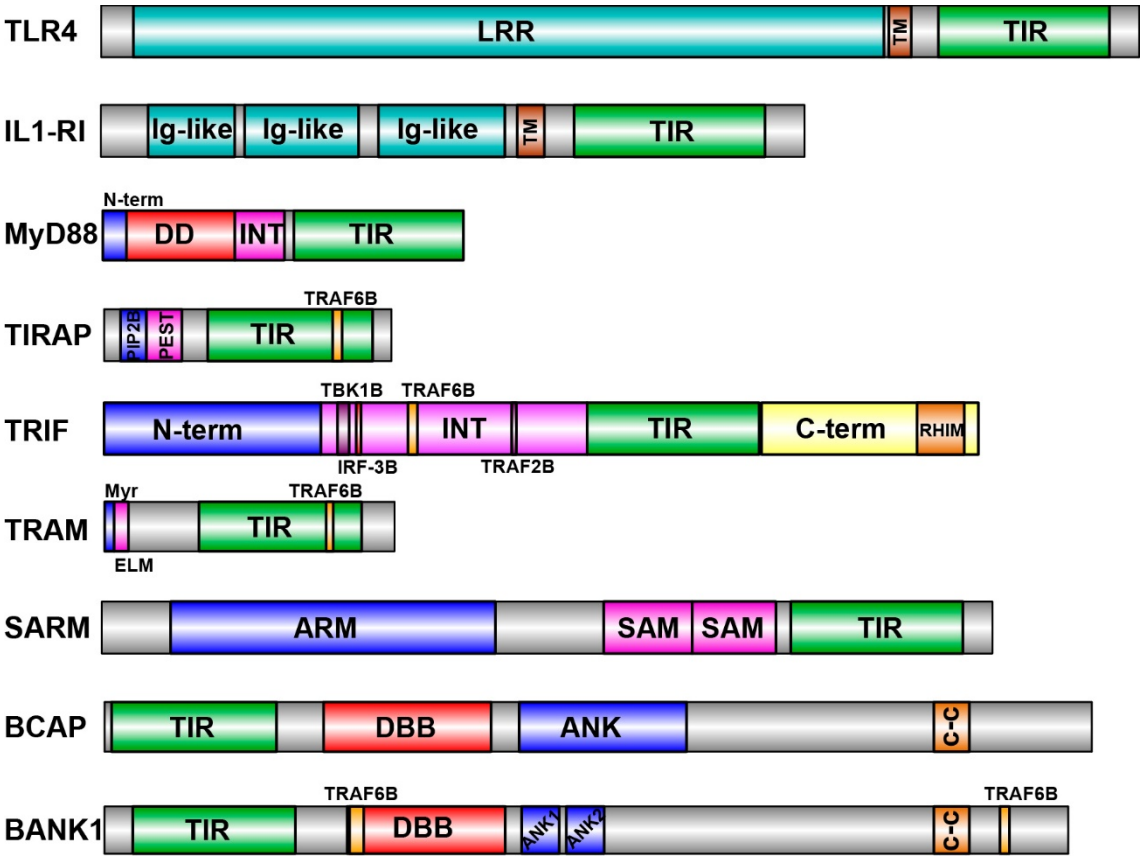

Fig 4.- Architecture of human TIR proteins.

TLR4 (Płóciennikowska *et al.*, 2015a; Ullah *et al.*, 2015), IL-1RI, UniProt accession number P14778.1 (Consortium, 2018) and TM region calculated with TMHMM (Krogh *et al.*, 2001), MyD88 (Avbelj *et al.*, 2011; Avbelj *et al.*, 2018), TIRAP (Ullah *et al.*, 2016), TRIF (Matsumoto *et al.*, 2013; Ullah *et al.*, 2013),

TRAM (Ullah *et al.*, 2016), SARM1 (Horsefield *et al.*, 2019), BCAP (Lauenstein *et al.*, 2020; Luo *et al.*, 2019; Troutman *et al.*, 2012), and BANK1 (Georg *et al.*, 2019). Generated with Illustrator for Biological Sequences (IBS) (Liu *et al.*, 2015b). Abbreviations: Transmembrane (TM), Intermediate domain (INT), PtdIns(4,5)P_2 binding motif (PIP2B), Pro-Glu-Ser-Thr-rich domain (PEST), TRAF6 binding motif (TRAF6B), TBK1 binding motif (TBK1B), IRF-3 binding pLxIS motif (IRF-3B), TRAF2 binding motif (TRAF2B), endosomal localization motif (ELM), Armadillo domain (ARM), Sterile α-motif (SAM), Dof/BANK/BCAP domain (DBB), Ankyrin domain (ANK), coiled-coil region (c-c).

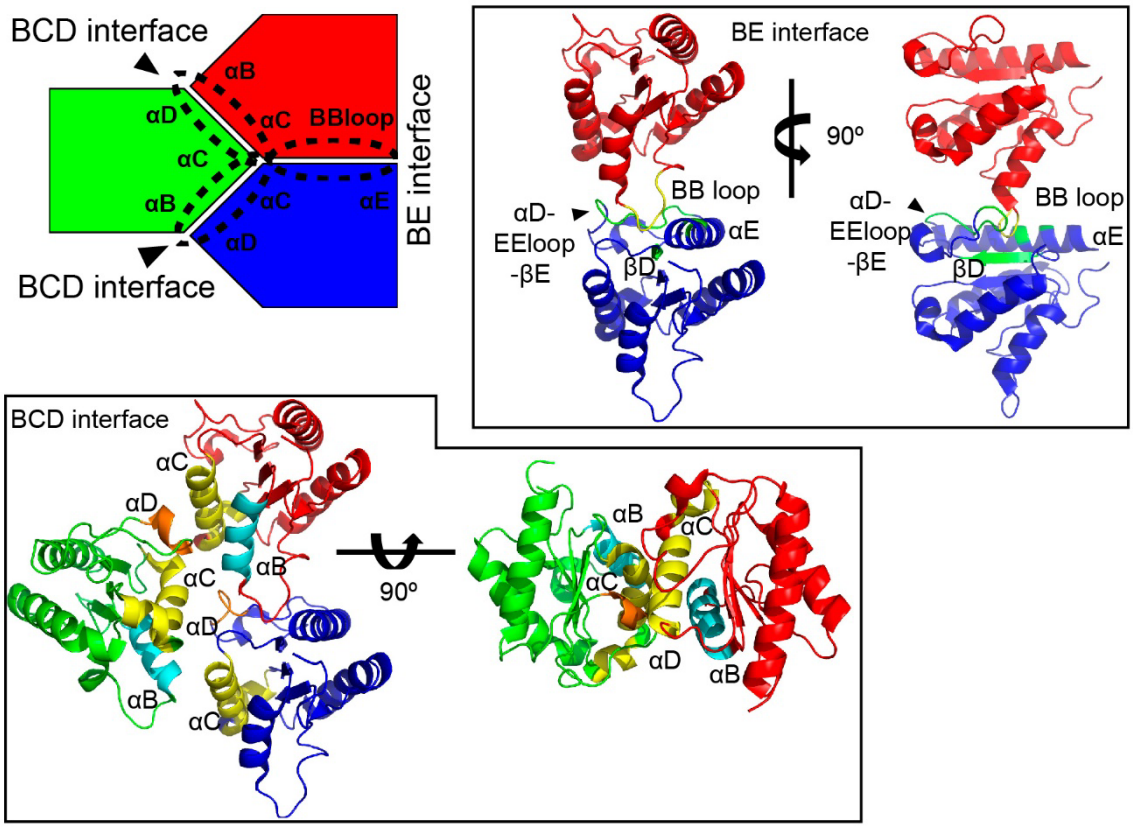

Fig 5.- TIRAP self-interacting interfaces.

Upper: BE interface comprises residues between the BB loop (yellow) in the red chain and the αD-EE loop-βE-αE surface (green) on the blue molecule. Lower: BCD interface connects the green monomer to the other two chains. αC (yellow) connects to the αB(cyan) from the upper (red) molecule and the αD (orange) from the lower (blue) chain. Based on (Ve *et al.*, 2017) (PDB 5UZB).

2.3.1.- Transmembrane TIR-containing proteins.

Like TLRs, the Interleukin Receptors (IL-R) family of transmembrane proteins bear a cytoplasmic TIR domain. Both have distinctive extracellular regions and roles. TLRs detect PAMPs and DAMPS through their outer LRR whereas IL-Rs recognize host-produced cytokines (IL-1, IL-18, IL-33) employing three Immunoglobulin (Ig)-like domains (Ve *et al.*, 2015) (Fig 4).

Among human **TLRs,** TLR1/2/6/10 TIR domains have available structures (Table 5). Although there is no TLR4-TIR 3D assembly yet reported, mutagenic studies and molecular modeling propose that it may form homodimers through its BE surface. This way, BCD interfaces become exposed to the TIR domains of TLR4 adaptors to bind (Bovijn *et al.*, 2012; Guven-Maiorov *et al.*, 2015). A recent study points out that differently charged BB loop surfaces on "protein-sensing" TLRs (TLR1/2/4/6/10) and "nucleic acid-sensing" TLRs (TLR3/7/8/9) may explain the need for intermediate adaptors such as TIRAP or TRAM (Mahita and Sowdhamini, 2018a).

IL-Rs are devoted to activation and specification of adaptive immunity and control inflammatory reactions (Garlanda *et al.*, 2009). Generally, the ligand (for example IL-1) binds to its specific receptor (IL-RI) which in turn interacts with an accessory protein (AcP) receptor (IL-1RAcP) that may be shared by other IL-R. Cytosolic TIR domains of IL-1RI and IL-1RAcP then associate, recruit MyD88 and thus activate myddosome signaling (Krumm *et al.*, 2014). Various inhibitory mechanisms have been described (Garlanda *et al.*, 2013). Among them, modified receptors, such as IL-RII, with no TIR side, or SIGIRR (a.k.a TIR8/IL-1R8) which has a modified TIR domain that fails to recruit MyD88. SIGIRR is also known to act as an inhibitor for not only IL-Rs but also TLRs (Garlanda *et al.*, 2013; Gong *et al.*, 2010). The 3D structure of one IL-R, IL-1RAPL-(TIR), has been solved (Khan *et al.*, 2004) (Table 5).

2.3.2.- TIR adaptor proteins.

To date, seven human TIR adaptors have been identified. Their protein architecture appears in Fig 4, while Tables 6 and 7 sum up posttranslational modifications and relevant variants such as Single Nucleotide Polymorphisms, (SNPs) and splicing variants.

Table 6.- Posttranslational modifications of human TIR adaptors.

Modification	Residues	Enzyme	Comments	Ref.
MyD88				
Ser-phosphorylation	S242	Unknown kinase /PP2A phosphatase	Inhibits signaling.	(Vyncke *et al.*, 2016; Xie *et al.*, 2013)
	S244		Enhances signaling.	
Tyr-phosphorylation	Y180, Y227, Y278	Syk	Upon LPS / IL-1α signal. Degradation.	(Gurung *et al.*, 2017; Han *et al.*, 2010)
Disulfide bonds	All Cys in TIR	Reduced by Nrx	Signaling downregulation.	(Stottmeier and Dick, 2016)
K48-ubiquitination	-	Smurf1/2 and Smad6 (TFG-β induced)	Proteasomal degradation.	(Jenkins and Mansell, 2010; Lee *et al.*, 2011; Naiki *et al.*, 2005)
	-	Nrdp1		(Wang *et al.*, 2009)
K63-ubiquitination	K231	Bacterial induced. Deubiquitinated by CYLD	Required for signaling. CYLD is an inhibitor.	(Lee *et al.*, 2016)
NEDDylation	-	NEDDylase E1, UBC12 and NEDP1 (deNEDDylase)	Antagonizes ubiquitination, impairs dimerization.	(Yan *et al.*, 2017)

TIRAP				
Thr-phosphorylation	T28	IRAK1/4	Impairs PIP binding. Triggers degradation.	(Dunne *et al.*, 2010; Zhao *et al.*, 2017)
Tyr-phosphorylation	Y86 Y106 Y159 Y187	Btk	Upon TLR activation, required for signaling and later degradation.	(Gray *et al.*, 2006; Jenkins and Mansell, 2010; Piao *et al.*, 2008)
	Y106	PKCδ		(Kubo-Murai *et al.*, 2007; Paracha *et al.*, 2014)
Glutathionyla-tion	C91	Oxidizing environment, maybe GSTO1-1	Needed for signaling.	(Hughes *et al.*, 2017)
K48-ubiquitination	K15 K16	SOCS-1	Proteasomal degradation.	(Mansell *et al.*, 2006; Sheedy and O'Neill, 2007)
Proteolytic cleavage	D198	Caspase-1	Down-regulation.	(Miggin *et al.*, 2007; Ulrichts *et al.*, 2010)
TRIF				
Ser/Thr-phosphorylation	S210, S212, T214	TBK1	IRF-3 recruitment.	(Liu *et al.*, 2015a; Zhao *et al.*, 2016)
Tyr-phosphorylation	Y375 (mouse)	Syk	Promotes degradation.	(Han *et al.*, 2010)
K48-ubiquitination	K228	TRIM38	Proteasomal degradation.	(Hu *et al.*, 2015; Li and Zhong, 2018)
	-	WWP2		(Li and Zhong, 2018; Yang *et al.*, 2013)
K63-ubiquitination	-	TRAF2/6	Activation.	(Sasai *et al.*, 2010)
TRAM				
Ser-phosphorylation	S16	PKCε	Release form PM, required for signaling.	(McGettrick *et al.*, 2006)
Tyr-phosphorylation	Y167	PTPN4 (phosphatase)	Release from PM and TRIF interaction.	(Huai *et al.*, 2015)
Myristoylation	G2	-	Membrane linking.	(Rowe *et al.*, 2006)
SARM1				
Ser-phosphorylation	S548	JNK	Upon oxidative stress enhances NADase activity.	(Murata *et al.*, 2018)

NEDDylation is the conjugation of NEDD8 a small molecule that regulates localization, activity, and interaction of proteins. Abbreviations: Phosphatase 2A (PP2A), Spleen tyrosine kinase (Syk), Nucleoredoxin (Nrx), Smad ubiquitin regulatory factor 1 (Smurf), SMAD family member 6 (Smad), Transforming growth factor-β (TGF), RING-Type E3 ubiquitin transferase (Nrdp1), K63-deubiquitinase (CYLD), (UBC12), deNEDDylase 1 (NEDP1), Bruton's tyrosine kinase (Btk), Protein kinase C (PKC), Glutathione transferase Omega 1 (GSTO1-1), Suppressor of Cytokine Signaling-1 (SOCS1), Tripartite Motif-Containing Protein 38 (TRIM38), WW domain-containing protein (WWP2), Protein tyrosine phosphatase nonreceptor type 4 (PTN4).

Table 7.- Relevant human TIR adaptors splicing variants and SNPs.

Variant	ID	Details	Relevance	Ref
MyD88				
Splicing	MyD88s	Lacks INT	Down-regulator.	(Janssens *et al.*, 2002)
SNP	rs1319438 (S34Y)	Death-Domain	Reduced self- and IRAK4 binding. Infection susceptibility.	(George *et al.*, 2011)
	rs878852993 (E52del)	Death-Domain	Loss-of-function.	(von Bernuth *et al.*, 2008)
	rs137853065 (L93P)	Death-Domain	Reduced self-binding and susceptibility to Gram(+) bacteria.	(O'Carroll *et al.*, 2018; von Bernuth *et al.*, 2008)
	rs199396 (R98C)	Death-Domain	Reduced self- and IRAK4 binding. Infection susceptibility.	(George *et al.*, 2011)
	rs137853064 (R196C)	BB loop	Reduced self-binding and susceptibility to Gram(+) bacteria.	(O'Carroll *et al.*, 2018; von Bernuth *et al.*, 2008)
	rs387907272 (L252P)	βD	Gain-of-function. Lymphoma.	(Ngo *et al.*, 2011; Zhan *et al.*, 2016)
TIRAP				
Splicing	2 Isoforms	Longer Ct	Both isoforms a (221aa) and b (235aa) are functional.	(Misch and Hawn, 2008)
SNP	rs8177369 (A9P)	N-term	Possibly loss-of-function.	(Sheedy and O'Neill, 2007)
	rs8177399 (R13W)			
	rs3802813 (S55N)	PEST domain	Functional.	(An *et al.*, 2011)
	rs138228187 (R81C)	Before TIR	Probably loss-of-function.	Ensembl.org
	rs8177400 (D96N)	αA	Loss-of-function. No MyD88 interaction/ posttranslational modification.	(George *et al.*, 2010; Nagpal *et al.*, 2009)
	rs144258412 (A100T)	αA	Probably loss-of-function.	(An *et al.*, 2011)
	rs3802814 (Q101Q)	Synony-mous	Protective against atopic dermatitis.	(An *et al.*, 2011)
	rs548742559(R121W)	BB loop	Probably loss-of-function.	Ensembl.org
	rs147530219 (E132K)	BBloop/αB	Loss-of-function.	(An *et al.*, 2011)
	rs74937157 (C134R)	αB	Probably loss-of-function.	Ensembl.org
	rs199917692(R143Q)	βC	Loss-of-function.	(An *et al.*, 2011)
	rs200632029(R143W)	βC	Probably loss-of-function.	(An *et al.*, 2011)
	rs8177374 (S180L)	DD loop	Protective in heterozygosis against Malaria, bacteremia, *Pneumococcus,* TB, sepsis, *Helicobacter pylori,* and premature birth.	(Ferwerda *et al.*, 2009; Fulgione *et al.*, 2016; Jenkins and Mansell, 2010; Karody *et al.*, 2013; Khor *et al.*, 2007; Misch and Hawn, 2008)
	rs7932766 (A186A)	Synony-mous	Susceptibility to meningeal TB.	(Hawn *et al.*, 2006)
	E190D	αD	Loss-of-function. Alters TRAF6 binding.	(An *et al.*, 2011; Mansell *et al.*, 2004)
	rs7932976 (V197I)	βE	Benign.	
	rs17853052 (X222W)	Stop to Trp	Generates a 256 aa protein.	(Sheedy and O'Neill, 2007)
TRIF				
SNP	rs7255265 (T4T)	Synony-mous	Worse measles vaccine outcome.	(Ovsyannikova *et al.*, 2011)
	rs2292151 (D557D)			
	rs387907307 (R141stop)	Prema-ture stop	Herpes simplex encephalitis.	(Sancho-Shimizu *et al.*, 2011)
	rs146550489 (S186L)	TBK1B		

TRAM				
Splicing	TAG	+ GOLD	Endosomal location inhibitor.	(Palsson-McDermott *et al.*, 2009)
SNP	rs2288384	3'UTR variant	TB association.	(Mekonnen *et al.*, 2018)
SARM1				
Splicing	Two Isoforms	Longer Nt	Both isoform 1 (724aa) and 2 (690aa) are functional.	(Mink *et al.*, 2001)
BCAP				
Splicing	BCAPs	Lacks TIR domain	No longer inhibit TLR signaling.	(Halabi *et al.*, 2017; Matsumura *et al.*, 2010)
BANK1				
Splicing	BANK1-D2	Lacks TIR domain	Enhanced TRAF6 binding.	(Georg *et al.*, 2019)
SNP	rs35978636 (W40C)	TIR	Increased binding to MyD88.	(Georg *et al.*, 2019)
	rs10516487 (R31L)	TIR	Susceptibility to autoimmune disease.	(Bae and Lee, 2017)
	rs3733197 (A383T)	2nd ANK		

After a literature and Ensembl.org (Yates *et al.*, 2019) search, preferably coding sequence variations that had suggested or demonstrated clinical implications were included. Abbreviations: Tuberculosis (TB), TRAM adaptor with GOLD domain (TAG), Golgi dynamics domain (GOLD), 3' untranslated region (3'UTR).

MyD88 is composed of an unstructured N-terminal region, a Death-Domain (DD), an intermediate domain (INT), and a C-terminal TIR (Fig 4). Recently, it has been reported that the first 21 aa form a localization motif that binds phosphatidic acid in PM, which likely acts as a signaling lipid (Avbelj *et al.*, 2018). Its N-terminal motif further interacts with IRF-7, leading to Type I IFN production upon TLR9 stimulation (Deguine and Barton, 2014; Honda *et al.*, 2004). The DD bears six antiparallel α-helixes (Ferrao and Wu, 2012) and binds to DD-containing IRAK kinases (Lin *et al.*, 2010). INT is not only a spacer region between domains, but it helps IRAK4 binding. The isolated INT peptide inhibits TLR signaling (Avbelj *et al.*, 2011) and is absent in MyD88s inhibitory splicing variant (Janssens *et al.*, 2002), while the expression of DD + INT leads to its constitutive activation (Burns *et al.*, 1998).

The MyD88-TIR domain interacts with TIRAP through the BCD surface, helped by an additional region in the DE and EE loops (Vyncke *et al.*, 2016). Alternate homodimerization by both BE and BCD interfaces forms a left-handed helix compatible with further DD assembly models (Vyncke *et al.*, 2016). Recently it has been proposed that preassembled MyD88 hexamers, clustered by their DDs, can be found in resting cells forming a left-handed helix. Upon TLR activation, MyD88 TIR units bind receptor or adaptor TIRs via BCD surface, so that the IRAK4 interface becomes available, allowing myddosome formation (Moncrieffe *et al.*, 2020).

TIRAP has an N-terminal, positively charged, PtdIns(4,5)P_2 binding motif (PBM) (Kagan and Medzhitov, 2006; Zhao *et al.*, 2017), followed by a Pro-Glu-Ser-Thr-rich (PEST) domain, present in short-lived proteins (Jenkins and Mansell, 2010). The C-terminal TIR includes a TRAF6 binding

motif within αD helix (Mansell *et al.*, 2004; Verstak *et al.*, 2009) and a caspase-1 cleavage site on its βE strand (Miggin *et al.*, 2007; Sheedy and O'Neill, 2007) (Fig 4). TIRAP activity is tightly regulated via posttranslational modifications, listed in Table 6. It is also a highly polymorphic gene; clinically relevant variants are summarized in Table 7.

Several resolved TIRAP-TIR structures are available (Table 5) plus one of the N-terminal domain (Zhao *et al.*, 2017). The first crystal structures obtained displayed an atypical fold: they had an unusually long AB loop and lack αB helix or BB loop. All of them bear two disulfide bonds (Lin *et al.*, 2012; Snyder *et al.*, 2014; Valkov *et al.*, 2011). Nevertheless, the latest structures, solved by NMR (Hughes *et al.*, 2017) and cryo-electron microscopy (Cryo-EM) (Ve *et al.*, 2017), have revealed a TIRAP-TIR fold much like typical TIR assemblies.

Hughes and collaborators explored TIRAP under reducing conditions and using a monomeric functional mutant. Elimination of those disulfide bridges showed intact αB helix and BB loop motifs (Hughes *et al.*, 2017). Ve and colleagues examined the *in vitro* assembled TIRAP protofilament. Although such filaments are not likely to happen under physiological conditions, they unraveled precise intra-strand (BE interface) and inter-strand (BCD interface) TIRAP homo-oligomerization surfaces (Ve *et al.*, 2017) (Fig 5). They also propose that TIRAP-TLR4-TIR interaction occurs via the BCD surface (Ve *et al.*, 2017).

TRIF binds directly to TRAM and endosomal TLR3. 712 aa long, it is composed of an N-terminal protease-resistant domain, an unstructured proline-rich intermediate region, a central TIR, and a C-terminal disordered region in which a RIP homotypic interaction motif (RHIM) domain is found (Ullah *et al.*, 2013) (Fig 4). Inside the intermediate region, binding sites for TBK1, TRAF2, and TRAF6 have been identified (Sasai *et al.*, 2010; Tatematsu *et al.*, 2010). The N-terminal domain belongs to the Interferon-induced protein with tetratricopeptide repeats (IFIT) family of proteins (Pidugu *et al.*, 2019; Ullah *et al.*, 2013) and plays an autoinhibitory role blocking TIR interfaces (Mahita and Sowdhamini, 2017). Both its TIR domain and C-terminal region are required for TRIF homo-oligomerization (Funami *et al.*, 2008). RHIM also binds to Receptor interacting protein 1 (RIP1) and RIP3, both DD containing kinases, to activate cell death pathways (Ullah *et al.*, 2013).

P434 in the TIR domain BB loop of TRIF is needed for self-association but not for binding TLR3 or TRAM (Funami *et al.*, 2008). TRIF is rather proposed to bind them by electrostatic interactions: its RK site basic motif connects to the acidic EDD site on a TRAM molecule (Enokizono *et al.*, 2013; Funami *et al.*, 2017) (Fig 6), and to the negatively charged TLR3 dimer BB loops (Mahita and Sowdhamini, 2018a). Additionally, the TRIF QI site on TRIF binds to a second TRAM unit via

its TS site (Enokizono *et al.*, 2013) (Fig 6). At resting state, TRIF is expressed at low levels and diffuses in the cytosol. After a transient association with active TLR3, it forms speckle-like structures in the cytoplasm, where downstream signaling molecules are recruited (Funami *et al.*, 2007). TRIF overexpression also triggers the formation of the speckles (Funami *et al.*, 2007).

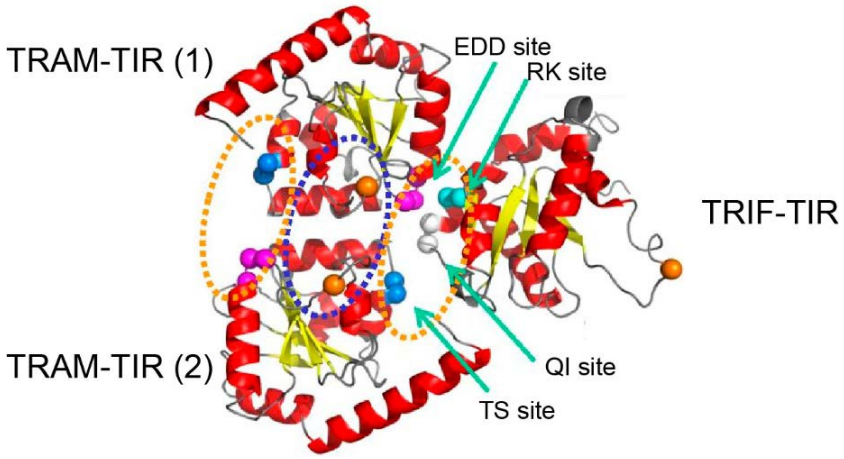

Fig 6.- TRIF and TRAM key interacting residues.

Docking model of the TIR domains of TRAM and TRIF, adapted from (Enokizono *et al.*, 2013). The docking structure is comprised of a TRAM dimer and a TRIF monomer. TRAM-TRAM interfaces are enclosed in blue dotted lines, TRIF-TRAM in orange dotted lines. TRAM T155 and S156 (TS site) and E87, D88, and D89 (EDD site) are colored in blue and magenta respectively. TRIF R522 and L523 (RK site) are shown in cyan, and Q518 and I519 (QI site) appear in white. In this model, BB loop residues C117 in TRAM and P434 in TRIF, highlighted in orange, have been substituted by His.

TRAM, apart from bridging the TLR4-TIR domain and TRIF at the cytosolic side of the early endosomal membrane (Funami *et al.*, 2015; Yamamoto *et al.*, 2003), it binds MyD88 to enable endosomal TLR2 (Stack *et al.*, 2014), TLR7 (Shevlin and Miggin, 2014), and IL-18-R signaling (Ohnishi *et al.*, 2012). TRAM has 235 aa, beginning with a bipartite sorting signal (myristoylation signal, a polybasic region) and a TIR domain (Kagan *et al.*, 2008) with a TRAF6-binding domain on its DD loop (Verstak *et al.*, 2014) (Fig 4).

TRAM homodimerization happens via its BB loop (Enokizono *et al.*, 2013; Funami *et al.*, 2017), but it is predicted that both BE or BCD interfaces could be used, as for TIRAP (Ve *et al.*, 2017). The C117H BB loop mutant, although able to bind TLR4-TIR, does neither homodimerize nor interact with TRIF (Oshiumi *et al.*, 2003). TRAM dimers use one molecule EDD site to bind the positively charged BB loop region from the TLR4 dimer (Mahita and Sowdhamini, 2018a), whereas the EDD motif on the other unit faces the TRIF RK site (Enokizono *et al.*, 2013) (Fig 6).

D91/E92, in TRAM αA helix, are key for signaling but not for TRIF binding. They are proposed to play a role in TRAM endosomal localization, as the corresponding Ala mutations lead to TRAM mislocation in the cytosol, even though it maintains an intact myristoylation signal (Funami *et al.*, 2015; Funami *et al.*, 2017). Moreover, association with MyD88 is thought to occur similarly to TIRAP-MyD88 binding (Ohnishi *et al.*, 2012). TRAM overexpression leads to auto-aggregation and subsequent activation of TRIF without TLR4 stimulation (Funami *et al.*, 2015; Oshiumi *et al.*, 2003).

The B-cell adaptor for phosphatidylinositol 3-kinase (**BCAP** a.k.a PI3KAP1) links signals from TLR, IL-1, and IL-8 receptors to the Phosphatidylinositol 3-kinase (PI3K) and Phospholipase Cγ2 (PLCγ2) pathways (Halabi *et al.*, 2017; Troutman *et al.*, 2012). Composed of 805 aa, it displays an N-terminal TIR followed by a central Dof/BANK/BCAP (DBB) domain, an ankyrin motif (ANK), and a short coiled-coil region (Lauenstein *et al.*, 2020) (Fig 4). Among other roles, (Deason *et al.*, 2018; Lauenstein *et al.*, 2020; Luo *et al.*, 2019; Singh *et al.*, 2018) it binds TIRAP and MyD88 and downregulates inflammation (Troutman *et al.*, 2012). PI3K activation promotes PtdIns(4,5)P_2 conversion into phosphatidylinositol-3,4,5-*tris*phosphate (PtdIns(3,4,5)P_3), which further inhibits TIRAP PM binding (Luo *et al.*, 2019).

The B-cell scaffold protein with ankyrin repeats 1 (**BANK1**), a BCAP paralog, has been related to autoimmune diseases through various genetic studies (Bae and Lee, 2017; Georg *et al.*, 2019). With 785 aa, it has an N-terminal TIR, followed by a DBB domain, two ANK repeats, and a C-terminal coiled-coil (Fig 4). It interacts with MyD88 through its TIR domain and TRAF6 by various motifs.

SARM1 is a human TIR adaptor, although more phylogenetically related to bacterial and plants than to animal TIR proteins (Horsefield *et al.*, 2019; Zhang *et al.*, 2011). First identified as a specific inhibitor of both TRIF- and MyD88-mediated signaling (Peng *et al.*, 2010; Zhang *et al.*, 2011), it was later found to have a role in axonal degeneration (Gerdts *et al.*, 2013; Osterloh *et al.*, 2012) and, recently, it was the first TIR protein to be acknowledged as a NADase enzyme (Essuman *et al.*, 2017; Essuman *et al.*, 2018; Summers *et al.*, 2016). Nonetheless, many other roles have been assigned to SARM1, reviewed in Carty and Bowie (Carty and Bowie, 2019).

With 724 aa, SARM1 contains an N-terminal heat Armadillo repeat motif (ARM), two central sterile α-motifs (SAMs), and a C-terminal TIR domain (Horsefield *et al.*, 2019) (Fig 4). It is found at mitochondria (targeted by the initial 106 aa), cytoplasm, and at the axonal cytosol in neurons (Carty and Bowie, 2019). Besides, the N-terminal ARM region may play an autoinhibitory role (Summers *et al.*, 2016). SARM1 self-association is required for its catalytic function (Horsefield

et al., 2019). SAM domains, which are conserved protein-protein interaction motifs, have been recently found to homo-oligomerize rendering a functionally relevant octameric ring (Horsefield *et al.*, 2019; Sporny *et al.*, 2019). The TIR domain BB loop has proved to be important in axon degeneration (Summers *et al.*, 2016), as well as in mediating inhibition of MyD88 and TRIF signaling via direct TIR-TIR interaction (Carlsson *et al.*, 2016). In both features, G601 was described as an essential residue.

Notably, the NADase enzymatic activity of the SARM1 TIR domain relies on the glutamic acid E642 belonging to the WxxxE motif (Essuman *et al.*, 2017). The latter is a conserved pattern in Guanine-nucleotide Exchange Factors (GEF), and some bacterial translocated effectors (detailed later) (Felix *et al.*, 2014; Orchard and Alto, 2012). The motif is absent in other human TIR adaptors but conserved in most TLRs (Fig 3). SARM1 NAD^+ degrading ability is not exclusive, instead, several studies have proved NADase activity on various other animal (Table 8), plant (Table 9), and bacterial (Table 10) TIR domains.

Table 8.- Animal TIR proteins known to be NAD^+ cleaving enzymes, all of them related to SARM1.

Protein	Species	Substrates	Products	Function	Ref
SARM1	*H. sapiens* (Human)	NAD^+ $NADP^+$ 3apAD sNAD NHD NGD	Nam, ADPR, cADPR	TIR adaptor and axonal degeneration	(Essuman *et al.*, 2017; Horsefield *et al.*, 2019)
SARM1	*Mus musculus* (mouse)	NAD^+	Nam, ADPR, cADPR		(Essuman *et al.*, 2017; Osterloh *et al.*, 2012)
dSarm	*D. melanogaster* (fly)				(Essuman *et al.*, 2017; Osterloh *et al.*, 2012)
SARM1	*D. rerio* (Zebrafish)			TIR adaptor	(Essuman *et al.*, 2017; Jault *et al.*, 2004)
TIR-1	*C. elegans* (worm)		-	Axonal degeneration	(Horsefield *et al.*, 2019; Summers *et al.*, 2016)

Abbreviations: Nicotinamide adenine dinucleotide phosphate ($NADP^+$), 3-acetylpyridine adenine dinucleotide (3apAD), Thionicotinamide adenine dinucleotide (sNAD), Nicotinamide hypoxanthine dinucleotide (NHD), Nicotinamide guanine dinucleotide (NGD), Nicotinamide (Nam), ADPribose (ADPR), cyclic ADPR (cADPR), *C. elegans* TIR protein (TIR-1).

2.3.3.- NAD^+ as a modulator of both metabolism and immunity.

NAD^+, and its reduced form NADH, are essential players not only in eukaryotic metabolism, energy homeostasis, redox balance, and cell survival but also in the modulation of signaling in immunity and inflammatory pathways (Singhal and Cheng, 2019). This coenzyme is consumed as a substrate in multiple reactions or acts as an electron carrier in redox reactions. NAD^+ is an electron acceptor in glycolysis, fatty acid oxidation, or the tricarboxylic acid cycle, whereas NADH donates electrons in mitochondrial oxidative phosphorylation or the cytosolic conversion of pyruvate to lactate yielding ATP (Singhal and Cheng, 2019).

Introduction

Host NAD^+ consuming enzymes are classified into sirtuins, ADP-ribosyltransferases, and NAD^+ glycohydrolases. Sirtuins are histone deacetylases that transfer the acetyl group to the ADP-ribose (ADPR) moiety of NAD^+, and thus epigenetically regulate multiple processes from energy metabolism to inflammation and apoptosis (Audrito *et al.*, 2019). ADP ribosyltransferases, such as poly-ADPR polymerases (PARP), add ADPR to substrate proteins, while NAD^+ glycohydrolases, such as CD38, use NAD^+ as a precursor of secondary messengers, for example, the Ca^{2+} mobilizing ADPR and cyclic ADPR (cADPR) (Audrito *et al.*, 2019; Singhal and Cheng, 2019). Interestingly, SARM1 also produces such metabolites when consuming NAD^+ (Table 8).

The immunometabolism describes the metabolic reprogramming induced in immune cells upon stimulation. This allows fitting the inflammatory requirements, such as increasing their phagocytic power, being NAD^+ a central player in this regulation (Singhal and Cheng, 2019). Macrophages exist as two different populations regarding their metabolic stage (Fig 7). Proinflammatory classically activated macrophages (M1), occur upon LPS stimulation, and experience the Warburg effect, favoring glucose consumption via glycolysis to quickly obtain ATP (Gomes *et al.*, 2013). These changes are required for cytoskeleton dynamics, adhesion, and phagocytosis, all critical features of active macrophages (Venter *et al.*, 2014b), and also promote a myriad of biosynthetic pathways that enable large scale cytokine production, such as TNFα (van Teijlingen Bakker and Pearce, 2020). On the other hand, IL-4 induces alternative activation of macrophages (M2), which are anti-inflammatory, promote wound healing, and obtain their energy mainly from mitochondrial oxidative phosphorylation, a slower but more efficient mechanism (van Teijlingen Bakker and Pearce, 2020).

In M1 cells, NAD^+ is required to maintain such a high glycolytic flux, it is nonetheless consumed during signaling events. For example, reactive oxygen species (ROS) accumulate due to the oxidative phosphorylation blockage. Apart from having an anti-microbial effect helping M1 function, ROS can damage DNA (van Teijlingen Bakker and Pearce, 2020). Subsequent overactivation of PARP signaling by DNA double-strand breaks, which poly-ADPribosylate proteins, can lead to a drop in the levels of its substrate, NAD^+ (Fehr *et al.*, 2020; Singhal and Cheng, 2019). To avoid glycolysis blockage by a lack of this cofactor, TNFα can induce the expression of the Nicotinamide phosphoribosyltransferase (NAMPT, a.k.a PBEF) (Al-Shabany *et al.*, 2016), which regenerates NAD^+ from nicotinamide (Nam), a by-product from PARP activity (van Teijlingen Bakker and Pearce, 2020) (Fig 7). Indeed, increasing NAD^+ levels act as positive feedback for TNFα production, as it is regulated by sirtuins (Al-Shabany *et al.*, 2016). On the other hand, M2 macrophages are actively respiring cells that easily maintain NAD^+ homeostasis and redox balance through oxidative phosphorylation, thus NAD+ biosynthesis is repressed (van

Teijlingen Bakker and Pearce, 2020). In fact, these cells have lower NAD^+ cellular concentrations compared to M1 (Al-Shabany *et al.*, 2016).

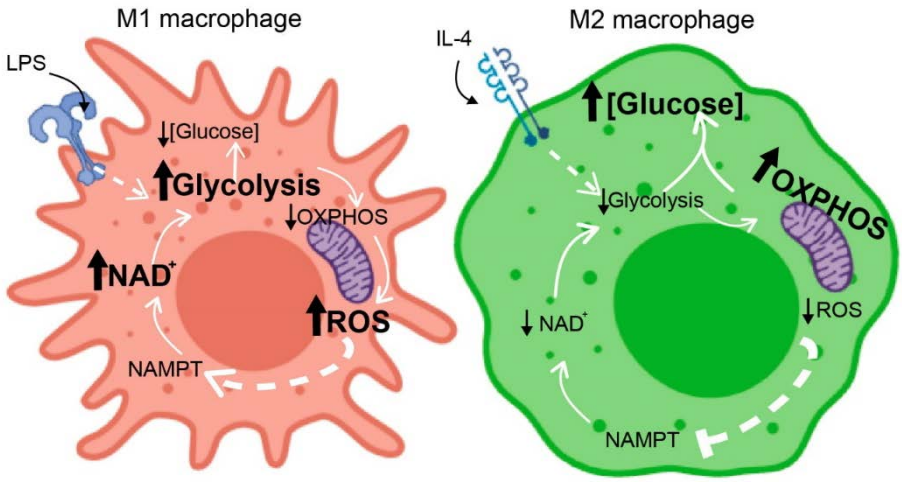

Fig 7.- NAD^+ as an immunometabolic modulator in macrophages.

Classically activated M1 macrophages (left) appear upon LPS activation and are pro-inflammatory. They obtain energy mainly through glycolysis, and a blockage in mitochondrial oxidative phosphorylation (OXPHOS) increases the reactive oxygen species (ROS) levels. High NAD^+ levels are maintained by nicotinamide phosphoribosyltransferase (NAMPT) and allow a high glycolytic flux. Alternative activated M2 macrophages (right) become activated by IL-4 and have an increased OXPHOS flux, leading to higher cytosolic glucose concentrations and lower NAD^+ and ROS levels. Drawings were generated using BioRender and Adobe Illustrator CS6.

2.4.- Animal TIR proteins.

TIR domains are conserved across the animal kingdom (Table 4). Compared to humans, mice have extra TLRs: TLR11/12/13 but lack a counterpart to human TLR10 (Takeda and Akira, 2015). Some non-mammalian vertebrate clades have unique features. For example, amphibians, such as frogs, display both fish-specific and mammalian-specific TLRs. Fish display at least 20 TLRs, some of them lacking human orthologs (Zhang *et al.*, 2014). *Drosophila melanogaster* is the best-studied model among arthropods. Toll-1 signaling plays a role in both immunity and embryo development, following a pathway in which general features are conserved (Lemaitre *et al.*, 1996; Valanne *et al.*, 2011). *Caenorhabditis elegans* is a nematode model organism which, although displaying only some components, is still able to signal effectively (Tenor and Aballay, 2008), playing both immune and developmental roles. It has TIR-1, a SARM1 ortholog related to axonal degeneration (Summers *et al.*, 2016), which is also a NADase (Horsefield *et al.*, 2019) (Table 8). Echinoderms such as *Strongylocentrotus purpuratus* (sea urchin) display an impressive figure of TIR proteins: up to 222 TLR and 26 adaptors. Receptors bear extraordinary diverse LRR regions and probably match different ligands (Hibino *et al.*, 2006). Through evolution, species

may have maintained only the TLRs that were relevant in their environment or, if advantageous, expander their repertoire.

2.5.- Plant TIR proteins.

Plant immunity relies on cytosolic NLRs to fight intracellular pathogen-derived effectors, eventually activating a programmed cell death pathway (Wang *et al.*, 2020). Among them, TIR-NBS-LRR receptors (TNLs) consist of an N-terminal TIR, a central nucleotide-binding site (NBS), and a C-terminal LRR domain (Wang *et al.*, 2020). While TNLs are characteristic of dicotyledon angiosperms, they are absent from monocotyledons (Shao *et al.*, 2016). Instead, they have other kinds of TIR proteins, also involved in disease resistance but lacking NBS and LRR domains, the so-called "TIR-only" proteins (Wan *et al.*, 2019) (Table 4). TNLs are required to dimerize via their TIR domains to effectively signal, as reflected in some crystal structures (Table 5). Again, NADase activity is identified among certain TNLs and "TIR-only" plant proteins (Table 9). Some generate as a product a variant of cyclic ADP-ribose (v-cADPR), distinct from cADPR produced by hSARM1 (Table 8). This chemical represents a novel biomarker for plant TIR enzymatic activity and it is discussed whether it may act as a secondary messenger (Wan *et al.*, 2019).

Table 9.- Plant TIR proteins known to be NAD^+ cleaving enzymes.

Protein	Species	Substrates	Products	Function	Ref
L6	*Linum usitatissimum* (Flax)	NAD^+, $NADP^+$	Nam, ADPR	TNL	(Bernoux *et al.*, 2011; Horsefield *et al.*, 2019)
RUN1	*Muscadinia rotundifolia* (Grapevine)				
RPS4	*Arabidopsis thaliana*	NAD^+	Nam, ADPR v-cADPR	TNL	(Wan *et al.*, 2019; Williams *et al.*, 2014)
RPP1					
RBA1	*A. thaliana*	NAD^+, $NADP^+$	Nam, ADPR v-cADPR	"TIR-only" protein	(Wan *et al.*, 2019)
BdTIR	*Brachypodium distachyon* (grass)				

Abbreviations: Response to HopBA1 (RBA1), TIR-NBS-LRR plant receptor (TNL), a variant of cyclic ADPR (v-cADPR).

2.6- Bacterial TIR Proteins.

Bacteria exhibit a wider diversity of TIR-containing proteins (Toshchakov and Neuwald, 2020). TIR domains are located either in N- or C- terminal regions of bacterial proteins, accompanied by highly heterogeneous sequences (Patterson and Werling, 2013). A few of them have their structures resolved (Table 5). They are considered multi-purpose protein-protein interaction motifs (Spear *et al.*, 2009), they can mimic and impair mammalian TIR interactions (Cirl *et al.*, 2008; Rana *et al.*, 2013), some bear NADase activity (Table 10), and recently they have been also related to a new anti-phage system (Doron *et al.*, 2018). The Thoeris System consists of two proteins, Thoeris system A (ThsA), bearing NAD binding properties, and ThsB, a bacterial TIR

protein. NAD binding and hydrolysis are probably key for effective anti-phage defense (Doron *et al.*, 2018). While both functional proteins are required, *Bacillus cereus* ThsA, but not ThsB, act as NADase *in vitro* (Ka *et al.*, 2020).

Still, the best-characterized bacterial TIR-proteins are virulence factors (Rosadini and Kagan, 2015) (Table 4). They can (i) interfere with host cell TLR and IL-R signaling, as TcpC from uropathogenic *Escherichia coli* (Cirl *et al.*, 2008; Yadav *et al.*, 2010), (ii) control dendritic cell (DC) activation, as BtpA/B from *Brucella* spp. (Salcedo *et al.*, 2013; Salcedo *et al.*, 2008), (iii) stabilize microtubules, as BtpA (Felix *et al.*, 2014; Radhakrishnan *et al.*, 2011), (iv) alter endosomal trafficking and cytokine signaling, as PumA from *Pseudomonas aeruginosa* (Imbert *et al.*, 2017), (v) impair inflammasome function, as TcpC (Waldhuber *et al.*, 2016), (vi) trigger the Unfolded Protein Response (UPR) ER stress pathway, as BtpA (Smith *et al.*, 2013), and (vii) degrade NAD^+ (Essuman *et al.*, 2018) (Table 10).

In many cases, genes for bacterial TIR effectors are found within genetic fragments of phage origin (Wagner *et al.*, 2018), or chromosomal cassettes related to antibiotic resistance as in the case of *Staphylococcus aureus* TirS (Patot *et al.*, 2017). Bacterial effectors can access their targets either by being secreted or introduced inside the cells after bacterial phagocytosis (Patterson and Werling, 2013). *E. coli* TcpC is secreted to the extracellular environment and then is directly taken up by macrophages (Cirl *et al.*, 2008). Intracellular pathogens, such as *Brucella* spp. rely on secretion systems to translocate their factors into host cells (Felix *et al.*, 2014), which will be discussed in the next section.

Table 10.- Bacterial and archaeal TIR proteins known to be NAD^+ cleaving enzymes.

Protein	Species	Substrates	Products	Function	Ref
BtpA	*Brucella* spp.	NAD^+	Nam, ADPR, v-cADPR	T4SS effector	(Coronas-Serna *et al.*, 2020a; Essuman *et al.*, 2018; Kaplan-Türköz *et al.*, 2013)
TirS	*S. aureus*	NAD^+, $NADP^+$, 3apAD, sNAD	Nam, ADPR	Bacterial virulence factor	(Essuman *et al.*, 2018)
TcpC	*E. coli* (UPEC)				
AbTIR	*Acinetobacter baumannii*	NAD^+	Nam, ADPR, v-cADPR		
PdTIR	*P. denitrificans*		Nam, ADPR	-	(Chan *et al.*, 2009; Essuman *et al.*, 2018)
TcpA	*Theionarchaea archaeon* (Archaea)	NAD^+	Nam, ADPR	-	(Essuman *et al.*, 2018)
TcpO	*Methanobrevibacter olleyae* (Archaea)		Nam, ADPR, v-cADPR	-	

Abbreviations: *Acinetobacter baumannii* TIR protein (AbTIR), TIR containing protein O (TcpO).

3.- *Brucella.*

Brucella is a genus of Gram-negative coccobacilli and the etiologic agent of brucellosis, an endemic zoonosis causing abortion and sterility in livestock and wild animals (Byndloss and Tsolis, 2016; Głowacka *et al.*, 2018). In humans, it causes chronic debilitating disease. Acute symptoms are unspecific influenza-like, followed by chronic undulating fever, arthritis, osteomyelitis, muscular pain, hepatosplenomegaly, and rarely endocarditis and neurological signs (Byndloss and Tsolis, 2016; Celli, 2019). Species are relatively host-specific. Relevant for human disease are *B. melitensis, B. abortus, B. suis,* and *B. canis* (Byndloss and Tsolis, 2016; Głowacka *et al.*, 2018).

Transmission occurs through inhalation, ingestion, and contact with mucosal membranes or damaged skin from animal to human (Głowacka *et al.*, 2018) and seldom among humans (Tuon *et al.*, 2017). Typically, it is related to occupational risk and/or to the ingestion of unprocessed dairy products (Głowacka *et al.*, 2018). Nevertheless, it is one of the most common laboratory-acquired diseases around the world, as it is aerosol-transmitted (Byndloss and Tsolis, 2016). The latter feature leads it to be considered as a potential biological weapon (Pappas *et al.*, 2006).

A worldwide public health issue, brucellosis causes considerable economic losses, particularly in developing countries (Franc *et al.*, 2018). The most affected areas are the Middle East, Mediterranean rim, South and Central America, Asia, and Africa (European Food Safety *et al.*, 2019). In the European Union (EU) there has been a constant decrease in *Brucella* spp. infection both in humans and livestock over the last 10 years, thanks to comprehensive surveillance programs. The most prevalent countries are Greece, Italy, Portugal, and Spain, bearing 70% of all human EU cases in 2018 (European Food Safety *et al.*, 2019). In the latest years, an increase in cases has been detected, related to travel and migration, plus uncontrolled food import. Moreover, France (officially free from bovine brucellosis) has recently reported the presence of *B. melitensis* in wild mountain goats (European Food Safety *et al.*, 2019), and a new *B. microti*-like strain was isolated in a frog farm for human consumption, whose human pathogenicity is still to be determined (Jaý *et al.*, 2018).

3.1.- The inner life of an intracellular pathogen.

As an intracellular pathogen, *Brucella* spp. have developed various mechanisms to turn down immunity responses and ensure their survival within host cells (Głowacka *et al.*, 2018). As they reach a new host, they invade epithelial cells in mucosal membranes, where they can resist up to 72h. Once released, they reach phagocytic cells (macrophages and DCs) and they manage to replicate intracellularly. *Brucella* takes advantage of cellular tropism and colonizes lymph nodes,

the reproductive tract, liver, and spleen (Głowacka *et al.*, 2018). Transmission of the disease occurs mainly after abortion. Once in its chronic stage, it infects pregnant animal trophoblasts, which are fetal-derived placental cells that ensure embryo nutrition and hormone secretion (Dehio and Tsolis, 2017). Damaged trophoblasts suffer intense ER stress, leading to apoptosis and inflammation, which follows into a necrotizing placentitis and subsequent fetal death (Byndloss *et al.*, 2019; Dehio and Tsolis, 2017).

3.1.1.- Tricks to subvert innate immunity.

Brucella has an impressive ability to hide from host immunity in different ways, including the use of modified LPS and a Type IV Secretion System (T4SS). LPS is one of the most important antigens in Gram-negative bacteria. It is composed of Lipid A, oligosaccharide core, and O-antigen and lies on the external side of the outer membrane. *Brucella* spp. have modified their LPS in various ways: (i) longer lipid A fatty acid chains (C_{28}, instead of usual C_{12}-C_{16}) impairing TLR4 recognition; (ii) a distinct glycosylation pattern on the oligosaccharide core that hides it from MD-2; and (iii) an O-antigen resistant to recognition by the complement system (Byndloss and Tsolis, 2016). *Brucella* strains may be classified into rough (R-LPS) or smooth (S-LPS), according to their lacking or not of the O-antigen in their LPS, respectively. The latter, beyond subverting complement action, is required for lipid raft-mediated internalization into macrophages (Głowacka *et al.*, 2018). Modified flagellin, lacking the domain that TLR5 usually detects, is also an effective way to hide from TLRs (Byndloss and Tsolis, 2016; Głowacka *et al.*, 2018).

Cyclic β1-2 glucans, known as Osmoregulated Periplasmic Glucans (OPG) have both pro and anti-inflammatory properties. Apart from stabilizing the periplasmic space to ensure flagella and T4SS function, OPGs modulate host lipid rafts, preventing lysosome bactericidal actions (Arellano-Reynoso *et al.*, 2005; Guidolin *et al.*, 2018). Moreover, its two T4SS effectors and TIR-containing proteins BtpA/B further down-regulate TLR signaling and DC maturation (Salcedo *et al.*, 2013; Salcedo *et al.*, 2008), and will be discussed later.

3.1.2.- The intracellular cycle.

Upon *Brucella* cells contact with either phagocytic or non-phagocytic cells, bacteria are internalized generating the *Brucella* containing vacuole (BCV) (Fig 8). Initially, 0-8 h post-infection (pi), endosomal BCV (eBCV) gains markers of early endosomes, such as the Ras-related protein 5 (Rab5), then those of late endosomes, including the Lysosome-associated membrane protein 1 (LAMP1) and Rab7, and eventually being acidified to phagolysosomal-like levels (pH 4,5-5) (Celli, 2019) (Fig 8A). Although around 90% of bacteria are killed within lysosomes,

surviving cells need this eBCV conditions to effectively reach the next step (Celli, 2019; Celli *et al.*, 2003).

At 8-12 h pi, the eBCV switches to replicative BCV (rBCV), connected to both the endoplasmic reticulum (ER) and Golgi. This is an ER-derived organelle as evidenced by markers like calreticulin, calnexin, or by bearing glucose-6-phosphate dehydrogenase (G6PDH) activity in its lumen (Celli, 2019). *Brucella* cells take advantage of their T4SS effectors (Table 11) to modify host vesicle trafficking in the ER exit site (ERES) as well as inducing the Unfolded Protein Response (UPR), a sort of ER stress via the Inositol-requiring enzyme 1α (IRE1α) pathway, and even recruiting some autophagy initiation factors (Celli, 2019) (Fig 8B). Intense bacterial replication is detected in rBCV 12-48 h pi, and the ER network is reorganized (Celli, 2019). Eventually, 48-72 h pi, *Brucella* exits the cell in a non-lytic way, preventing cell death. Autophagic-derived membranes engulf rBCV, rendering the multilayered autophagic BCV (aBCV), which mediates bacterial exocytosis, closing the intracellular cycle (Celli, 2019) (Fig 8C).

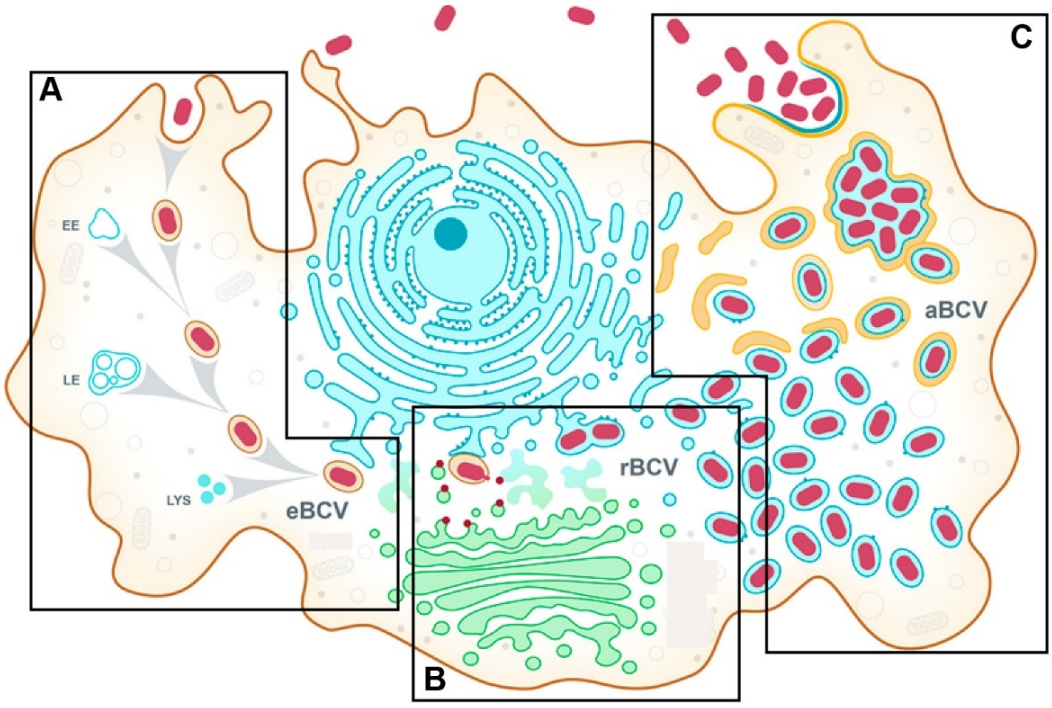

Fig 8.- Model of the *Brucella* intracellular cycle in macrophages.

Modified form (Celli, 2019). (A) The *Brucella* containing vacuole (BCV) acquire from early endosomes (EE), late endosomes (LE), and lysosomes (Lys) the endosomal BCV (eBCV) features. (B) eBCV maturation promotes the translocation of T4SS effectors (red dots). They enable the acquisition of ER (blue) and Golgi (green) derived membranes, generating replicative BCVs (rBCVs). (C) rBCVs, in which bacteria extensively replicate, are captured within autophagosome-like structures (dark orange) to become autophagic BCVs (aBCVs), required for bacterial egress and new cycles of intracellular infections.

3.2.- Type IV Secretion System (T4SS) and its effectors.

Brucella T4SS is a multiprotein complex devoted to efficient substrate export into the host cell. It is homologous to the well-known T4SS (type IVA subfamily) of another α-proteobacterium, the *Agrobacterium tumefaciens* plant pathogen (Celli, 2019; Głowacka *et al.*, 2018; Ke *et al.*, 2015; Lacerda *et al.*, 2013). The 12 components (VirB1-12) of the Brucella T4SS are found within the *virB* operon (Ke *et al.*, 2015; Lacerda *et al.*, 2013). Their expression is upregulated upon acidification of the eBCV and nutrient starvation and is down-regulated at the replicative stage (Lacerda *et al.*, 2013). For example, the two-component regulatory system BvrS/BvrR senses nutrient starvation and thus induces the transcription of vacuolar hijacking *Brucella* regulator (VjbR). This is a transcriptional factor that activates the *virB* operon promoter (Altamirano-Silva *et al.*, 2018; Głowacka *et al.*, 2018; Lacerda *et al.*, 2013).

T4SS is a large complex that goes through bacterial inner and outer membranes plus the BCV membrane, reaching the host cytosol. Their subunits can be classified into 4 groups: the cytosolic ATPase energy center, the bacterial inner membrane platform, the outer membrane core complex, and the stretching needle (or pilus) assembly that injects bacterial effectors into the host cytosol through the vacuolar membrane (Grohmann *et al.*, 2018; Ke *et al.*, 2015; Lacerda *et al.*, 2013).

T4SS and its secreted effectors play a crucial role in *Brucella* spp. pathogenesis: they enable intracellular replication and persistence, modulate host innate immunity, and are key for the transition from eBCV to rBCV, and to the later aBCV (Byndloss *et al.*, 2019; Celli, 2019; Lacerda *et al.*, 2013). Several T4SS-secreted effectors have been identified, but only some have their roles deciphered (Table 11) (Celli, 2019; Ke *et al.*, 2015). To find them, various bioinformatic approaches have been employed, considering the presence of secretory signals, positively charged C-terminal motifs, eukaryotic- or virulence factor-homolog domains, and its conservation among α-proteobacteria, among others (Marchesini *et al.*, 2011; Myeni *et al.*, 2013). Then putative effectors have been checked for their ability to be secreted in wild-type and T4SS defective mutants. One method is the TEM1-β-lactamase assay (de Jong *et al.*, 2008; Myeni *et al.*, 2013), in which bacteria, bearing a TEM1-fused effector, infect macrophages treated with a fluorescent TEM beta-lactamase substrate. Translocated effectors are detected by a shift, from green to blue, of the substrate color on fluorescence microscopy.

Table 11.- *Brucella* spp. T4SS secreted effectors described so far and their functions.

Effector	Target	Function	Refs
VceA	ER	It inhibits autophagy and promotes trophoblast apoptosis. Transcriptionally co-regulated by *VirB* operon.	(de Jong *et al.*, 2008; Zhang *et al.*, 2019a)
VceC	BiP	It binds BiP ER chaperone, activates UPR, via the IRE1α pathway, and induces placentitis and abortion. Its role in UPR induced trophoblast apoptosis is controversial. Co-regulated by *VirB* operon.	(Byndloss *et al.*, 2019; de Jong *et al.*, 2013; de Jong *et al.*, 2008; Zhi *et al.*, 2019)
RicA	Rab2	It recruits Rab2 small GTPase to the BCV, modulates ER-Golgi traffic, and is regulated by BspB.	(de Barsy *et al.*, 2011; de Bolle *et al.*, 2012; Smith *et al.*, 2020)
BPE005	cAMP	It alters cAMP/PKA signaling and induces autophagy and liver fibrosis.	(Arriola Benitez *et al.*, 2018; Marchesini *et al.*, 2011)
BPE043	Unknown	Unknown. It has 4 apolipoprotein domains and may interfere with lipid transport.	(Marchesini *et al.*, 2011)
BPE275	Unknown	Unknown. It is a serine protease from the rhomboid family.	(Marchesini *et al.*, 2011)
BPE123	α-enolase 1	It recruits the α-enolase 1 to the BCV, so it may alter glucose metabolism.	(Marchesini *et al.*, 2011; Marchesini *et al.*, 2016)
BspA	Unknown	It inhibits host protein secretion, prior to the rBCV biogenesis.	(Myeni *et al.*, 2013)
BspB	COG	It redirects ER-Golgi trafficking to generate the rBCV and modulates RicA effects on Rab2.	(Miller *et al.*, 2017; Myeni *et al.*, 2013; Smith *et al.*, 2020)
BspC	Unknown	Unknown. It displays an N-terminal Sec-dependent signal peptide.	(Myeni *et al.*, 2013)
BspE	Unknown	Unknown. It bears a coiled-coil and a TM domain.	(Myeni *et al.*, 2013)
BspF	Unknown	It promotes intracellular replication and inhibits host protein secretion, before the rBCV biogenesis.	(Myeni *et al.*, 2013)
BtpA	TIRAP, microtubules	It downregulates TLR signaling, activates UPR, stabilizes microtubules, and has NADase activity.	(Salcedo *et al.*, 2013; Salcedo *et al.*, 2008)
BtpB	Unknown	It downregulates TLR signaling.	(Salcedo *et al.*, 2013)
SepA	Unknown	It promotes early intracellular survival and eBCV lysosomal resistance.	(Döhmer *et al.*, 2014)
BspL	Herp (ERAD)	It interacts with Herp, an ERAD factor, and activates UPR via the IRE1α pathway. It delays aBCV formation.	(Luizet *et al.*, 2019)

Abbreviations: *virB*-coregulated effector (Vce), Unfolded protein response (UPR), Inositol requiring enzyme 1α (IRE1α) Binding immunoglobulin protein (BiP), Rab2 interacting conserved protein A (RicA), *B. abortus* putative effector proteins (BPE), cyclic adenosine monophosphate (cAMP), Protein kinase A (PKA), *Brucella* secreted proteins (Bsp), Conserved Oligomeric Golgi (COG), secretory pathway (Sec), *Brucella* TIR-containing protein (Btp), Secreted effector protein A (SepA), ER-associated protein degradation (ERAD).

3.2.1.- BtpA, a multitasking expert.

Discovered by two groups, in *B. abortus* (Btp1) (Salcedo *et al.*, 2008) and *B. melitensis* (TcpB) (Cirl *et al.*, 2008) simultaneously, it later was given a third name, following the international guidelines for bacterial nomenclature: *Brucella* TIR-containing protein A (BtpA) (Salcedo *et al.*, 2013). This T4SS effector (Salcedo *et al.*, 2013) has been assigned multiple roles. As a TIR-

containing virulence factor, it was identified to be a TLR2/4/5 pathway down-regulator, blocking NF-κB activation and cytokine secretion in a MyD88-dependent manner, and interfering with DC maturation (Cirl *et al.*, 2008; Salcedo *et al.*, 2013; Salcedo *et al.*, 2008). BtpA also impairs adaptive immunity, as it inhibits CD8+ T cell killing of bacterial infected cells and results in a lesser immunological memory (Durward *et al.*, 2012). Besides, it was recently found to also down-regulate non-canonical inflammasome activation, via induction of ubiquitination and degradation of caspases 1/4/11 (Jakka *et al.*, 2017).

Regarding TLR signaling downregulation, on one hand, BtpA was suggested to mimic TIRAP properties, including phosphoinositide binding (Radhakrishnan *et al.*, 2009), and proposed to trigger phosphorylated TIRAP, but not TIRAP(P125H) for ubiquitination and degradation (Li *et al.*, 2016; Sengupta *et al.*, 2010). On the other hand, other groups described its ability to bind MyD88-DD, disrupting DD-DD interactions in the myddosome (Chaudhary *et al.*, 2012). Further studies showed BtpA interacting with MyD88, TIRAP, and TLR4, but only disrupting the TLR4-TIRAP interface (Alaidarous *et al.*, 2014).

Beyond its immunomodulatory properties, BtpA manipulates microtubule dynamics (Radhakrishnan *et al.*, 2011) and induces the UPR (Smith *et al.*, 2013). The latter re-structures the ER (Smith *et al.*, 2013), while the control of the cytoskeleton helps BCV maturation (Alves-Silva *et al.*, 2017), both favoring *Brucella* cell replication. BtpA acts as a stabilization factor for microtubules, in a similar way to paclitaxel, and prevents drug-induced depolymerization (Alves-Silva *et al.*, 2017; Radhakrishnan *et al.*, 2011). The BtpA interactor Cytoplasmic linker protein 170 (CLIP170) also integrates two effector functions (Jakka *et al.*, 2018). Located at the plus end of growing microtubules, CLIP170 does not only work as a cytoskeleton modulator but also inhibits TLR signaling by enhancing TIRAP ubiquitination and degradation, probably collaborating on the BtpA-dependent TIRAP downregulation (Jakka *et al.*, 2018).

Structurally, BtpA has a phosphoinositide binding region within the N-terminal half (Radhakrishnan *et al.*, 2009) and a C-terminal TIR domain. Conserved features of the TIR domain are the BB loop, with a functionally relevant glycine (G183 in *B. abortus* gene (Felix *et al.*, 2014), also numbered G158 when referring to the *B. melitensis* gene (Alaidarous *et al.*, 2014; Ke *et al.*, 2016) and the above-described WxxxE motif in αC' helix (Felix *et al.*, 2014). The TIR domain homodimerizes via hydrogen bonds among DD and EE loops, helped by residues in αD, αC, and αE helixes (Fig 9A), similarly to *Paracoccus denitrificans* PdTIR (Alaidarous *et al.*, 2014; Kaplan-Türköz *et al.*, 2013; Snyder *et al.*, 2014). Besides, there is a second homodimer interface within αA and αE helixes, and BB loop (Fig 9B) (Kaplan-Türköz *et al.*, 2013; Snyder *et al.*, 2014). The N-

terminal domain is important for dimer stabilization (Alaidarous *et al.*, 2014; Kaplan-Türköz *et al.*, 2013), as shown by the α-tail at the 4LZP PDB structure (Kaplan-Türköz *et al.*, 2013) (Fig 9). Both full-length BtpA and its TIR domain alone disrupt TLR4-TIRAP connections (Alaidarous *et al.*, 2014). The dimer conformation makes the BB loops available for TLR4/TIRAP binding, facing opposite directions (Alaidarous *et al.*, 2014; Snyder *et al.*, 2014), as nicely illustrated by an *in silico* study (Saqib and Baig, 2019). Nonetheless, MyD88 interaction occurs independently of the Gly residue at the BtpA BB loop (Alaidarous *et al.*, 2014). For microtubule stabilization, both the BB loop (Radhakrishnan *et al.*, 2011) and the WxxxE motif (Felix *et al.*, 2014) are crucial. The WxxxE motif binds to the end of the BB loop, which positions G183 close to the WxxxE pocket (Fig 9C).

Interestingly, decoy peptides from BtpA-TIR have been tested to inhibit TLR2/4 signaling. They may become a new immunomodulatory treatment, for example in osteoarthritis (Hong *et al.*, 2019). In addition, BtpA DD loop- and αD helix-DE loop-βE strand-derived peptides have been shown to inhibit both MyD88 and TRIF signaling, and promote intracellular survival of a *ΔbtpA B. melitensis* mutant strain in macrophages (Ke *et al.*, 2016).

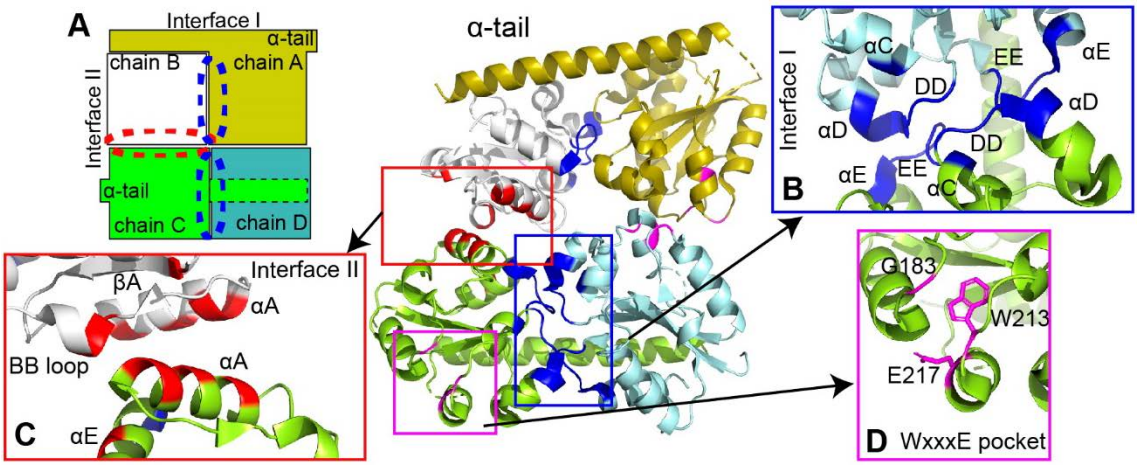

Fig 9.- BtpA self-interacting interfaces and the WxxxE motif.

(A) Scheme showing interface I, in a blue dotted line, and interface II, in a red dotted line. (B) Interface I, in a blue square, linking chains C (green) and D (light blue). (C) Interface II, in a red square, binds chains B (white) and C. (D) In a pink square, a detail of the functionally relevant WxxxE pocket. Chains A (yellow) and C have an additional α-tail, N-terminal to the TIR domain, that stabilizes the conformation. Based on (Felix *et al.*, 2014; Kaplan-Türköz *et al.*, 2013) (PDB 4LZP).

3.2.2.- BtpB, the second TIR effector.

Discovered in 2013 (Salcedo *et al.*, 2013), BtpB is a second *Brucella* T4SS-secreted TIR-protein. Despite sharing only an 11% sequence homology with BtpA, BtpB also displays a C-terminal TIR domain with a conserved WxxxE motif on the αC' helix (Felix *et al.*, 2014).

BtpB controls innate immunity, inhibiting TLR2/4/5/9 signaling, probably via MyD88, as TLR3-TRIF signaling was unaffected. It also impairs DC activation (Salcedo *et al.*, 2013) and modulates immunity at an early stage of the placental infection (Mol *et al.*, 2014). Besides, like BtpA, it is also capable to stabilize microtubules using the WxxxE motif (Felix *et al.*, 2014). It often co-localizes with the microtubule-organizing center (MTOC) and is recruited to intracellular compartments, where ubiquitinated proteins accumulate, when ectopically expressed in HeLa cells (Felix *et al.*, 2014).

4.- *Saccharomyces cerevisiae* as a model organism.

The budding yeast *Saccharomyces cerevisiae* is a unicellular eukaryotic microscopic fungus. Yeasts can be considered the oldest domesticated organisms, evolved in household or community environments to obtain fermented beverages and food, even though its historic use has been empirical. Yeasts have been isolated from ancient Egypt clay vessels (about 5100 years ago) and succeed to produce beer these days (Aouizerat *et al.*, 2019). It was not until the 19th century that they were regarded as living beings and their metabolism was linked to fermentation processes (Barnett, 1998, 2000).

Over the last fifty years, *S. cerevisiae* has proved to be a valuable research model in molecular and cellular biology (Botstein and Fink, 1988; Botstein and Fink, 2011). It is a powerful model for classical genetics, as it has a haploid and diploid life cycle and undergoes both meiosis and mitosis (Herskowitz, 1988). Besides, yeast genetic manipulation tools have quickly developed: the ease of transformation and homologous recombination allowed an impressive spread of gene-protein-function association data. Nowadays, thanks to the collaborative efforts of the yeast research community, most of the engineered technology and functional data are available. It was the first eukaryotic genome to be sequenced in 1996 (Goffeau *et al.*, 1996), and to date over 85% of its Open-Reding Frames (ORF) are annotated in open-access databases such as the *Saccharomyces* Genome Database (Cherry *et al.*, 2012).

There is a myriad of yeast genetic editing methods. Plasmid transformation or genomic integration protocols are well established. Genes can be introduced (or removed) using a wide range of auxotrophic or drug resistance selectable markers. ORF expression can be controlled using different constitutive or inducible promoters or varying plasmid copy number (Alberti *et al.*, 2007; Lee *et al.*, 2015). Moreover, *S. cerevisiae* whole-genome deletion, overexpression, and reduced expression collections are useful systems for screening for genetic interactions (Khurana and Lindquist, 2010). Tagged-ORF libraries are used to check protein localization (GFP-tagged) or to “pull-down” protein complexes (GST-tagged or epitope-tagged) (Botstein and Fink, 2011). The yeast two-hybrid system, based on a transcriptional activator split into its DNA-binding and activator domains, has been widely used to verify direct protein-protein interactions. Query proteins X and Y are then fused to either domain and, only if they are interacting, the transcriptional activator promotes the expression of a reporter gene (Fields and Song, 1989). This 30-year-old strategy is still widely used and has become a paradigm of the contribution of yeast-based tools to research in molecular biology (Paiano *et al.*, 2019).

4.1.- Yeast models for human disease.

Any organism must display two features to become a suitable model for human disease: conservation of the biological process and feasibility of laboratory analysis (Khurana and Lindquist, 2010). Despite having separately evolved over hundreds of millions of years, humans and yeast pathways and physiological processes share considerable homology. About 31% of *S. cerevisiae* genes have human orthologs (Kachroo *et al.*, 2015), and up to 60% of yeast proteins have at least one conserved domain also present in humans (Khurana and Lindquist, 2010). In a study performed on essential genes, 47% of the human orthologs were able to complement the corresponding yeast deletion mutants (Kachroo *et al.*, 2015).

Beyond genetic similarities, elemental cellular processes are preserved too. As a eukaryote, *S. cerevisiae* has a complex subcellular organization, with membrane-coated organelles and its genetic material inside a nucleus. Its characteristic cell division mechanism, cell cycle regulation, DNA replication and transcription plus RNA processing and translation, organelle biogenesis and function, cytoskeletal dynamics, intracellular trafficking, protein targeting and secretion, cell signaling, and metabolic pathways are highly similar to human cells (Khurana and Lindquist, 2010; Smith and Snyder, 2006). Notably, various processes genetically elucidated and characterized originally in yeast became Nobel Prize awarded: among them cell cycle regulation in 2001 (Hartwell, 1974; Nobel-Assembly, 2001), vesicle trafficking in 2013 (Nobel-Assembly, 2013; Novick and Schekman, 1979), and autophagy in 2016 (Nobel-Assembly, 2016; Takeshige *et al.*, 1992).

S. cerevisiae is cheap, safe, and easy to manipulate. Growth conditions are highly reproducible by using chemically defined media. Its short generation time and its stability make it a suitable candidate for large-scale screenings, and even for industrial drug production (Otero *et al.*, 2013). Additionally, the impressive amount of data and genetic tools available makes yeast research straightforward. Investigators benefit for over 30 years from all these characteristics to humanize yeasts (modifying them to carry human genes) (Kim *et al.*, 2020). Several approaches have been proposed to study human biology: from searching for new drug activities and targets to reconstructing whole human pathways or complexes into thus “humanized” yeasts (Laurent *et al.*, 2016). If the human disease-causing gene has a known yeast ortholog, it may be replaced, checked for complementarity, and then SNPs from patients further analyzed in the yeast system. Other strategies rely on humanizing only some conserved residues or motifs on the yeast ORF (Laurent *et al.*, 2016). Lastly, human genes can be expressed in yeast regardless of the existence or absence of functional or structural homologs. If the expression of the human gene leads to a detectable phenotype, an interference assay for functional analysis can be set up. Heterologous

expression of human genes has proved its effectivity in providing new insight into the understanding of various disease mechanisms (Laurent *et al.*, 2016).

Neurodegenerative diseases are caused, in many cases, by a mutated protein unable to properly fold. It aggregates and becomes cytotoxic, sometimes showing a prionic behavior (Khurana and Lindquist, 2010). Yeast lacks functions related to most neuron-specific traits, but they have conserved vesicle trafficking mechanisms (key for neuronal function) and have their own prion-like proteins (Khurana and Lindquist, 2010; Lindquist, 1997). Thus, heterologous expression of human neuropathogenic proteins in yeast provides a good model, being their features easily reproduced. As an example, the amyloid beta-peptide from Alzheimer's disease is toxic when expressed in yeast, disrupting endocytic traffic. A whole-genome overexpression screen led to the discovery of disease-related human genes (Treusch *et al.*, 2011). Other models have served as a platform for drug screening, and the outcome was further checked in neuron cell culture and higher organisms (Khurana and Lindquist, 2010; Treusch *et al.*, 2011).

Cell signaling is fundamental in many aspects of cellular life. As in the case of other biological processes, *S. cerevisiae* has pioneered eukaryotic signaling research (Botstein and Fink, 1988; Botstein and Fink, 2011). In many cases, oncogenesis results in dysregulation of a signaling pathway, ending up in uncontrolled cell proliferation and survival. One of these has been modelized in yeast over the last 15 years by our research group: the PI3K/PTEN/Akt oncogenic pathway (Coronas-Serna *et al.*, 2020b; Rodríguez-Escudero *et al.*, 2005b) (Fig 10). Phosphatidylinositol-3 kinase (PI3K), upon recruitment to PM via active receptor tyrosine kinases, transforms PtdIns(4,5)P_2 into PtdIns(3,4,5)P_3. The latter is a key signaling lipid that recruits relevant factors for different processes like cell proliferation and survival. Akt (a.k.a PKB) is recruited to PM via PtdIns(3,4,5)P_3-binding, becomes activated by PDK1 and mTORC2 kinases, and further spreads downstream the signal to activate cell proliferation. This is downregulated by tumor suppressor PTEN, the lipid phosphatase that balances PI3K activity (Manning and Toker, 2017). *S. cerevisiae* lacks class I PI3K activity, and no PtdIns(3,4,5)P_3 is naturally found (De Craene *et al.*, 2017). Heterologous expression of PM-targeted PI3K, or PI3K co-expressed with Akt, leads to yeast cell death by alterations in the actin cytoskeleton and vesicle traffic (Coronas-Serna *et al.*, 2018; Fernández-Acero *et al.*, 2015; Oliver *et al.*, 2017; Rodríguez-Escudero *et al.*, 2005b). This is indeed counteracted by PTEN co-expression, allowing functional characterization of cancer-related mutations in this tumor suppressor (Fernández-Acero *et al.*, 2019; Rodríguez-Escudero *et al.*, 2015). Also, known PI3K inhibitors (potential anti-tumoral drugs) restore cell growth in this humanized yeast setting (Fernández-Acero *et al.*, 2012). Taking advantage of these phenotypes, screens to test new drug candidates and mutations found in patients have been

developed. Examples of engineered yeast settings either growth- or fluorescence-based are reviewed in Coronas-Serna *et al.* (Coronas-Serna *et al.*, 2020b).

4.2.- Yeast as a model to understand bacterial effectors.

Frequently, bacterial pathogens deliver effector proteins as virulence factors through sophisticated mechanisms, such as Type III/IV Secretion Systems (T3SS and T4SS). Such effectors trigger physiologically relevant processes within the host cell, to ensure the proliferation and/or survival of the intracellular pathogen. Nonetheless, deciphering their roles is not straightforward, as previously commented.

S. cerevisiae has helped to understand the mode-of-action of some bacterial virulence factors by heterologous expression. It offers conserved molecular targets, processes, and putative activities in a simple cellular environment, which highlights the effector-derived phenotype and uncovers its subcellular localization. Besides, its scalability and the abundant genetic and genomic editing protocols make it easy to develop screening assays to either find host interactors and specific drug inhibitors or to drive structure-function studies using random or site-directed mutagenesis (Curak *et al.*, 2009; Popa *et al.*, 2016; Siggers and Lesser, 2008). Still, yeast has some limitations in heterologous expression assays. For example, some effectors may require pathogen-derived posttranslational modifications that cannot be reproduced in yeast. It also lacks higher eukaryotic relevant immunity pathways, such as TLR or inflammasome signaling that play a crucial role in the host-pathogen dialogue (Popa *et al.*, 2016).

Growth inhibition is the most typical phenotype upon yeast heterologous expression of a bacterial virulence factor (Popa *et al.*, 2016). Several approaches have been developed to exploit this feature and gain further clues to their function. Suppression or enhancement of effector-derived yeast toxicity can be screened using yeast whole-genome deletion or overexpression collections. For example, the yeast pathogenic genetic array (PGA) strategy is based on previous classic screens for synthetic lethality (i. e. two mutants are individually healthy, but the double mutant is no longer viable). If expressing the heterologous effector inhibits the growth of any of the mutants in the collection, its phenotype should be comparable to the deletion of the synthetic lethal partner of that gene (Bosis *et al.*, 2011; Lee *et al.*, 2019). Yeast ORF overexpression collections are used to screen for growth inhibition suppressors too. In this case, an increase in the copies of its target may rescue the toxic features of the effector (Fernandez-Piñar *et al.*, 2012). Moreover, small compound libraries can be used to find specific inhibitors that rescue effector-induced yeast phenotypes. These would be potential new drugs for infectious diseases therapy or may help in further investigations (Arnoldo *et al.*, 2008; Huang *et*

al., 2008). On the other hand, libraries of putative bacterial effector-coding genes have also been tested for growth inhibition in yeast to identify novel activities (Alemán *et al.*, 2009; Rangel *et al.*, 2019).

All these studies revealed varied mechanisms ruling bacterial effector-induced yeast cell growth inhibition or death. Cytoskeleton perturbation, arresting cell cycle, organelle traffic impairment, and altered signaling are among the principal causes, as reviewed in Popa *et al.* (Popa *et al.*, 2016). Interference with the yeast cytoskeleton often leads to cell polarity loss or cell cycle blockage. In many cases effectors tune small Guanosine triphosphate hydrolase (GTPase) signaling, mimicking host modulators. GTPases regulate membrane trafficking, actin dynamics, cell cycle, or nuclear import, and are switched on by Guanine nucleotide exchange factors (GEFs) and off by GTPase activating proteins (GAPs). Bacterial effectors resembling GEFs usually bear a conserved WxxxE motif (Bulgin *et al.*, 2010). Vesicle trafficking and membrane composition are frequently targeted by invasive bacteria, to avoid phagocytosis or to ensure intracellular survival (Popa *et al.*, 2016).

MAPK signaling is also commonly altered by bacterial effectors. Often, MAPK pathways are among the first clues to learn about the effector's activity in the host cell, as the high degree of conserved signaling elements in yeast MAPK cascades with those of higher eukaryotes eases the analysis. Bacterial effectors may prevent phosphorylation or directly trigger the degradation of a component. In other cases, they can alter proteins shared by more than one pathway (Popa *et al.*, 2016).

It is not rare that the same effector causes phenotypes by more than one mechanism. For example, our research group found that SopB (a.k.a SigD) from *Salmonella* Typhimurium, which has a C-terminal inositol phosphatase domain, interacts with and blocks small GTPase Cdc42 activation through its N-terminal region, both in human and yeast (Alemán *et al.*, 2005; Rodríguez-Escudero *et al.*, 2011; Rodríguez-Escudero *et al.*, 2006). Expressing the intact protein shows the phosphatidylinositol phosphatase-derived effects, in which cell wall integrity pathway MAPK Slt2 is strongly activated and toxicity is mainly a consequence of PtdIns(4,5)P_2 depletion. Using a phosphatase-dead mutant, cells die otherwise: Cdc42-driven actin polarization is lost, the cell-cycle becomes arrested in G2, and instead of strongly activating Slt2, it inhibits Kss1, a MAPK from the filamentation pathway (Alemán *et al.*, 2005; Rodríguez-Escudero *et al.*, 2011; Rodríguez-Escudero *et al.*, 2006). To sum up, a sole effector has proved to cause growth inhibition in several MAPK pathways.

Our research team has pioneered the bacterial effector yeast expression approach testing effectors from Enteropathogenic *Escherichia coli* (EPEC) (Rodríguez-Escudero *et al.*, 2005a), *Coxiella burnetii* (Rodríguez-Escudero *et al.*, 2016), *Klebsiella pneumoniae* (Storey *et al.*, 2020) and *Salmonella* including the already described SopB, SopE2 and SptP (Rodríguez-Pachón *et al.*, 2002), SteC (Fernandez-Piñar *et al.*, 2012), and SteA (Domingues *et al.*, 2016) (Fig 10C). Moreover, we designed a screen to identify *Salmonella* proteins inhibiting yeast growth when overproduced (Alemán *et al.*, 2009). Altogether, we have proved *S. cerevisiae* to be an invaluable system to assess bacterial virulence factors.

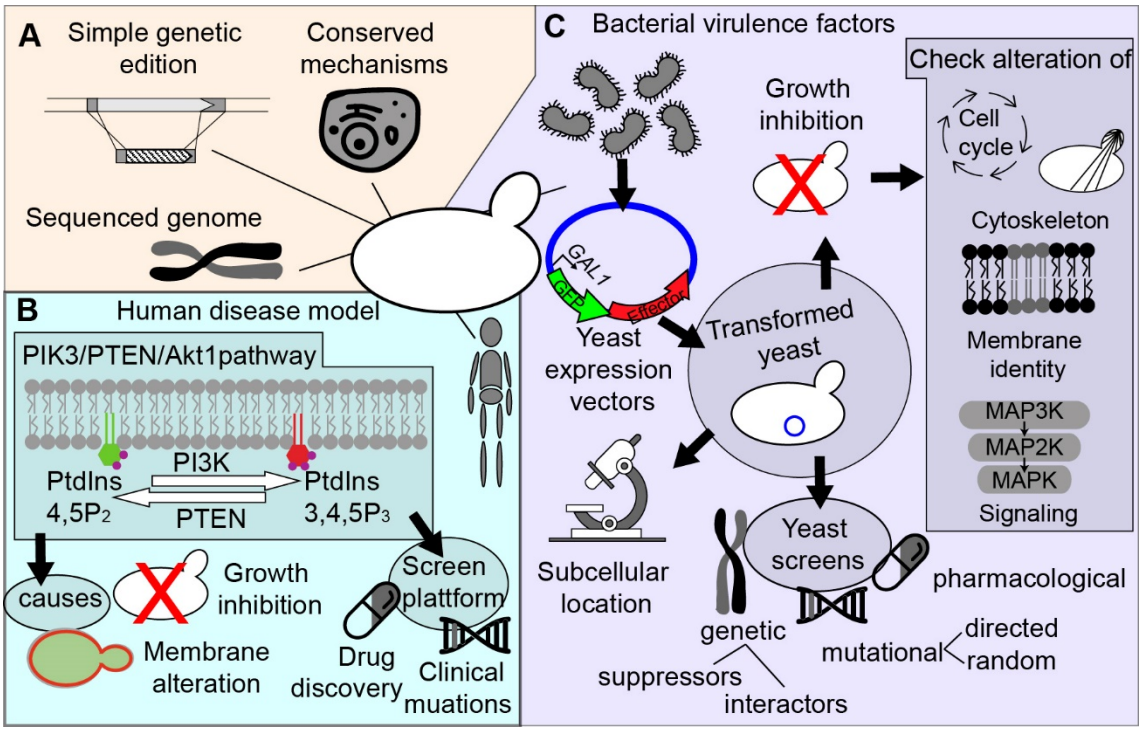

Fig 10.- *Saccharomyces cerevisiae* as a model organism.

(A) Budding yeast is an excellent eukaryotic model, as it has conserved mechanisms with higher eukaryotes, simple genetic edition tools, plus its genome is sequenced and data are freely available. (B) Example of a human disease yeast model developed by our group, the PI3K/PTEN/Akt1 pathway. The expression of the protooncogene PI3K induces yeast growth and alteration of membrane composition. Both phenotypes are counteracted by the tumor suppressor PTEN and set the basis for yeast-based screen platforms for either drug discovery or the assessment of clinical mutations. (C) General strategies for the study of bacterial virulence factors in yeast, performed by our group. Bacterial effectors are transformed into yeast expression vectors, controlled under the *GAL1* promoter. Their subcellular localization and growth inhibitory properties are checked, and the lying mechanisms are further investigated. Yeast can serve as a platform for genetic (looking for suppressor genes or interactors), mutational (either directed or random), or pharmacological screens. Drawings were generated with Adobe Illustrator CS6.

Background and Objectives

Background and Objectives

For several years, our research group has been employing *S. cerevisiae* yeast as a model organism. Heterologous expression strategies were preferred, targeting either human diseases, as the human PI3K/PTEN/Akt pathway reconstruction (Coronas-Serna *et al.*, 2020b; Rodríguez-Escudero *et al.*, 2005b), or bacterial virulence, for example, by the expression of *Salmonella* type 3 secretion system (T3SS) effectors (Domingues *et al.*, 2016; Rodríguez-Escudero *et al.*, 2006). In the context of a collaborative project, Dr. Suzana Salcedo (CNRS, Université de Lyon1), an expert on *Brucella* host-pathogen interactions, shared with us the genes of putative *B. abortus* T4SS effectors to elucidate their mode of action via yeast expression. Among them, BtpB, and to a lesser extent BtpA, caused yeast growth inhibition. At that time, María Rodríguez-Escudero proved that yeast expressing BtpB had depolarized actin patches, blocked endocytosis, and impaired MAPK signaling and that all those phenotypes relied on the TIR domain. Besides, she developed a random mutagenesis screen and found twelve loss-of-function mutations on BtpB.

The fact that those *Brucella* effectors bear a TIR domain drew our attention to the TLR signaling and its SMOC-based pathways. So, we started a collaboration with Dr. Jonathan C. Kagan (Harvard University), an expert in innate immunity and SMOCs, to reconstruct the myddosome and triffosome in yeast. This way we could give a new perspective to the field, by analyzing such intricate complexes in a cellular environment lacking potentially interfering elements, and provide a platform to study those *Brucella* effectors. Moreover, we could set the basis for yeast-based screen platforms to find new antimicrobial or immunomodulating drugs, to test clinically relevant SNPs on the human adaptors, or to evaluate other TIR-containing bacterial effectors. Altogether, we proposed for the present Thesis the following **objectives**:

1.-Reconstruction of the TLR4-associated SMOCs through yeast heterologous expression, assessment of the interactions among human TIR proteins plus their downstream kinases, and analysis of clinically relevant mutations.

2.-Understanding the yeast phenotypes derived from the heterologous expression of *Brucella* TIR effectors, through a screen for toxicity suppressor yeast genes and the characterization of loss-of-function mutants found on a previous screen.

3.-Connection of both human and bacterial TIR protein yeast models to evaluate their interactions and the phenotypes induced in yeast.

Materials and Methods

Materials and Methods

1.- Microorganisms.

The *Escherichia coli* DH5α F′(K12Δ(*lacZYA-argF*)U169 *deoR supE44 thi-1 recA1 endA1 hsdR17 gyrA96 relA1* (*ϕ80lacZΔM15*)F′) was the routine strain used for general molecular biology. For the Gateway cloning techniques, the *S. cerevisiae* Advanced Gateway Destination Vectors collection from Susan Lindquist (Addgene Kit # 1000000011) (Alberti *et al.*, 2007), was provided transformed in an *E. coli ccdB* resistant strain. YPH499 (*MATa ade 2-101 trp1-63 leu2-1 ura3-52 his3-200 lys2-801*) (Sikorski and Hieter, 1989) was the *S. cerevisiae* strain for general use in these studies unless otherwise stated. W303-1A (*MAT*a *leu2-3,112 trp1-1 can1-100 ura3-1 ade2-1 his3-11,15*, (Thomas and Rothstein, 1989) was employed for the Yeast ORF overexpression library screening.

2.- Culture media, growth, and conservation conditions.

The general medium for *S. cerevisiae* culture was the yeast-peptone-dextrose (YPD) (1% yeast extract, 2% peptone, and 2% glucose). Yeast bearing plasmids were selected and maintained employing the minimum synthetic dextrose media (SD) (0.17% yeast nitrogen base without amino acids, 0.5% ammonium sulfate, and 2% glucose), supplemented with the required amino acids or nitrogenous bases, excepting the ones corresponding to the auxotrophies targeted by the plasmids. Additionally, the synthetic raffinose (SR) and synthetic galactose (SG) media shared SD composition, but bear 1.5% raffinose or 2% galactose respectively, instead of glucose. *E. coli* was cultured using the Luria Bertani (LB) medium (1% tryptone, 0,5 yeast extract, 0.5% NaCl), supplemented for plasmid selection with 100 µg/mL Ampicillin or 50 µg/mL Kanamycin, added after sterilization. The water used for dissolution was deionized through Millipore purification systems. The media were autoclaved at 121°C and 1-atmosphere over-pressure for 20 minutes. To obtain solid media, 2% agar was added to the usual composition.

E. coli was cultured at 37 ^{o}C, shaking at 200-220 rpm when using in liquid media. Unless otherwise stated, *S. cerevisiae* was cultured at 30 ^{o}C, with 180-220 rpm shaking in liquid media. Liquid culture growth was followed through optical density (OD) measurements, at 600nm wavelength, on a Beckman DU640 spectrophotometer, and using the optimal dilutions. For experiments requiring *GAL1* promoter-derived expression induction, transformed yeast cells were pre-inoculated for 18 h in SR liquid media. Then, cultures were inoculated to an OD_{600} of 0.3 into new liquid SR supplemented with 2% galactose and were cultured for 5h, unless

otherwise stated. The use of raffinose optimizes the *GAL1* promoter induction process as it does not repress (unlike glucose) nor induces it.

To stimulate yeast signaling pathways, the following compounds were used: (i) Congo Red (30 µg/mL, Millipore), is a compound that binds chitin, alters proper yeast cell wall building, and thus activates the Cell Wall Integrity (CWI) MAPK pathway, and (ii) the α-Factor pheromone (3 µM, Innovagen) triggers the mating MAPK pathway. Cells expressing a *GAL1* controlled gene grew for 2.5 h in the galactose-added media before the addition of any of those stimuli.

Yeast and *E. coli* strains were long-term conserved at -80 ^{o}C in glycerol solutions at 25% or 50% (v/v) respectively. To avoid plasmid loss, *E. coli* was previously cultured on LB carrying the appropriate antibiotic.

2.1.- Ten-fold serial dilution drop assay.

This assay evaluates the effects of the expression of heterologous genes on yeast growth. Transformants were cultured on SD media for 18 h. Cells were then suspended in sterile water to an OD_{600} of 0.5 as the first dilution. Subsequently, three more ten-fold serial dilutions were generated on a final volume of 180 µL of sterile water, using a sterile 96-well plate. 5 µL of each dilution were plated using a Multi-blot replicator (VP407, V&P Scientific, INC) in SD, as a control, and SG, for expression induction, solid media. Plates were cultured at 30 ^{o}C for 72 h.

3.- Molecular biology techniques.

Basic molecular biology techniques including *E. coli* alkaline lysis plasmid DNA extraction, restriction enzyme digestion, polymerase chain reaction (PCR) DNA amplification with a MiniCycler PTC-150 (MJ Research), were pursued following classical protocols (Ausubel, 2001; Sambrook and Russell, 2001). Plasmid transformations on *E. coli* and *S. cerevisiae* were performed following the Inoue method (Sambrook and Russell, 2006) and the lithium acetate single-step method (Chen *et al.*, 1992) respectively. Plasmid extraction and purification were achieved using either NZTMiniprep (NZYTech) and NucleoSpin Plasmid (MacheryNagel) commercial kits. For restriction enzyme cloning, PCR products were generated using the Expand High Fidelity DNA polymerase (Roche) and were subcloned into pGEM-T vector system kit (Promega) for sequencing and the insert was then subcloned into a yeast expression vector. Restriction enzymes came from either NZYTech or Roche, and vectors opened with a single enzyme were treated with the rAPid alkaline DNA phosphatase (Roche) to remove the 5' end phosphate, before ligation using the T4-DNA ligase (Roche). For Gateway cloning (Thermofisher) primers containing the *attB* sequences were designed and inserts were amplified using KAPA

HiFi DNA polymerase (KAPA biosystems), and later introduced into pDONR221 (Thermofisher) using the BP clonase II (Thermofisher) to obtain the entry plasmid. Destination vectors were chosen from the *S. cerevisiae* Advanced Gateway Destination Vectors collection (Addgene Kit # 1000000011) (Alberti *et al.*, 2007), and sequenced entry plasmids were subcloned into the chosen destination vectors using the LR clonase II (Thermofisher) to generate the yeast expression plasmids. As destination vectors bearing the *ccdB* gene are not suitable for *E. coli* DH5α retransformation, the polylinker region of the pEG(KG) vector has been cloned to remove *ccdB* and obtain a suitable control plasmid for the yeast expression experiments.

DNA electrophoresis was done on 1% agarose gel on TAE buffer (40 mM Tris base, 20 mM acetic acid, 1 mM EDTA, pH=7.75), the gel was subsequently stained on a GelRed (Sigma) solution (GelRed 1 X in 0.1M NaCl) and visualized on a UV transilluminator MiniLumi (DNR Bioimaging systems). To elute DNA fragments from agarose gels the Geneclean Turbo (MP Biomedicals) commercial kit was used. DNA concentration was measured at a Nanodrop (Thermo Scientific) and was sequenced via the Sanger method at the Genomics Unit of the Complutense University of Madrid.

All plasmids and primers issued in this work are listed in Table 12 and Table 13 respectively. For insert amplification, human cDNA of TLR4 and the adaptors MyD88, TIRAP, TRIF, and TRAM were kindly donated by Dr. Jonathan C. Kagan, and *Brucella abortus* ORFs of BtpA and BtpB were kindly shared by Dr. Suzana P. Salcedo (Salcedo *et al.*, 2013; Salcedo *et al.*, 2008). These proteins were cloned in fusion to fluorescent protein tags such as Green Fluorescent Protein (GFP), enhanced GFP (EGFP) or mCherry (a red fluorescence protein), or the Glutathione S-transferase (GST) for co-purification experiments.

Table 12.- List of vectors and yeast expression plasmids used in this study.

Plasmid	Description (marker, promoter, type)	Source/Reference
Cloning vectors and control plasmids		
pYES2	Control yeast empty vector (URA3, GAL1, episomal)	Invitrogen
pYES2-GFP	Yeast expression episomal plasmid for N-terminal GFP fusions (URA3, GAL1, episomal)	(Rodríguez-Escudero et al., 2009)
pYES2-mCherry	Yeast expression episomal plasmid for N-terminal mCherry fusions (URA3, GAL1, episomal)	Dr. Isabel Rodriguez-Escudero
pYES3	Control yeast empty vector (TRP1, GAL1, episomal)	Invitrogen
pYES3-GFP	Yeast expression episomal plasmid for N-terminal GFP fusions (TRP1, GAL1, episomal)	Dr. Isabel Rodriguez-Escudero

pYES3-mCherryCt	Yeast expression episomal plasmid for C-terminal mCherry fusions (TRP1, GAL1, episomal)	Dr. Ahmad Ismail
pYES3-mCherryNt	Yeast expression episomal plasmid for N-terminal mCherry fusions (TRP1, GAL1, episomal)	Dr. Isabel Rodriguez-Escudero
pAG425GAL-EGFP-ccdB	Gateway destination vector (LEU2, GAL1, episomal)	Dr. Susan Lindquist (via Addgene)
pAG425GAL-EGFP	Control plasmid from pAG425GAL-EGFP-ccdB bearing the polylinker region from pEG(KG) cloned via Gateway (LEU2, GAL1, episomal)	Elba del Val
YCpLG	Control yeast empty vector (LEU3, GAL1, centromere)	Dr. Jeremy Thorner
YCpLG-GFP	Yeast expression centromeric plasmid for C-terminal GFP fusions (LEU2, GAL1, centromere)	(Rodríguez-Escudero et al., 2006)
pEG(KG)	Yeast expression episomal plasmid for N-terminal GST fusions (URA3-leu2d, GAL1, episomal)	(Mitchell et al., 1993)
myr-pEG(KG)	Modified pEG(KG) for myristoylated GST N-terminal fusions (URA3-leu2d, GAL1, episomal)	This work
Yeast expression plasmids		
pYES3-mCherry-MyD88	Human MyD88 cDNA mCherry fusion for yeast expression (TRP1, GAL1, episomal)	This work
pYES2-GFP-MyD88	Human MyD88 cDNA GFP fusion for yeast expression (URA3, GAL1, episomal)	This work
pAG425GAL-EGFP-MyD88	Human MyD88 cDNA EGFP fusion for yeast expression, via gateway cloning (LEU2, GAL1, episomal)	Elba del Val
YCpLG-TIRAP-GFP	Human TIRAP (isoform b) cDNA GFP fusion for yeast expression (LEU2, GAL1, centromere)	This work
pYES3-TIRAP-mCherry	Human TIRAP (isoform b) cDNA, mCherry Ct fusion for yeast expression (TRP1, GAL1, episomal)	This work
pYES2-mCherry-TIRAP	Human TIRAP (isoform b) cDNA, mCherry Nt fusion for yeast expression (URA3, GAL1, episomal)	Nicola Paccione
pAG425GAL-EGFP-TRIF	Human TRIF cDNA EGFP fusion for yeast expression, via gateway cloning (LEU2, GAL1, episomal)	This work, Costanza Giraudo
pYES3-TRIF-mCherry	Human TRIF cDNA mCherry fusion for yeast expression (TRP1, GAL1, episomal)	This work
YCpLG-TRAM-GFP	Human TRAM cDNA GFP fusion for yeast expression (LEU2, GAL1, centromere)	This work
pYES3-TRAM-mCherry	Human TRAM cDNA mCherry fusion for yeast expression (TRP1, GAL1, episomal)	This work
pEG(KG)-GST-TLR4-TIR	Human TLR4 C-terminal region cDNA, GST fused for yeast expression (URA3-leu2d, GAL1, episomal)	This work
pEG(KG)-myrGST-TLR4-TIR	Human TLR4 C-terminal region cDNA, myr-GST fused for yeast expression (URA3-leu2d, GAL1, episomal)	This work

pEG(KG)-GST-IRAK4	Human IRAK4 cDNA, GST fused for yeast expression (URA3-leu2d, GAL1, episomal)	Giulia Genna
pEG(KG)-GST-IRAK1	Human IRAK1 cDNA, GST fused for yeast expression (URA3-leu2d, GAL1, episomal)	Giulia Genna
pEG(KG)-GST-IRAK2	Human IRAK2 cDNA, GST fused for yeast expression (URA3-leu2d, GAL1, episomal)	Giulia Genna
pYES2-GFP-BtpA	*B. abortus* BtpA full-length GFP fusion for yeast expression (URA3, GAL1, episomal)	María Rodríguez-Escudero
pYES2-GFP-BtpB	*B. abortus* BtpB full-length GFP fusion for yeast expression (URA3, GAL1, episomal)	María Rodríguez-Escudero
pYES3-GFP-BtpB	*B. abortus* BtpB full-length GFP fusion for yeast expression (TRP1, GAL1, episomal)	María Rodríguez-Escudero
pYES2-GFP-BtpA-N	N-terminal (1-126) non-TIR domain of BtpA GFP fusion for yeast expression (URA3, GAL1, episomal)	This work
pYES2-GFP-BtpA-TIR	C-terminal (127-275), TIR domain of BtpA´s GFP fusion for yeast expression (URA3, GAL1, episomal)	This work
pYES3-GFP-BtpA-TIR	C-terminal (127-275), TIR domain of BtpA´s GFP fusion for yeast expression (TRP1, GAL1, episomal)	This work, Lucía Sastre
pYES2-GFP-BtpB-N	N-terminal (1-139) non-TIR domain of BtpB´s GFP fusion for yeast expression (URA3, GAL1, episomal)	María Rodríguez-Escudero
pYES2-GFP-BtpB-TIR	C-terminal (140-292), TIR domain of BtpB´s GFP fusion for yeast expression (URA3, GAL1, episomal)	María Rodríguez-Escudero
pYES3-GFP-BtpB-TIR	C-terminal (140-292), TIR domain of BtpB´s GFP fusion for yeast expression (TRP1, GAL1, episomal)	This work, Lucía Sastre
pEG(KG)-GST-BtpB-TIR	C-terminal (140-292), TIR domain of BtpB´s GST fusion for yeast expression (URA3-leu2d, GAL1, episomal)	Dr. Victor J. Cid
pLA10H	S.cerevisiae Cdc10 fusion to GFP, which was used to visualize the yeast septin ring. (HIS3, MET25, centromere)	Dr. Victor J. Cid
pRS426-GFP2XPH(PLCδ)	A fluorescent reporter for PtdIns4,5P_2 (URA3, GAL1, episomal)	(Stefan et al., 2002)
pYES3-GFP-Akt1	Yeast plasmid for heterologous Akt1expression (TRP1, GAL1, episomal)	(Andrés-Pons et al., 2007)
YCpLG-PI3Kα-CAAX	Yeast plasmid for heterologous PI3K expression (LEU2, GAL1, centromere)	(Rodríguez-Escudero et al., 2009)
Yeast ORF collection	A library of yeast ORF for overexpression (URA3, GAL1, episomal)	GE Healthcare
Site-directed mutants		
pEG(KG)-GST-IRAK4 KD	Human IRAK4 kinase death (KD) K213A/K214A mutant (URA3-leu2d, GAL1, episomal)	Giulia Genna
pYES3-mCherry-MyD88 x2SA	MyD88 mutant on two phosphorylatable serines, S242A S244A (TRP1, GAL1, episomal)	This work
pYES3-mCherry-MyD88 P200H	MyD88 mutant on the BB loop P200H (TRP1, GAL1, episomal)	This work

pYES3-mCherry-MyD88 L252P	MyD88 gain-of-function, oncogenic mutant (TRP1, GAL1, episomal)	This work
YCpLG-TIRAP P125H-GFP	TIRAP mutant on the BB loop P125H (LEU2, GAL1, centromere)	This work
pYES3-TIRAP P125H mCherry	TIRAP mutant on the BB loop proline (TRP1, GAL1, episomal)	This work
pYES3-TIRAP K15-16A mCherry	TIRAP mutant on two PM targeting lysines K15A K16A (TRP1, GAL1, episomal)	This work
pYES3-TIRAP K31-32A mCherry	TIRAP mutant on two other PM targeting lysines K31A K32A (TRP1, GAL1, episomal)	This work
pYES3-TIRAP x4KA mCherry	TIRAP mutant on the4 PM targeting lysines K15A K16A K31A K32A (TRP1, GAL1, episomal)	This work
pYES3-TRAM C117H-mCherry	TRAM mutant on the BB loop C117H (TRP1, GAL1, episomal)	This work
pYES3-TRAM G2A-mCherry	TRAM lacking myristoylation signal G2A (TRP1, GAL1, episomal)	This work
pYES3-TRAM DEAA-mCherry	TRAM without an acidic motif D91A E92A (TRP1, GAL1, episomal)	This work
YCpLG-TRAM C117H-GFP	TRAM mutant on the BB loop C117H (LEU2, GAL1, centromere)	This work
YCpLG-TRAM G2A-GFP	TRAM lacking myristoylation signal G2A (LEU2, GAL1, centromere)	This work
YCpLG-TRAM DEAA-GFP	TRAM without an acidic motif D91A E92A (LEU2, GAL1, centromere)	This work
pAG425GAL-EGFP-TRIF P434H	TRIF mutant on the BB loop P434H (LEU2, GAL1, episomal)	This work
pYES2-GFP-BtpA E217A	BtpA catalytically inactive mutant E217A (URA3, GAL1, episomal)	This work
pYES2-GFP-BtpA-TIR E217A	BtpA-TIR catalytically inactive mutant E217A (URA3, GAL1, episomal)	This work
pYES2-GFP-BtpB E234A	BtpB catalytically inactive mutant E234A (URA3, GAL1, episomal)	This work
pYES3-GFP-BtpB E234A	BtpB catalytically inactive mutant E234A (TRP1, GAL1, episomal).	This work
pYES2-GFP-BtpB-TIR E234A	BtpB-TIR catalytically inactive mutant E234A (URA3, GAL1, episomal)	This work
pYES2-GFP-BtpB-TIR D158G	D158G random mutagenesis screen hit mutation, introduced on BtpB-TIR (URA3, GAL1, episomal)	This work
pYES2-GFP-BtpB-TIR S162P	S192P random mutagenesis screen hit mutation, introduced on BtpB-TIR (URA3, GAL1, episomal)	This work
pYES2-GFP-BtpB-TIR Y225C	Y225C random mutagenesis screen hit mutation, introduced on BtpB-TIR (URA3, GAL1, episomal)	This work

Table 13.- List of the primers used in this study.

Primer	Sequence (5'->3')	Purpose
Cloning primers		
MyD88-Up	5'-ttaagcttatggctgcaggaggtcccgg-3'	To amplify hMyD88 and clone it into pYES3-mCherryNt and pYES2-GFP (*Hind*III-*Bam*HI)
MyD88-Lo	5'-ttggatccatggctgcaggaggtcccgg-3'	
TIRAP-*Bam*HI-Up	5'-ttggatccatggcatcatcgacctccct-3'	To amplify hTIRAP (isoform b) and clone it into YCpLG-GFP (*Bam*HI-*Bam*HI) and pYES3-mCherryCt (*Hind*III-*Bam*HI)
TIRAP-*Hind*III-Up	5'-ttaagcttatggcatcatcgacctccct-3'	
TIRAP-Lo	5'-ttggatccaagtagatcagatactgtagc-3'	
TRIF-*Hind*III-Up	5'-ttaagcttatggcctgcacaggcccatc-3'	To amplify hTRIF and clone it into pYES3-mCherryCt (*Hind*III-*Hind*III)
TRIF-*Hind*III-Lo	5'-ttaagcttttctgcctcctgcgtcttgtc-3'	
TRIF-Nt-attB1-Up	5'-ggggacaagtttgtacaaaaaagcaggcttcatggcctgcacaggcccatca-3'	To amplify hTRIF to clone it N-terminally tagged via gateway cloning in pAG425GAL1-EGFP
TRIF-Nt-attB2-Lo	5'-ggggaccactttgtacaagaaagctgggttttatcattctgcctcctgcgtc-3'	
TRAM-*Bam*HI-Up	5'-ttggatccatgggtatcgggaagtcta-3'	To amplify hTRAM and clone it into YCpLG-GFP and pYES3-mCherryCt (*Bam*HI-*Bam*HI)
TRAM-*Bam*HI-Lo	5'-ttggatccggcaataaattgtctttgtac-3'	
TLR4-TIR-Up	5'-ttggatcccacctgatgcttcttgctg-3'	To amplify hTLR4 (657-839) and clone it into pEG(KG) and myr-pEG(KG) (*Bam*HI-*Hind*III)
TLR4-TIR-Lo	5'-ttaagctttcagatagatgttgcttcctg-3'	
BtpA-Up	5'-cgcggatccatgagttcgtactcttctaata-3'	To amplify *B. abortus* BtpA FL, N (1-126) or TIR (127-275) and clone them into pYES2-GFP or pYES3-GFP (*Bam*HI-*Eco*RI)
BtpA-Lo	5'-ggaattctcagataagggaatgcagttc-3'	
BtpA-126stop-Lo	5'-ggaattctcatgattgtttgatgaaagcttca-3'	
BtpA-*Bam*HI127-Up	5'-cgggatccttgagctccatgcgaacaac-3'	
BtpB-Up	5'-cgcgggatccatgtacaatttatttgtttcggg-3'	To amplify *B. abortus* BtpB FL, N (1-139), or TIR (140-292) and clone them into pYES2-GFP (*Bam*HI-*Xba*I, or *Bam*HI-*Eco*RI for BtpB-N) or pYES3-GFP (*Bam*HI-*Bam*HI, or *Bam*HI-*Eco*RI for BtpB-TIR)
BtpB-Lo	5'-gctctagactaggtgatgagggcgacg-3'	
BtpB-pYES3-Up	5'-cgggatccatgtacaatttatttgtttcgggc-3'	
BtpB-pYES3-Lo	5'-cgggatccctaggtgatgagggcgac-3'	
BtpB-140stop-Lo	5'-ggaattcctacagagttattcct-3'	
BtpB-*Bam*HI140 Up	5'-cgggatccatgccgtcgtggacgcgacag-3'	
BtpB-*Eco*RI-Lo	5'-ggaattcctaggtgatgagggcgacg-3'	
Mutagenic primers		
InsMyrKG-Up	5'-ctcatgggaactagtaagtcttcccctatactaggttattggaaaatt-3'	Insertion of the myristoylation signal before GST in pEG(KG)
InsMyrKG-Lo	5'-ggaagacttactagttcccatgagctcgaattgatccggtaat-3'	
MyD88 x2SA-Up	5'-gcactcgccctcgctccaggtgcccatcagaagc-3'	To generate MyD88 S242A S244A mutant
MyD88 x2SA-Lo	5'-ctggagcgagggcgagtgcaaatttggtctggaagtcaca-3'	
MyD88 PH-Up	5'-gatgtcctgcatggcacctgtgtctggtcta-3'	To generate MyD88 P200H BB loop mutant
MyD88 PH-Lo	5'-ggtgccatgcaggacatcgcggtcag-3'	
MyD88 LP-Up	5'-cagaagcgaccgatccccatcaagtacaag-3'	To generate MyD88 L252P oncogenic mutant
MyD88 LP-Lo	5'-ggggatcggtcgcttctgatgggca-3'	
TIRAP PH-Up	5'- caacccacggcggcgctatagtgtccg-3'	To generate TIRAP P125H BB loop mutant
TIRAP PH-Lo	5'- gccgccgtgggttgcatcccggagtt-3'	
TIRAP K15-16A-Up	5'- cggcctgcggcgcctctaggcaagatgg-3'	To generate TIRAP K15A K16A mutant
TIRAP K15-16A-Lo	5'- tagaggcgccgcaggccgagagccagga-3'	
TIRAP K31-32A-Up	5'- ctgctggcggcgcccaagaagaggccc-3'	To generate TIRAP K31A K32A mutant
TIRAP K31-32A-Lo	5'- ttgggcgccgccagcagggtctgcctg-3'	
TRAM C117H-Up	5'- tgagatgccacatggcagacagcatttacag-3'	To generate TRAM C117H BB loop mutant
TRAM C117H-Lo	5'- gctgtctgccatgtggcatctcagcaaagat-3'	
TRAM G2A-Up	5'-ggatccatggctatcgggaagtctaaaataaattcct-3'	To generate TRAM G2A mutant in YCplG and pYES3 vectors
TRAM G2A pYES3-Lo	5'- cttcccgatagccatggatccgagctc-3'	

TRAM G2A-YCpLG-Lo	5'- gacttcccgatagccatggatccggttc-3'	
TRAM DEAA-Up	5'-gatgacacagctgcagccctcagagtccag-3'	To generate TRAM D91A E92A mutant
TRAM DEAA-Lo	5'-tctgagggctgcagctgtgtcatcttctgcatg-3'	
TRIF P343H-Up	5'- ggtgcacgggcgcggggagctga-3'	To generate TRIF P343H BB loop mutant
TRIF P343H-Lo	5'- cgcccgtgcacctggaaatcctcgca-3'	
BtpA E217A-Up	5'-agcaatggcccgcaagagcattagatggactgacggc-3'	To generate BtpA E217A catalytically inactive mutant
BtpA E217A-Lo	5'-gccgtcagtccatctaatgctcttgcgggccattgct -3'	
BtpB E234A-Up	5'-aaaagactggtgcggcgtcgcgttccgcgcgattcgcgaa-3'	To generate BtpB E234A catalytically inactive mutant
BtpB E234A-Lo	5'-ttcgcgaatcgcgcggaacgcgacgccgcaccagtctttt-3'	
BtpB D158G-Up	5'-cacgattttggcgtcggtctctcttttccc-3'	To generate BtpB D158G mutation on BtpB-TIR
BtpB D158G-Lo	5'-gagaccgacgccaaaatcgtgctgagtgata-3'	
BtpB S162P-Up	5'-cgtcggtctccctttttcccggtgag-3'	To generate BtpB S162P mutation on BtpB-TIR
BtpB S162P-Lo	5'-ccgggaaaagggagaccgacgtcaaaatc-3'	
BtpB Y225C-Up	5'-ggcgacgactgtcagcgaaaagactggt-3'	To generate BtpB Y225C mutation on BtpB-TIR
BtpB Y225C-Lo	5'-ttttcgctgacagtcgtcgccgacgaaga-3'	
Sequencing primers		
M13Fw	5'-tgtaaaacgacggccagt-3'	Universal forward primer
M13Rv	5'-caggaaacagctatgacc-3'	Universal reverse primer
GAL1	5'-gttaatatacctctatac-3'	To read downstream *GAL1* promoter
TRIF 800-Up	5'-gccagcccaccagagctg-3'	To completely cover the TRIF ORF
EGFP 600 Up	5'-tacctgagcacccagtcc-3'	To read downstream the EGFP tag
GST sec-Lo	5'-tatcaccttcatcgcgct-3'	To check the insertion of myr in pEG(KG)
attB-Up	5'-aaaaaagcaggctacaaa-3'	Universal *attB* primers to identify the overexpression screen hits
attB-Lo	5'-accactttgtacaagaaa-3'	

3.1.- Site-directed mutagenesis.

Point mutations or insertions were generated via the site-directed mutagenesis method (Wang and Malcolm, 1999) using the *PfuI* Turbo DNA polymerase (Agilent), for robust, high-fidelity PCRs. Primers were designed following the guidelines on the QuikChange kit (Agilent) instructions and contained the desired mutation. In some cases, for example, the insertion of a myristoylation signal N-terminally to the GST tag on pEG(KG), an improved primer design protocol was followed (Liu and Naismith, 2008), in which primer-template annealing was enhanced, while primer-primer dimerization was reduced. The entire plasmid was amplified, and the PCR product was digested with the *DpnI* restriction enzyme to remove the methylated template plasmid and then transformed into *E. coli.* Finally, the presence of the mutation was checked by Sanger sequencing. To maintain its versatility, when a mutation of a gene cloned via Gateway cloning was desired, it was preferably mutated on the entry clone, to be later subcloned into any destination vector.

4.- Microscopy techniques.

To visualize the fluorescent protein tags mCherry, GFP, and EGFP on live yeast, transformed yeast were induced to express the *GAL1* promoter-controlled genes as described earlier for 5 h

unless otherwise stated. Cells were harvested by room temperature (RT) centrifugation (1min, 5000 rpm) and 3 µL of the pellet were mounted on a microscope slide and covered by a cover glass. Cells were examined in Eclipse TE2000U microscope (Nikon, Tokyo, Japan) and digital images were acquired with an Orca C4742-95-12ER charge-coupled-device camera (Hamamatsu Photonics, Hamamatsu City, Japan) and processed by HC Image (Hamamatsu). Confocal images were acquired by Dr. Víctor J Cid using a Zeiss LSM 510 confocal microscope (Carl Zeiss, Oberkochen, Germany) at Dr. Jonathan C. Kagan's laboratory on the Boston Children's Hospital facility and processed with SlideBook6 (3i Intelligent imaging). Images were analyzed using FiJi (ImageJ, NIH) and Adobe Photoshop CS6.

4.1.- Fluorescent staining methods.

To monitor vacuolar morphology and endocytosis, staining with FM4-64 (Molecular Probes) was carried out, following the described protocol (Vida and Emr, 1995). After 5 h of *GAL1* protein expression induction, cells were harvested by RT centrifugation (2 min, 3000 rpm). Pellet was resuspended on 200uL of SG medium with FM4-64 added to a 40µM final concentration. Cells were cultured at 30 ^{o}C and 900 rpm shaking for the time required for the experiment, usually 1h, then washed twice with PBS, and mounted to be examined under the microscope.

Nuclear labeling was performed by adding DAPI at 1:1000 directly to the harvested cells and washed once with PBS.

4.2.- Indirect yeast immunofluorescence.

To visualize yeast tubulin microtubules, indirect yeast immunofluorescence was performed as previously described (Cid *et al.*, 2001). After *GAL1* promoter induction, cells were fixed first with 3.7% formaldehyde for 10 min RT, and a second fixation was done with 3.7% formaldehyde in 0.1 M KPO_4, pH=6.5, and 0.5 mM $MgCl_2$, for 15 min RT and washed in 0.1 M KPO_4, pH=6.5. Fixed cells were resuspended in 0.2 M Tris-HCl, pH=8.8, containing 20 mM EDTA, pH=8, 1 M NaCl, and 80 mM β-mercaptoethanol, incubated at RT for 10 min, washed once with KPO_4-sodium citrate buffer, pH=5.8, containing 1 M NaCl and twice with KPO_4-sodium citrate, pH=5.8 with 1M sorbitol, resuspended in 1 ml of solution A (1.2 M sorbitol, 40 mM KPO_4, pH=6.5, 0.5 mM $MgCl_2$) containing 0.14 M β-mercaptoethanol, and digested with 110 µl of Glusulase (Dupont) and 0.6 mg/ml Zymolyase 100T (MP biomedical). The digested cells were washed twice with solution A, applied to the wells of poly-l-lysine (Sigma)-coated multi-well microscope slides, and permeabilized by treatment at −20°C with, successively, methanol for 6 min and acetone for 30 s. Permeabilized cells were rehydrated in PBS, blocked in PBS-BSA (1 mg/ml bovine serum albumin (BSA) in PBS), and incubated overnight at 4°C with anti-αtubulin primary antibody

(Table 14). After incubation, cells were washed five times with PBS-BSA and incubated for 2 h in the dark with the Alexa 594 anti-rat antibody secondary antibody. Finally, stained cells were washed five times with PBS, DAPI was added at 1:1000 for nuclear labeling, and samples were observed at the fluorescence microscope.

Table 14 .- List of antibodies used in this study.

Antibody	Species	Details	Dilution	Purpose
Primary antibodies				
Anti-αTubulin	Rat (mc)	Serotec. YOL1/34	1:500	IF visualization of yeast tubulin
Anti-mCherry	Rabbit (pc)	Living Colors. Anti-DsRed	1:1000	WB detection of mCherry-tagged proteins
Anti-GFP	Mouse (mc)	Living Colors. JL-8	1:1000	WB detection of GFP and EGFP-tagged proteins
Anti-GST	Rabbit (pc)	Santa Cruz. z5	1:1000	WB detection of GST-tagged proteins
Anti-P-MAPK	Rabbit (pc)	Cell Signaling. Anti-phospho-p44/ p42 MAPK (T202/Y204)	1:1000	WB detection of dually phosphorylated Slt2, Kss1 and Fus3 yeast MAPKs
Anti-Slt2	Rabbit (pc)	(Martín *et al.*, 1993)	1:1000	WB detection of total Slt2
Anti-G6PDH	Rabbit (pc)	Sigma	1:50000	WB loading control
Anti-actin	Mouse (mc)	MP biomedicals. C4	1:2000	WB loading control
Secondary antibodies				
Alexa 594 anti-rat	Chicken (pc)	Invitrogen	1:1000	IF
IRDye-680 anti-rabbit	Goat (pc)	LI-COR	1:5000	WB
IRDye-800 anti-rabbit	Goat (pc)	LI-COR	1:5000	WB
IRDye-680 anti-mouse	Goat (pc)	LI-COR	1:5000	WB
IRDye-800 anti-mouse	Goat (pc)	LI-COR	1:5000	WB

Abbreviations: Monoclonal (mc), Polyclonal (pc), immunofluorescence (IF), Western blotting (WB), New England Biolabs (NEB). Glucose-6-phosphate dehydrogenase (G6PDH).

5.- Protein detection via Western blotting.

5.1.- Extraction obtention and sample preparation.

Cells were harvested, after 5h of *GAL1* promoter induction unless otherwise stated, by centrifugation at 2500 rpm and 4 ^{o}C for 3 min, and supernatants were completely removed. Yeast protein extracts were obtained following the procedure previously described (Martín *et al.*, 2000). Cell pellets were resuspended in 150 µL of protein lysis buffer (50 mM Tris-HCl PH=7.5, 10% glycerol, 1% Triton X-100, 0.1% SDS, 150 mM NaCl, 5 mM NaF, 50 mM β-glycerophosphate, 5 mM sodium pyrophosphate, and 1 mM sodium orthovanadate) and shortly before use was supplemented with phenylmethylsulfonyl fluoride (PMSF) up to 1 mM and 1 tablet/10 mL of Complete Mini, EDTA-free, Protease inhibitor cocktail (Roche). Samples were added approximately 150 µL of 0.75-1 mm diameter glass beads (Reesch) and cells were bead blasted at 5.5 m/s using a FastPrep-24 (MP Biomedicals) for 30 sec twice, allowing a 5 min incubation on ice in between. Tubes were centrifugated at 13000 rpm and 4 ^{o}C for 10 min, supernatants

containing the protein extract were recovered, and total protein concentration was estimated measuring OD_{280} at the Beckman DU640 spectrophotometer. Samples from the same experiment were diluted using the protein lysis buffer to be set to the same concentration. Protein denaturalization was achieved by adding the samples an equal volume of the 2X loading SDS-PAGE buffer (125 mM Tris-HCl pH=6.8, 5% SDS, 25% glycerol, 0.6g bromophenol blue) supplemented shortly before use with Dithiothreitol (DTT) to a final concentration of 0.25 M, and subsequently boiling them for 5 min.

5.2.- Protein electrophoresis, membrane transfer, and immunodetection.

Proteins on the extracts were separated by sodium dodecyl sulfate-polyacrylamide gel electrophoresis (SDS-PAGE) using a 10% resolving gel (10% acrylamide-*bis*acrylamide mixture, 0.38 M Tris HCl pH=8.8, 0.1% SDS, 0.05% APS, and 1.3 µL/mL TEMED) and a 5% stacking gel (5% acrylamide-*bis*acrylamide mixture, 0.13 M Tris HCl pH=6.8, 0.1% SDS, 0.1% APS, and 1 µL/mL TEMED). Electrophoresis was carried out in either a Mini-PROTEAN 3 or Tetra (Bio-Rad) cells, at a 150-200V voltage using an electrophoresis buffer (196 mM glycine, 0.1% SDS, 50 mM Tris-HCl pH=8.3). A pre-stained protein ladder standard (Bio-Rad or Invitrogen) was included to estimate protein size. Separated proteins were transferred to a 0.45 µm nitrocellulose membrane (Hybond, Amersham) on a wet Mini Trans-Blot Transfer Cell (Bio-Rad) at a constant voltage of 110V for 1 h. Gel and membrane were protected with two layers of 3 mm Whatman paper and a sponge on each side. Transfer buffer was obtained mixing 1 volume of 10 X transfer buffer (58 g/L Tris-HCl, 29 g/L glycine, and 3,7g/L SDS) to 2 volumes of ethanol and 7 volumes of distilled water.

Proteins on nitrocellulose membranes were visualized via fluorescently tagged secondary antibodies using the Odyssey Infrared Imaging System (LI-COR). After transference, blots were blocked on 5% skimmed milk in PBS for 1 h RT and were subsequently incubated with the corresponding primary antibody (Table 14) diluted in PBS-tween (0.1% Tween-20 in PBS) plus 1% skimmed milk for 1 h RT or 4 ^{o}C overnight under gentle shaking. Membranes were then washed with PBS-Tween 5 times of 5 min each and incubated with the desired fluorescently labeled secondary antibody (Table 14), diluted on the same solution used for the primary antibodies, for 1 h RT and protected from light. Finally, after 5 more PBS-Tween washes membranes were scanned on the Odyssey Infrared Imaging System (LI-COR) scan, images were processed, and band intensity was measured with Image Studio (LI-COR).

5.3.- Protein co-purification assays.

Transformed cells were treated to induce *GAL1* promoter expression and harvested as previously described in section 5.1. Protein extraction followed the same guidelines described in that section, apart from using a different lysis buffer to ensure protein-protein interactions: the precipitation lysis buffer (50 mM Tris-HCl PH=7.5, 10% glycerol, 0.1% NP40, 150 mM NaCl, 5 mM EDTA pH=8, 50 mM NaF, 50 mM β-glycerophosphate, 5 mM sodium pyrophosphate, and 1 mM sodium orthovanadate). Once protein extracts on the same experiment were diluted to the same concentrations, 10 µL of extracts were saved as input samples, treated with 2X loading SDS-PAGE buffer, and boiled 5min to for protein denaturation.

The resting extracts were treated with either Glutathione Sepharose 4B (GE Healthcare Life Sciences) for GST pull-down experiments or GFP-TrapA, (Chromotek), which is a slurry of anti-GFP nanobody-coated agarose beads for GFP Co-Immunoprecipitation (Co-IP) settings. Before the addition to the samples, slurries were treated following the manufacturer's instructions. To equilibrate the Sepharose slurry for GST pull-down, 3 washes with 2 volumes of precipitation lysis buffer at 4 ^{o}C 3000 rpm and 1 min were carried out, with a final 1:1 dilution in precipitation lysis buffer and 50 µL of the mixture was added to each sample. In the case of the GFP-TrapA, 25 µL slurry was equilibrated per sample by washing three times with 500 µL of dilution buffer (10 mM Tris-HCl PH=7.5, 150 mM NaCl, 0.5 mM EDTA pH=8) at 4 ^{o}C 5000 rpm for 2 min, followed by a complete supernatant removal before sample addition. To ensure proper slurry-sample mixing, the final volume was increased up to 600 µL with precipitation lysis buffer in either case and tubes were tumbled end-over-end overnight at 4 ^{o}C. Samples were subsequently centrifuged at 4 ^{o}C, the supernatant was discarded, and pellets were washed 6 times at 4 ^{o}C and 3000 rpm for 1 min (GST pull-down) or 4 ^{o}C 5000 rpm for 2 min (GFP Co-IP). Washed pellets were treated with 2X loading SDS-PAGE buffer and boiled for 5 min to denature and elute the proteins from the slurry. These samples, together with the input samples were loaded on the same polyacrylamide gel to be visualized by Western blotting as described in section 5.2.

5.4.- Phosphopeptide identification by mass spectrometry.

5.4.1.- Protein extraction and enrichment.

Yeast co-transformed with pYES3-mCherry-MyD88 and pEG(KG)-GST-IRAK4 were induced for *GAL1* promoter-dependent expression, harvested, and proteins were extracted as described in section 5.3. Samples were treated with RFP-TrapA (Chromotek), a slurry of anti-RFP nanobody-coated agarose beads that also targeted mCherry tagged proteins, as indicated in the previous section. Nanobody-bound proteins were eluted, denaturized, and loaded into a 10% SDS-

polyacrylamide gel. After electrophoresis, bands were visualized in-gel by Coomassie blue staining, and three of them corresponding to the slow and regular migrating mCherry-MyD88, and the one of GST-IRAK4 were selected for further analysis.

5.4.2.- Digestion and desalting of peptides.

The proteomic analysis described here was performed by the technical staff at the Proteomics Unit of the Complutense University of Madrid. For the trypsin digestion, selected bands were cut, in-gel reduced with DTT, alkylated with Iodacetamide, and digested with a 1/20 (w/w) ratio of recombinant Trypsin (Trypsin sequencing grade, Roche) overnight at 37 ^{o}C, according to (Sechi and Chait, 1998). The peptides from proteins digested were desalted and concentrated with C18 reverse phase chromatography (OMIX C18, Agilent technologies) and the peptides were eluted with 50% acetonitrile / 0,1% trifluoroacetic acid. Finally, the samples were freeze-dried in Speed-vac and resuspended in 2% AN, 0, 1% formic acid before the Nano LC-MS/MS analysis. The supernatants were stored at -20 ^{o}C before the analysis.

5.4.3.- Liquid chromatography and mass spectrometer analysis.

The desalted protein digest was analyzed by RP-LC-ESI-MS/MS in an EASY-nLC 1000 System coupled to the Q-Exactive HF mass spectrometer through the Nano-Easy spray source (all from Thermo Scientific).

Peptides were loaded first onto an Acclaim PepMap 100 Trapping column (Thermo Scientific, 20mm x 75 µm ID, 3 µm C18 resin with 100 Å pore size) using buffer A (mobile phase A: 2% acetonitrile, 0.1% formic acid) and then were separated and were eluted on a C18 resin analytical column NTCC (Nikkyo Technos Co., Ltd. de 150 mm x 75 µm ID, 3 µm C18 resin with 100 Å pore size) with an integrated spray tip. A 55 minutes gradient of 5% to 35% Buffer B (100% acetonitrile, 0.1% formic acid) in Buffer A at a constant flow rate of 250 nL/min was used.

Data acquisition was performed with a Q-Exactive HF. Data were acquired using an ionspray voltage 1.8 Kv and ion transfer temperature of 250 ^{o}C. All data were acquired using data-dependent acquisition and in positive mode with Xcalibur 4.0 software. For the MS2 scan, were selected top 10 most abundant precursors with charges of 2–6 in MS 1 scans for higher energy collisional dissociation fragmentation with a dynamic exclusion of 20 s. The MS1 scans were acquired at the m/z range of 375–2000 Da with a mass resolution of 60,000 and automatic gain control (AGC) target of 3E6 at a maximum Ion Time (ITmax) of 100 ms. The threshold to trigger MS2 scans was 1.6E5; the normalized collision energy was 27%; the resolved fragments were scanned at a mass resolution of 30,000 and AGC target value of 1E5 in an ITmax of 50ms.

5.4.4.- Protein identification.

Peptide identification from raw data was carried out using the Mascot v. *2.3.2* search engine through the Protein Discoverer *2.2* Software (Thermo Scientific). Database searches were performed against the Swiss Prot database without taxonomic restriction (553089 sequences, 2017/02/21) and a home-made database with the sequences of the target proteins (8 sequences). The following parameters were used for the searches: tryptic cleavage after Arg and Lys, up to two missed cleavage sites allowed, and tolerances of 10 ppm for precursor ions and 0.6 Da for MS/MS fragment ions and the searches were performed allowing optional Methionine oxidation, S, T, Y phosphorylation and fixed carbamidomethylation of Cysteine. The search against the decoy database (integrated decoy approach) was used to calculate the false discovery rate (FDR). The acceptance criteria for protein identification were an FDR < 1% and at least one peptide identified with high confidence (CI>95%). The probability of phospho-site localization in peptides with these modifications was estimated by the ptm-RS node in proteome discoverer 2.2 software and the probability threshold accepted was 75%.

6.- Determination of yeast metabolites.

6.1.- Yeast cellular ATP measurement by luciferase assay.

ATP levels were measured using the ENLITEN ATP Assay System (Promega) following the manufacturer´s instructions. Yeast cells were cultured in SR for 18 h and then new SG was added for *GAL1*-driven gene expression to a final OD_{600} of 0.3 and cultured for 3 h at 30 ^{o}C. Approximately $1.8x10^{7}$ cells were harvested in 3 mL of culture and then concentrated by centrifugation for 3 min at 2500 rpm at 4 ^{o}C. Pellets were washed with 1 mL PBS at 4 ^{o}C and stored at -80 ^{o}C for further analysis. For ATP extraction, pellets were resuspended with trichloroacetic acid (TCA, 5 %, 10 µL) and immediately neutralized using 500 µL of TAE buffer. The samples were centrifuged for 15 sec at 13000 rpm and then 1:100 diluted in more TAE buffer. 10 µL of this solution was mixed with 100 µL of the rL/L reagent provided by the kit and luminescence was measured in Relative Light Units (RLU) using OPTOCOMP1 luminometer (MGM instruments). To correlate RLU data with the ATP concentrations and thus allow the quantification, a standard curve was prepared using the kit´s reagents, for each experimental set.

6.2.- Yeast cellular NAD^+ measurement by mass spectrometry.

6.2.1.- Yeast NAD^+ extraction.

Yeast cells were cultured as stated for the ATP luciferase assay. Approximately $6x10^7$ cells were harvested in 10 mL of culture and then concentrated by centrifugation for 3 min at 2500 rpm at 4 ºC. Pellets were washed with 1 mL PBS at 4 ºC and stored at -80 ºC for further analysis.

The yeast NAD^+ extraction protocol is a simplified version of the one previously described (Sporty *et al.*, 2008). Pellets were resuspended in ammonium acetate (600 µL of 50 mM in MS grade water) and approximately 300 µL of 0.5-0.75 mm diameter glass beads (Reesch) was added to the tube, and cells were bead blasted as described in section 5.1. The supernatant was recovered by perforation of the bead-blasting tube´s base with a red-hot 0.9 x 40 mm needle. The pierced tube was placed inside a capless 1.5 mL microfuge tube and both tubes were centrifuged together for 3 min at 2000 rpm at 4 ºC. This first cell lysate was stored in a new 1.5 microfuge tube on ice. The glass beads in the bead-blasting tube were then washed one more time with 600 µL of a 3:1 v/v mixture of acetonitrile (MS grade) and ammonium acetate (50 mM in MS grade water). The rinsate was then mixed with the first lysate. The mixture was clarified by centrifugation for 3 min at 13000 rpm at 4 ºC and the supernatant was transferred to an ice-cold 1.5 mL microfuge tube. To standardize results, 150 µL of these lysates were kept for protein concentration measurement by the Bradford method.

6.2.2.- NAD^+ mass spectrometry measurement.

Mass spectrometry measurements were performed by the staff of the Mass Spectrometry Unit at Universidad Complutense de Madrid (UCM). Samples were filtered with a 0.22 µm PTFE filter (JASCO) and analyzed by liquid chromatography (LC) coupled to a QQQ mass spectrometer equipped with a turbo ion spray source operating in positive ion mode (LCMS 8030, Shimadzu). Chromatographic separation was performed on a Gemini C18 analytical column (50 mm×2.1 mm I.D., 2.7 µm particle size; Poroshell 120 PhenylHexyl). The injection volume was 10 µL. Samples were delivered over 11 min at a flow rate of 0.3 mL/min through the analytical column at 45 °C. The mobile phase was composed of A (3 % methanol, 10 mM tributylamine, 3 mM acetic acid in water LC grade, 0.1 % formic acid in water) and B (methanol). Mobile phase composition began with 0 % B and was increased to 45 % B in 2 min, to 50 % in 5 more minutes, and up to 95 % in one minute. The mobile phase was then maintained at 95 % B for 2 min and followed by re-equilibration with 0 % B over the next 2 min, before injection of the next sample. Quantification of NAD^+ was performed by multiple reactions monitoring (MRM) mode to monitor the parent ion-product ion (m/z) of the analyte. Mass transitions of m/z 662.10 to 540.00 (CE = +16 V) were

used for quantification and m/z 662.10 to 407.90 (CE = +30 V) for identification with a dwell-time of 100 ms. The calibration curve was determined by plotting the peak area of the analyte (Y) versus the nominal concentration (X) with the least square linear regression. All analyses were made under ISO 9001:2008 quality management system certification.

7.- Yeast whole genome ORF overexpression library screening.

A pooled *S. cerevisiae* whole genome ORF library (Yeast ORF collection, GE Healthcare), containing 4500 *URA3*-based plasmids for overexpression under *GAL1* promoter and protein A-tagged, was split into three groups. The W303-1A wild type yeast strain was co-transformed with pYES3-GFP-BtpB and one of the three library pools in each set. BtpB toxicity suppression by overexpression of a specific cDNA was tested by its ability to grow in SG agar plates. Candidates were sequenced via yeast colony PCR, using attB-Up and attB-Lo, specifically designed to amplify any ORF cloned into the library. Once identified, candidate plasmids were individually retransformed and checked by the ten-fold serial dilution growth assay (section 2.1). 20 different candidates were selected and tested for specificity by co-transformation with YCpLG-PI3Kα-CAAX (Rodríguez-Escudero *et al.*, 2005b), another toxic construct for yeast cells that acts by a different mechanism. Eventually, GFP-BtpB and yeast ORF protein expression levels of the 7 hits were verified by western blotting.

8.- Statistical analysis and bioinformatics support.

All data sets were tested for normality using the Shapiro-Wilkinson test. When a normal distribution was confirmed a One-Way ANOVA test with a Bonferroni correction was used for statistical comparison of multiple data sets and Students t-test for two-sample comparison. For data sets that did not show normality, a Kruskal-Wallis test was applied, with Dunn's correction.

During the completion of this Thesis, several bioinformatics databases, software, and resources were used. The more relevant among them are listed in Table 15.

Table 15.- List of the main bioinformatics resources and software used in this study.

Resource	Description
Bibliography	
PubMed	Digital repository of scholarly articles that have been published within the biomedical and life sciences journal literature. Developed by the NCBI.
Gene and protein information	
SGD	The SGD provides comprehensive integrated biological information for the budding yeast *S. cerevisiae* along with search and analysis tools to explore these data. Developed by Stanford University.
NCBI Gene	The NCBI Gene database integrates information from a wide range of species. Developed by the NCBI.

NCBI Protein	The NCBI Protein database is a collection of protein sequences from several sources. Developed by the NCBI.
UniProt	The UniProt database provides the scientific community with a comprehensive, high-quality, and freely accessible resource of protein sequence and functional information. From NIH, EMBL, and SIB.
Domain identification and interactions	
ExPASy-Prosite	A database of protein domains, families, and functional sites, it includes a scan mode to find domains out of protein sequences. From the SIB.
Conserved domains	For searching and identification for conserved domains within a protein or coding nucleotide sequence. Developed by the NCBI.
BioGRID	A public repository of genetic and protein interaction data from model organisms and humans. Developed by (Oughtred *et al.*, 2019).
iGPS	Predictor algorithm of *in vivo* kinase-specific phosphorylation sites on substrate proteins. Developed by (Song *et al.*, 2012).
Alignments and structural data	
NCBI BLAST	BLAST compares nucleotide or protein sequences to sequence databases and calculates the statistical significance. Developed by the NCBI.
Clustal Omega	Multiple sequence alignment tool. From the EMBL.
PBD	The Protein Data Bank collects and allows online visualization of protein and other macromolecules 3D structural data. Developed by (Berman *et al.*, 2000).
Posttranslational modifications and SNP	
dbSNP	It contains human SNP, microsatellites, and small-scale insertions and deletions along with publication, population frequency, molecular consequence. Developed by the NCBI.
Ensembl	Integrates experimental and reference genomic data from vertebrates and model organisms. Developed by EMBL (Yates *et al.*, 2019).
Phosphosite Plus	A collection of experimentally observed modifications as phosphorylation acetylation, methylation, ubiquitination, and O-glycosylation. Developed by Cell Signaling (Hornbeck *et al.*, 2015).
iPTMnet	iPTMnet is a bioinformatics resource for an integrated understanding of protein posttranslational modifications in a systems biology context. Developed by (Huang *et al.*, 2017).
Gene edition and primer design	
Gene Runner	Nucleic acid and protein sequence visualization and edition, primer design, and restriction site analysis. Developed by Frank Buquicchio and Michael Spruyt.
Image analysis	
FiJi	Fiji distributes the open-source software ImageJ focused on biological-image analysis. Developed by (Schindelin *et al.*, 2012).
Photoshop CS6	An image editing software that is used to adjust contrasts on microscopy and blot images and generate merge images. Developed by Adobe.
Statistics	
Excel	Data collection and management. Developed by Microsoft.
SPSS	Statistical analysis. Developed by IBM.
Origin	Statistical analysis and graph generation. Developed by OriginLab.
Manuscript writing	
Word	Writing and table management. Developed by Microsoft.
EndNote X9	Reference management software. Developed by Clarivate.
Figure arrangement	
PowerPoint	Figure sketching and data presentation. Developed by Microsoft.
Illustrator CS6	Figure arrangement and scheme drawing. Developed by Adobe.
BioRender	Scientific drawing resources. From BioRender.com
IBS	An illustrator of biological sequences that enables easy and accurate sequence schemes drawing. Developed by (Song *et al.*, 2012).
PyMol	Visualization of protein structural data on PDB file and structural picture and movie generation. From (Schrödinger, 2020)
ESPript	A program that renders sequence similarities and secondary structure information from aligned sequences for analysis and publications. Developed by (Robert and Gouet, 2014)

Materials and Methods

Abbreviations: Nacional Center of Biotechnology Information (NCBI), *Saccharomyces* Genome Database (SGD), National Institutes of Health (NIH), European Molecular Biology Laboratory (EMBL), Swiss Institute of Bioinformatics (SIB).

Results

Results

1.- Reconstruction of Toll-Like Receptor (TLR)-associated supramolecular complexes through yeast heterologous expression.

1.1.- Expression and subcellular localization of human TIR adaptors in yeast.

1.1.1.- Overproduction of human TIR adaptors in yeast does not interfere with growth.

MyD88, TIRAP, TRIF, and TRAM, the four adaptors involved in TLR4 signaling were chosen to be expressed in *S. cerevisiae*. The corresponding human cDNAs were cloned into yeast plasmids as either GFP, EGFP, or mCherry fusions under the control of the strong inducible *GAL1* promoter, which is repressed in glucose-based media and induced when cultured on galactose-based media. The expression of the heterologous proteins was verified via Western blotting (Fig 11). Serial dilution growth assays on solid media revealed that none of the overexpressed adaptors impaired yeast growth (Fig 12).

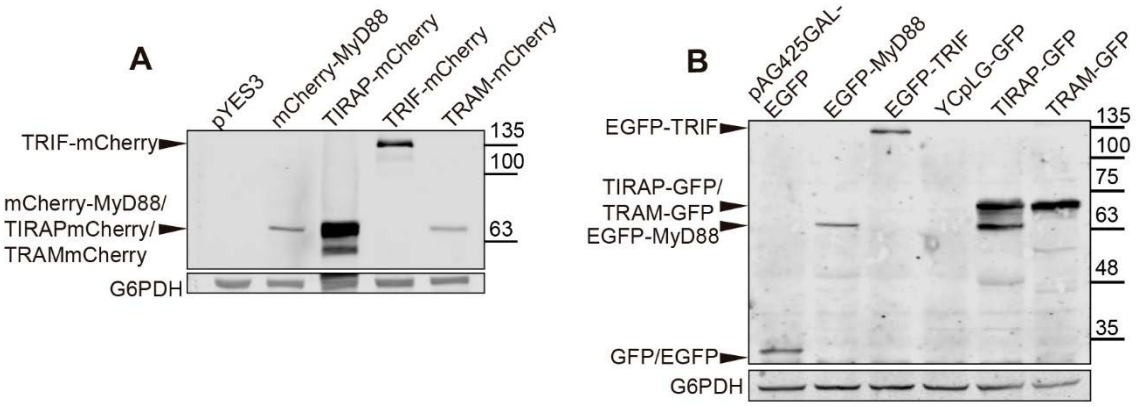

Fig 11.- Expression of human TIR adaptors in yeast.

Western blotting of YPH499 strain extracts from cells grown in SG for 5 h bearing the indicated pYES3 (A) and either pAG425GAL-EGFP (EGFP-MyD88 and EGFP-TRIF) or YCpLG-GFP (TIRAP-GFP and TRAM-GFP) (B) derivative plasmids using antibodies anti-mCherry (A, upper panels) and anti-GFP (B, upper panels) followed by anti-G6PDH as a loading control (lower panels). The molecular weights of the constructs are: mCherry-MyD88 (60 kDa), TIRAP-mCherry (52 kDa), TRIF-mCherry (103 kDa), TRAM-mCherry (54 kDa), EGFP (29 kDa), EGFP-MyD88 (62 kDa), EGFP-TRIF (105 kDa), GFP (27 kDa), TIRAP-GFP (52 kDa), TRAM-GFP (54 kDa). Approximate molecular weights on the figure are expressed in kDa.

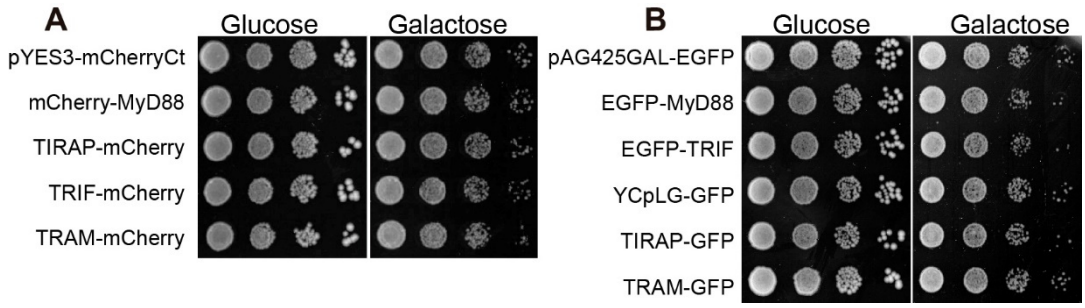

Fig 12.- Human TIR adaptors do not alter yeast growth.

Ten-fold serial dilution assay of YPH499 yeast cells bearing as control pYES3-mCherryCt (A), pAG425GAL-EGFP, and YCpLG-GFP (B) and expressing the indicated constructs from pYES3 derivative plasmids (A), or EGFP-MyD88 and EGFP-TRIF from pAG425GAL derivative plasmids or TIRAP-GFP and TRAM-GFP cloned into YCpLG vector (B). Cells were cultured under repression in SD agar medium (Glucose) and induction in SG agar medium (Galactose) for 72h.

1.1.2.- Subcellular localization of human TIR adaptors in *Saccharomyces cerevisiae*.

Subcellular localization of the GFP or mCherry fusions was next addressed. Both TIRAP N-terminal and C-terminal mCherry fusions were found on yeast PM, probably driven by their polybasic region (Kagan and Medzhitov, 2006) and forming peripheral clusters (Fig 13). Further focal analyses revealed that mCherry-TIRAP clusters were often filamentous on yeast PM, possibly generated via self-interaction (Fig 13B). Remarkably, mCherry-TIRAP was often concentrated near the bud region, close but never coincident with the septin ring (Fig 13C).

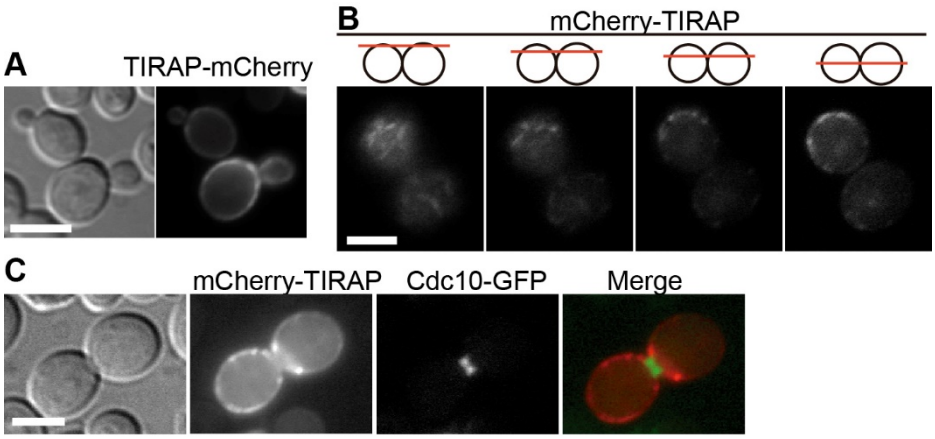

Fig 13.- TIRAP localizes in the yeast PM.

Nomarski and fluorescence microscopy of YPH499 yeast cells transformed with (A) pYES3-TIRAP-mCherry, expressing TIRAP-mCherry and (C) pYES2-mCherry-TIRAP expressing mCherry-TIRAP (red) and pLA10H plasmid, expressing the septin ring marker Cdc10-GFP (green). (B) Focal planes of a YPH499 yeast cell expressing mCherry-TIRAP from pYES2-mCherry-TIRAP. Scale bars represent 5 µm.

TIRAP is proposed to bind PM via recognition of the PtdIns(4,5)P_2 phospholipid in mammalian cells (Kagan and Medzhitov, 2006). Therefore its co-localization with the PM PtdIns(4,5)P_2 fluorescent reporter GFPx2PH(PLCδ) was checked by laser confocal microscopy. Cellular middle plane confocal sections revealed that, while PtdIns(4,5)P_2 was more abundant at growing buds and bud necks, as expected (Garrenton *et al.*, 2010), TIRAP-mCherry was excluded from bud necks (Fig 14A), as observed with mCherry-TIRAP (Fig 13Fig 13C). Besides, the TIRAP-mCherry signal was more intense in the mother cell in the case of emerging and growing buds but had similar levels in larger buds (Fig 14A). Surface planes showed that most TIRAP-mCherry patches were not coincident with the PtdIns(4,5)P_2 marker (Fig 14B). This indicates that TIRAP was associated with microdomains different to those preferentially recognized by the GFPx2PH(PLCδ) marker.

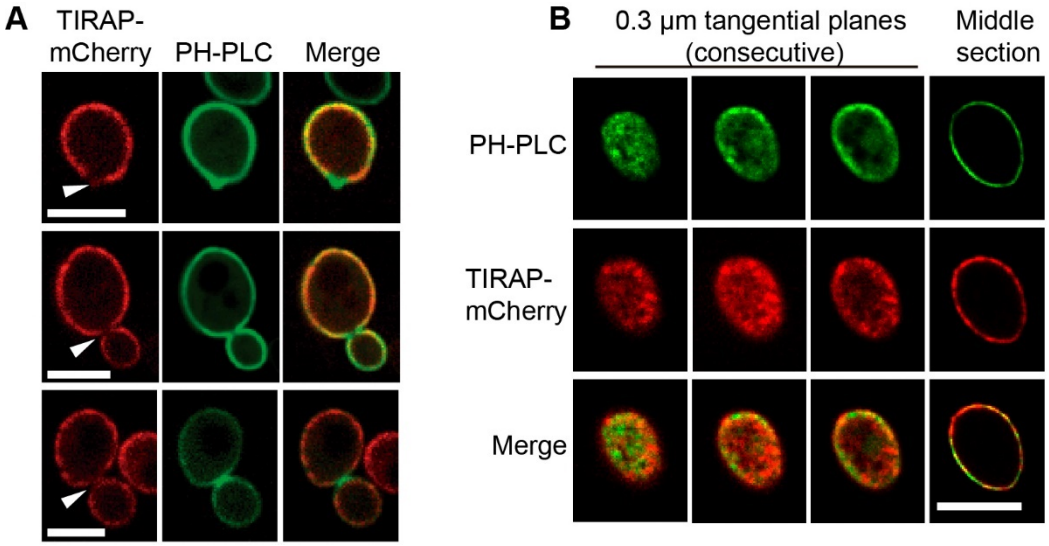

Fig 14.- TIRAP does not fully co-localize with a PtdIns(4,5)P_2 marker.

Confocal microscopy of YPH499 yeast cells expressing TIRAP-mCherry from pYES3-TIRAP-mCherry and the PtdIns(4,5)P_2 marker GFPx2PH(PLCδ) (PH-PLC) from pRS426-GFP2XPH(PLCδ) plasmid, (A) white arrows indicate emerging buds and bud necks. (B) Consecutive tangential planes of a single cell. Scale bars represent 5 µm.

TRAM has a bipartite sorting signal, composed of a myristoylation signal and endosomal localization motif (ELM), that targets it to PM and endosomal membranes in the mammalian cell (Kagan *et al.*, 2008). Interestingly, TRAM constructs expressed in yeast formed long curly filaments along the cell surface (Fig 15). Probably, those filaments are ruled by TIR-TIR interactions. Indeed, the TIR domain of TIRAP can assemble into filaments via self-interaction *in vitro*, and the TIR domain of TRAM has been suggested to do so (Ve *et al.*, 2017). Confocal imaging of yeast cells co-expressing TRAM-mCherry and the PtdIns(4,5)P_2 marker showed both

signals coincident at the middle plane (Fig 15B). These data indicate that TRAM structures are located at the PM, probably driven by its natural myristoylation signal.

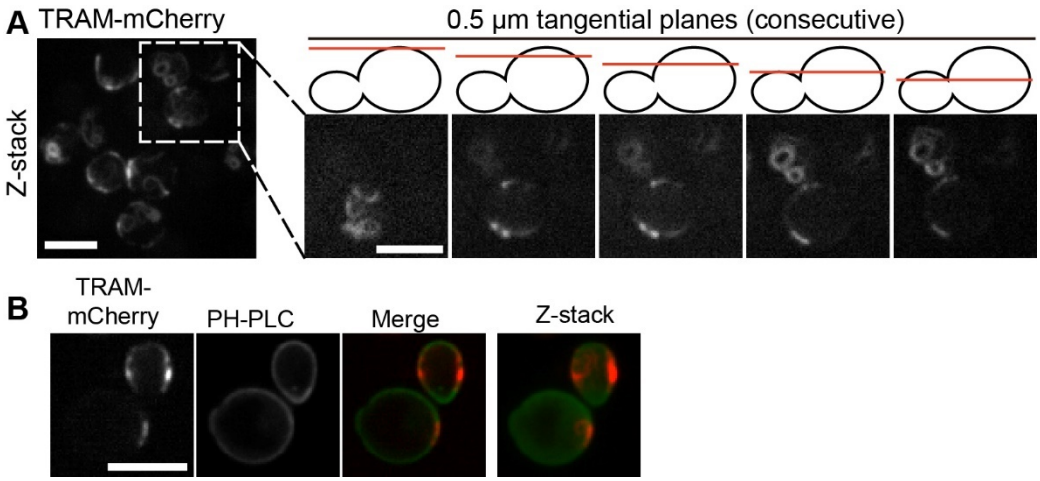

Fig 15.- TRAM forms PM filaments in yeast.

Confocal images of YPH499 yeast cells expressing TRAM-mCherry (A) from pYES3-TRAM-mCherry plasmid or co-expressing it with the PtdIns(4,5)P_2 marker GFPx2PH(PLCδ) (PH-PLC) from pRS426-GFP2XPH(PLCδ) plasmid (B). Z-stacks are the projection of 19 planes (0.25 µm per step) (A) or 15 planes (0.3 µm per step) (B). Scale bars represent 5 µm.

MyD88 and TRIF fluorescent tag fusions appear as cytoplasmic puncta upon heterologous expression in yeast (Fig 16). mCherry-MyD88 -expressing yeast cells usually bear 1 to 4 cytosolic spots (Fig 16A). Regarding TRIF, N-terminal tagged construct EGFP-TRIF shows 1 o 2 dots, whereas C-terminally tagged TRIF-mCherry, typically displays between 2 and more than 5 puncta per cell (Fig 16B). Co-expression of both TRIF fusion proteins exhibited a clear co-localization (Fig 16C), indicating that they co-aggregate at the same place.

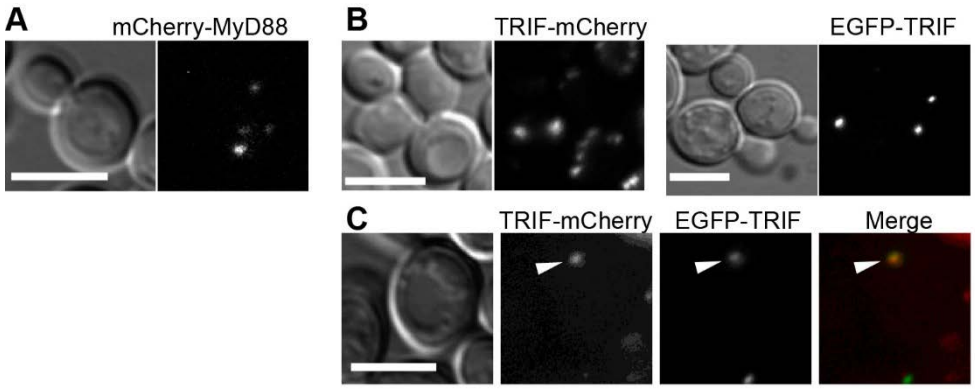

Fig 16.- MyD88 and TRIF appear in spots in yeast.

Nomarski and fluorescence microscopy of YPH499 yeast cells expressing mCherry-MyD88 from plasmid pYES3-mCherry-MyD88 (A), either TRIF-mCherry or EGFP-TRIF (B) from plasmids pYES3-TRIF-mCherry and

pAG425GAL-EGFP-TRIF respectively or co-expressing both TRIF constructs (C). The white arrow indicates a co-localization event. Scale bars represent 5 µm.

1.1.3.- Recapitulating interactions among human TIR adaptors in yeast.

It is well established that human TIR-containing adaptors interact with other TIR proteins. As proof of principle, we aimed to reproduce these properties in the heterologous *S. cerevisiae* intracellular environment. Therefore, two pairs of known interactors, namely MyD88 and TIRAP (Vyncke *et al.*, 2016) and TRIF and TRAM (Enokizono *et al.*, 2013), were co-expressed in yeast. Microscopic observations revealed a clear co-localization of TIRAP and MyD88. Both were found in either PM patches or the MyD88 spots, recruiting each other to their original location in the yeast cell (Fig 17A). On the other hand, we were not able to detect any co-localization between TRIF and TRAM under the conditions assayed (Fig 17B). This may reflect, that additional components or cellular processes necessary for their co-occurrence in cellular compartments are missing in the yeast model, compared to the mammalian cell scenario.

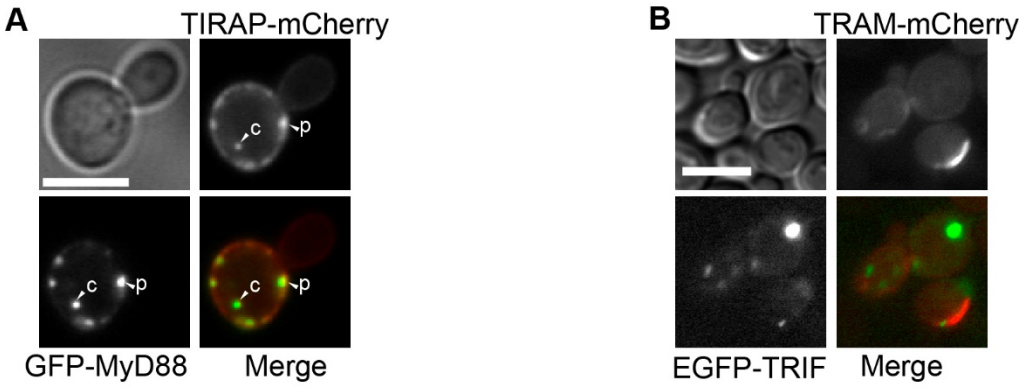

Fig 17.- Co-expression of MyD88 and TIRAP and TRIF and TRAM.

Nomarski and fluorescence microscopy of YPH499 yeast cells co-transformed with (A) pYES3-TIRAP-mCherry (TIRAP-mCherry, red) and pYES2-GFP-MyD88 (GFP-MyD88, green), (B) pYES3-TRAM-mCherry (TRAM-mCherry, red), and pAG425GAL-EGFP-TRIF (EGFP-TRIF, green). White arrows indicate cytosolic spots (c) or PM patches (p). Scale bars represent 5 µm.

Protein-protein interactions were subsequently assessed *in vitro* via co-immunoprecipitation. We used commercial anti-GFP nanobody agarose beads to precipitate GFP or EGFP-tagged constructs. Effective co-immunoprecipitation of TIRAP-GFP and mCherry-MyD88 was acknowledged, as expected (Fig 18A). Surprisingly, EGFP-TRIF also co-immunoprecipitated TRAM-mCherry (Fig 18B), despite the lack of co-localization observed (Fig 17B). A possible explanation for this fact is that homotypic TIR-TIR interaction or subcellular localization clues predominate over heterotypic interaction *in vivo*. On the other hand, during cell disruption for

the obtention of lysates, such restrictions are lacking, enabling the detection of TRIF-TRAM interacting ability *in vitro*.

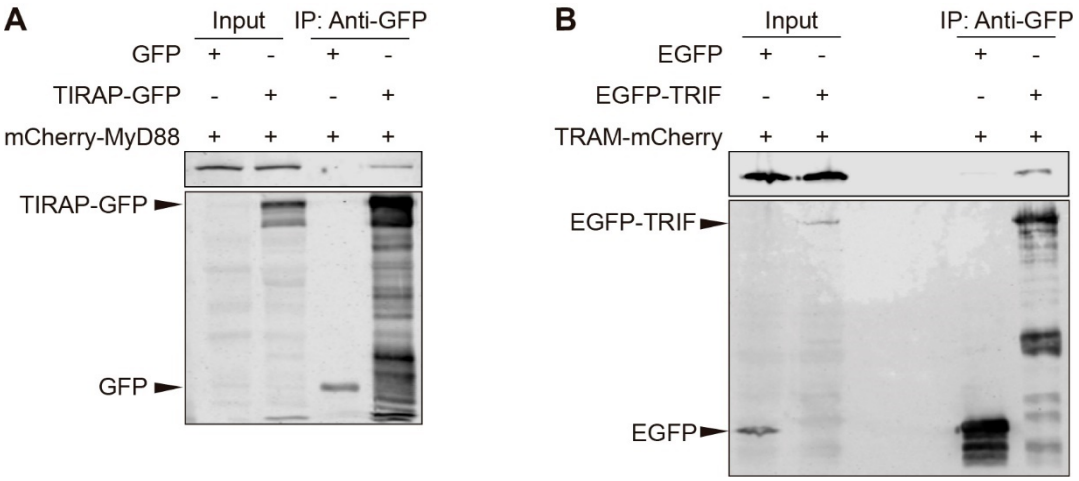

Fig 18.- Immunoprecipitation assays of MyD88-TIRAP and TRIF-TRAM.

YPH499 yeast cells were co-transformed with plasmids (A) pYES3-mCherry-MyD88 (mCherry-MyD88) and YCpLG-TIRAP-GFP (TIRAP-GFP) or YCpLG-GFP as control (GFP) or (B) pYES3-TRAM-mCherry (TRAM-mCherry) and pAG425GAL-EGFP-TRIF (EGFP-TRIF) or pAG425GAL-EGFP as a control (EGFP). Extracts were immunoprecipitated using anti-GFP nanobody agarose beads (GFP-TrapA, Chromotek), followed by Western blotting analysis. Input lanes show the whole extract, whereas IP lanes display immunoprecipitated proteins. Blots were developed using antibodies anti-mCherry (upper panels) and anti-GFP (lower panels).

1.2.- Introducing the TIR domain of TLR4.

To further reconstruct the TLR signaling pathway in *S. cerevisiae*, we next included the TLR4 receptor. Budding yeast has a thick cell wall (Jiménez-Gutiérrez *et al.*, 2020). Under these conditions, getting a functional full-length TLR4 receptor would be quite difficult, as PAMP recognition by the extracellular side would be impaired. Instead, only the cytosolic C-terminal region (657-839), containing the TIR domain, was expressed. We designed an N-terminal fusion to GST, to favor TLR4-TIR dimerization. In parallel, a myristoylation (myr) signal was added before the GST tag, to target the construct to the PM (Fig 19A). The expressed fusions did not alter yeast growth (Fig 19B).

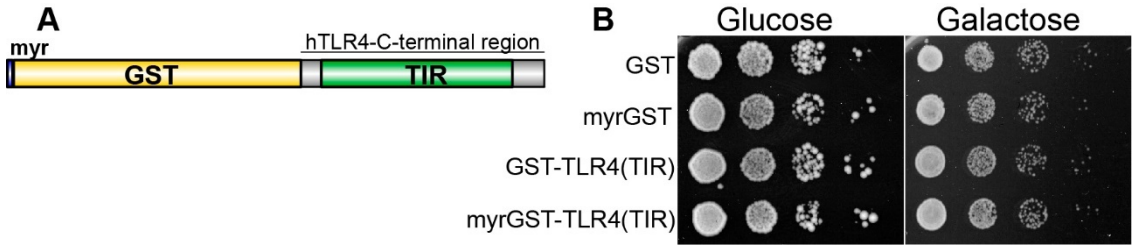

Fig 19.- TLR4-TIR does not alter yeast growth.

(A) Scheme of myristoylation signal (myr) and GST fusion to the C-terminal region of human TLR4. (B) Ten-fold serial dilution assay of YPH499 yeast cells expressing GST, myrGST, and the fusions GST-TLR4-TIR and myrGST-TLR4-TIR from pEG(KG) derivative plasmids. Cells were cultured under repression in SD agar medium (Glucose) and induction in SG agar medium (Galactose) for 72h. Both media lacked uracil and leucine to ensure maximum plasmid copy number, as pEG(KG) bears a *leu2d* defective gene apart from *URA3*.

The TLR4-TIR constructs generated were then checked for their ability to interact *in vitro* with both adaptor pairs already expressed in yeast. Triple transformants bearing either GST-TLR4-TIR fusion plus TIRAP and MyD88 or plus TRAM and TRIF were assayed by pull-down experiments, using glutathione-coated beads. Both myristoylated and non-myristoylated versions interacted with MyD88 and TIRAP (Fig 20A), and TRIF and TRAM (Fig 20B).

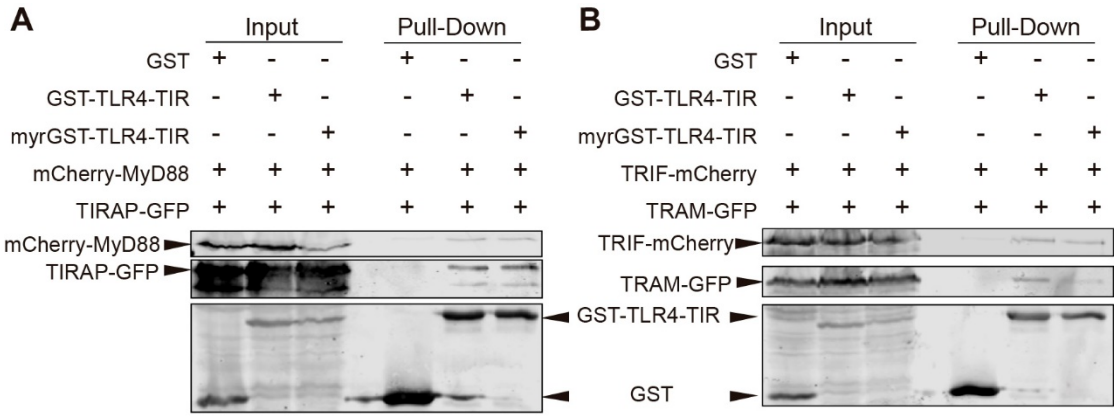

Fig 20.- Pull-down assay of TLR4-TIR and the adaptors.

YPH499 yeast cells were co-transformed with either GST, GST-TLR4-TIR, or myr-GST-TLR4-TIR from pEG(KG) derivative plasmids and mCherry-MyD88 plus TIRAP-GFP from pYES3-mCherry-MyD88 or YCpLG-TIRAP-GFP respectively (A) or TRIF-mCherry plus TRAM-GFP from pYES3-TRIF-mCherry or YCpLG-TRAM-GFP respectively (B). Extracts were treated with glutathione agarose beads (GE Healthcare), followed by Western blotting analysis. Input lanes show the whole extract, whereas pull-down lanes display precipitated proteins. Blots were developed using antibodies anti-mCherry (upper panels), anti-GFP (central panels), and anti-GST (lower panels).

Next, the TLR4-TIR fusions were co-transformed only with the fluorescent protein-tagged versions of either TIRAP or TRAM. This way, any changes in the localization of these adaptors driven by the receptor expression would be detected under a microscopic examination. TIRAP-mCherry, which usually only decorates yeast PM, was also found in a few cytosolic spots when non-myristoylated GST-TLR4-TIR was co-expressed, but not in control cells expressing either GST or myrGST alone. In cells bearing the PM-targeted construct myr-GST-TLR4-TIR, TIRAP-mCherry was driven to dots of similar size, which were PM-bound in this case (Fig 21).

Receptor co-expression also altered the characteristic TRAM-mCherry PM filaments. Either myristoylated or non-myristoylated TLR4-TIR constructs made TRAM-mCherry localize in PM puncta in virtually all TRAM expressing cells (Fig 22A-B). Further confocal imaging revealed that those spots were shortened filaments while GST-TLR4-TIR co-expression, and discrete dots when myrGST-TLR4-TIR was present (Fig 22C).

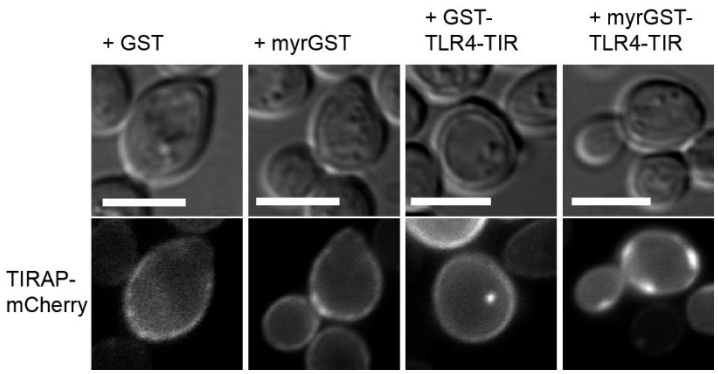

Fig 21.- TLR4-TIR recruits TIRAP in yeast.

Nomarski and fluorescence microscopy of YPH499 yeast cells co-transformed with pEG(KG) derivatives expressing bare (GST) or myristoylated GST (myrGST), bare (GST-TLR4-TIR) or myristoylated (myrGST-TLR4-TIR) GST fusion to TLR4-TIR together with pYES3-TIRAP-mCherry expressing TIRAP-mCherry. Cultures were grown on SR lacking not only uracil and tryptophan but also leucine to ensure maximum pEG(KG)-derivatives plasmid copy number. Scale bars correspond to 5 µm.

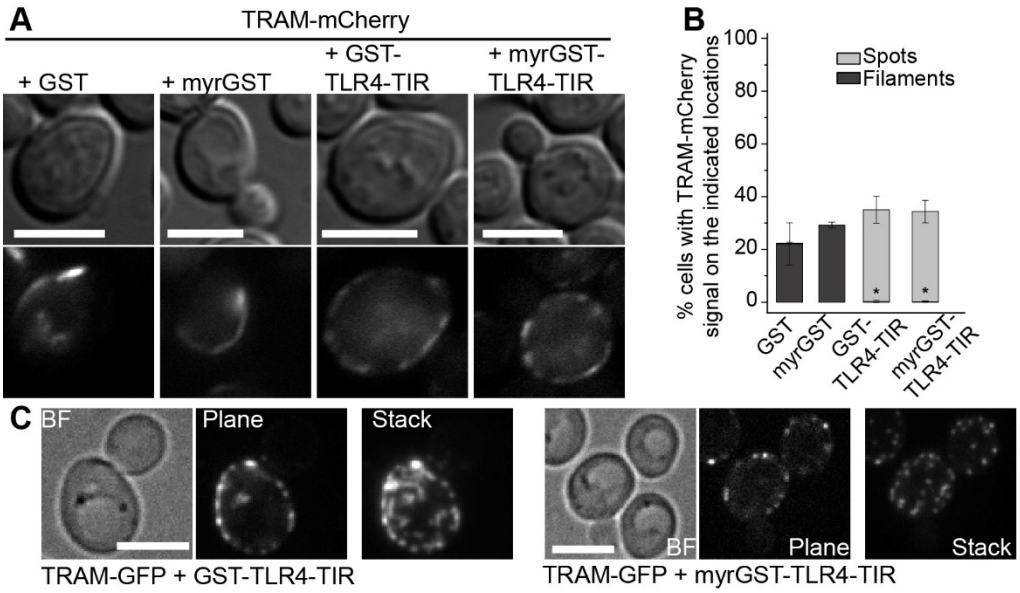

Fig 22.- TLR4-TIR relocates TRAM and impairs filament formation.

(A) Nomarski and fluorescence microscopy of YPH499 yeast cells co-transformed with pEG(KG) derivatives expressing bare (GST) or myristoylated GST (myrGST), and bare (GST-TLR4-TIR) or myristoylated (myrGST-TLR4-TIR) GST fusion to TLR4-TIR together with pYES3-TRAM-mCherrry (TRAM-mCherry). Cultures were grown on SR lacking not only uracil and tryptophan but also leucine to ensure maximum pEG(KG)-derivatives plasmid copy number. (B) Stacked bar graph displaying the percentage of cells showing TRAM-mCherry fluorescent signal as PM filaments (black section) or as PM puncta (gray section), out of all cells on a field. Data correspond to means ± standard deviation of three independent transformants (n ≥ 100). Statistical comparison of the filament data was done with Kruskal-Wallis ANOVA with a p-value < 0.05 (*) for myrGST vs GST-TLR4-TIR (p=0.016) and myrGST-TLR4-TIR (p=0.026). (C) Bright-field (BF) and confocal microscopy of YPH499 yeast cells co-transformed with YCpLG-TRAM-GFP (TRAM-GFP) and either GST-TLR4-TIR or myr-GST-TLR4-TIR from pEG(KG) derivative plasmids. Stacks are the Z projection of 15 planes (GST-TLR4-TIR) or 14 planes (myrGST-TLR4-TIR) of 0.3µm per step. Scale bars correspond to 5 µm.

1.3.- Interaction of MyD88 and TIRAP with downstream IRAK kinases.

1.3.1.- MyD88 interacts and becomes phosphorylated by IRAK4.

In mammalian cells, after assembling the TIR side of the SMOC, MyD88 recruits via DD-DD interactions the downstream kinases called IRAKs (Moncrieffe *et al.*, 2020). Taking advantage of the simplicity of a model that lacks potential interfering elements, such direct interactions were next tested in yeast. We first co-expressed GST N-terminal fusions of IRAK1, 2, and 4 together with mCherry-MyD88 and performed a pull-down assay (Fig 23A). MyD88 strongly interacted with IRAK4, its downstream factor, whereas only a subtle interaction was detected with IRAK1/2. Interestingly, a slow migrating band was identified in MyD88 when co-expressed with IRAK4, and that new band was more intense on the pull-down compared to the input, indicating that

IRAK4 preferably binds this form. To test whether kinase activity was determinant for MyD88-IRAK4 interaction, a second pull-down was performed, comparing IRAK4 wild type (WT) and its catalytically inactive (kinase-dead, KD) point mutant (Fig 23B). IRAK4 KD was still able to interact with MyD88 to the same extent as the WT, but the previously described lower mobility band no longer appeared, suggesting that it was a consequence of phosphorylation events directly exerted by the GST-IRAK4 kinase on mCherry-MyD88 as a substrate *in vivo*. To our knowledge, this is the first time that direct MyD88 phosphorylation by IRAK4 is detected.

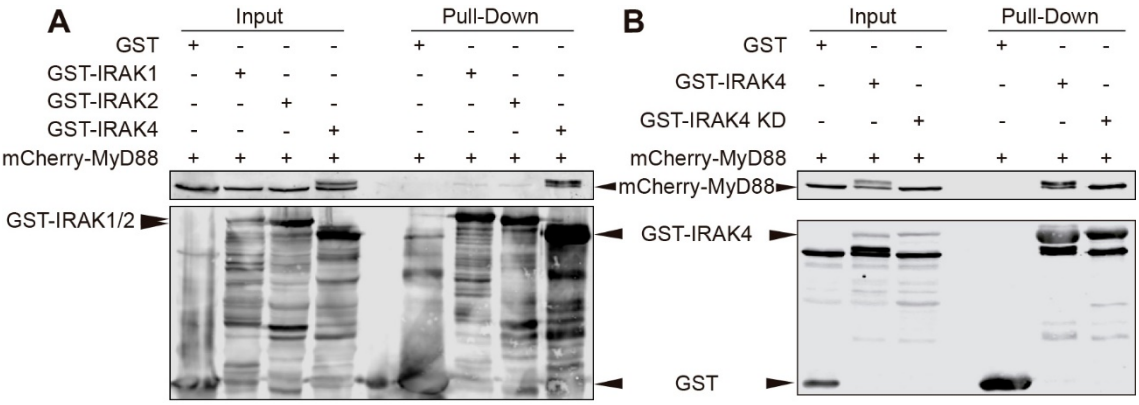

Fig 23.- Pull-down assay of the IRAK1/2/4 and MyD88.

YPH499 yeast cells were co-transformed with pYES3-mCherry-MyD88 plasmid and either GST, GST-IRAK1, GST-IRAK2, or GST-IRAK4 (A) or either GST, GST-IRAK4 WT or the kinase-dead mutant (KD) (B) all from pEG(KG) derivatives. Cultures were grown on SR lacking not only uracil and tryptophan but also leucine to ensure maximum pEG(KG)-derivatives plasmid copy number. Extracts were treated with glutathione agarose beads (GE Healthcare), followed by Western blotting analysis. Input lanes show the whole extract, whereas pull-down lanes display precipitated proteins. Blots were developed using antibodies anti-mCherry (upper panels), and anti-GST (lower panels).

MyD88 S242 and S244 phosphorylated residues were reported to be dephosphorylated by Phosphatase 2A (PP2A), which causes TLR signaling downregulation (Xie *et al.*, 2013). They become phosphorylated upon TLR stimulation, but no responsible kinase has been identified so far. To test whether IRAK4 could phosphorylate S242 and S244, a serine to alanine double mutant (S242A-S244A, designated x2SA from now on) was generated on mCherry-MyD88 yeast expression construct. Then, a pull-down assay using GST-IRAK4 WT and KD was performed (Fig 24). MyD88 x2SA was still able to interact with either IRAK4 WT or KD constructs. As expected, the slow mobility band only appeared upon IRAK4 WT co-expression, but it was barely seen on the input lanes and co-precipitated less intensely with IRAK4 WT, compared to the regular mobility band. This result contrast with the MyD88 WT behavior, in which the upper band is predominantly co-precipitated in the presence of IRAK4 WT. This suggests that S242 and S244,

together with other residues, are probably phosphorylated by overexpressed IRAK4 in the yeast model, although they are not responsible themselves for the mobility shift.

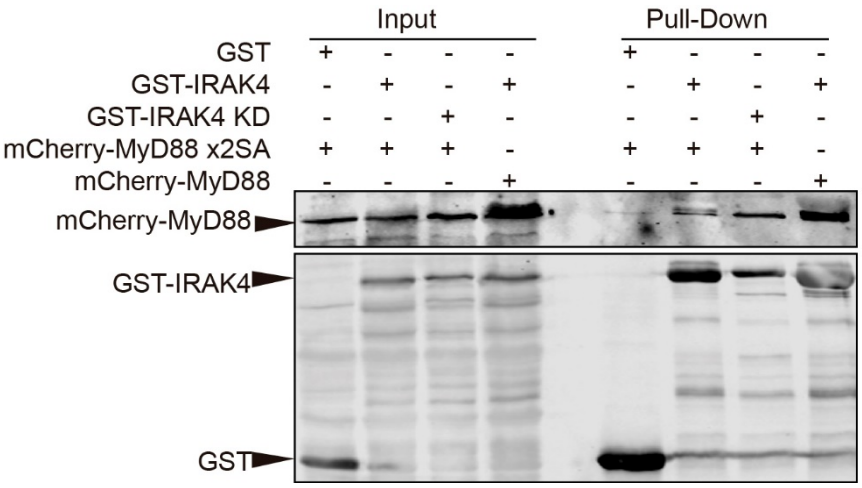

Fig 24.- Pull-down assay of IRAK4 and a MyD88 mutant.

YPH499 yeast cells were co-transformed with pEG(KG) plasmid derivatives expressing either GST, GST-IRAK4 WT, or the kinase-dead mutant (KD) and either mCherry-MyD88 WT or the S242A-S244A double mutant (x2SA) from pYES3 plasmid derivatives. Cultures were grown on SR lacking not only uracil and tryptophan but also leucine to ensure maximum pEG(KG)-derivatives plasmid copy number. Extracts were treated with glutathione agarose beads (GE Healthcare), followed by Western blotting analysis. Input lanes show the whole extract, whereas pull-down lanes display precipitated proteins. Blots were developed using antibodies anti-mCherry (upper panels), and anti-GST (lower panels).

To identify which MyD88 residues were targeted by IRAK4 in these conditions, we search for MyD88 phosphopeptides by using mass spectrometry techniques. Yeast protein extracts expressing both mCherry-MyD88 and GST-IRAK4 were co-immunoprecipitated using anti-mCherry nanobody agarose beads (RFP-TrapA, Chromotek), and enriched samples were loaded in a 10% SDS-polyacrylamide gel. Three bands were identified via Coomassie blue staining: slow migrating MyD88 band (UP), regular MyD88 band (DOWN), and the band corresponding to IRAK4 (Fig 25A). These bands were cut from the gel and trypsin-digested. The resulting peptides were separated via liquid chromatography and analyzed by mass spectrometry (MALDI-TOF-TOF) (Fig 25A). Peptides containing S, T, and/or Y phosphorylated residues were identified against a tailored database containing our tagged-construct sequences. Sequence coverage reached for mCherry-MyD88 a 94.67%, 79.23%, and 62.50%, while for GST-IRAK4 it was 57.51%, 28.18%, and 58.66% for the UP, DOWN, and KINASE bands respectively.

In the MyD88 protein sequence, ten phosphorylated serine and threonine residues were found, five (T148, T149, S242, T281, S283) were exclusively found on the UP band, three of them, (T141,

S244, and T272), also appeared in the DOWN band, S10 was found on both UP and KINASE bands, whereas S19 exclusively appeared in the KINASE band (Fig 25B). S10 is located on the N-terminal region, S19 belongs to the DD, and T141, T148, and T149 are inside the INT domain. The other 5 belong to the TIR side of MyD88 (Fig 25B). Looking at the resolved MyD88 TIR structure (PDB: 4DOM) (Vyncke *et al.*, 2016), these residues are found on the surface (Fig 25C). S242 and S244 are at the end of αC' helix and play a role in the BCD interface (Vyncke *et al.*, 2016). T281 and S283 belong to the EE loop, close to the Box 3 motif, and take part in the MyD88 BE surface (Vyncke *et al.*, 2016). T272 is on the DE loop, and previous studies found it key for TIRAP-MyD88 interaction although it only slightly altered NF-kB activation (Vyncke *et al.*, 2016).

Nevertheless, up to 12 other serine/threonine phosphorylation events were detected on the mCherry fusion tag, including one on the cloning linker region (Fig 25B). Eight IRAK4 putative autophosphorylation events, although phosphorylation by a yeast kinase cannot be ruled out, were also identified, one of them on the GST tag (Fig 25D). These data suggest that overexpressed IRAK4 acts as a highly reactive enzyme in the yeast environment and has the ability to phosphorylate its upstream recruiter MyD88.

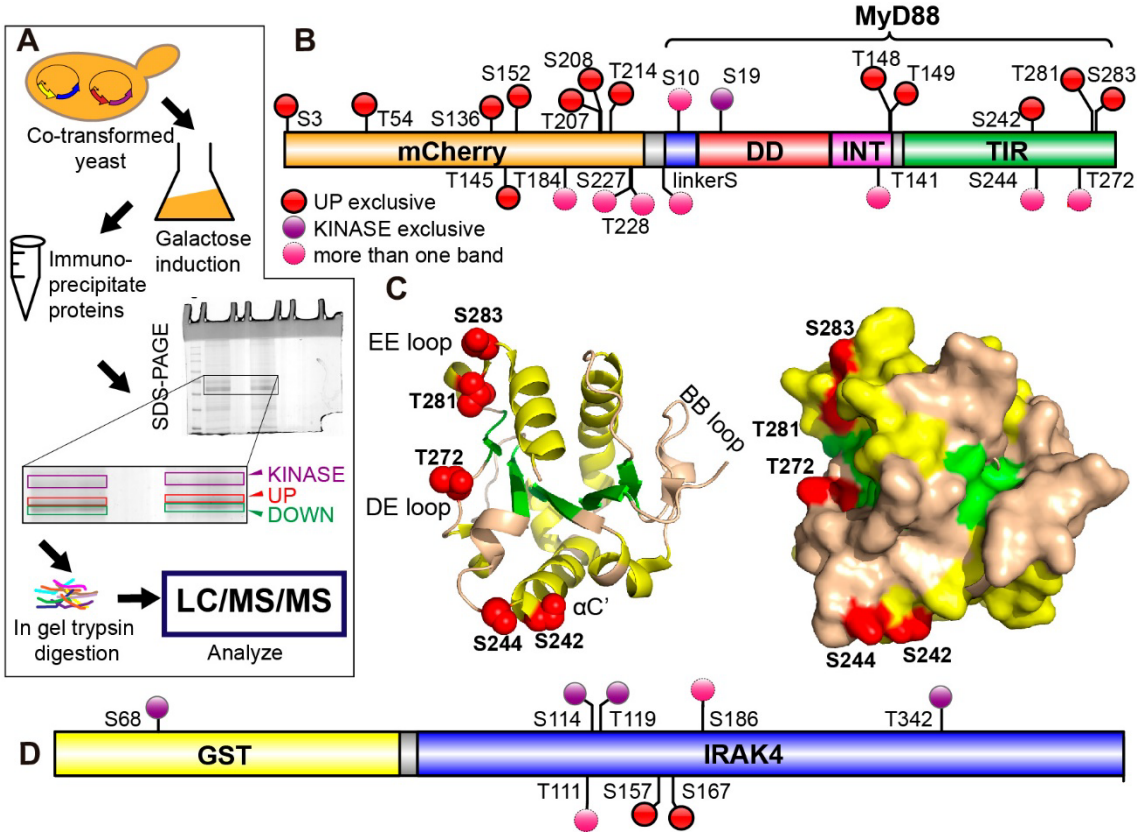

Fig 25.- The phosphorylated residues on MyD88.

(A) Scheme of the proteomics assay, including a picture of the Coomassie blue-stained gel with the selected bands highlighted, both lanes containing a duplicate of the sample. YPH499 yeast cells were co-

transformed with pEG(KG)-GST-IRAK4 and pYES3-mCherry-MyD88, and cultures were grown on SR lacking not only uracil and tryptophan but also leucine to ensure maximum pEG(KG)-GST-IRAK4 plasmid copy number. (B) Phosphorylated residues that were identified on the mCherry-MyD88 construct. Residue names and numbers refer to the notation for each ORF. LinkerS is a serin residue found on the cloning linker region between both constructs. Residues found exclusively on the UP or the KINASE band are colored in red or violet respectively. Pink circles indicate that those residues were found in more than one band. (C) Cartoon (left) and surface (right) structures of MyD88-TIR domain (PDB: 4DOM) showing the location of the MyD88-TIR phosphorylated residues by IRAK4 as red spheres. α-helixes appear in yellow and β-strands in green. (D) Phosphorylated residues that were detected on the GST-IRAK4 construct. Drawings generated with IBS, PyMol, and Adobe Illustrator CS6. Abbreviations: SDS-polyacrylamide gel electrophoresis (SDS-PAGE); liquid chromatography (LC); mass spectrometry (MS); Death domain (DD); Intermediate domain (INT); TIR domain (TIR).

1.3.2.- TIRAP interacts with IRAK1/2 and IRAK4 KD in the yeast model.

In the mammalian cell context, TIRAP has been described as an interactor of WT IRAK2 (Fitzgerald *et al.*, 2001) and the catalytically inactive KD mutants of IRAK1 and IRAK4 (Dunne *et al.*, 2010). So, we aimed to reconstruct those interactions in the yeast model. WT GST-IRAK1/2/4 were co-transformed with TIRAP-mCherry. In this case, not only IRAK2 but also WT IRAK1 interacted with TIRAP (Fig 26A). There was also slight co-purification with WT IRAK4, which became stronger when IRAK4 KD mutant was co-expressed (Fig 26B).

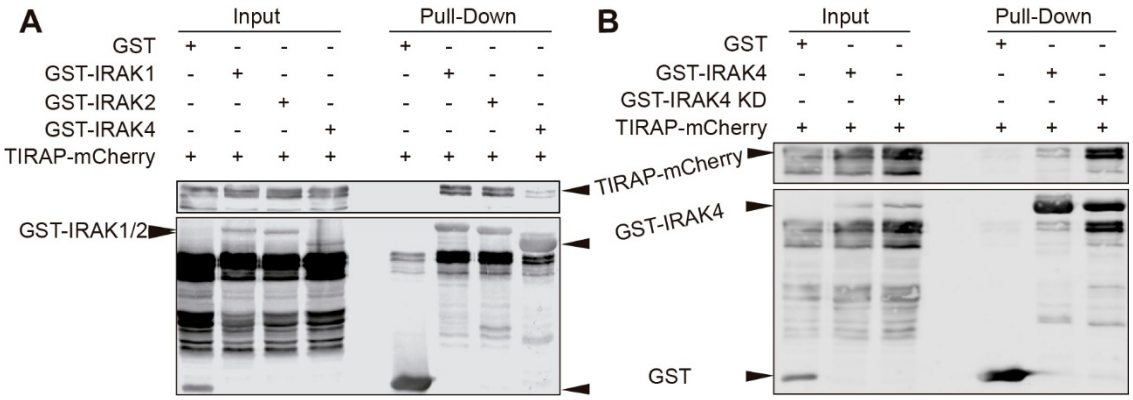

Fig 26.- Pull-down assay of IRAK1/2/4 and TIRAP.

YPH499 yeast cells were co-transformed with pYES3-TIRAP-mCherry plasmid and either GST, GST-IRAK1, GST-IRAK2, or GST-IRAK4 (A) or either GST, GST-IRAK4 WT or the kinase-dead mutant (KD) (B) all from pEG(KG) derivative plasmids. Cultures were grown on SR lacking not only uracil and tryptophan but also leucine to ensure maximum pEG(KG)-derivatives plasmid copy number. Extracts were treated with glutathione agarose beads (GE Healthcare), followed by Western blotting analysis. Input lanes show the whole extract, whereas pull-down lanes display precipitated proteins. Blots were developed using antibodies anti-mCherry (upper panels), and anti-GST (lower panels).

One of the key elements driving TIR-TIR interactions is the BB loop. A point mutation switching a conserved proline to histidine (TIRAP P125H) (Ve *et al.*, 2017) impairs TLR signaling and TIRAP TIR domain interacting properties. To test whether this BB loop region was responsible for its interactions with IRAK1 or 2, which lack TIR domains, the P125H mutation was introduced in TIRAP via site-directed mutagenesis. No significant changes in the interaction with IRAK1 or 2 were detected, suggesting that IRAK1/2 and TIRAP interaction in yeast occurs independently of the BB loop of TIRAP (Fig 27).

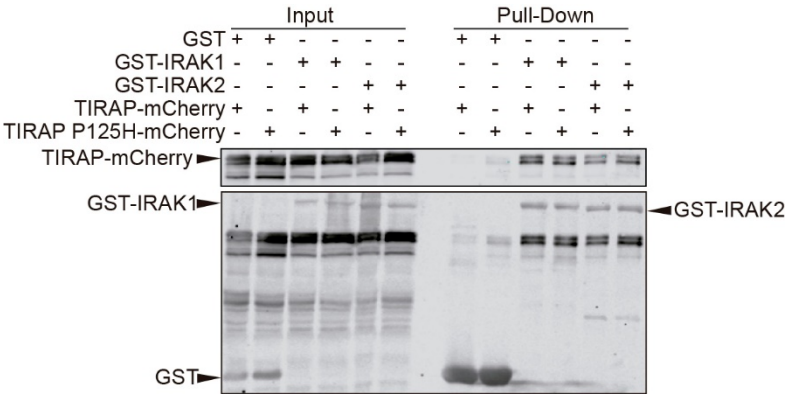

Fig 27.- Pull-down assay of IRAK1/2 and a TIRAP mutant.

YPH499 yeast cells were co-transformed with pEG(KG) plasmid derivatives expressing either GST, GST-IRAK1, or GST-IRAK2 and with either TIRAP-mCherry WT or the P125H mutant from pYES3 derivative plasmids. Cultures were grown on SR lacking not only uracil and tryptophan but also leucine to ensure maximum pEG(KG)-derivatives plasmid copy number. Extracts were treated with glutathione agarose beads (GE Healthcare), followed by Western blotting analysis. Input lanes show the whole extract, whereas pull-down lanes display precipitated proteins. Blots were developed using antibodies anti-mCherry (upper panels), and anti-GST (lower panels).

1.4.- Mutational analyses of human TIR adaptors in the yeast model.

Once determined the features of human TIR adaptors upon yeast heterologous expression, we next aimed to generate, by site-directed mutagenesis, point mutations in residues potentially relevant for their function to test them in the yeast system.

1.4.1.- TIRAP N-terminal lysine clusters play a role in PM localization in *S. cerevisiae*.

Besides the aforementioned BB loop mutation (TIRAP P125H, section 1.3.2, Fig 27), key N-terminal lysine residues involved in proper TIRAP PM localization and PtdIns(4,5)P2 binding (Kagan and Medzhitov, 2006) were also targeted. Three lysine-to-alanine mutants were generated on the TIRAP-mCherry construct: two double mutants K15A-K16A (K15-16A) and K31A-K32A (K31-32A) plus another mutant containing all four mutations K15A-K16A-K31A-

K32A, designated as x4KA. Neither TIRAP P125H, either fused to GFP or mCherry nor any of the four TIRAP-mCherry mutants induced toxicity in yeast (Fig 28A). The expression of these TIRAP mutants was checked via Western blotting (Fig 28B-C). TIRAP x4KA mutant behaved differently on the immunoblot, as the signal was much less intense than that observed in TIRAP WT or the other mutants (Fig 28B). This may indicate that the loss of these residues compromises protein stability.

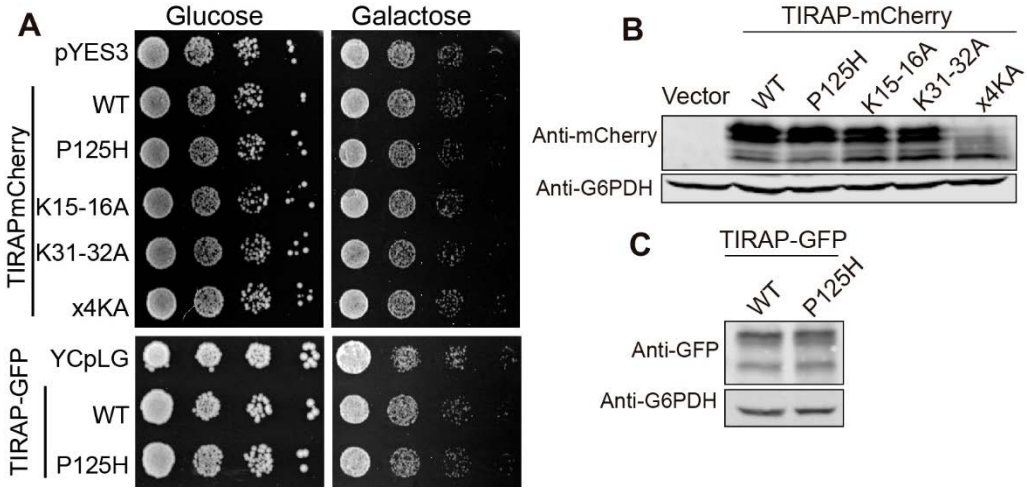

Fig 28.- Expression of TIRAP mutants.

(A) Ten-fold serial dilution assay of YPH499 yeast cells bearing empty vector (pYES3) and expressing TIRAP-mCherry WT and the indicated mutants from pYES3 derivative plasmids (upper panel) and empty vector (YCpLG) followed by TIRAP-GFP WT and P125H mutant, expressed from YCpLG plasmid (lower panel). Cells were cultured under repression in SD agar medium (Glucose) and induction in SG agar medium (Galactose) for 72h. Western blotting of YPH499 yeast extracts transformed with (B) pYES3 (vector) and the same TIRAP-mCherry constructs as in (A, upper), or (C) YCpLG TIRAP-GFP WT and P125H mutant. It was developed using antibodies anti-mCherry (B, upper panels) and anti-GFP (C, upper panels) followed by anti-G6PDH as a loading control (lower panels).

Fluorescence microscopy showed that TIRAP-mCherry x4KA was less frequently found on PM, compared to TIRAP-mCherry WT. Double mutants K15-16A and K31-32A decorate the PM like the WT, although in a lower percentage of cells. The BB loop P125H mutant did not change its location compared to WT but had a more homogeneous and less intense signal (Fig 29). These data point out that this lysine cluster is involved in heterologous TIRAP-mCherry PM targeting in yeast, similar to what was reported for mammalian cells by Kagan and Medzhitov (Kagan and Medzhitov, 2006).

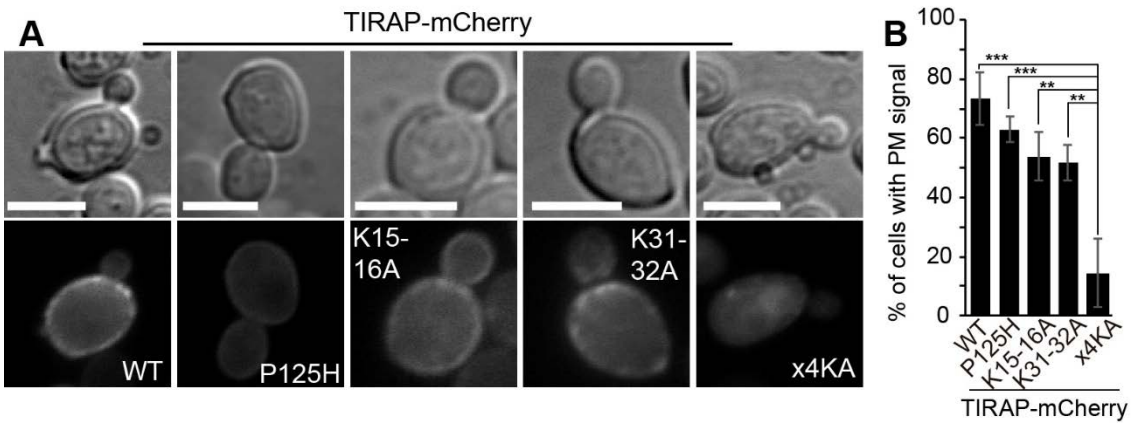

Fig 29.- The TIRAP polybasic region targets it to the yeast PM.

(A) Nomarski and fluorescence microscopy of YPH499 cells expressing TIRAP-mCherry WT and the indicated mutants from pYES3 derivative plasmids. Scale bars correspond to 5 µm. (B) Graph displaying the percentage of cells showing PM mCherry fluorescent signal. Data correspond to means ± standard deviation of three independent transformants (n ≥ 100). One-way ANOVA statistical comparison produced a p-value < 0.001 (***) for x4KA vs WT and P125H and a p < 0.01 (**) vs K15-16A (p=0.001) and vs K31-32A (p= 0.002).

1.4.2.- The MyD88 BB loop mutant displays a lower frequency of cytoplasmic spots.

On the MyD88 sequence, three mutations were studied: (i) the previously generated MyD88 x2SA mutant (Section 1.3.1. Fig 24), lacking two phosphorylatable serines; (ii) the proline to histidine mutation in the BB loop (MyD88 P200H), equivalent to that in TIRAP P125H (Ve *et al.*, 2017; Vyncke *et al.*, 2016) that impairs TIR-TIR interactions, and (iii) a well-established oncogenic mutation reported to display stronger interacting properties (MyD88 L252P) (Avbelj *et al.*, 2014; Ngo *et al.*, 2011; Zhan *et al.*, 2016). None of the MyD88 mutants caused toxicity in yeast (Fig 30A) and expression was verified via Western blotting. In the case of the L252P mutant, the band was less intense as compared to the other MyD88 constructs, perhaps indicating lower stability (Fig 30B).

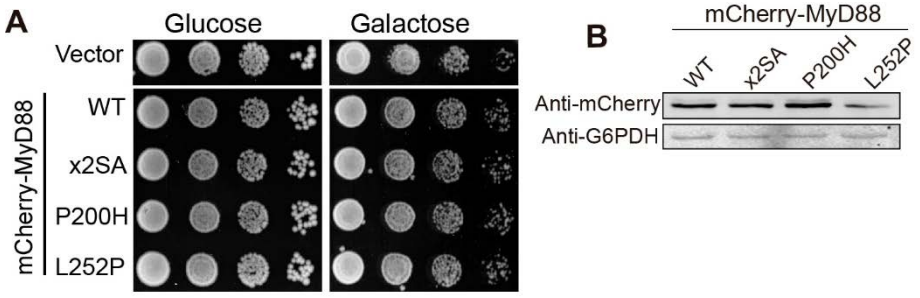

Fig 30.- Expression of MyD88 mutants.

(A) Ten-fold serial dilution assay of YPH499 yeast cells bearing empty vector (pYES3) and expressing mCherryMyD88 WT and the indicated mutants from pYES3 derivative plasmids. Cells were cultured under

repression in SD agar medium (Glucose) and induction in SG agar medium (Galactose) for 72h. (B) Western blotting of YPH499 yeast extracts transformed with the same mCherry-MyD88 constructs as in A, developed using antibodies anti-mCherry (upper), followed by anti-G6PDH as a loading control (lower).

Fluorescence microscopy showed all mCherry MyD88 mutants displaying typical 1 to 4 mCherry-MyD88 cytosolic spots (Fig 31). Nevertheless, the samples expressing each of the three mutants had fewer cells bearing dots. This difference was statistically significant in the case of the BB loop mutant P200H (Fig 31B). If we consider self-interaction as a requirement for spot formation, these data would reflect that mutants, especially those with compromised TIR-TIR interaction ability, are less able to form cytosolic spots because of their altered TIR interacting properties, as in the case of MyD88 P200H. However, if cytoplasmic spots were fully dependent on TIR-TIR interactions, the gain-of-function L252P mutant should produce more conspicuous spots, so other determinants may be involved in this localization.

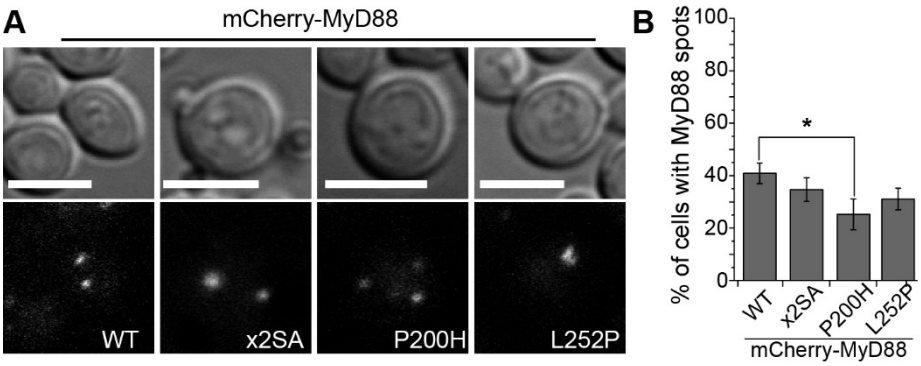

Fig 31.- The MyD88 mutants also form spots.

(A) Nomarski and fluorescence microscopy of YPH499 yeast cells bearing mCherry-MyD88 WT and the indicated mutants, from pYES3 derivative plasmids. Scale bars correspond to 5 µm. (B) Graph displaying the percentage of yeast cells showing MyD88 spots. Data correspond to means ± standard deviation of three independent transformants (n ≥ 100). One-way ANOVA statistical comparison retrieved a p-value=0.021 (*) for WT vs P200H mutant.

Next, both proline-to-histidine BB loop mutants on MyD88 and TIRAP were examined for their ability to co-localize in the yeast cell. Neither TIRAP P125H nor MyD88 P200H mutants co-localized with their partner (Fig 32). Indeed, they kept the localization observed when expressed alone (Fig 29 and 31) despite the presence of the second TIR protein, contrasting with the recruitment displayed by intact TIRAP and MyD88 when co-expressed (Fig 17and 32).

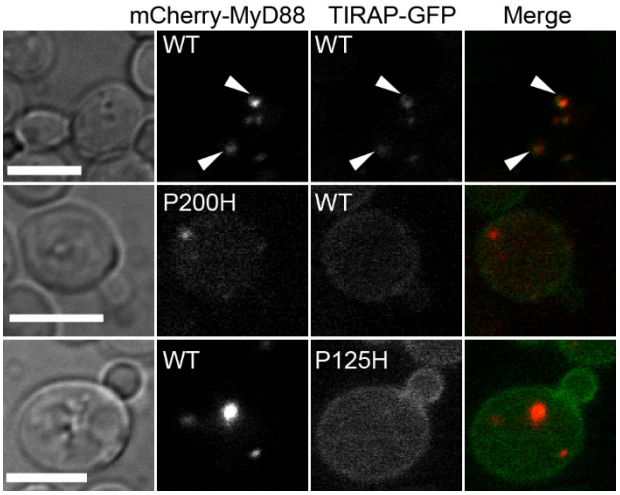

Fig 32.- Co-expression of TIRAP and MyD88 BB loop mutants.

Nomarski and fluorescence microscopy of YPH499 cells co-expressing mCherry-MyD88 and TIRAP-GFP, either WT or the indicated mutants, and from pYES3-mCherry-MyD88 or YCpLG-TIRAP-GFP plasmid derivatives. White arrows show co-localization events. Scale bars correspond to 5 µm.

1.4.3.- Role of the TRAM myristoylation signal, BB loop, and D91 E92 acidic residues in filament formation.

Three TRAM mutations were chosen to be tested on the yeast model: (i) a conserved BB loop mutation, in this case, cysteine 117 into histidine (Ve *et al.*, 2017); (ii) a version bearing an inactive myristoylation signal (TRAM G2A) (Funami *et al.*, 2017); and (iii) two acidic residues identified as key for proper TRAM endosomal location (Funami *et al.*, 2017), were turned into alanines (D91A E92A, designated as TRAM DEAA). None of the mutants altered yeast growth and they were efficiently expressed upon induction in the yeast cell as determined by Western blotting (Fig 33). The TRAM DEAA protein band appeared as a slightly faster-migrating band, compared with the other versions. This was already reported in transfected human cell experiments (Funami *et al.*, 2015), probably caused by global changes in the electrostatic charges of the protein.

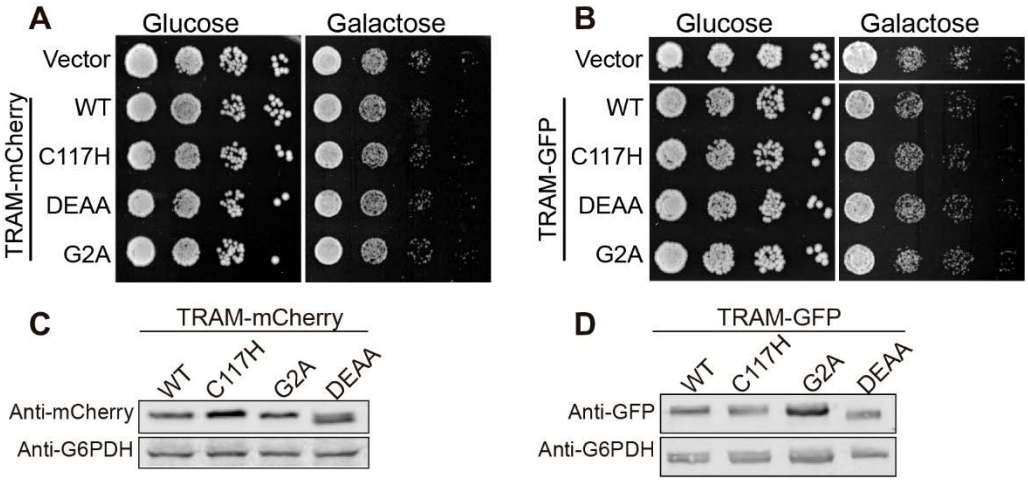

Fig 33.- Expression of TRAM mutants.

Ten-fold serial dilution assay of YPH499 yeast cells bearing empty vector (pYES3) and expressing TRAM-mCherry WT and the indicated mutants from pYES3 derivative plasmids (A) or another empty vector (YCpLG), and expressing TRAM-GFP WT and corresponding mutants form YCpLG derivative plasmids (B). Cells were cultured under repression in SD agar medium (Glucose) and induction in SG agar medium (Galactose) for 72h. Western blotting of YPH499 yeast extracts transformed with (C) pYES3 (vector) and the same TRAM-mCherry constructs as in (A), or (D) YCpLG TIRAP-GFP WT and the same samples as in (B). Blots were developed using antibodies anti-mCherry (C, upper panels) and anti-GFP (D, upper panels) followed by anti-G6PDH as a loading control (lower panels).

Interestingly, each TRAM mutant showed a different location when analyzed by fluorescence microscopy (Fig 34). Instead of forming the typical PM-associated long filaments described above for TRAM WT, the BB loop mutant TRAM C117H, predominantly decorated inner membranes, presumably the yeast vacuole, as well as the PM. This reflects that, despite keeping intact its membrane-targeting signal, it cannot generate filaments, probably because self-interaction is impaired. Besides, the vacuolar signal may result from endocytosis. On the other hand, the TRAM G2A mutant, lacking the N-terminal myristoylation signal, appears ubiquitously along the cytosol. Thus, it has lost both filament formation and membrane targeting features. This indicates that efficient PM targeting is a prerequisite for TRAM filament formation in the yeast model. The TRAM DEAA mutant was mostly found in inner membranes, like C117H, but about 3-4% of cells were still able to generate the typical filaments. In some cells, both filaments and vacuoles could be identified (Fig 35). This points out that the two acidic residues are important but not critical for TRAM filament formation in the yeast model.

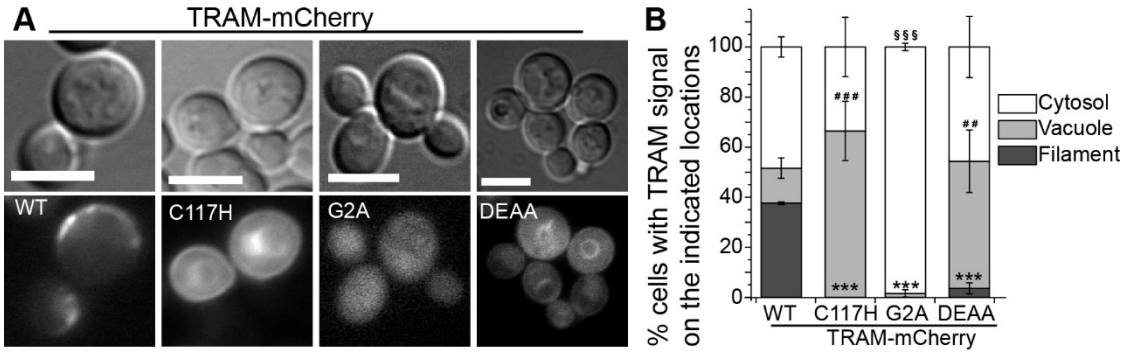

Fig 34.- The TRAM mutants vary their location.

(A) Nomarski and fluorescence microscopy of YPH499 yeast cells bearing TRAM-mCherry WT and the indicated mutants expressed from pYES3 derivative plasmids. Scale bars correspond to 5 µm. (B) Graph displaying the percentage of yeast cells showing TRAM-mCherry signal on either PM filaments, vacuoles, or along the cytosol. Data correspond to means ± standard deviation of three independent transformants (n ≥ 100). One-way ANOVA statistical comparison: (i) of filament data led a p-value < 0.001 (***) for WT vs the other three mutants, (ii) of vacuole data led a p-value < 0.001 (###) for WT vs CH, and a p=0.006 (##) for WT vs DEAA; and (iii) of cytosol data led a p-value < 0.001 (§§§) for WT vs G2A.

To verify that the inner membranes in which TRAM C117H and TRAM DEAA mutants localize correspond to yeast vacuoles, the FM4-64 vital dye was used (Vida and Emr, 1995). This non-permeable molecule gets internalized into the yeast cell following the endocytic pathway. After 1h of incubation, it stains the vacuole with a fluorescent red signal. The FM4-64 signal was coincident with the inner membranes where these TRAM mutants localize (Fig 35), confirming their vacuole targeting in yeast.

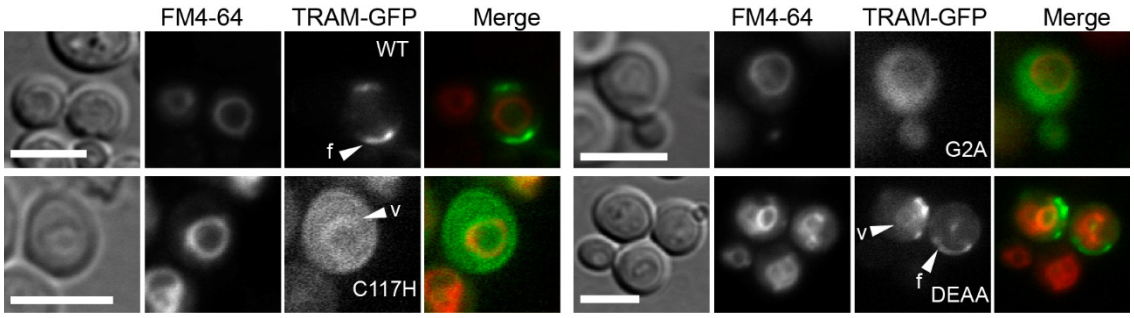

Fig 35.- Vacuole visualization using FM4-64.

Nomarski and fluorescence microscopy of YPH499 yeast cells bearing TRAM-GFP and the indicated mutants, from YCpLG plasmid derivatives, after 1h treatment with FM4-64 vital dye. White arrows indicate TRAM on vacuolar membranes (v) or filaments (f). Scale bars correspond to 5 µm.

1.4.4.- The release of TRAM from PM-associated filaments does not favor co-localization with TRIF.

Having lost their ability to form filaments by self-interaction, TRAM mutants may expose now interacting interfaces that remained hidden inside the filament. This may plausibly allow for its partner TRIF to co-localize in the yeast cell. Nevertheless, the co-expression of EGFP-TRIF with the C117H, G2A, and DEAA TRAM-mCherry mutants did not show any co-localization events (Fig 36), indicating that none of these TRAM changes favored TRIF recruitment.

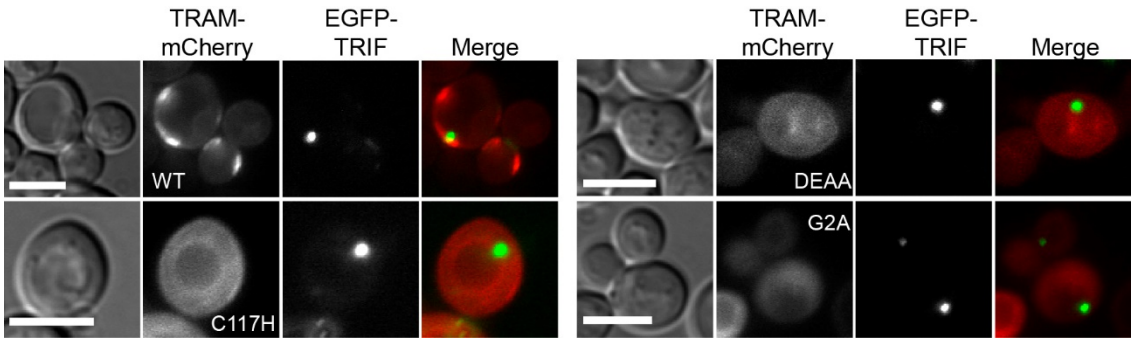

Fig 36.- Co-expression of TRIF and the TRAM mutants.

Nomarski and fluorescence microscopy of YPH499 yeast cells co-expressing EGFP-TRIF and TRAM-mCherry WT or the indicated mutants, from pAG425GAL-EGFP-TRIF or pYES3-TRAM-mCherry plasmid derivatives. Scale bars correspond to 5 µm.

1.4.5.- Mutation of the TRIF BB loop does not alter its localization in yeast.

On the TRIF construct, a single point mutation was introduced: the conserved BB loop proline was turned into histidine (Ve *et al.*, 2017). The TRIF P343H mutant did not cause any toxicity in yeast (Fig 37A) and was expressed properly, as verified by immunoblotting (Fig 37B). Like WT TRIF, the mutant localized in 1-2 cytoplasmic spots per cell (Fig 37). Thus, the canonic BB loop mutation in the TRIF TIR domain did not alter its localization pattern in yeast.

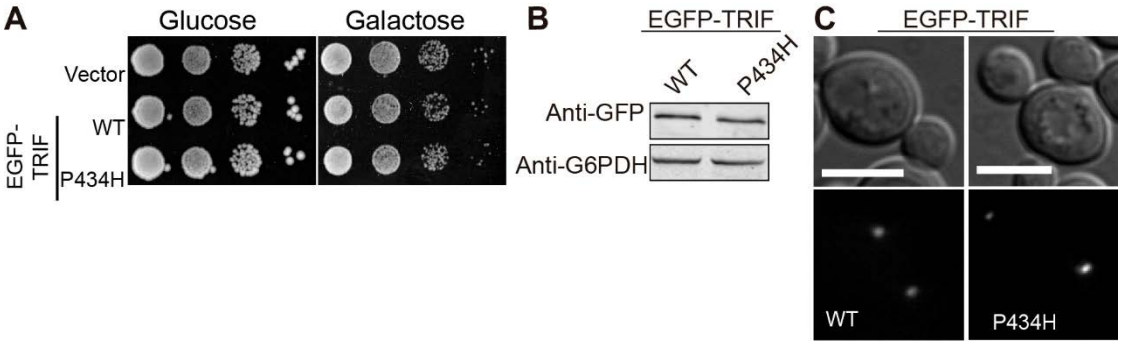

Fig 37.- Expression of the TRIF BB loop mutant.

(A) Ten-fold serial dilution assay of YPH499 yeast cells bearing pAG425GAL-EGFP plasmid (vector) and expressing EGFP-TRIF WT and the P434H mutant from pAG425GAL-EGFP derivative plasmids. Cells were

cultured under repression in SD agar medium (Glucose) and induction in SG agar medium (Galactose) for 72h. (B) Western blotting of YPH499 yeast extracts transformed with the same EGFP-TRIF constructs as in (A), developed using antibodies anti-GFP (upper), followed by anti-G6PDH as a loading control (lower). (C) Nomarski and fluorescence microscopy of YPH499 yeast cells bearing EGFP-TRIF WT and the P434H mutant from pAG425GAL-EGFP derivative plasmids. Scale bars correspond to 5 µm.

2.- Assessing TIR-containing effectors from *Brucella abortus* in *Saccharomyces cerevisiae*.

2.1.- Expression of *Brucella abortus* TIR-domain containing proteins in yeast.

2.1.1.- BtpA and BtpB induce yeast growth inhibition through their TIR domains.

To bring a new perspective into the research of *Brucella* T4SS-translocated TIR-containing proteins BtpA and BtpB and decipher additional roles in modulation of cellular functions, *B. abortus* genes *btpA* and *btpB* were cloned on yeast expression pYES2 derivative plasmids. They were set under the control of the *GAL1* promoter-and fused to an N-terminal GFP tag. Serial dilution agar plate growth assays showed both GFP-BtpA and GFP-BtpB to be inhibitory for yeast growth, although the expression of the latter was much more toxic (Fig 38). Both effectors have their TIR domains on the C-terminal region, but their N-terminal sides are quite different. To tell apart which domain was responsible for yeast toxicity, both bacterial effectors were split to individually express the N- and C-terminal halves of the proteins. Thus, GFP fusions to BtpA-N (1-126) and BtpA-TIR (127-275), and BtpB-N (1-139) and BtpB-TIR (140-292) were produced. Both isolated TIR domains were still able to cause toxicity. In contrast, the N-terminal regions did not affect yeast growth (Fig 38). Interestingly, the TIR domain of BtpA was more toxic than the full-length protein, suggesting that the N-terminal region may play a regulatory role in the TIR domain activity of BtpA.

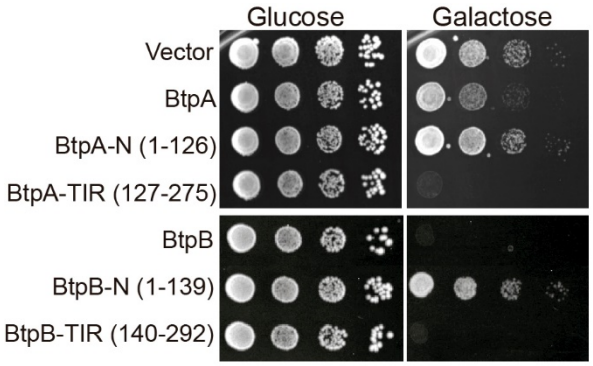

Fig 38.-The *Brucella* TIR effectors inhibit yeast growth.

Ten-fold serial dilution assay to monitor growth in YPH499 yeast strain expressing the pYES2 empty vector or the BtpA or BtpB indicated versions (full-length, N, and TIR) from pYES2-GFP plasmid derivatives. Cells were cultured under repression in SD agar medium (Glucose) and induction in SG agar medium (Galactose) for 72h.

2.1.2.- The *Brucella* TIR domains form filamentous structures in the yeast cell.

At the fluorescence microscope, GFP-BtpA was enriched in yeast nuclei, as its signal coincides with DAPI staining (Fig 39A). On the other hand, GFP-BtpB is localized in 1-4 cytoplasmic spots per cell (Fig 39B). Regarding truncated versions, N-terminal sides kept a similar subcellular localization as their respective full-length proteins: BtpA-N being at the nucleus and BtpB-N forming spots (Fig 39C). Despite their limited sequence identity (19.92%), TIR domains from both GFP-BtpA-TIR and GFP-BtpB-TIR behaved in the same way, assembling themselves into long cytoplasmic filaments (Fig 39D).

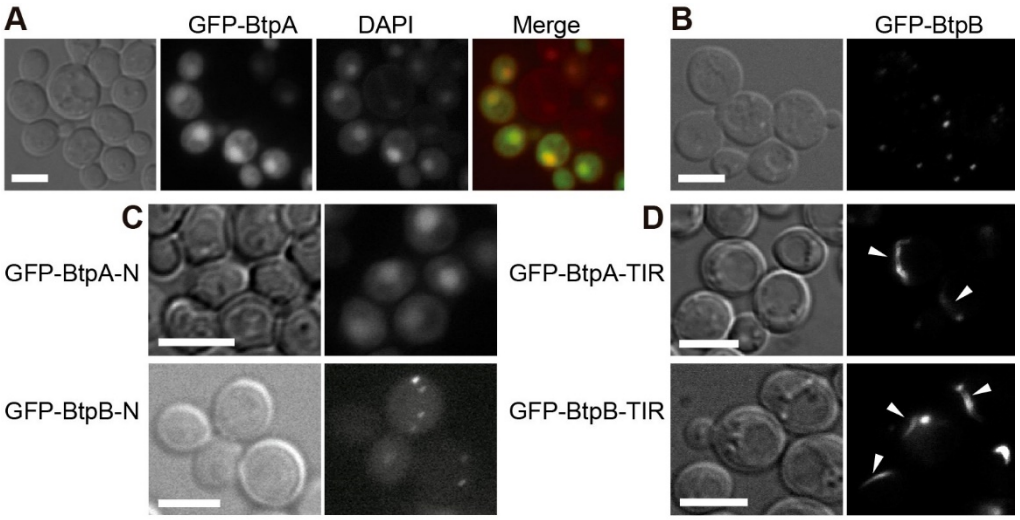

Fig 39.- Localization of the *Brucella* TIR effectors.

Nomarski and fluorescence microscopy of YPH499 yeast strain expressing from pYES2 plasmid derivatives the following fusion proteins: (A) full-length GFP-BtpA (green) and stained with DAPI (red), after 6h induction; (B) full-length GFP-BtpB after 4h induction; the GFP-fused N-terminal regions (C) or TIR domains (D) of BtpA and BtpB after 5h and 4h induction respectively. Arrows indicate the cytosolic filaments. Scale bars represent 5 µm.

Such stable long filaments inside the cytoplasm, marked by the TIR domains, suggested that they could belong to internal yeast filamentous structures, like the tubulin cytoskeleton. Indeed, BtpA had been described to have microtubule-stabilizing properties (Radhakrishnan *et al.*, 2011). Therefore, to test whether the filaments co-localized with microtubules, immunofluorescence was performed, using an anti-tubulin antibody on GFP-BtpA/B-TIR-expressing cells, and DAPI was used for nuclear staining (Fig 40). Although the heterologous structures occasionally surrounded or contacted the yeast nucleus, no co-localization between TIR filaments and tubulin was detected. While we cannot completely exclude the possibility that *Brucella* TIR domains are interacting with other internal yeast filamentous structures, our data indicate that they can

assemble into complex structures via self-interaction. Moreover, their N-terminal counterpart is probably downregulating this feature, as full-length BtpA and BtpB do not form such filaments.

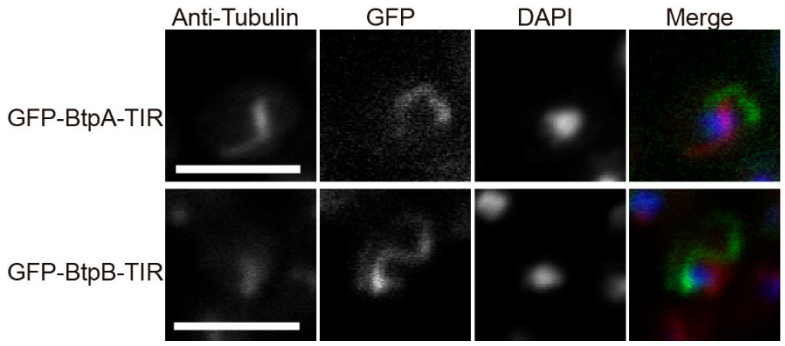

Fig 40.- BtpA-TIR and BtpB-TIR do not coincide with yeast tubulin.

Indirect immunofluorescence of YPH499 yeast cells expressing GFP-BtpA-TIR or GFP-BtpB-TIR (green) after 4h induction from pYES2 plasmid derivatives. Microtubules are stained using an anti-tubulin antibody (red). Nuclei are labeled with DAPI (blue). Scale bars represent 5 µm.

2.2.- BtpB depolarizes actin patches, severely blocks endocytosis, and globally downregulates cell signaling in *S. cerevisiae.*

Prior to this Ph.D. project, preliminary experiments performed in our lab by María Rodríguez-Escudero on BtpB-expressing yeast lead to the observation of actin depolarization. The actin cytoskeleton is required for polarized growth in *S. cerevisiae* during budding, so it could be probably targeted by bacterial effectors to arrest cell growth. Indeed, staining of actin cortical patches with rhodamine-conjugated phalloidin showed that BtpB promoted a dramatic loss of polarization of actin structures towards the growing bud and septum region. Besides, such phenotype fully relied on the BtpB TIR domain, and no alterations were identified on yeast expressing the BtpB-N terminal domain (Coronas-Serna *et al.*, 2020a) (Fig 41).

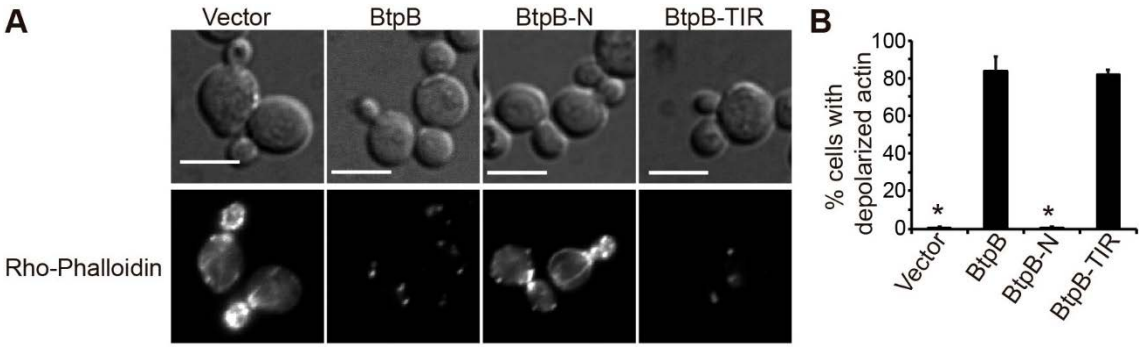

Fig 41.- BtpB depolarizes actin patches in yeast.

(A) Nomarski and fluorescence microscopy of a rhodamine-phalloidin (Rho-Phalloidin) staining of YPH499 cells expressing pYES2-GFP empty vector, BtpB, BtpB-N, or BtpB-TIR after 4h induction. (B) Graph showing

the percentage of small- to medium-budded cells with depolarized actin. Data correspond to means ± standard deviation of three independent transformants (n ≥ 100) and statistical comparison was done with Kruskal-Wallis ANOVA with p-values referring to BtpB of 0.024 (*) for vector and BtpB-N. Scale bars represent 5 µm. These data were obtained prior to this Ph.D. project (Coronas-Serna *et al.*, 2020a).

Actin is not only fundamental for supporting budding, its function is also relevant for endocytosis. Indeed, preliminary data pointed out to an endocytic blockage upon BtpB expression. We took advantage of the FM4-64 fluorochrome to track endocytic traffic (Vida and Emr, 1995). Yeast cells actively expressing GFP-BtpB (showing intense green fluorescent dots) were unable to internalize FM4-64, unlike control cells expressing GFP alone (Fig 42A, C). Truncated versions were also examined (Fig 42B), being the TIR domain fully responsible for this phenotype. This result points out that BtpB, and its isolated TIR domain, vastly block yeast endocytosis.

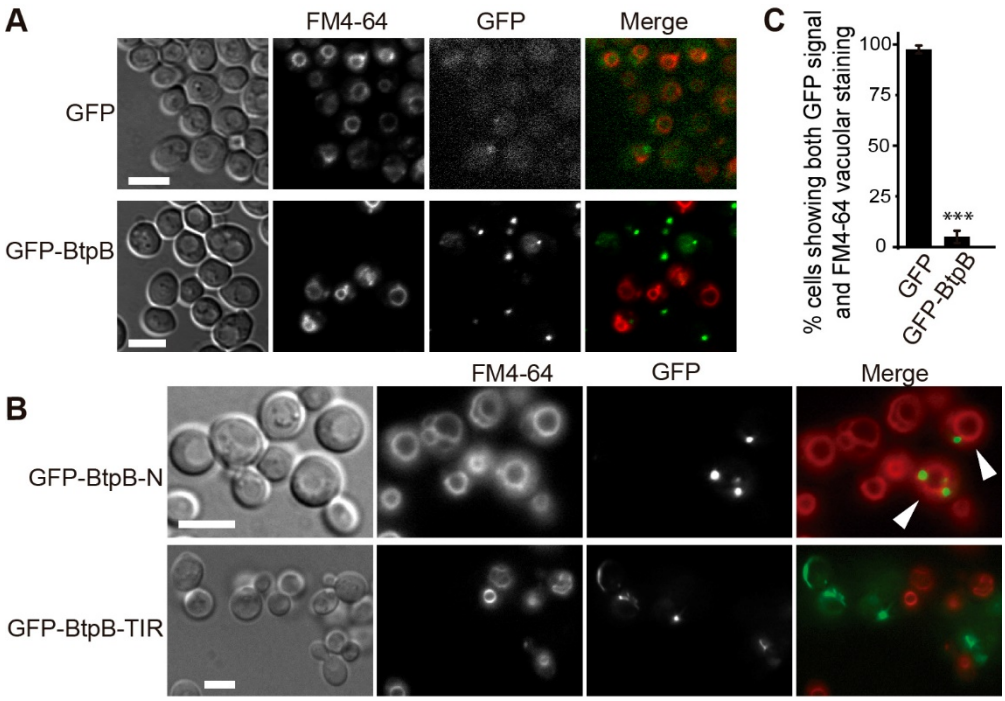

Fig 42.- BtpB impairs yeast endocytosis.

Nomarski and fluorescence microscopy of YPH499 cells expressing pYES2-GFP or pYES2-GFP-BtpB (A) or the truncated versions, from pYES2 plasmid derivatives (B), after 4h induction, stained with the endocytic marker FM4-64 for 1h. (C) Graph representing the percentage of cells expressing pYES2-GFP or pYES2-GFP-BtpB that show both GFP and FM4-64 vacuolar signal. Data correspond to means ± standard deviation of three independent transformants (n ≥ 100) and statistical comparison was done with Student´s t-test, $p < 0.0001$ (***). Scale bars represent 5 µm.

Frequently, mitogen-activated protein kinase (MAPK) signaling pathways become activated by stressors spoiling actin function, like the cell wall integrity (CWI) pathway, engaging the Slt2 MAPK (Harrison *et al.*, 2001). Previous research from our group showed that yeast expressing *Salmonella* effectors SopB and SteC (Fernandez-Piñar *et al.*, 2012; Rodríguez-Escudero *et al.*, 2006) alter actin polarization by switching off small GTPases, triggering parallel dephosphorylation of downstream Fus3 and Kss1 MAPKs of the mating pathway. Preliminary results from our lab also showed an alteration in MAPK phosphorylation levels in yeast cells expressing BtpB. In the present Thesis, we decided to further analyze this effect both in BtpB and BtpA. As shown in Fig 43 all Slt2, Fus3, and Kss1 MAPK basal phosphorylation levels were downregulated upon BtpB, but not BtpA, yeast expression.

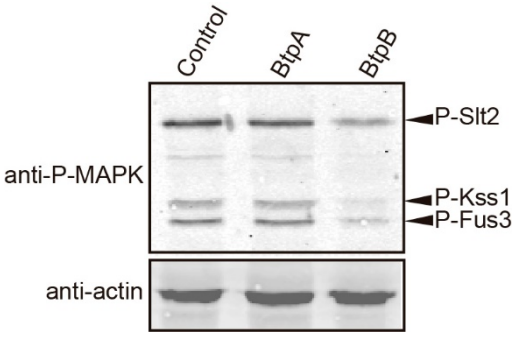

Fig 43.- BtpB impairs yeast MAPK basal activation.

Western blotting from YPH499 cells extracts bearing the empty vector pYES2 (control), BtpA, or BtpB from pYES2-GFP plasmid derivatives, developed with anti-P-MAPK antibody to detect dually-phosphorylated Slt2, Kss1, and Fus3 (upper panel) and anti-actin as a loading control (lower panel).

Next, we tested if BtpB would downregulate MAPK activation not only at basal levels but also under an effective stimulation of the pathways. To stimulate the CWI route, yeasts were incubated at higher temperatures (39ºC) or treated with the cell wall-stressing compound Congo red. The mating pheromone α-factor was also used to activate Fus3 and Kss1. Although BtpB still allowed activation of these pathways by the corresponding stimuli, MAPK phosphorylation was always less efficient (Fig 44).

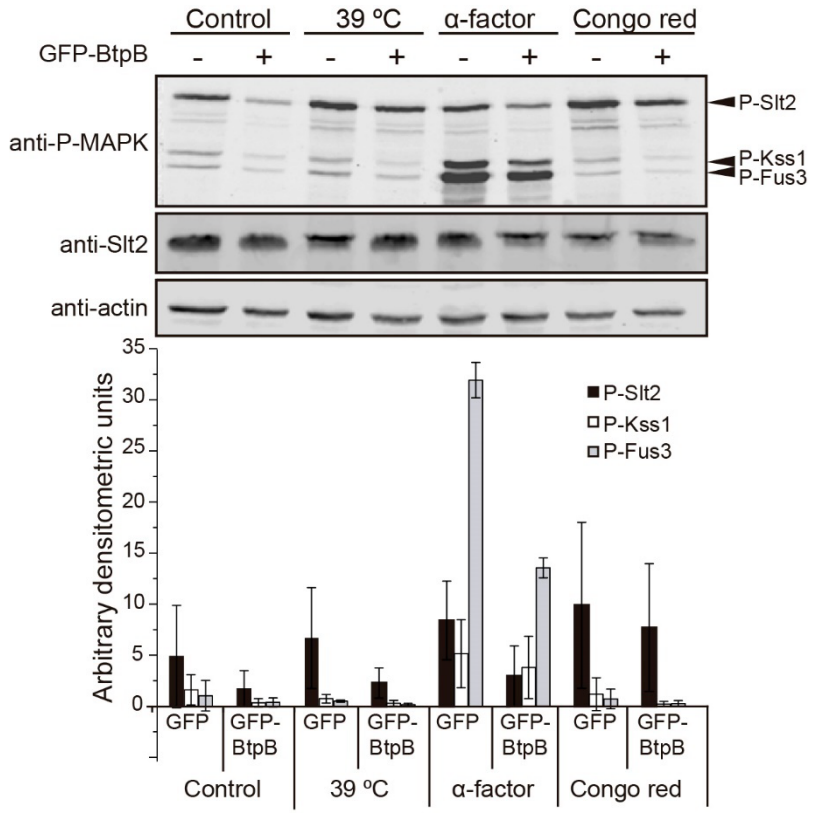

Fig 44.- BtpB reduces MAPK activation upon stimulation.

(A) Western blotting from YPH499 yeast cell lysates bearing pYES2 (-) or pYES2-GFP-BtpB (+) and upon different conditions: 30ºC (control), high temperature (39ºC), pheromone (α-factor) or Congo red, using anti-P-MAPK (upper panel), anti-Slt2 (medium panel) and anti-actin (lower panel) as a loading control. (B) Densitometric measurement of bands corresponding to phosphorylated MAPKs Slt2, Kss1, and Fus3. The graph displays densitometric data of phosphorylated MAPKs normalized against actin and error bars show the standard deviation from three independent experiments on different transformant clones.

Other experiments, previously performed in our lab, pointed out that other non-related kinases, such as the Hog1 MAPK from the high osmolarity pathway (Brewster and Gustin, 2014) or the mammalian Akt1, which becomes phosphorylated by conserved PDK-like kinases when expressed in yeast (Rodríguez-Escudero *et al.*, 2005b), were also less efficiently phosphorylated when BtpB was present (Coronas-Serna *et al.*, 2020a). Such a wide effect in protein phosphorylation might reflect a general impairment of cellular phosphorylation events.

2.3.- A genetic screen for yeast genes that suppress BtpB-induced lethality.

Aiming to identify possible yeast target genes of BtpB, we carried out a genetic screen using a whole-genome yeast ORF collection (GE Healthcare), consisting of all *S. cerevisiae* predicted ORFs cloned into a vector for inducible *GAL1* promoter-driven overexpression. The collection,

transformed in *E. coli*, was pooled into three non-overlapping libraries, which in turn were independently co-transformed with a plasmid expressing GFP-BtpB also from the *GAL1* promoter. Once plated on galactose medium, only yeast overexpressing a yeast ORF able to suppress BtpB toxicity were recovered (Fig 45).

Seven suppressor genes listed in Table 16 were selected when growth rescue (i) was confirmed after individual re-transformation, (ii) was specific for BtpB-induced growth inhibition, but not that caused by other toxic heterologous protein (PI3Kα-CAAX) (Rodríguez-Escudero *et al.*, 2005b), and (iii) was not due to lower production of GFP-BtpB, as verified by Western blotting (Fig 46B). As shown in Fig 46A, suppression was partial in all cases.

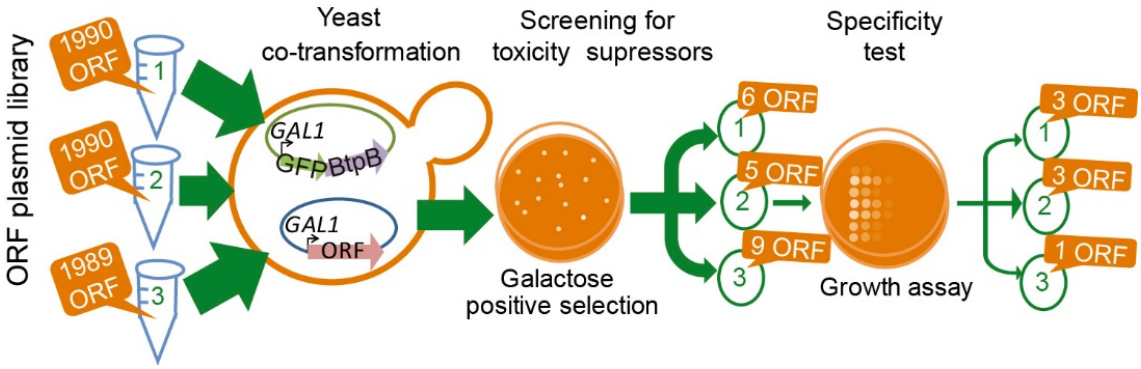

Fig 45.- Scheme of the screen by yeast ORF overexpression.

Drawings were generated using Microsoft PowerPoint and Adobe Illustrator CS6.

Table 16.- Yeast genes that suppress BtpB-induced toxicity when overexpressed.

GO	ORF	Protein	Protein function (times isolated)
Metabolism	*YHR043C*	*DOG2*	2-deoxyglucose-6-phosphate phosphatase; confers 2-deoxyglucose resistance when overexpressed. (1)
	YCR036W	*RBK1*	Putative ribokinase. (1)
	YGR259C	*YGR259C*	Dubious open reading frame; overlaps almost completely with the verified ORF *TNA1/YGR260W.* (3)
	YDR287W	*INM2*	Inositol monophosphatase, involved in the biosynthesis of inositol. (1)
Ubiquitin-proteasome	*YMR022W*	*UBC7*	Ubiquitin-conjugating enzyme; involved in the ERAD pathway and in the inner nuclear membrane-associated degradation pathway. (3)
	YGL004C	*RPN14*	19S proteasome regulatory particle (RP) assembly-chaperone; putatively involved in the assembly of the proteasome base subcomplex. (1)
pH regulation	*YGR122W*	*YGR122W*	A protein of unknown function, a probable ortholog of *Aspergillus nidulans* PalC, which is involved in pH regulation and binds to the ESCRT-III complex. (1)

Gene data come from the *Saccharomyces* Genome Database (Cherry *et al.*, 2012). Abbreviations: Gene ontology (GO).

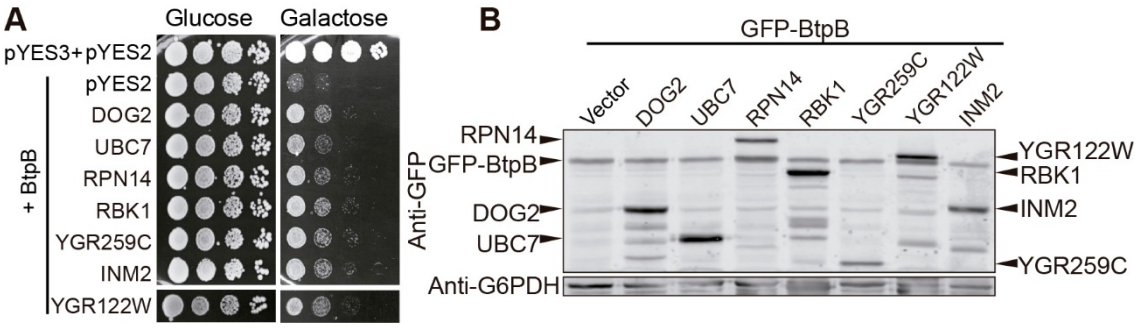

Fig 46.- Checking the hits from the yeast ORF overexpression screen.

(A) Ten-fold serial dilution assay of W303-1A yeast cells co-expressing BtpB from the pYES3-GFP-BtpB plasmid and each of the seven indicated suppressor ORFs isolated from a yeast genetic screen, from the yeast ORF collection (GE Healthcare). pYES3 and pYES2 are the corresponding empty vectors for BtpB and the overexpressed genes, respectively. Cells were cultured under repression in SD agar medium (Glucose) and induction in SG agar medium (Galactose) for 72h. (B) Western blotting of W303-1A yeast strain co-expressing GFP-BtpB, from pYES3-GFP-BtpB, and each of the proteins encoded by the suppressor genes, from the yeast ORF collection (GE Healthcare), plus pYES2 as a control (vector). Antibodies anti-GFP to detect GFP-BtpB (upper panel) and Anti-G6PDH as a loading control (lower panel) were used. The anti-GFP antibody allows the detection of the indicated protein A-tagged proteins due to the affinity of the tag with the Fc region of IgG-type antibodies.

The co-transformation of these suppressors with BtpB-TIR led to the same rescue levels, although no growth recovery was detected when co-expressed with BtpA-TIR (Fig 47). Thus, either these suppressors are specific for BtpB-TIR domain derived toxicity in yeast, or the effect of BtpA-TIR on the cells is too strong to allow partial suppression.

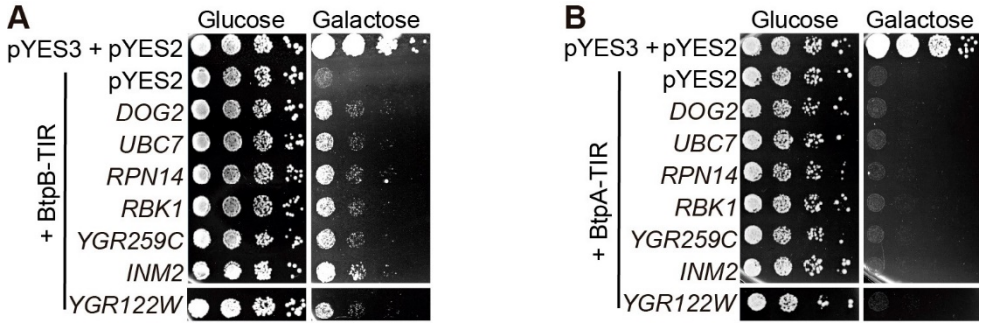

Fig 47.- Testing the suppressor genes vs BtpB-TIR and BtpA-TIR.

Ten-fold serial dilution assays of yeast cells co-expressing BtpB-TIR (A) or BtpA-TIR (B) from pYES3 derivatives, and the indicated suppressor genes, from the yeast ORF collection (GE Healthcare). pYES3 and

pYES2 are the corresponding empty vectors for BtpB- or BtpA-TIR and the overexpressed genes, respectively. Cells were cultured under repression in SD agar medium (Glucose) and induction in SG agar medium (Galactose) for 72h.

Although most of these genes have not been yet assigned a well-established function in yeast, three of them, INM2, RBK1, and DOG2 are sugar or inositol phosphorylating/dephosphorylating enzymes related to metabolic pathways (Table 16). DOG2 encodes a 2-deoxyglucose-6 phosphate phosphatase and its overexpression overcomes the toxicity of this glycolytic inhibitor (Randez-Gil *et al.*, 1995), and RBK1 encodes a putative ribokinase, which has been recently shown to be catalytically active (Schroeder *et al.*, 2018). These results suggest that metabolic changes related to carbon source usage partially prevent BtpB toxicity.

2.4.- BtpA and BtpB deplete ATP and NAD^+ in the yeast cell.

Previously observed phenotypes caused by BtpB yeast expression, affecting actin function, endocytosis, and a general impairment of MAPK signaling and protein phosphorylation, may be related to low cellular ATP levels. Moreover, the fact that three sugar kinase/phosphatases were able to suppress BtpB toxicity, points out that energy metabolism is compromised in BtpB-expressing yeast cells. Thus, we next measured the ATP levels in yeast cells expressing the *Brucella* TIR effectors. As shown in Fig 48A, cells bearing BtpB or the TIR domains of either BtpB or BtpA, showed a significant loss of ATP intracellular levels, as determined by luciferase assay.

During the development of this Ph.D. project, Essuman and collaborators reported that the TIR-domain of proteins from phylogenetically diverse bacteria, including BtpA, displayed enzymatic activity as NAD^+ hydrolases (Essuman *et al.*, 2018). Then, we decided to determine also the NAD^+ levels in yeast cells expressing the *Brucella* TIR effectors. Quantitative mass spectrometry measurements led to the detection of significant depletion of yeast cellular NAD^+ in the presence of the same constructs that dropped ATP levels (Fig 48). Interestingly, NAD^+ levels were lowered about one order of magnitude upon BtpB overexpression. Besides, a slight but significant reduction of NAD^+ was detected upon BtpA expression (Fig 48B). This reduction in ATP and NAD^+ correlated very well with the toxicity of the constructs (Fig 38): for example, BtpA-TIR caused a stronger effect on cellular NAD^+ and ATP than its full-length. As a control, we generated a BtpB catalytically inactive mutant (E234A), by changing to Ala the equivalent Glu residue described to be essential for catalysis in other TIR domains (Essuman *et al.*, 2018). As expected, the mutant neither affects NAD^+ nor ATP intracellular levels (Fig 48), indicating that the observed depletion of ATP is a consequence of the NAD+ elimination by the enzymatic activity of the TIR proteins.

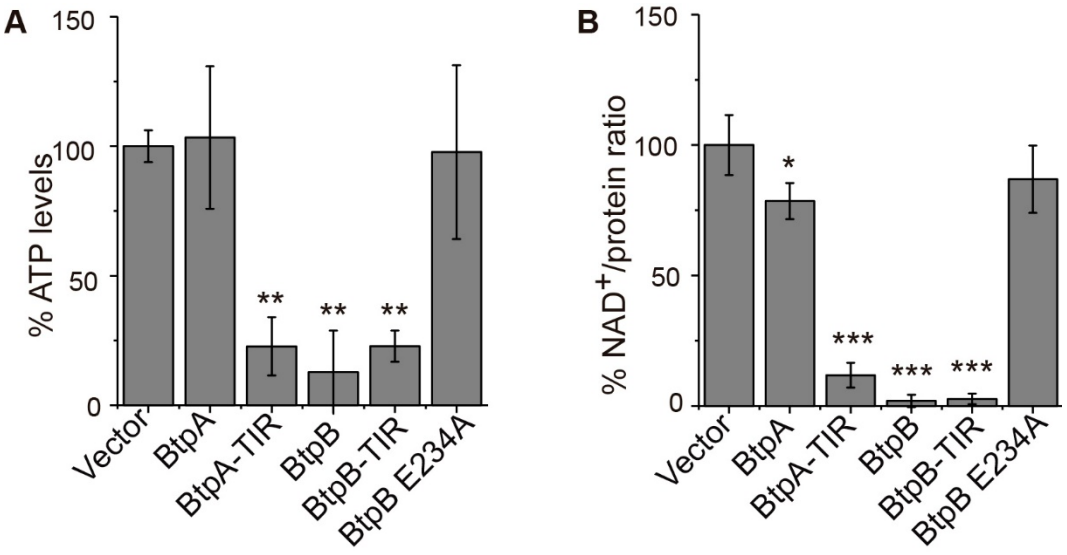

Fig 48.- Measurements of ATP and NAD^+ yeast levels.

(A) Cellular ATP measurement by luciferase assay in YPH499 cells transformed with pYES2 empty vector and pYES2 plasmid derivatives bearing both full-length and TIR domain versions of BtpA and BtpB and the catalytically inactive BtpB E234A mutant. The graph shows ATP levels as a percentage relative to the ATP levels measured on empty vector control cells. Results correspond to means ± standard deviation of three different transformants and statistical comparison was done with one-way ANOVA with p-values < 0.01 (**) referred to Vector of p=0.0045 vs BtpA-TIR, p=0.0017 vs BtpB and p=0.0046 vs BtpB-TIR. (B) Cellular NAD^+ levels measured by mass spectrometry, standardized as a NAD^+/extract protein ratio, from YPH499 cells transformed with the same plasmids as in (A). The graph shows the NAD^+/protein ratio as a percentage of the empty vector control cells NAD^+/protein ratio. Data correspond to means ± standard deviation of four different transformants and statistical comparison was done with one-way ANOVA with p-values < 0.0001 (***) for vector vs BtpA-TIR, BtpB and BtpB-TIR, and p=0.0134 (*) vs BtpA.

2.5.- Structure-function studies on the TIR effectors.

2.5.1.- Mapping of residues essential for NAD^+ hydrolase function at the TIR domain of BtpB.

Taking advantage of the severe toxicity of BtpB in yeast, a screen for the isolation of loss-of-function mutations by random mutagenesis was performed in our lab. This was performed by plasmid gap-repair (Andrés-Pons *et al.*, 2007), forcing *in vivo* homologous recombination between an open gapped plasmid and a partially overlapping insert encoding a BtpB-TIR containing fragment (118-292), which had been generated by error-prone PCR. This way, recombinant clones bearing mutations that make BtpB no longer toxic were directly selected in a galactose-based medium. Plasmid recovery and sequencing yielded ten single and two double BtpB mutants, two of them displaying a partial phenotype suppression (Fig 49).

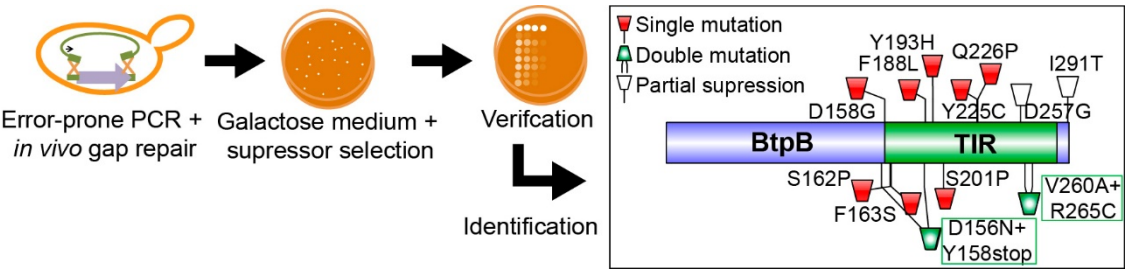

Fig 49.- Scheme of the random mutagenesis screen on BtpB including the mutations identified. See the text for more details. Drawings were generated using IBS, Microsoft PowerPoint, and Adobe Illustrator CS6.

Most mutations corresponded to non-conservative amino acid changes in highly conserved regions between BtpA and BtpB TIR domains, namely D158G, S162P, F163S, F188L, Y193H, S201P, Y225C, Q226P, and I291T (Fig 50). Some of these residues were also conserved in the TIR-domain of human SARM1 and plant RUN1, in which the NAD^+ hydrolytic activity had been recently described (Essuman *et al.*, 2017; Horsefield *et al.*, 2019).

```
BtpB-TIR      -------FDVGLSFPGEARGLVEQVARELEARV--GPNAYFYDNNYVSQLARPSLDTLLQ  208
BtpA-TIR      -------YDFFISHASEDKE---AFVQDLVAALRDLGAKIFYDA-YTL-KVGDSLRRKID  191
HsSARM-TIR    -------PDVFISYRRNSGS---QLASLLKVHLQLHGFSVFIDV-EKL-EAGKFEDKLIQ  609
RUN1-TIR      SNARTITYDVFLSFRGEDTR--FNFTDHLYSALGRRGIRTFRDD--KL-RRGEAIAPELL  74
                      *. :*.  :     .   : *:  :       * *    : . .      :

BtpB-TIR      DIYRNRCKLIVVFVGD--------DYQRKDWCGVEFRAIREIIMARAEQR----IMFVRV  255
BtpA-TIR      QGLANS-KFGIVVLSE--------HFFSKQWPARELDGLTAMEI---GGQTRILPIWHKV  239
HsSARM-TIR    SVMGAR-NFVLV-LSPGALDKCMQDHDCKDWVHKEIVT--A--L---SCGKNIVPIIDGF  660
RUN1-TIR      KAIEES-RSSVIVFSE--------NYARSRWCLDELVKIMECHKDKKDPGHAVFPIFYHV  125
                 .    .  :: ..         ..  . *   *:                 :   .

BtpB-TIR      D-------DGAVDGVFRTDGYVDARRFNPSEIAQF---IAERVAL---------------  290
BtpA-TIR      S-------------------YDEVRRFSPS--------LADKVALNTSLKSVEEIAKELH  272
HsSARM-TIR    E-------------------WPEPQVLPED--------MQAVLTFNGIKWSHEYQEATIE  693
RUN1-TIR      DPSHVRKQEGSFGEAFAG--YGENLK---DKIPRWRTALTEAANLSGWPL-QDGYESNQI  179
              .                   : :      .       :     :

BtpB-TIR      --ITT-------------------------  292
BtpA-TIR      SLI-------------------------  275
HsSARM-TIR    KIIRFLQGRS-SRDSSAGSDTSLEGAAP  720
RUN1-TIR      KEITDSIFRRLKCKRLDAG---------  198
                *
```

Fig 50.- Alignment of protein sequences of the TIR domains of BtpB, BtpA, human SARM1, and plant RUN1. Conserved residues that were found mutated in the screen are marked according to their properties (see Fig 51A) and in magenta, the WxxxE residues W213 and E217, which belong to the catalytic site for NADase activity.

To understand the effects of the mutations on BtpB properties, we used a resolved structure of the BtpA-TIR domain (PDB: 4LZP) (Kaplan-Türköz *et al.*, 2013), as the BtpB structure is not yet solved. With the help of Dr. Laurent Terradot (CNRS, France), we mapped on the BtpA structure, the corresponding residues to those found in BtpB-TIR (Fig 51). None of the residues mutated belonged to the TIR-TIR interface. S162 (S149 in BtpA) and F163 (H150 in BtpA) belong to the βA strand. Y225 (F208 in BtpA) and Q226 (F209 in BtpA) are part of the small helix αC. Mutations of

these residues are likely to disrupt the inner core and thus destabilize the whole structure. Mutation of BtpB S201P (S185 in BtpA) probably perturbs the NAD^+ catalytic site. In the recent crystal structure of the $NADP^+$-bound RUN1-Tir domain (Horsefield *et al.*, 2019) (PDB: 6O0W), the substrate lies in a pocket formed by the BB-loop and the loop containing the conserved catalytic WxxxE motif (Felix *et al.*, 2014) (Fig 51B). In BtpA structure S185 lies in the BB loop and interacts with the W213 (W231 in BtpB) of the WxxxE motif, which contains the essential catalytic E217 residue (E234 in BtpB). Finally, D158 (D145 in BtpA), F188 (F174 in BtpA), Y193 (Y178 in BtpA), and I291 (I275 in BtpA) residues clustered in two patches at the protein surface (Fig 51A).

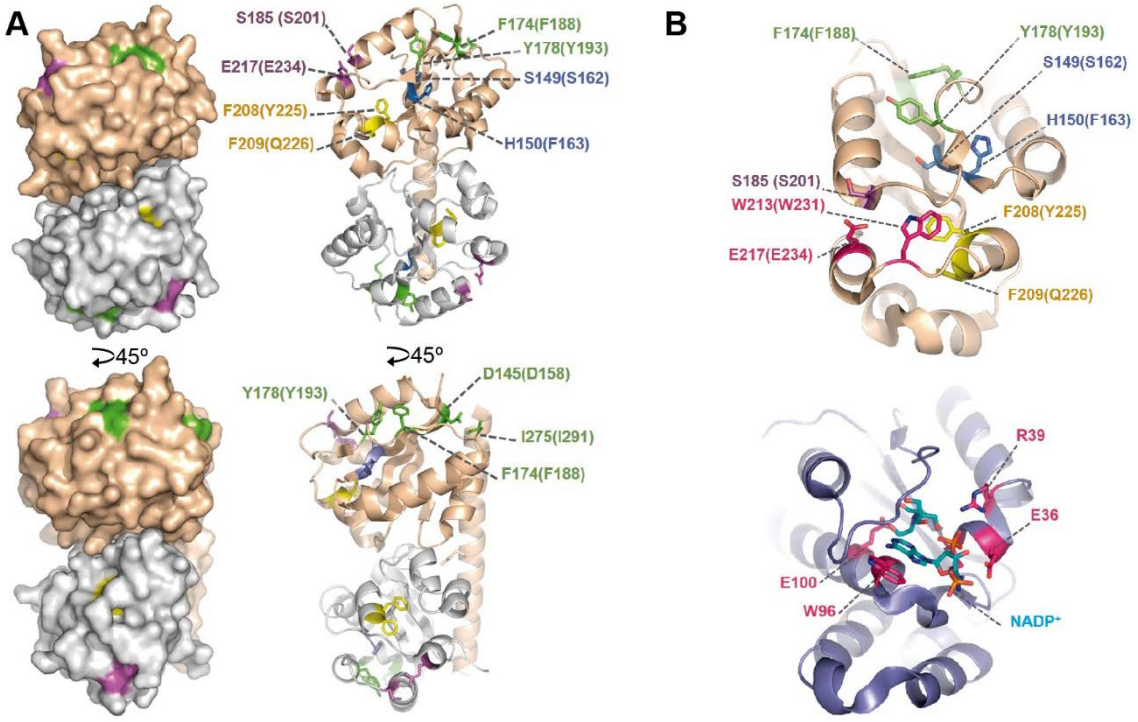

Fig 51.- Mapping on the BtpA-TIR structure the BtpB mutations found on the screen.

(A) Structure of the BtpA-TIR domain showing the positions equivalent to those identified as loss-of-function in BtpB by yeast random mutagenesis screening. Left panels: two views of BtpA-TIR dimer structure (PDB: 4LZP) with chain A colored in wheat and chain B in grey. Residues identified are colored according to their assigned properties. Positions of the mutations putatively affecting protein folding are colored in blue (βA strand) and yellow (αC helix). Mutations at the active site are colored in magenta. Mutations at the surface outside the active site are colored in green. Right panels: views in the same orientation of the BtpA dimer depicted as a cartoon with the side chains of mutated residues displayed as ball-and-stick. Residue numbers are indicated for BtpA and the corresponding residues in BtpB are in parenthesis. (B) Structure of BtpA-TIR (upper; PDB: 4LZP)) and RUN1-$NADP^+$ complex (lower; PDB: 6O0W), showing the equivalent positions of residues mutated in BtpB isolated in the yeast screen. Both cartoon structures are displayed in the same orientation. Side chains of mutated residues of BtpA relevant for this study are colored as in (A). The side chains of residues of the catalytic site of RUN1 are shown as ball-and-

stick and colored in pink and the $NADP^+$ ligand is colored in cyan. Specific atoms are colored as follows: nitrogen in blue, oxygen in red, and phosphorus in orange. Generated with PyMol.

2.5.2.- NAD^+ hydrolase activity and filament formation depend on different residues.

Knowing that the mutants obtained from the screen were able to avoid BtpB-derived yeast toxicity and, therefore, presumably had impaired NAD^+ hydrolase activity, we next checked whether these residues were or not required for the TIR domain filament formation. So, mutations D158G, S162P, and Y225C, as well as the catalytically inactive E234A, were transferred to the GFP-BtpB-TIR construct. This way, a correlation between loss of toxicity and the ability of the TIR domain alone to produce filaments would be identified. Interestingly, only E234A, S162P, and, partially, Y225C mutations eliminated BtpB-TIR toxicity in yeast cells, even though all four mutations fully prevented toxicity and endocytosis defects in full-length BtpB (Fig 52).

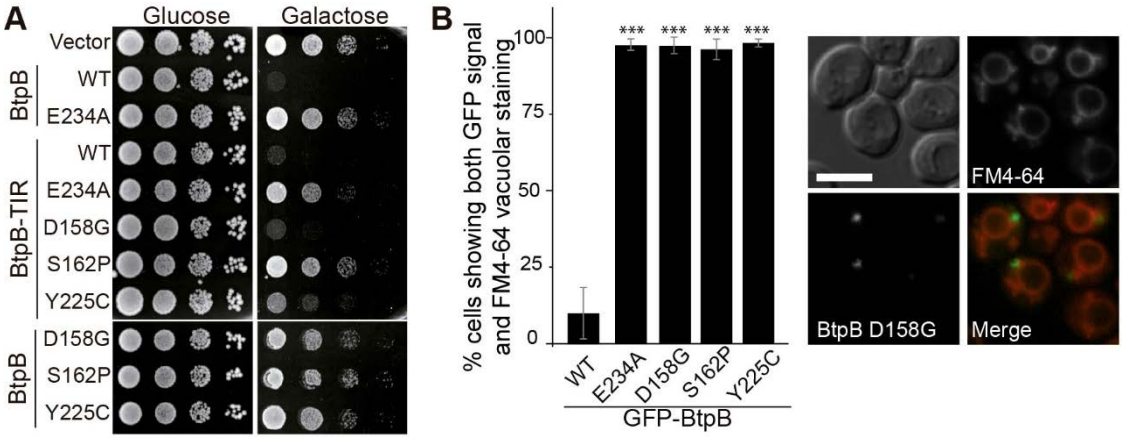

Fig 52.- Expressing the BtpB and BtpB-TIR mutants.

(A) Ten-fold serial dilution growth assay of YPH499 cells expressing pYES2 empty vector, BtpB full-length, BtpB-TIR, and the indicated mutants from pYES2 plasmid derivatives. Cells were cultured under repression in SD agar medium (Glucose) and induction in SG agar medium (Galactose) for 72h. (B) Graph representing the percentage of YPH499 cells, transformed with GFP-BtpB and the indicated mutants that, in 4h induction, display both GFP and FM4-64 vacuolar signal after 1h incubation (left) and representative Nomarski and fluorescence microscopy from BtpB D258G as an example (right). Results correspond to means ± standard deviation of three independent transformants ($n \geq 100$) and statistical comparison was done with one-way ANOVA with a p-value < 0.0001 (***) for all four mutants versus WT. Scale bars represent 5µm.

Regarding filament formation, only the GFP-BtpB-TIR S162P mutant significantly lost the ability to form protein filaments (Fig 53), probably because that mutation damaged the inner core (Fig 51A). These results indicate a segregation between filament formation and growth inhibitory

functions of BtpB-TIR in yeast and highlight the importance of the Glu234 residue specifically for NAD^+ hydrolase activity, while Ser162 is key for both features.

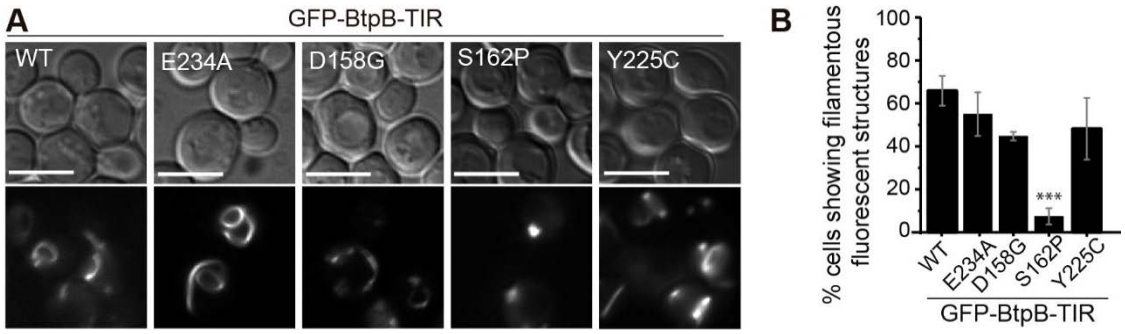

Fig 53.- Testing BtpB-TIR mutants for their ability to form filaments.

(A) Normarski and fluorescence microscopy of YPH499 cells expressing GFP-BtpB-TIR and the indicated mutants, from pYES2 derivative plasmids, after 4h induction. Scale bars represent 5 µm. (B) Graph displaying the percentage of cells showing filamentous fluorescent structures. Data correspond to means ± standard deviation of three independent transformants (n ≥ 100) and statistical comparison was done with one-way ANOVA with a p-value < 0.0001 (***) between BtpB-TIR WT and S162P.

All BtpB mutants and truncated versions were checked via Western blotting, to assess not only their protein expression levels but their ability to downregulate yeast MAPK phosphorylation. Growth inhibitory constructs BtpB WT, BtpB-TIR WT, and BtpB-TIR D158G (Fig 52A) showed fewer protein levels, compared with the N terminal half BtpB-N or the non-toxic mutants (Fig 54). On the other hand, BtpB-TIR Y225C, although displaying partial growth inhibition (Fig 52A), displayed a band as intense as other harmless mutants. Slt2 MAPK phosphorylation nicely correlated with toxicity, being not only BtpB WT and BtpB-TIR WT, but also BtpB-TIR D158G, and to a lower extent BtpB-TIR Y225C, able to cause a drop in P-Slt2 basal levels (Fig 54). In agreement, both Glu to Ala inactive mutants E234A, the full-length mutants, BtpB-TIR S162P, (Fig 52A), and BtpB-N (Fig 38) that do not cause growth inhibition displayed similar basal levels of P-Slt2 (Fig 54).

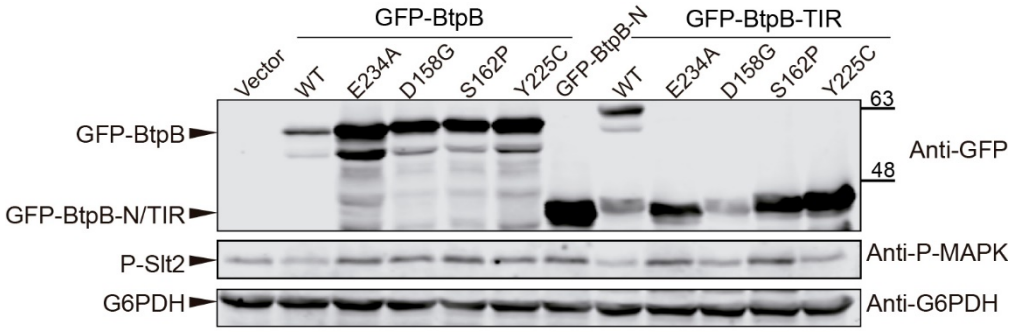

Fig 54.- Expression levels of the BtpB mutants.

Western blotting of YPH499 cells extracts bearing the indicated GFP-BtpB versions from pYES2 plasmid derivatives, and empty pYES2 as a control (vector), after 4h induction. The antibodies used were anti-GFP (upper panels), anti-P-MAPK to detect dual phosphorylation of Slt2 MAPK, and anti-G6PDH as a loading control (lower panels). The molecular weights of the constructs are: GFP-BtpB (60 kDa) GFP-BtpB-N (44 kDa) GFP BtpB-TIR (44kDa). Approximate molecular weights on the figure are expressed in kDa.

We also changed by site-directed mutagenesis the catalytic E217 residue to Ala in both full-length and the TIR domain alone of BtpA. As expected, the mutants lost their toxicity in yeast (Fig 55A). Although a statistically significant reduction in the percentage of cells showing BtpA-TIR filaments was found (Fig 55C), these structures were larger and more intense for the mutant than for the WT version (Fig 55B). Importantly, these results indicate that, as observed for BtpB, the catalytic E217 residue is essential for yeast growth inhibition but still allows assembly of the BtpA TIR domain into ordered structures (Fig 55B).

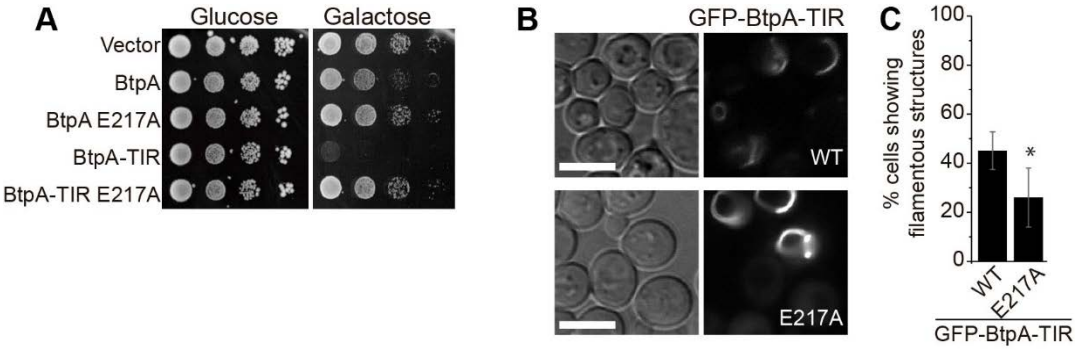

Fig 55. Expression of the BtpA Glu to Ala mutant.

(A) Ten-fold serial dilution growth assay, of YPH499 yeast bearing pYES2 empty vector and pYES2 derivative plasmids expressing BtpA and BtpA-TIR both their corresponding catalytically inactive mutants (E217A). Cells were cultured under repression in SD agar medium (Glucose) and induction in SG agar medium (Galactose) for 72h. (B) Nomarski and fluorescence microscopy of yeast cells expressing pYES2-GFP-BtpA-TIR WT and E217A mutant, after 4h induction. Scale bars represent 5 µm. (C) Graph displaying the percentage of cells showing filamentous fluorescent structures. Data correspond to means ± standard deviation of four independent transformants (n ≥ 100) and statistical comparison was done by the Student´s t-test with a p-value = 0.0431 (*).

Western blotting analysis of all BtpA constructs showed that only BtpA-TIR WT, indeed the most toxic construct (Fig 38), can reduce MAPK phosphorylation and has the lowest expression levels (Fig 56), consistent with high toxicity. The Glu to Ala inactive E217A mutant was tolerated at high expression levels and did not diminish basal Slt2 MAPK phosphorylation (Fig 56), just like the equivalent E234A BtpB mutant (Fig 54).

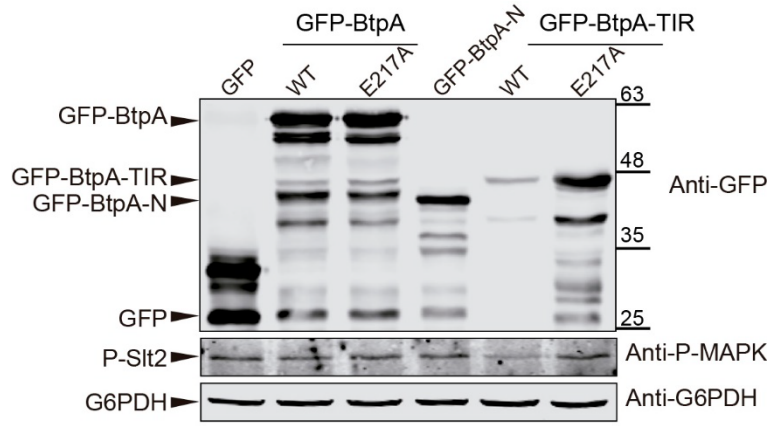

Fig 56.- BtpA-TIR impairs yeast MAPK activation.

Western blotting of YPH499 cells extracts bearing the indicated BtpA versions from pYES2-GFP plasmid derivatives, after 4h induction. The antibodies used were anti-GFP (upper panels), anti-P-MAPK to display dual phosphorylation of Slt2 yeast MAPK, and anti-G6PDH as a loading control (lower panels). The molecular weights of the constructs are: GFP (27 kDa), GFP-BtpA (58 kDa), GFP-BtpA-N (41 kDa), GFP-BtpA-TIR (44 kDa). Approximate molecular weights on the figure are expressed in kDa.

NADase inactive glutamic acid mutants in both TIR domains of BtpA and BtpB form cytosolic filaments, that appear at the microscope more robust than their WT equivalents (see Fig 53 and Fig 55). This might reflect the higher expression levels of these mutant proteins that are tolerated by yeast cells (Fig 54 and 56). Yeast immunofluorescence with anti-tubulin showed that, as in the case of the corresponding BtpA/B-TIR WT (Fig 40), those long filaments were extranuclear and did not co-localize with yeast tubulin (Fig 57). Thus, they should be presumably assembled by self-interaction.

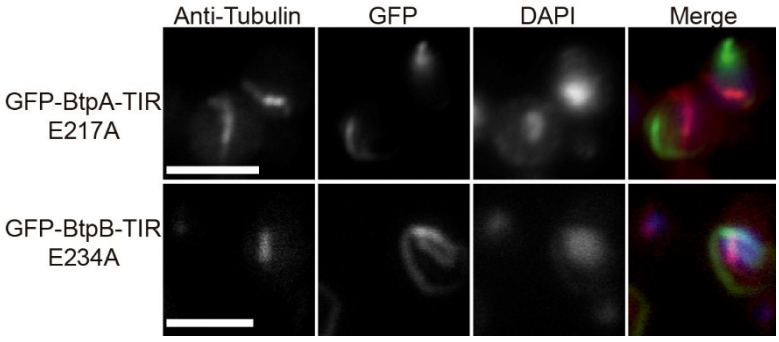

Fig 57.- Glu to Ala mutants of BtpA-TIR and BtpB-TIR do not coincide with yeast tubulin.

Indirect immunofluorescence of YPH499 yeast cells expressing GFP-BtpA-TIR E217A or GFP-BtpB-TIR E234A (green), from pYES2 plasmid derivatives. Microtubules are stained using an anti-tubulin antibody (red). Nuclei are labeled with DAPI (blue). Scale bars represent 5 µm.

2.6.- Co-expressing human TIR adaptors and bacterial TIR effectors.

2.6.1.- Human TIR adaptors do not vary effector-derived toxicity in yeast.

Before their NADase activity was elucidated, bacterial TIR domains were thought to downregulate innate immunity in host cells, for the establishment of the pathogen intracellular niche, by interfering with SMOC assembly. This could be assessed in the yeast model. As a further step, we decided to exploit the two experimental settings developed in the present Thesis by co-expressing human TIR adaptors with the *Brucella* TIR effectors. Since growth inhibition is one of the most characteristic phenotypes of BtpA/B protein expression in yeast (Fig 38), we first tested whether human TIR adaptor co-expression would enhance or buffer the toxicity of the bacterial effectors. Neither adaptor did alter BtpA, BtpA-TIR, BtpB, or BtpB-TIR growth inhibitory phenotype nor affect the lack of toxicity upon the expression of either N-terminal sides (Fig 58). This result indicates that, if a direct interaction exists, it is not strong enough to block the NADase activity of these *Brucella* effectors.

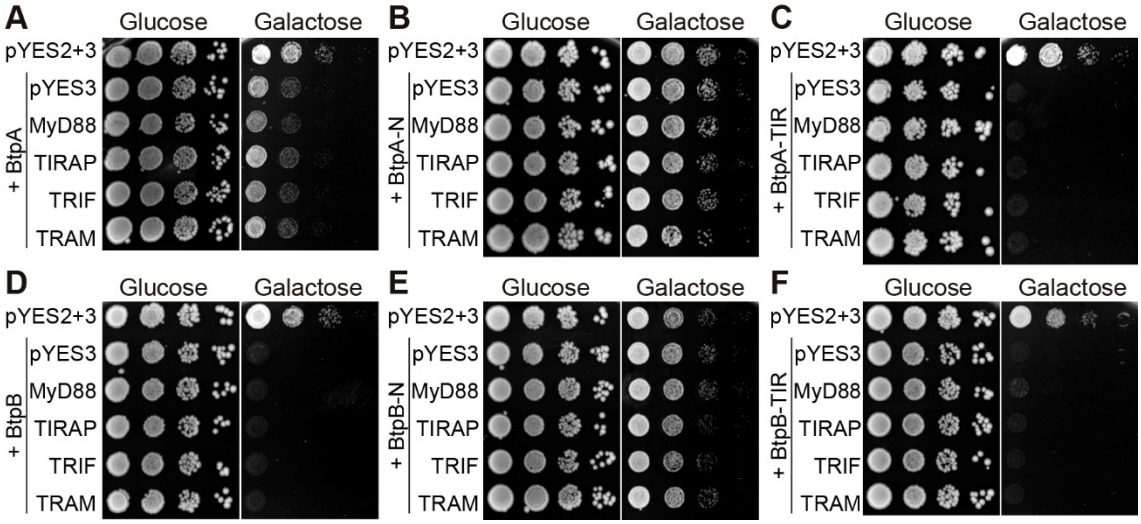

Fig 58.- Co-expression of the human TIR adaptors does not alter the *Brucella* TIR effectors yeast toxicity. Ten-fold serial dilution assay of YPH499 yeast cells bearing as control pYES3-mCherryCt and pYES2-GFP (pYES2+3) and co-expressing pYES3-mCherryCt (pYES3), MyD88, TIRAP, TRIF, and TRAM from pYES3 plasmid derivatives together with BtpA (A), BtpA-N (B), BtpA-TIR (C), BtpB (D), BtpB-N (E), and BtpB-TIR (F) from pYES2-GFP plasmid derivatives. Cells were cultured under repression in SD agar medium (Glucose) and induction in SG agar medium (Galactose) for 72h.

2.6.2.- Looking for effector-adaptor interactions.

To evaluate protein-protein interactions among *Brucella* TIR effectors and the four human adaptors, co-precipitation assays were set. Direct interaction has already been described for BtpA with MyD88 and TIRAP (Alaidarous *et al.*, 2014). We expressed in the yeast cell GFP-BtpA

or GFP-BtpA-TIR together with individual human TIR adaptors, to later immunoprecipitate protein extracts using commercial anti-GFP nanobody agarose beads. In the yeast model, GFP-BtpA co-immunoprecipitated, more efficiently than GFP alone, with MyD88 and TRIF, but not with TIRAP, and only a subtle band was appreciated in the case of TRAM. (Fig 59A-B). In contrast, BtpA-TIR does not seem to interact over the control with any of the adaptors (Fig 59C-D). Protein levels of the adaptors on the input lanes were lower when BtpA-TIR was co-expressed, probably due to the severe toxicity induced by the construct, which reduces protein yield in cell extracts (Fig 58).

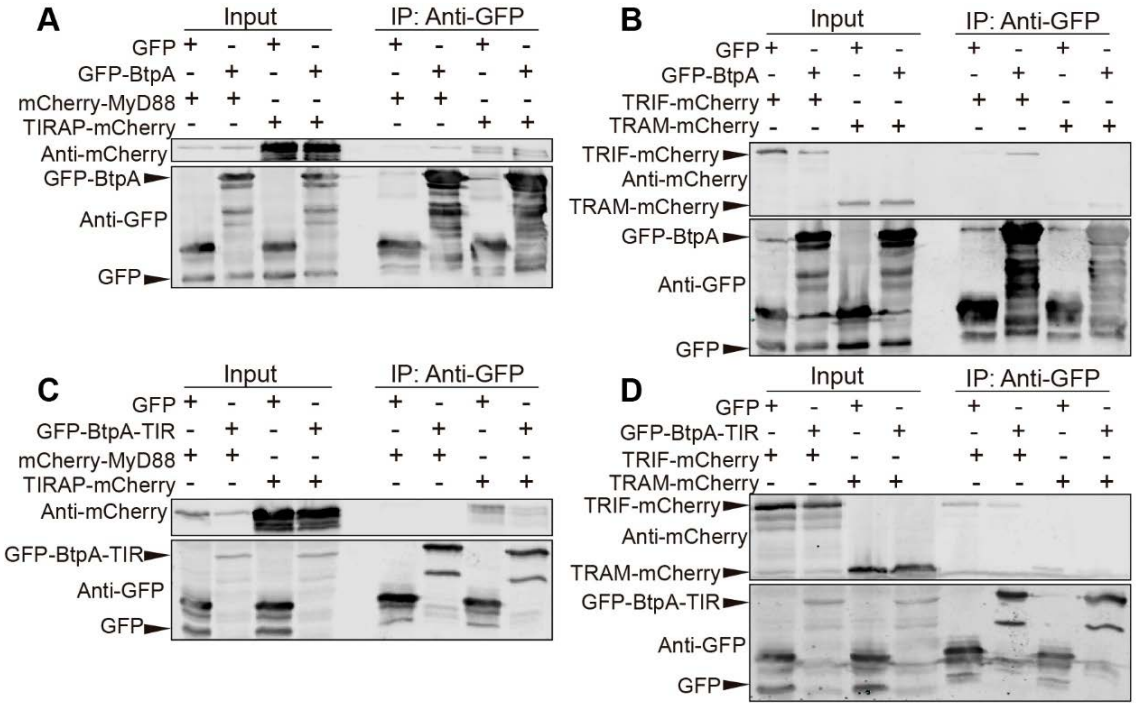

Fig 59.-Immunoprecipitation assay of BtpA and BtpA-TIR with the human adaptors.
YPH499 yeast cells bearing either pYES2-GFP (GFP) or GFP-BtpA-pYES2 (GFP-BtpA) (A-B) or GFP-BtpA-TIR-pYES2 (GFP-BtpA-TIR) (C-D) were co-transformed with mCherry-MyD88 and TIRAP-mCherry (A,C) or TRIF-mCherry and TRAM-mCherry (B,D), all from pYES3 plasmid derivatives. Extracts were immunoprecipitated using anti-GFP nanobody agarose beads (GFP-TrapA, Chromotek), followed by Western blotting analysis. Input lanes show the whole extract, whereas IP lanes display immunoprecipitated proteins. Blots were developed using antibodies anti-mCherry (upper panels) and anti-GFP (lower panels).

On the other hand, little is known about the ability of BtpB to bind human TIR proteins. Thus, we precipitated yeast cell extracts containing one of the human adaptors and either GFP-BtpB or a GST N-terminal fusion of the BtpB-TIR fraction (Fig 60). None of the adaptors co-precipitated with either construct in the conditions assayed. Like in the case of BtpA-TIR samples (Fig 59C-D),

input lanes having BtpB or BtpB-TIR showed lower protein levels of the adaptor, again reflecting the severe toxicity of these proteins (Fig 58).

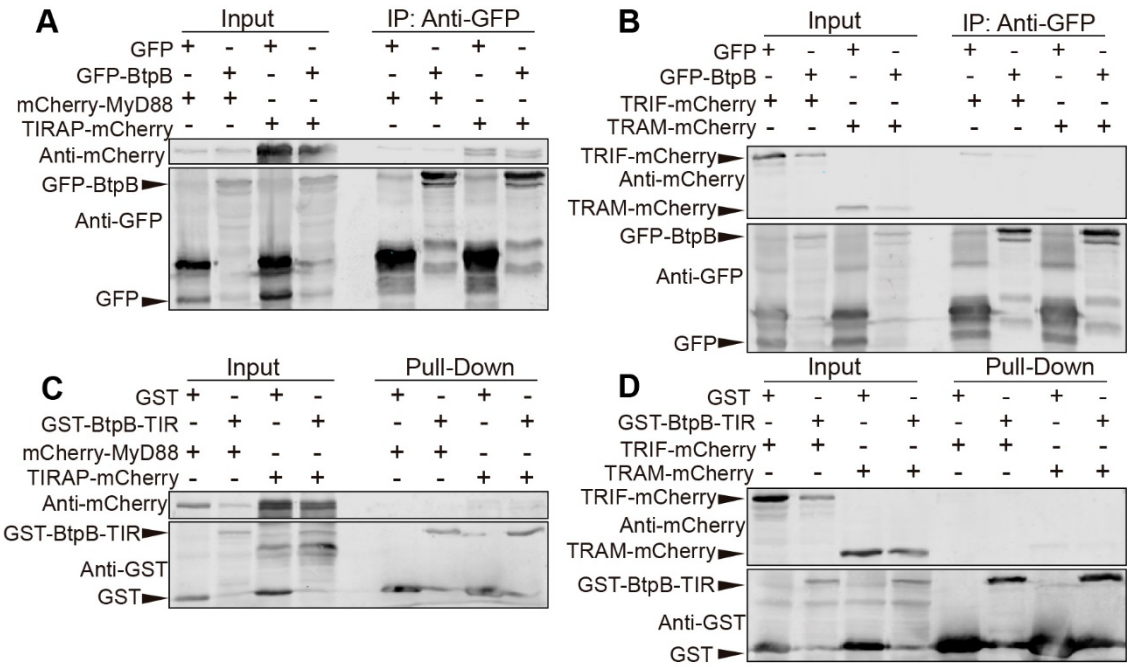

Fig 60.- Precipitation assays of BtpB and BtpB-TIR with the human adaptors.

YPH499 yeast cells bearing GFP or GFP-BtpB (A-B) or GST or GST-BtpB-TIR (C-D) were co-transformed with mCherry-MyD88 and TIRAP-mCherry (A, C) or TRIF-mCherry and TRAM-mCherry (B, D). Extracts were immunoprecipitated using Anti-GFP nanobody agarose beads (GFP-TrapA, Chromotek) (A-B) or treated with glutathione agarose beads (GE Healthcare) (C-D) followed by Western blotting analysis. Input lanes show the whole extract, whereas IP (A-B) and pull-down (C-D) lanes display precipitated proteins. Blots were developed using antibodies anti-mCherry (upper panels), anti-GFP (A-B lower panels), and anti-GST (C-D lower panels).

2.6.3.- *Brucella* TIR effectors impair TRAM filament formation.

We next addressed a microscopic examination of co-transformed yeast cells, to assess whether adaptor expression may alter effector location and *vice versa*. No substantial changes in GFP-BtpA localization were identified upon the co-expression of human adaptors (Fig 61A). However, BtpB signal co-localized or are close to cytosolic MyD88 and TRIF dots. TIRAP keeps its usual location on PM but sometimes is recruited to fade cytosolic spots that fit those of BtpB. Interestingly, TRAM did not form its characteristic filaments in cells bearing BtpB-signal, acquiring a cytosolic distribution with some aggregates that coincide with BtpB spots (Fig 61B).

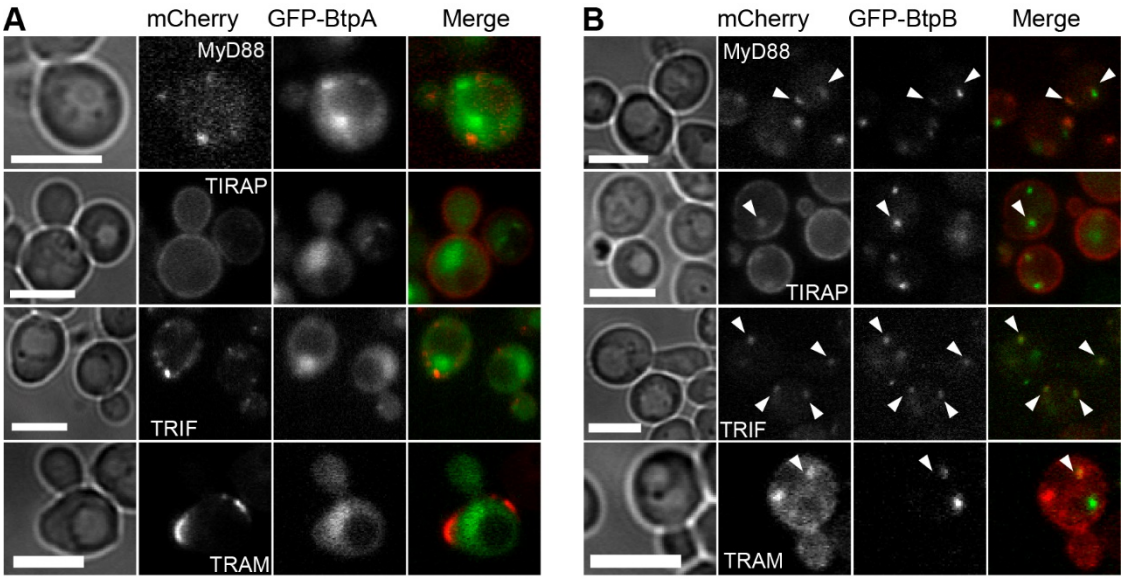

Fig 61.- Visualization of yeast cells co-expressing BtpA/B and the human adaptors.

Fluorescence microscopy of YPH499 yeast cells expressing mCherry-MyD88 (MyD88), TIRAP-mCherry (TIRAP), TRIF-mCherry (TRIF), or TRAM-mCherry (TRAM) from pYES3 derivative plasmids, (red) and GFP-BtpA (A) or GFP-BtpB (B) from pYES2 derivative plasmids (green), after 4h induction. White arrows indicate interesting events. Scale bars represent 5 µm.

Both TIR domains of BtpA and BtpB maintained their cytosolic filamentous structures in the presence of the human adaptors, which do not co-localize with them (Fig 62). Remarkably, as in the case of BtpB expression (Fig 61B), TRAM is no longer able to form its typical PM filaments when either BtpA or BtpB TIR domain is present (Fig 62). These results suggest that TRAM filaments are impaired in a yeast cellular environment altered by BtpB or the isolated TIR domains of both BtpA and B, which are the constructs that reduce ATP and NAD^+ cellular concentrations (Fig 48) and display the strongest toxicity (Fig 38). Thus, we suspected that the lack of TRAM filaments in BtpA/B-TIR-expressing cells may reflect a requirement of ATP rather than a direct sequester of TRAM by interaction.

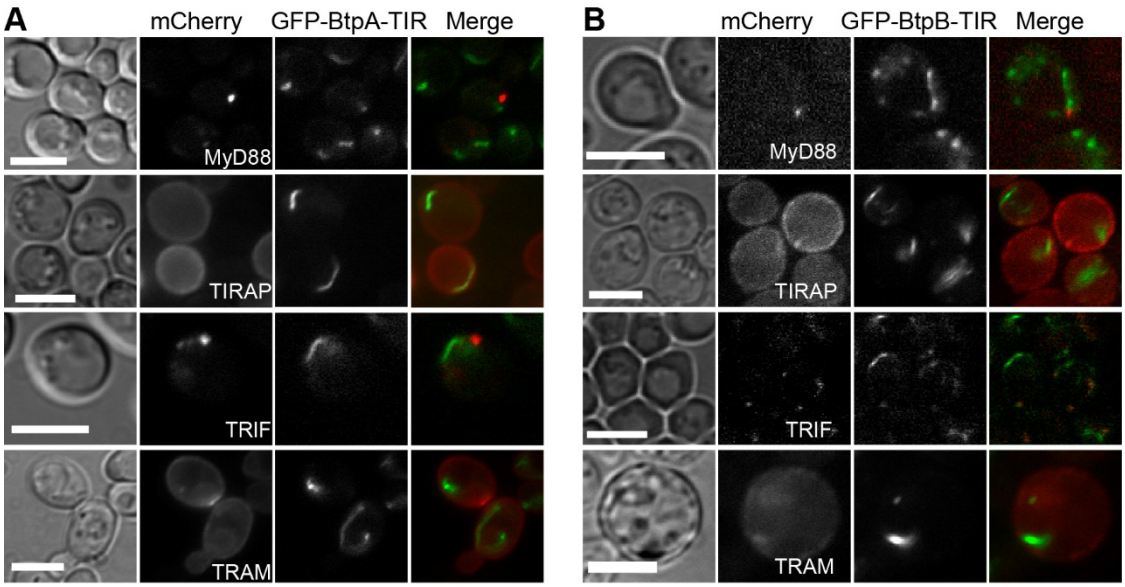

Fig 62.- Visualization of yeast cells co-expressing BtpA/B-TIR and the human adaptors.
Fluorescence microscopy of YPH499 yeast cells expressing mCherry-MyD88 (MyD88), TIRAP-mCherry (TIRAP), TRIF-mCherry (TRIF), or TRAM-mCherry (TRAM) from pYES3 derivative plasmids, (red) and GFP-BtpA-TIR (A) or GFP-BtpB-TIR (B) from pYES2 derivative plasmids (green), after 4h induction. Scale bars represent 5 µm.

To test this hypothesis, TRAM-mCherry was co-expressed with the catalytically inactive Glu to Ala mutants of BtpA-TIR and BtpB-TIR (E217A and E234A respectively). These mutants, that do not inhibit yeast growth (Fig 52A and 55A), allowed TRAM assembly into filaments (Fig 63). These data confirm that the alterations in TRAM filament formation require the presence of catalytically active BtpA/B TIRs.

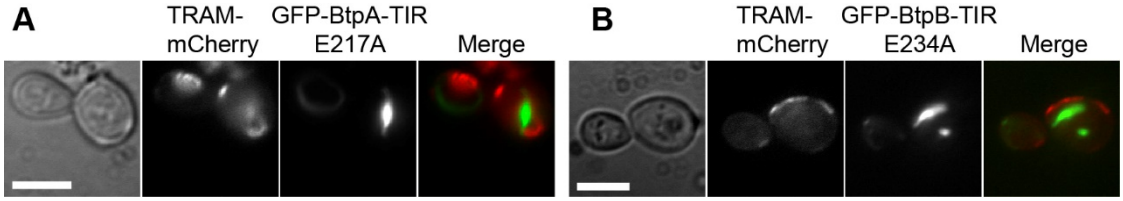

Fig 63.- Visualization of yeast cells co-expressing BtpA/B-TIR Glu to Ala mutants and the human adaptors.
Fluorescence microscopy of YPH499 yeast cells expressing TRAM-mCherry (red), from pYES3-TRAM-mCherry, and GFP-BtpA-TIR E217A (A) or GFP-BtpB-TIR E234A (B) catalytically inactive mutants, from pYES2 plasmid derivatives, after 4h induction. Scale bars represent 5 µm.

To sum up, the expression of the *Brucella* TIR-proteins in yeast allowed the assessment of bacterial-human TIR interactions in a new cellular context and revealed strong alterations of yeast biology, which mainly derived from their NADase activity.

Discussion

Discussion

TIR domain-containing proteins are widespread, found along diverse branches of the tree of life, their functions ranging from innate immunity signaling in animals, disease resistance in plants, and virulence factors or anti-phage systems in bacteria. In this Thesis, we present an approach to their study based on heterologous expression in *S. cerevisiae*. We have expressed both human TIR adaptor proteins involved in TLR4 signaling, and *Brucella abortus* TIR-containing T4SS effectors known to downregulate innate immunity during infection. Briefly, the TIR proteins issued in this study could be classified according to their ability or not to cause two major yeast phenotypes: (i) their toxicity in yeast, (BtpA, BtpB, and their TIR domains) vs their innocuousness (MyD88, TIRAP, TRIF, TRAM, and TLR4-TIR) and (ii) their ability to form visible filaments in yeast (TRAM, TIRAP, BtpA-TIR, and BtpB-TIR) or not (MyD88 and TRIF). Moreover, we have been able to determine that, in the case of BtpA and BtpB TIR domains, these two features depend on different molecular motifs, as non-toxic mutants still generated such filamentous structures.

The formation of TIR domain-derived filaments in yeast.

The human adaptors MyD88, TIRAP, TRIF, and TRAM function by spreading and amplifying TLR stimulation signals via TIR-TIR interactions. Considerable efforts have been carried out to uncover the basis of their interacting mechanisms (Enokizono *et al.*, 2013; Funami *et al.*, 2017; Mahita and Sowdhamini, 2018a; Nimma *et al.*, 2017; Ve *et al.*, 2017; Vyncke *et al.*, 2016). TIRAP generates long filaments *in vitro*, whose cryo-EM analysis led to the elucidation of a highly detailed structure (Ve *et al.*, 2017). These authors suggest that TRAM could produce similar filaments *in vitro*. Indeed, TRIF and TRAM TIR domains oligomerize and precipitate in solution. Therefore, to obtain their crystal structures, they had to be monomerized via the introduction of their corresponding BB loop mutations (TRIF P434H, TRAM C117H) (Enokizono *et al.*, 2013). This evidences that an intact BB loop is required for oligomerization, probably derived from robust self-interaction. On the other hand, the MyD88 TIR domain oligomerizes in a dose-dependent manner in the presence of TIRAP TIR domains, but not in the presence of those of TRAM or TLR4 (Ve *et al.*, 2017). Additional cell-free expression experiments unraveled that both DD and TIR domains are required for MyD88 polymerization (O'Carroll *et al.*, 2018). This reflects again that precipitation in solution, polymerization, and filament formation are features that evidence TIR-TIR interactions.

Brucella TIR effectors also have self-interacting properties within their TIR domains: structural details of these interactions have been thoroughly described for BtpA (Alaidarous *et al.*, 2014;

Kaplan-Türköz *et al.*, 2013; Saqib and Baig, 2019; Snyder *et al.*, 2014). Moreover, our results from BtpA and BtpB yeast expression show the ability of their TIR domains, once their N-terminal halves are removed, to form long cytoplasmic filaments, that are independent of yeast tubulin. Full-length TRAM also produces such filaments in the yeast model in support of the idea that they have homo-oligomerization properties. Those filaments may have not been detected in mammalian cells, because they may not appear at physiological concentrations, and thus yeast overexpression might evidence their intrinsic *in vivo* self-aggregation ability. TRAM, as well as TIRAP, have relatively small non-TIR regions, which are unlikely to mask TIR-TIR interactions. While TRAM displayed evident filaments in yeast, TIRAP is rather localized at the PM following a relatively patchy pattern. We hypothesize that TIRAP builds PM attached micro-filaments, that appear as PM clusters, clearly observed in the focal analysis of the mCherry-TIRAP construct. The fact that the bud neck, covered by a mesh of septin-based array of filaments, excludes TIRAP favors this idea, as septin filaments act as a barrier and should not leave room for the assembly of similar structures. In contrast, core adaptors MyD88 and TRIF are found in spots inside the yeast cell and do not render any evident filaments, at least within the resolution limits of our fluorescence microscope. They were expressed as full-length proteins, with their additional domains having interacting properties too, such as the DD in MyD88 and both the C-terminal RHIM motif and the autoinhibitory N-terminal region in TRIF. The latter has structural similarity to IFIT proteins, with tetratricopeptide repeats, also involved in protein-protein interactions (Pidugu *et al.*, 2019). These extra motifs may interfere with their ability to assembly into filaments in yeast, as we show in the case of *Brucella* BtpA and BtpB, which only form filaments when lacking their N-terminal region.

MyD88 and TRIF appear in spots in yeast cells.

Prior to the yeast model developed in the present Thesis, other groups have expressed some TIR proteins in mammalian cell lines. Overexpression of MyD88 in human cells led to signaling activation (Latty *et al.*, 2018). Similarly, TRIF overexpression led to its characteristic speckle formation (Funami *et al.*, 2007). It seems like the more adaptor expression levels, the larger complex is generated, and the stronger the signal is conveyed. Recently, Latty and collaborators established for the first time the kinetics of myddosome formation via *in vivo* single-molecule imaging, concluding that SMOC signal strength does not only depend on the size and number of complexes, but also on how quickly it disassembles (Latty *et al.*, 2018).

S. cerevisiae naturally lacks TLR signaling, so we cannot integrate its heterologous components into endogenous pathways. Instead, we can assume that the cytosolic spots upon MyD88 and

TRIF yeast expression could reflect their ability to aggregate, a crucial feature in SMOC formation. MyD88 P200H BB loop mutant, with its TIR-TIR interaction abilities altered (Ve *et al.*, 2017), has a significantly smaller number of cells bearing those puncta, which points out to the importance of MyD88 P200 residue in the formation of such aggregates in yeast. Nevertheless, the corresponding TRIF P434H mutant displayed no evident alterations in yeast localization, maybe because the effect of this mutation in TRIF oligomerization is masked by functional N-terminal IFIT and C-terminal RHIM domains in the *S. cerevisiae* model. The MyD88 L252P mutation (formerly annotated as L265P) (Zhan *et al.*, 2016) is a hyperactive mutation isolated in B-cell lymphoma (Avbelj *et al.*, 2014; Ngo *et al.*, 2011). MyD88 L252P homodimers get stabilized at their BCD surface, thus interactions within the myddosome are strengthened and signaling may occur without TLR activation (O'Carroll *et al.*, 2018; Zhan *et al.*, 2016). Unexpectedly, yeast expression of this oncogenic mutant did not lead to a higher number of cells with MyD88 spots, and even its expression levels were less intense than the other MyD88 constructs. However, a gain of function of this mutant may not be reflected in its subcellular localization, but on its ability to recruit and activate its downstream effectors.

IRAK4 can phosphorylate MyD88.

In this work, we report IRAK4 phosphorylation of MyD88 for the first time, to our knowledge. IRAKs are kinases acting immediately downstream of MyD88 in the myddosome, so we decided to include them in the yeast model to check if their interactions with MyD88 could be reproduced in a simple environment lacking other SMOC factors. IRAK4, but not IRAK1/2 clearly co-purified with MyD88, but surprisingly, we detected a slow migrating MyD88 upper band upon WT IRAK4 co-expression, that could reflect a phosphorylation event, as IRAK4 KD did not induce it.

Purification and further mass spectrometric analysis of MyD88 and IRAK4 bands led to the identification of several Ser/Thr phosphorylated residues. Among the phosphosites identified in MyD88, one was found in the N-terminal tail, a motif that displays phosphatidic acid binding properties (Avbelj *et al.*, 2018), plus another at the DD, which was exclusively found on the KINASE band, and is indeed the interacting domain with IRAK4. Three other, two among them being exclusively found at the UP band, are within the INT domain, which helps IRAK4 binding (Avbelj *et al.*, 2011), probably allowing the TIR and DD domains to acquire the required orientations (Moncrieffe *et al.*, 2020). Interestingly, five phosphorylated residues, three of them found exclusively at the UP band, belong to the TIR domain. All of them are exposed on the surface, likely because they are highly accessible residues, and are probably implicated in both

BE and BCD interfaces (Vyncke *et al.*, 2016). Moreover, S244 and T272 have been proposed to be part of the uropathogenic *E. coli* TIR effector TcpC binding site on MyD88-TIR (Snyder *et al.*, 2013) which may prevent TIRAP binding, S244 phosphorylation, and MyD88-TIR TIR interactions (Vyncke *et al.*, 2016).

To our knowledge, S242 and S244 are the only MyD88 phosphorylated Ser/Thr residues described to date. Previous studies had reported that the dephosphorylation of S242 and S244, by PP2A, downregulates MyD88 signaling (Xie *et al.*, 2013). However, further research showed that while a phosphomimetic mutant S244D enhances NF-κB activation, S242D plays the opposite role (Vyncke *et al.*, 2016). A double mutant, MyD88 x2SA, lacking those two phosphorylatable serines had a less intense slow migrating band upon IRAK4 co-expression in yeast, but no significant changes in the number of cells bearing spots were detected.

We also looked for phosphorylations on GST-IRAK4. Out of the seven residues bearing a phosphate in the IRAK4 protein, 4 had been already described as autophosphorylation events (Cheng *et al.*, 2007). Among them was T342, whose phosphorylation is required for IRAK4 complete activation (Cushing *et al.*, 2014). Apart from specific IRAK4 phosphorylations on Myd88 and autophosphorylations, several unexpected ones were found for example in GST. Either an increased intrinsic IRAK4 activity due to overexpression or the activity of spurious yeast kinases could account for such unspecific phosphorylations.

Altogether, some limitations to this assay must be considered: (i) the coverage, although high, was not complete, so there might be other phosphorylated residues that were still undetected, (ii) these phosphorylations were found when overexpressing both MyD88 and IRAK4 in a yeast cellular environment, which lacks the rest of the SMOC elements that may fine-tune its kinase activity, a setting that diverges from the physiological conditions, and (iii) we cannot rule out that some yeast kinases are responsible for unspecific phosphorylation of some of these residues. Yet, the yeast model usefulness relies on its capacity of providing hints: it undoubtedly proves that MyD88 phosphorylation by IRAK4 is possible and that no other elements of the pathway are involved.

Analyzing the localization of the sorting adaptors.

TIRAP and TRAM are two intermediate sorting adaptors linking receptors and the core adaptors, MyD88 and TRIF respectively, and are targeted to specific membranous regions in the mammalian cell via their localization motifs. At the first sight, only TIRAP seems to fit its expected location at the PM in the yeast cell. TRAM is also targeted to PM, in this case by its myristoylation signal, but the other side of its bipartite sorting signal, the endosomal localization motif, seems

to be masked. All three mutations tested in the TRAM yeast construct significantly impaired its ability to form filaments and led to alternative locations.

The addition of a myristoyl group is an effective mechanism that enhances membrane targeting of a protein and it is involved in a myriad of cell biology aspects, including innate immunity (Udenwobele *et al.*, 2017). The removal of the myristoylation signal (TRAM G2A) on the yeast construct led to its diffusion into the cytosol. This result raises the idea that, in the case of TRAM, effective PM targeting is a prerequisite for filament formation, contrasting with the ability of BtpA/B TIR, for example, to form strong cytosolic filaments. TRAM G2A diffusion into cytosol has already been described in mammalian cell lines, where the mutant is no longer able to spread the signal (Rowe *et al.*, 2006).

In higher cells, the BB loop mutant (TRAM C117H) no longer oligomerizes (Enokizono *et al.*, 2013), nor conveys the signal (Rowe *et al.*, 2006), and, as expected, no filaments were detected in yeast. Instead, it appeared attached to the yeast plasma and vacuolar membranes, partially in agreement with the results in human cell lines, where it appears at the PM (Funami *et al.*, 2015). The yeast vacuole is a big membranous compartment that acts as the cellular “drain”, the endpoint of the endocytic pathway where macromolecules become degraded (Feldmann, 2010). As a membrane-linked protein, TRAM mutants not forming filaments are possibly following the endocytic pathway, ending up bound to the yeast vacuolar membrane. In agreement, TRAM G2A, lacking the myristoylation signal, does not appear in vacuoles.

Overexpression of TRAM in human cells leads to unstimulated pathway activation (Oshiumi *et al.*, 2003). It has recently been described a conserved acidic motif (D91 and E92) that, when both residues are mutated to alanines, blocks such TRAM overexpression-derived signaling, while the mutant protein is still able to interact with TLR4 and TRIF. In the mammalian cell setting, the TRAM DEAA mutant, although effectively myristoylated, diffuses along the cytosol (Funami *et al.*, 2015), in contrast with our results in yeast, where TRAM DEAA appears at the PM and vacuolar membranes. The fact that a few cells still bear TRAM filaments indicates that D91 E92 residues are not as critical for TRAM-TRAM interaction in yeast as they are for TRAM localization and signal transduction in cell lines. In sum, effective signaling requires TRAM (i) to be able to self-interact (e.g., having an intact BB loop), and (ii) to be at a specific location (e.g., bearing a functional myr/endosomal localization motif/D91 E92 site). The yeast model generally recapitulates such behavior, but when the myristoylated protein is not able to form stable filaments at the PM due to loss of self-interaction, it seems prone to be endocytosed, ending up at the vacuolar membrane.

Discussion

An intriguing result from the yeast model is the fact that TRIF and TRAM do not co-localize, despite their apparent interaction in co-purification assays. This differs from the clear co-localization and interaction of the TIRAP-MyD88 pair in the yeast system, which requires an intact BB loop in both elements. A few explanations account for this result, (i) a third component is missing (other elements, a modification, a physicochemical parameter…) in the heterologous system compared with the mammalian cell, (ii) the N-terminal side of TRIF is preventing it from joining TRAM (Mahita and Sowdhamini, 2017), and (iii) as described for TLR3 signaling (Funami *et al.*, 2007), TRIF may be only transiently co-localizing with TRAM in the activated mammalian cell, moving quickly to its cytosolic speckle, and thus we are not able to reproduce or visualize that in *S. cerevisiae*.

TIRAP appears associated with yeast PM driven by its already described polybasic region (Kagan and Medzhitov, 2006), as TIRAP x4KA shows up in the cytosol. Nevertheless, TIRAP is rather forming PM clusters, a sort of micro-filaments, which disappear when looking at the BB loop mutant (TIRAP P125H), in which self-interactions are impaired. The polybasic region recognizes PtdIns(4,5)P_2, a phospholipid key for PM proper functionality (Hammond, 2016). Furthermore, lipid rafts containing PtdIns(4,5)P_2 play a role in TLR signal transduction (Ruysschaert and Lonez, 2015). Surprisingly, TIRAP clusters did not completely coincide with the Pleckstrin Homology (PH) domain of PLCδ, a reliable PtdIns(4,5)P_2 marker. Moreover, TIRAP, although accumulated near the bud, avoids yeast bud neck, which is a PtdIns(4,5)P_2 rich region (Bertin *et al.*, 2010). The bud neck is a PM stretch decorated by the septins, a group of proteins that form a stable filamentous ring that acts both as a diffusion barrier and as a scaffold to recruit the effectors required for bud development. One of those septins is Cdc10, which specifically binds PtdIns(4,5)P_2 (Farkašovský, 2020). Here we show that TIRAP is never coincident with the Cdc10-GFP-labeled septin ring, probably because its diffusion barrier properties prevent TIRAP from localizing there. Overall, the yeast system opens new and interesting clues for the study of TIRAP localization.

TIRAP interactions with the downstream IRAK kinases.

IRAK kinases interact with TIRAP in human cells, namely WT IRAK2 (Fitzgerald *et al.*, 2001) and the kinase-dead mutants of IRAK1/4 (Dunne *et al.*, 2010). In the yeast heterologous expression model, we effectively recapitulate the interactions of TIRAP with IRAK2 and IRAK4 KD. Besides, we detected an interaction between WT IRAK1 and TIRAP, demonstrating that active IRAK1, in contrast to active IRAK4, can bind TIRAP as well. Human cell studies indicate that those interactions relied on the TIRAP TIR domain since the isolated TIR domain of TIRAP alone still

interacted with IRAK2 (Fitzgerald *et al.*, 2001) and the BB loop mutant P125H no longer co-precipitated with IRAK4 KD (Dunne *et al.*, 2010). However, TIRAP P125H interacted with WT IRAK1/2 in yeast as intensely as WT TIRAP. These data might evidence that a functional BB loop is not required for direct TIRAP binding of IRAK1/2. The role of a putative TIRAP-IRAK binding in the absence of bridging MyD88 is still obscure, compared to the widely studied interactions between MyD88 and any of both proteins. Further testing of TIRAP P125H and IRAK4 KD co-purification from yeast cells, would be interesting to fully address the involvement of the TIRAP TIR domain in IRAKs interaction.

Recapitulating the TLR4-TIR domain interactions with TIRAP and TRAM.

The cytosolic side of human TLR4, bearing the TIR domain, has been introduced into the yeast model as two distinct versions, myristoylated or not at an N-terminal GST tag. TLR4 TIR interacted with both TIRAP and TRAM adaptors *in vitro*, and it can alter their location *in vivo*. When using the myristoylated myrGST-TLR4-TIR version, the change was more drastic, TIRAP appearing in large PM spots and TRAM losing all its filaments into PM dots. This suggests that the TLR4 TIR domain can interact and effectively recruit its adaptors in the yeast model. However, we still lack direct evidence of the myrGST-TLR4-TIR construct Is indeed at the PM. We have tried yeast immunofluorescence using antibodies vs GST or hTLR4, and even a cell protein lysate enrichment of membranous protein (data not shown) but no conclusive results were obtained to date.

Yeast phenotypes derived from BtpA and BtpB expression.

Our results indicate that *Brucella* TIR proteins induce yeast growth inhibition requiring their TIR domains, while N-terminal sides determine protein localization and, in the case of BtpA, modulate its toxicity. Here we also demonstrate that BtpA and BtpB TIR domains deplete NAD^+ from the yeast cell over one order of magnitude, in agreement with a recent report of bacterial TIR proteins being NADases, which included BtpA expressed in *E. coli* (Essuman *et al.*, 2018). Indeed, the results from our collaborator Dr. Suzana Salcedo and her team, published with our group in a joint paper, demonstrate that both proteins exhibit their enzymatic NADase activity when ectopically expressed in human cell lines, and more importantly, during *Brucella* infection (Coronas-Serna *et al.*, 2020a).

Yeast phenotypes caused by BtpB and the TIR domains of both effectors are plausibly a consequence of the metabolic alterations caused by NAD^+ and ATP removal. Indeed, ATP is required for phosphorylation events and microtubule disassembly (Bershadsky and Gelfand, 1981). Thus, a drop in cellular ATP availability may be the cause of actin and endocytosis

alterations and global downregulation of MAPK signaling detected in yeast. Intriguingly, TRAM does not form its filaments in the yeast model upon co-expression of either BtpB or the TIR domains of BtpA and BtpB suggesting that it may require normal NAD^+ or ATP cellular levels, as the co-expression of catalytically inactive BtpA or BtpB TIR mutants allowed TRAM to form those structures. However, the possibility that TRAM filament disassembly reflects a heterotypic TIR-TIR interaction rather than a requirement NAD^+ or ATP cannot be discarded.

In mammalian cells, the reduction of ATP levels may account for the reported BtpA prevention of drug-induced microtubule disassembly (Alves-Silva *et al.*, 2017; Radhakrishnan *et al.*, 2011). Endocytosis blockage also occurred upon ectopic expression of BtpB in human cell lines, but it was not significant in infection experiments using WT bacteria, compared to deletion mutants on either *btpA* or *btpB* genes (Coronas-Serna *et al.*, 2020a). Two explanations can be suggested: either the much smaller concentrations of *Brucella* TIR proteins translocated during infection do not produce such endocytic blockage or the presence of other effectors in the infection setting modulate this phenotype.

Regarding subcellular localization, BtpB and its truncated versions behaved similarly in human cells and yeast: Both BtpB and its non-TIR N-terminal extension alone kept their localization in dots, whereas BtpB-TIR displayed filaments along the cytosol, without co-localizing with neither tubulin nor with the intermediate filament marker vimentin (Coronas-Serna *et al.*, 2020a). Another bacterial TIR effector, TirS, form *S. aureus* displays very similar filaments upon ectopic expression in HeLa cells (Patot *et al.*, 2017). BtpB dots coincide, but not exclusively, with structures enriched of mono- and poly-ubiquitinated proteins in human cells and has sometimes been found on intercellular bridges resulting from cell division (Coronas-Serna *et al.*, 2020a; Felix *et al.*, 2014).

Unlike its nuclear-cytosolic distribution in yeast, full-length BtpA has been described to colocalize with microtubules upon expression in HeLa cells. Mutants on its WxxxE motif altered its localization and its cytoskeleton stabilizing features (Felix *et al.*, 2014), which play a role in the maturation of eBCV (Alves-Silva *et al.*, 2017). However, others have found BtpA at the PM, targeted to PtdIns(4,5)P_2, like TIRAP (Radhakrishnan *et al.*, 2009). *In vitro,* BtpA appears as a stable dimer and it requires both N-terminal and TIR domains to keep its conformation (Alaidarous *et al.*, 2014). Indeed, in one of the structures reported for this protein, an “α-tail” coming from the non-TIR side tightly packs the dimer (Kaplan-Türköz *et al.*, 2013). Despite our BtpA-TIR version lacking that α-tail, it forms stable filaments in *S. cerevisiae*, reflecting the

differences between the *in vitro* and *in vivo* conditions, making yeast an excellent living test tube for studying structural features.

Deciphering the roles of *Brucella* TIR proteins.

Our results and those of our collaborators (Coronas-Serna *et al.*, 2020a) highlight that *Brucella* can reduce NAD^+ levels in the host cell, probably to favor immunity evasion through modulation of cellular metabolism and signaling. The responsible enzymes, BtpA and BtpB, were previously reported to downregulate innate immunity signaling (Cirl *et al.*, 2008; Salcedo *et al.*, 2013; Salcedo *et al.*, 2008) and stabilize the microtubule network (Felix *et al.*, 2014) among other roles. Interfering with host TIR-TIR interactions is key to alter TLR signaling. BtpA has been described to interact with TIRAP, MyD88, and TLR4, and disrupt the TLR4-TIRAP interface (Alaidarous *et al.*, 2014). In yeast, although we did not observe any interaction with TIRAP, we were able to see BtpA co-purifying with MyD88 and TRIF. A reflection of self TIR-TIR interactions in the yeast model is the ability of the TIR domains to form long filaments in the cytosol, a property driven by residues different from the ones involved in yeast toxicity.

Indeed, not all point mutations found on a random mutagenesis screen to abrogate BtpB-derived yeast toxicity did interfere with BtpB-TIR filament formation, indicating that these two features rely on different structural determinants. The only BtpB-TIR mutant that was non-toxic and lost its filaments, S162P, belonged to a core region when mapped on BtpA structure, suggesting that the whole structure was likely disrupted. Besides, the fact that some mutations that prevented BtpB-induced phenotypes in yeast, such as growth inhibition or endocytosis blockage, still kept their toxicity and ability to form filaments when transferred to the BtpB TIR domain alone, agrees with the idea of the N-terminal domain buffering the enzymatic activity of *Brucella* TIR domains, as evidenced upon BtpA expression in yeast.

Mutations at the glutamic acid on the WxxxE motif yielded no yeast growth inhibition but kept forming filaments both in BtpA and BtpB TIR domains. This residue is required for *Brucella* TIR proteins NAD^+ depletion, as Glu to Ala mutations rendered them inactive in yeast and human cells (Coronas-Serna *et al.*, 2020a). Besides, it is key as well for BtpA microtubule stabilization (Felix *et al.*, 2014). The WxxxE signature is not exclusive of TIR domains, instead is conserved among a family of bacterial effectors mimicking Rho GEFs (Felix *et al.*, 2014; Orchard and Alto, 2012). The Rho family of small GTPases is devoted to cytoskeleton dynamics and cell morphology, and so, many bacterial effectors target them (Orchard and Alto, 2012). One of the GEF-like WxxxE effectors, the Mitochondrial associated protein (Map) form EPEC, activates the Rho small GTPase Cdc42 and induces the formation of host cell actin-rich cytoplasmic

projections called filopodia to favor pathogen adhesion (Berger *et al.*, 2009; Orchard and Alto, 2012). Interestingly, although BtpA is not classified as a bacterial GEF-like, it can also induce filopodia in transfected HeLa cells in a WxxxE and BB loop dependent manner (Felix *et al.*, 2014). Besides, like BtpB, Map has been shown by our group to induce actin depolarization in yeast (Rodríguez-Escudero *et al.*, 2005a). Nonetheless, the WxxxE is absent from MyD88, TIRAP, TRIF, and TRAM, which indeed are nontoxic upon yeast overexpression. TLR4-TIR, on the other hand, bears a WxxxE motif and did not alter yeast growth. To our knowledge, no NADase activity has been yet assigned to TLR-TIR domains, but their WxxxE motif contains a conserved Cys at the first "x", that is key for adaptor interaction and signaling (Shirey *et al.*, 2020). Indeed, our sequence alignment shows this Cys to be also present in MyD88, TIRAP, TRAM, plant TIRs, BtpB, PumA from *Pseudomonas aeruginosa,* and TirA from the social amoeba *Dictyostelium discoideum* (Fig 3). These results highlight the wide range of functions that derive from such a simple 5-residue motif, and probably many of them are yet to be unraveled.

Before the discovery of the TIR domain NADase activity (Essuman *et al.*, 2018), we developed a yeast ORF overexpression screen looking for suppressor genes. Although all produced a partial rescue, the ORFs found gave us hints pointing out to BtpB-derived yeast biology alterations. *UBC7* and *RPN14* are part of the ubiquitin-proteasome machinery, and their overexpression may favor the clearance of any toxic protein. Interestingly, Ubc7 is involved in ERAD, which is targeted by other *Brucella* effectors (Luizet *et al.*, 2019). Another two ORFs do not have a protein name yet: *YGR122W* is an ortholog of PalC from *Aspergillus nidulans*, while *YGR259C* is a small ORF that may act, when overexpressed, as an antisense RNA of *TNA1*, a high-affinity nicotinic acid PM permease involved in the NAD^+ salvage pathway (Ohashi *et al.*, 2013). Nonetheless, a yeast strain deleted on the *TNA1* gene suffered similar toxicity levels upon BtpB or BtpB-TIR expression (data not shown).

However, the screen most valuable hints came from the three sugar or inositol kinases/phosphatases found. Indeed, they told us about metabolic changes occurring in BtpB-challenged yeast cells, that may probably occur in *Brucella* host cells such as macrophages. The *DOG2* gene confers resistance to 2-deoxyglucose (Randez-Gil *et al.*, 1995), a glycolytic inhibitor also known to suppress macrophage inflammatory response and induce their apoptosis (Francis *et al.*, 2020; Venter *et al.*, 2014a). *RBK1* codes for a ribokinase form the Pentose-phosphate pathway (PPP), a side metabolic route that gets rid of glycolysis intermediates and displays an increased flux in pro-inflammatory M1 macrophages (Kelly and O'Neill, 2015; van Teijlingen Bakker and Pearce, 2020). Inm2 is one of the two yeast inositol monophosphatases. Inhibition of their human homolog selectively induced macrophage apoptosis in atherosclerotic plaques

without affecting neighboring endothelial or smooth muscle cells (De Meyer *et al.*, 2011) highlighting the importance of this enzyme among active macrophages. In sum, all three enzymes are related, in one way or another, to probable metabolic alterations undergone by active macrophages.

***Brucella* modulates host metabolism.**

Brucella cells use various mechanisms to evade host immunity and ensure their survival, including their T4SS effectors. Besides, they interplay with the different macrophage subpopulations. In the acute stages of infection, macrophages are mostly pro-inflammatory M1, and thus *Brucella* survival is limited. Bacteria resisting this initial challenge can establish chronic infection, in which M2 macrophages are predominant. These alternatively activated macrophages are less reactive against pathogens and have higher cytosolic glucose levels compared with M1, which offers a convenient environment for *Brucella* replication (Byndloss and Tsolis, 2016) (Fig 64). Indeed, *Brucella* cells adapt their metabolism to fit the available energy sources, for example using BPE123, a T4SS effector, to recruit the host glycolytic enzyme α-enolase 1 to the BCV (Marchesini *et al.*, 2016).

In this work, we show that BtpA and BtpB do not merely block TLR signaling or alter host microtubule dynamics, but they also display NADase activity. An intriguing question remains open: why would *Brucella* limit NAD^+ in the host cell? This is likely to occur in a highly regulated way, orchestrated together with other effectors to achieve bacterial intracellular survival. Nonetheless, the underlying mechanisms remain obscure and we can only speculate. Regarding the recent advances in immune metabolism, we can suggest that *Brucella* uses NAD^+ as a metabolic switch. The increase of intracellular NAD^+ is a hallmark of classical activation of macrophages (Al-Shabany *et al.*, 2016). Thus, *Brucella* might aim to maintain low host NAD^+ levels to prevent M1 activation as well as favoring the alternative M2 phenotype, in which replication is less repressed, and cytosolic glucose is more available (Byndloss and Tsolis, 2016) (Fig 64). Nonetheless, these changes must be tightly controlled, probably by the joint action of other T4SS effectors, as NAD^+ depletion induces necroptotic cell death in macrophages (Pajuelo *et al.*, 2018). Interestingly, the *Brucella abortus* nicotinamidase, an NAD^+ biosynthetic enzyme, is essential for bacteria replication and infectivity, reviewed in Mesquita *et al* (Mesquita *et al.*, 2016).

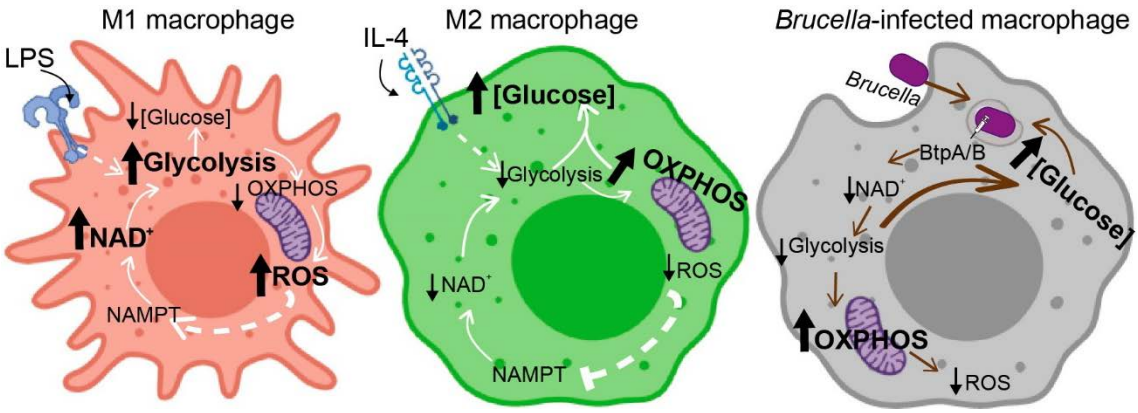

Fig 64.- *Brucella* could benefit from manipulating macrophage metabolism.

Classically activated M1 macrophages (left) are pro-inflammatory and maintain high NAD^+ levels to allow an increased glycolytic flux. Alternative activated M2 macrophages (center), in contrast, are anti-inflammatory and have an increased OXPHOS flux, leading to higher cytosolic glucose concentrations and lower NAD^+ and ROS levels. *Brucella* is proposed to modulate macrophage metabolism (right), though the secretion of the NAD^+ consuming effectors BtpA/B, which may favor replication by increasing cytosolic glucose availability and lowering the ROS levels. Drawings were generated using BioRender and Adobe Illustrator CS6.

Other pathogens play with NAD^+ concentrations, for example, HIV-infected lymphocytes have fewer NAD^+, while *Plasmodium*-containing erythrocytes have higher NAD^+ levels. *Streptococcus pyogenes* encodes an NAD^+ glycohydrolase, which depletes host NAD^+ and ATP, disrupts pro-inflammatory responses derived from PARP-1 signaling, and induces host cell death as reviewed in Mesquita *et al* (Mesquita *et al.*, 2016). In agreement, the addition of the NAD^+ precursor Nam to the cellular culture inhibited *S. pyogenes* growth (Hsieh *et al.*, 2020). Taken together, NAD^+ manipulation promotes *S. pyogenes* survival and chronic persistence, and *Brucella* is likely to act similarly.

Strategies targeting sirtuins, NAD^+ sensing proteins that activate various signaling routes towards immunomodulation, are also reported among pathogens. *Salmonella* induces low NAD^+ and ATP host levels, which may act as a trigger for the pathogen-derived SIRT1 lysosomal degradation, which eventually prevents bacterial clearance through autophagy (Ganesan *et al.*, 2017). Another example is *Mycobacterium tuberculosis,* which plays with host sirtuins, as both pharmacological enhancement of SIRT1 (Cheng *et al.*, 2017) or inhibition of SIRT2 (Bhaskar *et al.*, 2020) reduce bacterial survival. Besides, its Tuberculosis Necrotizing Toxin (TNT) acts as NAD^+ glycohydrolase, which depletes host NAD^+ and induces ROS, promoting necroptosis of macrophages and mycobacterial spreading (Pajuelo *et al.*, 2020).

Limitations and future prospects.

Our approach using *S. cerevisiae* as a model to study not only bacterial TIR effectors but also human TIR adaptors, is a new strategy in the field, as to our knowledge, this is the first time that TIR proteins are issued of yeast heterologous expression, apart from previous yeast-2-hybrid experiments (Enokizono *et al.*, 2013). We trust that it will provide new hints to TIR protein research, which are summarized in (Fig 65).

Among the limitations of the study, the most obvious is the impossibility of checking the signaling capacity of the adaptors tested. On the other hand, this approach offers a unique environment in which the one-to-one relationship of two proteins can be assessed. This leads to the second main limitation, which is due to technical issues of a plasmid-based heterologous expression. The yeast laboratory strains allow the transformation of a limited number of plasmids and require each to bear a different auxotrophic marker. To overcome this issue, different possibilities exist, as using plasmids bearing two opposite side directed promotors (Coronas-Serna *et al.*, 2018), mating two strains already transformed with different plasmids to get a transient expression, or integrating the heterologous constructs directly on the yeast genome, which is a more stable option. Nowadays exciting alternatives appear for yeast genetic manipulation, such as Golden Gate modular cloning (Lee *et al.*, 2015) or the CRISPR/Cas9-based technology for multiple gene integration (Giersch and Finnigan, 2017). Besides, using the *GAL1* promoter enables easy induction or repression of heterologous gene expression in yeast, but the more genes controlled under *GAL1* are introduced in the same cell, the less expression of each one is achieved. Indeed, it can sometimes be difficult to find two different fluorescently tagged proteins with similar brightness levels in the same cell, which renders co-localization experiments more complicated. Choosing different and constitutive promoters bypasses this problem but it is only recommended when expressing innocuous genes.

The present Thesis represents only a small part of the initial steps of a much larger project aiming at innate immunity SMOC signaling reconstruction in yeast, which our team is currently developing. Future aims are to look for easily measurable phenotypes to develop screen platforms enabling testing of pathological mutations or putative new antimicrobial or immunomodulating drugs, as we already did with our yeast PI3K/PTEN/Akt model (Coronas-Serna *et al.*, 2018; Coronas-Serna *et al.*, 2020b). Besides, another exciting branch of the project would be to include plant TIR proteins to test the phenotypes they may induce in yeast. Nevertheless, this work would have never been possible without our collaborators namely, the innate immunity and TLR signaling expert, Dr. Jonathan C. Kagan at Harvard University, and the

host-pathogen interactions and *Brucella* expert, Dr. Suzana Salcedo at CNRS-IBCP-Université de Lyon.

To sum up, *S. cerevisiae* has proved to be a feasible model to aid in the study of TIR domain-containing proteins, and that, together with other cellular models, will hopefully contribute to eventually unravel the nature beyond SMOC signaling and host-pathogen interactions.

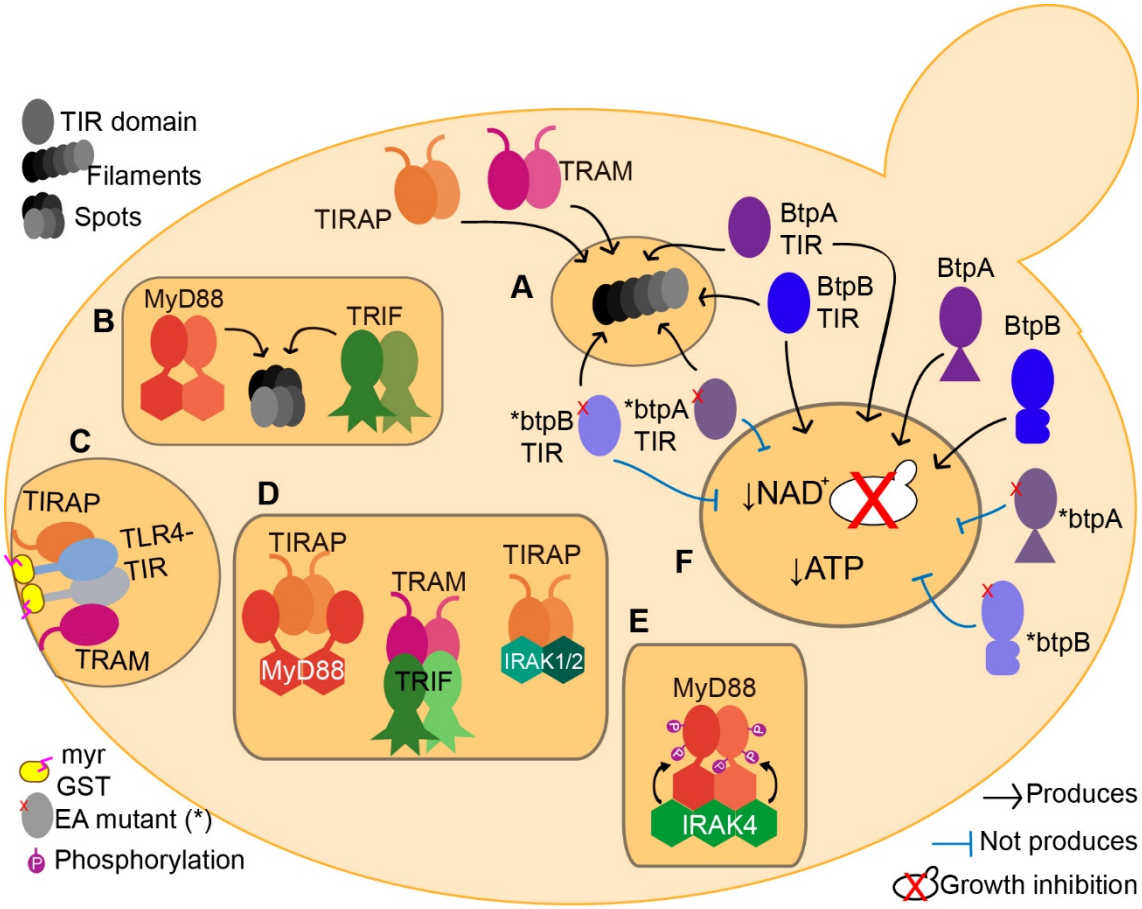

Fig 65.- Studying human TIR adaptors and the *Brucella* TIR effectors through their heterologous expression in *S. cerevisiae*.

(A) TRAM, TIRAP, the WT BtpA/B TIR domains, and the Glu to Ala (EA) mutants on the WxxxE motif, form filaments upon yeast expression. (B) MyD88 and TRIF locate in cytosolic spots. (C) The PM targeted myr-GST-TLR4-TIR construct redirects TIRAP and TRAM to PM patches. (D) Co-purification experiments revealed the interaction in the yeast model of MyD88 + TIRAP, TRIF + TRAM, and TIRAP + IRAK1/2. (E) IRAK4 can directly phosphorylate MyD88 in the yeast model. (F) BtpA, BtpB, and their TIR domains inhibited yeast growth and depleted yeast cellular NAD^+ and ATP levels, while their EA mutants did not cause any toxicity.

Conclusions

Conclusions

1.-The heterologous expression of the human TIR adaptors MyD88, TIRAP, TRIF, TRAM, and the cytosolic side of TLR4 does not alter yeast growth.

2.- TIR-TIR self-interactions are involved in the filament formation of TRAM, TIRAP, and the TIR domains of the *Brucella* effectors BtpA and BtpB upon yeast expression.

3.- MyD88 and TIRAP co-localize in the yeast cell, requiring an intact BB loop, whereas TRIF and TRAM do not co-localize, despite physically interacting.

4.-The yeast model recapitulates the interactions among human adaptors and the TIR domain of TLR4, including the recruitment of TIRAP and TRAM to plasma membrane patches.

5.-Overexpression in *S. cerevisiae* evidenced the ability of IRAK4 to phosphorylate MyD88 on several Ser/Thr residues.

6.- Both IRAK1 and IRAK2 interact with TIRAP, independently of its BB loop, in the yeast system.

7.-The formation of TRAM filaments at the yeast plasma membrane relies on the BB loop and the acidic residues D91 E92.

8.-The expression of *Brucella* TIR proteins in yeast allowed us to confirm the NADase activity of BtpA and to identify for the first time this activity on BtpB.

9.-The glutamic acid on the WxxxE motif of BtpB and the TIR domains of BtpA and BtpB is essential to deplete cellular NAD^+ and consequently to reduce ATP, impair MAPK signaling, and inhibit yeast growth.

10.-The N-terminal non-TIR extensions of BtpA and BtpB determine their subcellular location and modulate their NADase activity.

11.- BtpA and BtpB TIR domain filament formation and toxicity in yeast rely on distinct structural determinants.

12.-The TIR domains of BtpA and BtpB require their catalytic activity to interfere with TRAM filament formation.

Conclusiones

Conclusiones

1.-La expresión heteróloga de los adaptadores TIR humanos MyD88, TIRAP, TRIF, TRAM, así como la de la región citosólica de TLR no alteran el crecimiento de la levadura.

2.- Las interacciones TIR-TIR están implicadas en la formación de filamentos de TRAM, TIRAP y los dominios TIR de los efectores de *Brucella* BtpA y BtpB al expresarse en levadura.

3.- MyD88 y TIRAP co-localizan en la célula de levadura, requiriendo el *BB loop* intacto, mientras que TRIF y TRAM no co-localizan, a pesar de interaccionar físicamente.

4.- El modelo de levadura reproduce las interacciones entre los adaptadores humanos y el dominio TIR de TLR4, incluido el reclutamiento de TIRAP y TRAM a acúmulos en la membrana plasmática

5.- La sobreexpresión en *S. cerevisiae* evidenció la capacidad de IRAK4 de fosforilar MyD88 en varios residuos de Ser/Thr.

6.- Tanto IRAK1 como IRAK2 interaccionan con TIRAP, independientemente de su *BB loop*, en el sistema de levadura.

7.- La formación de los filamentos de TRAM en la membrana plasmática de levadura depende del *BB loop* y de los residuos ácidos D91 E92.

8.- La expresión de las proteínas TIR de *Brucella* en levadura nos ha permitido confirmar la actividad NADasa de BtpA e identificar esta actividad por primera vez en BtpB.

9.- El ácido glutámico del motivo WxxxE de BtpB y de los dominios TIR de BtpA y BtpB es esencial para la eliminación del NAD^+ celular y en consecuencia la reducción del ATP, el impedimento de la señalización por MAPK y la inhibición del crecimiento en levadura.

10.- La extensión N-terminal “no-TIR” de BtpA y BtpB determina su localización subcelular y modula su actividad NADasa.

11.- La formación de filamentos y la toxicidad de los dominios TIR de BtpA y BtpB en levadura dependen de distintos determinantes estructurales.

12.- Los dominios TIR de BtpA y BtpB requieren su actividad catalítica para interferir con la formación de los filamentos de TRAM.

References

References

Aashaq, S., Batool, A., and Andrabi, K.I. (2019). TAK1 mediates convergence of cellular signals for death and survival. Apoptosis *24*, 3-20.

Al-Shabany, A.J., Moody, A.J., Foey, A.D., and Billington, R.A. (2016). Intracellular NAD+ levels are associated with LPS-induced TNF-α release in pro-inflammatory macrophages. Biosci Rep *36*, e00301.

Alaidarous, M., Ve, T., Casey, L.W., Valkov, E., Ericsson, D.J., Ullah, M.O., Schembri, M.A., Mansell, A., Sweet, M.J., and Kobe, B. (2014). Mechanism of bacterial interference with TLR4 signaling by *Brucella* Toll/interleukin-1 receptor domain-containing protein TcpB. J Biol Chem *289*, 654-668.

Alberti, S., Gitler, A.D., and Lindquist, S. (2007). A suite of Gateway cloning vectors for high-throughput genetic analysis in *Saccharomyces cerevisiae*. Yeast *24*, 913-919.

Alemán, A., Fernández-Piñar, P., Pérez-Núñez, D., Rotger, R., Martín, H., and Molina, M. (2009). A yeast-based genetic screen for identification of pathogenic *Salmonella* proteins. FEMS Microbiol Lett *296*, 167-177.

Alemán, A., Rodríguez-Escudero, I., Mallo, G.V., Cid, V.J., Molina, M., and Rotger, R. (2005). The amino-terminal non-catalytic region of *Salmonella* Typhimurium SigD affects actin organization in yeast and mammalian cells. Cell Microbiol *7*, 1432-1446.

Altamirano-Silva, P., Meza-Torres, J., Castillo-Zeledón, A., Ruiz-Villalobos, N., Zuñiga-Pereira, A.M., Chacón-Díaz, C., Moreno, E., Guzmán-Verri, C., and Chaves-Olarte, E. (2018). *Brucella abortus* Senses the Intracellular Environment through the BvrR/BvrS Two-Component System, Which Allows *B. abortus* To Adapt to Its Replicative Niche. Infect Immun *86*.

Alves-Silva, J., Tavares, I.P., Guimarães, E.S., Costa Franco, M.M., Figueiredo, B.C., Marques, J.T., Splitter, G., and Oliveira, S.C. (2017). Modulation of Microtubule Dynamics Affects *Brucella abortus* Intracellular Survival, Pathogen-Containing Vacuole Maturation, and Pro-inflammatory Cytokine Production in Infected Macrophages. Front Microbiol *8*, 2217.

An, Y., Ohnishi, H., Matsui, E., Funato, M., Kato, Z., Teramoto, T., Kaneko, H., Kimura, T., Kubota, K., Kasahara, K*., et al.* (2011). Genetic variations in MyD88 adaptor-like are associated with atopic dermatitis. Int J Mol Med *27*, 795-801.

Andrés-Pons, A., Rodríguez-Escudero, I., Gil, A., Blanco, A., Vega, A., Molina, M., Pulido, R., and Cid, V.J. (2007). *In vivo* functional analysis of the counterbalance of hyperactive phosphatidylinositol 3-kinase p110 catalytic oncoproteins by the tumor suppressor PTEN. Cancer Res *67*, 9731-9739.

Aouizerat, T., Gutman, I., Paz, Y., Maeir, A.M., Gadot, Y., Gelman, D., Szitenberg, A., Drori, E., Pinkus, A., Schoemann, M*., et al.* (2019). Isolation and Characterization of Live Yeast Cells from Ancient Vessels as a Tool in Bio-Archaeology. mBio *10*.

Arellano-Reynoso, B., Lapaque, N., Salcedo, S., Briones, G., Ciocchini, A.E., Ugalde, R., Moreno, E., Moriyón, I., and Gorvel, J.P. (2005). Cyclic beta-1,2-glucan is a *Brucella* virulence factor required for intracellular survival. Nat Immunol *6*, 618-625.

Arnoldo, A., Curak, J., Kittanakom, S., Chevelev, I., Lee, V.T., Sahebol-Amri, M., Koscik, B., Ljuma, L., Roy, P.J., Bedalov, A*., et al.* (2008). Identification of Small Molecule Inhibitors of *Pseudomonas aeruginosa* Exoenzyme S Using a Yeast Phenotypic Screen. PLoS Genet *4*, e1000005.

Arriola Benitez, P.C., Pesce Viglietti, A.I., Herrmann, C.K., Dennis, V.A., Comerci, D.J., Giambartolomei, G.H., and Delpino, M.V. (2018). *Brucella abortus* Promotes a Fibrotic Phenotype in Hepatic Stellate Cells, with Concomitant Activation of the Autophagy Pathway. Infect Immun *86*.

Audrito, V., Managò, A., Gaudino, F., Sorci, L., Messana, V.G., Raffaelli, N., and Deaglio, S. (2019). NAD-Biosynthetic and Consuming Enzymes as Central Players of Metabolic Regulation of Innate and Adaptive Immune Responses in Cancer. Front Immunol *10*, 1720.

Ausubel, F.M. (2001). Current protocols in molecular biology.

Avbelj, M., Horvat, S., and Jerala, R. (2011). The Role of Intermediary Domain of MyD88 in Cell Activation and Therapeutic Inhibition of TLRs. The Journal of Immunology *187*, 2394.

References

Avbelj, M., Panter, G., and Jerala, R. (2018). The role of N-terminal segment and membrane association in MyD88-mediated signaling. Biochem Biophys Res Commun *495*, 878-883.

Avbelj, M., Wolz, O.O., Fekonja, O., Benčina, M., Repič, M., Mavri, J., Krüger, J., Schärfe, C., Delmiro Garcia, M., Panter, G.*, et al.* (2014). Activation of lymphoma-associated MyD88 mutations via allostery-induced TIR-domain oligomerization. Blood *124*, 3896-3904.

Bae, S.C., and Lee, Y.H. (2017). Association between BANK1 polymorphisms and susceptibility to autoimmune diseases: A meta-analysis. Cell Mol Biol (Noisy-le-grand) *63*, 29-35.

Barnett, J.A. (1998). A history of research on yeasts. 1: Work by chemists and biologists 1789-1850. Yeast *14*, 1439-1451.

Barnett, J.A. (2000). A history of research on yeasts 2: Louis Pasteur and his contemporaries, 1850-1880. Yeast *16*, 755-771.

Belvin, M.P., and Anderson, K.V. (1996). A conserved signaling pathway: the *Drosophila* toll-dorsal pathway. Annu Rev Cell Dev Biol *12*, 393-416.

Berger, C.N., Crepin, V.F., Jepson, M.A., Arbeloa, A., and Frankel, G. (2009). The mechanisms used by enteropathogenic *Escherichia coli* to control filopodia dynamics. Cell Microbiol *11*, 309-322.

Berman, H.M., Westbrook, J., Feng, Z., Gilliland, G., Bhat, T.N., Weissig, H., Shindyalov, I.N., and Bourne, P.E. (2000). The Protein Data Bank. Nucleic Acids Research *28*, 235-242.

Bernoux, M., Ve, T., Williams, S., Warren, C., Hatters, D., Valkov, E., Zhang, X., Ellis, J.G., Kobe, B., and Dodds, P.N. (2011). Structural and functional analysis of a plant resistance protein TIR domain reveals interfaces for self-association, signaling, and autoregulation. Cell Host Microbe *9*, 200-211.

Bershadsky, A.D., and Gelfand, V.I. (1981). ATP-dependent regulation of cytoplasmic microtubule disassembly. Proc Natl Acad Sci U S A *78*, 3610-3613.

Bertin, A., McMurray, M.A., Thai, L., Garcia, G., 3rd, Votin, V., Grob, P., Allyn, T., Thorner, J., and Nogales, E. (2010). Phosphatidylinositol-4,5-bisphosphate promotes budding yeast septin filament assembly and organization. J Mol Biol *404*, 711-731.

Beutler, B., and Rehli, M. (2002). Evolution of the TIR, tolls and TLRs: functional inferences from computational biology. Curr Top Microbiol Immunol *270*, 1-21.

Bhaskar, A., Kumar, S., Khan, M.Z., Singh, A., Dwivedi, V.P., and Nandicoori, V.K. (2020). Host sirtuin 2 as an immunotherapeutic target against tuberculosis. eLife *9*, e55415.

Blander, J.M., and Sander, L.E. (2012). Beyond pattern recognition: five immune checkpoints for scaling the microbial threat. Nature reviews Immunology *12*, 215-225.

Bonham, K.S., Orzalli, M.H., Hayashi, K., Wolf, A.I., Glanemann, C., Weninger, W., Iwasaki, A., Knipe, D.M., and Kagan, J.C. (2014). A promiscuous lipid-binding protein diversifies the subcellular sites of toll-like receptor signal transduction. Cell *156*, 705-716.

Bosis, E., Salomon, D., and Sessa, G. (2011). A simple yeast-based strategy to identify host cellular processes targeted by bacterial effector proteins. PLoS One *6*, e27698.

Botstein, D., and Fink, G.R. (1988). Yeast: an experimental organism for modern biology. Science *240*, 1439-1443.

Botstein, D., and Fink, G.R. (2011). Yeast: an experimental organism for 21st Century biology. Genetics *189*, 695-704.

Bovijn, C., Ulrichts, P., De Smet, A.S., Catteeuw, D., Beyaert, R., Tavernier, J., and Peelman, F. (2012). Identification of interaction sites for dimerization and adapter recruitment in Toll/interleukin-1 receptor (TIR) domain of Toll-like receptor 4. J Biol Chem *287*, 4088-4098.

Brewster, J.L., and Gustin, M.C. (2014). Hog1: 20 years of discovery and impact. Sci Signal *7*, re7.

Broz, P., and Dixit, V.M. (2016). Inflammasomes: mechanism of assembly, regulation and signalling. Nat Rev Immunol *16*, 407-420.

Brubaker, S.W., Bonham, K.S., Zanoni, I., and Kagan, J.C. (2015). Innate immune pattern recognition: a cell biological perspective. Annu Rev Immunol *33*, 257-290.

Bulgin, R., Raymond, B., Garnett, J.A., Frankel, G., Crepin, V.F., Berger, C.N., and Arbeloa, A. (2010). Bacterial guanine nucleotide exchange factors SopE-like and WxxxE effectors. Infect Immun *78*, 1417-1425.

Burns, K., Martinon, F., Esslinger, C., Pahl, H., Schneider, P., Bodmer, J.L., Di Marco, F., French, L., and Tschopp, J. (1998). MyD88, an adapter protein involved in interleukin-1 signaling. J Biol Chem *273*, 12203-12209.

Byndloss, M.X., Tsai, A.Y., Walker, G.T., Miller, C.N., Young, B.M., English, B.C., Seyffert, N., Kerrinnes, T., de Jong, M.F., Atluri, V.L.*, et al.* (2019). *Brucella abortus* Infection of Placental Trophoblasts Triggers Endoplasmic Reticulum Stress-Mediated Cell Death and Fetal Loss via Type IV Secretion System-Dependent Activation of CHOP. mBio *10*.

Byndloss, M.X., and Tsolis, R.M. (2016). *Brucella* spp. Virulence Factors and Immunity. Annu Rev Anim Biosci *4*, 111-127.

Carlsson, E., Ding, J.L., and Byrne, B. (2016). SARM modulates MyD88-mediated TLR activation through BB-loop dependent TIR-TIR interactions. Biochim Biophys Acta *1863*, 244-253.

Carty, M., and Bowie, A.G. (2019). SARM: From immune regulator to cell executioner. Biochem Pharmacol *161*, 52-62.

Celli, J. (2019). The Intracellular Life Cycle of *Brucella* spp. Microbiol Spectr *7*.

Celli, J., de Chastellier, C., Franchini, D.-M., Pizarro-Cerda, J., Moreno, E., and Gorvel, J.-P. (2003). *Brucella* evades macrophage killing via VirB-dependent sustained interactions with the endoplasmic reticulum. J Exp Med *198*, 545-556.

Chan, S.L., Low, L.Y., Hsu, S., Li, S., Liu, T., Santelli, E., Le Negrate, G., Reed, J.C., Woods, V.L., Jr., and Pascual, J. (2009). Molecular mimicry in innate immunity: crystal structure of a bacterial TIR domain. J Biol Chem *284*, 21386-21392.

Chan, S.L., Mukasa, T., Santelli, E., Low, L.Y., and Pascual, J. (2010). The crystal structure of a TIR domain from *Arabidopsis thaliana* reveals a conserved helical region unique to plants. Protein Sci *19*, 155-161.

Chaudhary, A., Ganguly, K., Cabantous, S., Waldo, G.S., Micheva-Viteva, S.N., Nag, K., Hlavacek, W.S., and Tung, C.-S. (2012). The *Brucella* TIR-like protein TcpB interacts with the death domain of MyD88. Biochem Biophys Res Commun *417*, 299-304.

Chen, D.C., Yang, B.C., and Kuo, T.T. (1992). One-step transformation of yeast in stationary phase. Curr Genet *21*, 83-84.

Chen, G., Zhuchenko, O., and Kuspa, A. (2007). Immune-like phagocyte activity in the social amoeba. Science *317*, 678-681.

Chen, J.Q., Szodoray, P., and Zeher, M. (2016). Toll-Like Receptor Pathways in Autoimmune Diseases. Clin Rev Allergy Immunol *50*, 1-17.

Cheng, C.Y., Gutierrez, N.M., Marzuki, M.B., Lu, X., Foreman, T.W., Paleja, B., Lee, B., Balachander, A., Chen, J., Tsenova, L.*, et al.* (2017). Host sirtuin 1 regulates mycobacterial immunopathogenesis and represents a therapeutic target against tuberculosis. Sci Immunol *2*.

Cheng, H., Addona, T., Keshishian, H., Dahlstrand, E., Lu, C., Dorsch, M., Li, Z., Wang, A., Ocain, T.D., Li, P.*, et al.* (2007). Regulation of IRAK-4 kinase activity via autophosphorylation within its activation loop. Biochem Biophys Res Commun *352*, 609-616.

Cherry, J.M., Hong, E.L., Amundsen, C., Balakrishnan, R., Binkley, G., Chan, E.T., Christie, K.R., Costanzo, M.C., Dwight, S.S., Engel, S.R.*, et al.* (2012). *Saccharomyces* Genome Database: the genomics resource of budding yeast. Nucleic Acids Res *40*, D700-705.

Chuenchor, W., Jin, T., Ravilious, G., and Xiao, T.S. (2014). Structures of pattern recognition receptors reveal molecular mechanisms of autoinhibition, ligand recognition and oligomerization. Curr Opin Immunol *26*, 14-20.

Cid, V.J., Shulewitz, M.J., McDonald, K.L., and Thorner, J. (2001). Dynamic localization of the Swe1 regulator Hsl7 during the *Saccharomyces cerevisiae* cell cycle. Mol Biol Cell *12*, 1645-1669.

Cirl, C., Wieser, A., Yadav, M., Duerr, S., Schubert, S., Fischer, H., Stappert, D., Wantia, N., Rodriguez, N., Wagner, H.*, et al.* (2008). Subversion of Toll-like receptor signaling by a unique family of bacterial Toll/interleukin-1 receptor domain-containing proteins. Nat Med *14*, 399-406.

Cohen, P., and Strickson, S. (2017). The role of hybrid ubiquitin chains in the MyD88 and other innate immune signalling pathways. Cell Death Differ *24*, 1153-1159.

References

Consortium, T.U. (2018). UniProt: a worldwide hub of protein knowledge. Nucleic Acids Research *47*, D506-D515.

Coronas-Serna, J.M., Fernández-Acero, T., Molina, M., and Cid, V.J. (2018). A humanized yeast-based toolkit for monitoring phosphatidylinositol 3-kinase activity at both single cell and population levels. Microb Cell *5*, 545-554.

Coronas-Serna, J.M., Louche, A., Rodríguez-Escudero, M., Roussin, M., Imbert, P.R.C., Rodríguez-Escudero, I., Terradot, L., Molina, M., Gorvel, J.P., Cid, V.J.*, et al.* (2020a). The TIR-domain containing effectors BtpA and BtpB from *Brucella abortus* impact NAD metabolism. PLoS Pathog *16*, e1007979.

Coronas-Serna, J.M., Valenti, M., Del Val, E., Fernández-Acero, T., Rodríguez-Escudero, I., Mingo, J., Luna, S., Torices, L., Pulido, R., Molina, M.*, et al.* (2020b). Modeling human disease in yeast: recreating the PI3K-PTEN-Akt signaling pathway in *Saccharomyces cerevisiae*. Int Microbiol *23*, 75-87.

Curak, J., Rohde, J., and Stagljar, I. (2009). Yeast as a tool to study bacterial effectors. Curr Opin Microbiol *12*, 18-23.

Cushing, L., Stochaj, W., Siegel, M., Czerwinski, R., Dower, K., Wright, Q., Hirschfield, M., Casanova, J.L., Picard, C., Puel, A.*, et al.* (2014). Interleukin 1/Toll-like receptor-induced autophosphorylation activates interleukin 1 receptor-associated kinase 4 and controls cytokine induction in a cell type-specific manner. J Biol Chem *289*, 10865-10875.

de Barsy, M., Jamet, A., Filopon, D., Nicolas, C., Laloux, G., Rual, J.-F., Muller, A., Twizere, J.-C., Nkengfac, B., Vandenhaute, J.*, et al.* (2011). Identification of a *Brucella* spp. secreted effector specifically interacting with human small GTPase Rab2. Cellular Microbiology *13*, 1044-1058.

de Bolle, X., Letesson, J.J., and Gorvel, J.P. (2012). Small GTPases and *Brucella* entry into the endoplasmic reticulum. Biochem Soc Trans *40*, 1348-1352.

De Craene, J.-O., Bertazzi, D.L., Bär, S., and Friant, S. (2017). Phosphoinositides, Major Actors in Membrane Trafficking and Lipid Signaling Pathways. International Journal of Molecular Sciences *18*, 634.

de Jong, M.F., Starr, T., Winter, M.G., den Hartigh, A.B., Child, R., Knodler, L.A., van Dijl, J.M., Celli, J., and Tsolis, R.M. (2013). Sensing of Bacterial Type IV Secretion via the Unfolded Protein Response. mBio *4*, e00418-00412.

de Jong, M.F., Sun, Y.H., den Hartigh, A.B., van Dijl, J.M., and Tsolis, R.M. (2008). Identification of VceA and VceC, two members of the VjbR regulon that are translocated into macrophages by the *Brucella* type IV secretion system. Mol Microbiol *70*, 1378-1396.

De Meyer, I., Martinet, W., Van Hove, C.E., Schrijvers, D.M., Hoymans, V.Y., Van Vaeck, L., Fransen, P., Bult, H., and De Meyer, G.R. (2011). Inhibition of inositol monophosphatase by lithium chloride induces selective macrophage apoptosis in atherosclerotic plaques. Br J Pharmacol *162*, 1410-1423.

Deason, K., Troutman, T.D., Jain, A., Challa, D.K., Mandraju, R., Brewer, T., Ward, E.S., and Pasare, C. (2018). BCAP links IL-1R to the PI3K-mTOR pathway and regulates pathogenic Th17 cell differentiation. J Exp Med *215*, 2413-2428.

Deguine, J., and Barton, G.M. (2014). MyD88: a central player in innate immune signaling. F1000Prime Rep *6*, 97-97.

Dehio, C., and Tsolis, R.M. (2017). Type IV Effector Secretion and Subversion of Host Functions by *Bartonella* and *Brucella* Species. Curr Top Microbiol Immunol *413*, 269-295.

Döhmer, P.H., Valguarnera, E., Czibener, C., and Ugalde, J.E. (2014). Identification of a type IV secretion substrate of *Brucella abortus* that participates in the early stages of intracellular survival. Cell Microbiol *16*, 396-410.

Domingues, L., Ismail, A., Charro, N., Rodríguez-Escudero, I., Holden, D.W., Molina, M., Cid, V.J., and Mota, L.J. (2016). The *Salmonella* effector SteA binds phosphatidylinositol 4-phosphate for subcellular targeting within host cells. Cell Microbiol *18*, 949-969.

Doron, S., Melamed, S., Ofir, G., Leavitt, A., Lopatina, A., Keren, M., Amitai, G., and Sorek, R. (2018). Systematic discovery of antiphage defense systems in the microbial pangenome. Science (New York, NY) *359*, eaar4120.

Drouin, M., Saenz, J., and Chiffoleau, E. (2020). C-Type Lectin-Like Receptors: Head or Tail in Cell Death Immunity. Front Immunol *11*, 251-251.

Dunne, A., Carpenter, S., Brikos, C., Gray, P., Strelow, A., Wesche, H., Morrice, N., and O'Neill, L.A. (2010). IRAK1 and IRAK4 promote phosphorylation, ubiquitination, and degradation of MyD88 adaptor-like (Mal). J Biol Chem *285*, 18276-18282.

Durward, M., Radhakrishnan, G., Harms, J., Bareiss, C., Magnani, D., and Splitter, G.A. (2012). Active evasion of CTL mediated killing and low quality responding CD8+ T cells contribute to persistence of brucellosis. PLoS One *7*, e34925.

Enokizono, Y., Kumeta, H., Funami, K., Horiuchi, M., Sarmiento, J., Yamashita, K., Standley, D.M., Matsumoto, M., Seya, T., and Inagaki, F. (2013). Structures and interface mapping of the TIR domain-containing adaptor molecules involved in interferon signaling. Proc Natl Acad Sci U S A *110*, 19908-19913.

Essuman, K., Summers, D.W., Sasaki, Y., Mao, X., DiAntonio, A., and Milbrandt, J. (2017). The SARM1 Toll/Interleukin-1 Receptor Domain Possesses Intrinsic NAD(+) Cleavage Activity that Promotes Pathological Axonal Degeneration. Neuron *93*, 1334-1343.e1335.

Essuman, K., Summers, D.W., Sasaki, Y., Mao, X., Yim, A.K.Y., DiAntonio, A., and Milbrandt, J. (2018). TIR Domain Proteins Are an Ancient Family of NAD(+)-Consuming Enzymes. Curr Biol *28*, 421-430.e424.

European Food Safety, A., European Centre for Disease, P., and Control (2019). The European Union One Health 2018 Zoonoses Report. EFSA Journal *17*, e05926.

Evavold, C.L., and Kagan, J.C. (2018). How Inflammasomes Inform Adaptive Immunity. J Mol Biol *430*, 217-237.

Farkašovský, M. (2020). Septin architecture and function in budding yeast. Biol Chem *401*, 903-919.

Fehr, A.R., Singh, S.A., Kerr, C.M., Mukai, S., Higashi, H., and Aikawa, M. (2020). The impact of PARPs and ADP-ribosylation on inflammation and host-pathogen interactions. Genes Dev *34*, 341-359.

Feldmann, H. (2010). Yeast molecular and cell biology.

Felix, C., Kaplan Türköz, B., Ranaldi, S., Koelblen, T., Terradot, L., O'Callaghan, D., and Vergunst, A.C. (2014). The *Brucella* TIR domain containing proteins BtpA and BtpB have a structural WxxxE motif important for protection against microtubule depolymerisation. Cell Commun Signal *12*, 53.

Fernández-Acero, T., Bertalmio, E., Luna, S., Mingo, J., Bravo-Plaza, I., Rodríguez-Escudero, I., Molina, M., Pulido, R., and Cid, V.J. (2019). Expression of Human PTEN-L in a Yeast Heterologous Model Unveils Specific N-Terminal Motifs Controlling PTEN-L Subcellular Localization and Function. Cells *8*.

Fernández-Acero, T., Rodríguez-Escudero, I., Molina, M., and Cid, V.J. (2015). The yeast cell wall integrity pathway signals from recycling endosomes upon elimination of phosphatidylinositol (4,5)-bisphosphate by mammalian phosphatidylinositol 3-kinase. Cell Signal *27*, 2272-2284.

Fernández-Acero, T., Rodríguez-Escudero, I., Vicente, F., Monteiro, M.C., Tormo, J.R., Cantizani, J., Molina, M., and Cid, V.J. (2012). A yeast-based *in vivo* bioassay to screen for class I phosphatidylinositol 3-kinase specific inhibitors. J Biomol Screen *17*, 1018-1029.

Fernandez-Piñar, P., Alemán, A., Sondek, J., Dohlman, H.G., Molina, M., and Martín, H. (2012). The *Salmonella* Typhimurium effector SteC inhibits Cdc42-mediated signaling through binding to the exchange factor Cdc24 in *Saccharomyces cerevisiae*. Molecular Biology of the Cell *23*, 4430-4443.

Ferrao, R., and Wu, H. (2012). Helical assembly in the death domain (DD) superfamily. Curr Opin Struct Biol *22*, 241-247.

Ferwerda, B., Alonso, S., Banahan, K., McCall, M.B., Giamarellos-Bourboulis, E.J., Ramakers, B.P., Mouktaroudi, M., Fain, P.R., Izagirre, N., Syafruddin, D*., et al.* (2009). Functional and genetic evidence that the Mal/TIRAP allele variant 180L has been selected by providing protection against septic shock. Proc Natl Acad Sci U S A *106*, 10272-10277.

Fessler, M.B., and Parks, J.S. (2011). Intracellular lipid flux and membrane microdomains as organizing principles in inflammatory cell signaling. J Immunol *187*, 1529-1535.

References

Fields, S., and Song, O. (1989). A novel genetic system to detect protein-protein interactions. Nature *340*, 245-246.

Fitzgerald, K.A., and Kagan, J.C. (2020). Toll-like Receptors and the Control of Immunity. Cell *180*, 1044-1066.

Fitzgerald, K.A., Palsson-McDermott, E.M., Bowie, A.G., Jefferies, C.A., Mansell, A.S., Brady, G., Brint, E., Dunne, A., Gray, P., Harte, M.T.*, et al.* (2001). Mal (MyD88-adapter-like) is required for Toll-like receptor-4 signal transduction. Nature *413*, 78-83.

Franc, K.A., Krecek, R.C., Häsler, B.N., and Arenas-Gamboa, A.M. (2018). Brucellosis remains a neglected disease in the developing world: a call for interdisciplinary action. BMC Public Health *18*, 125-125.

Francis, R., Singh, P.K., Singh, S., Giri, S., and Kumar, A. (2020). Glycolytic inhibitor 2-deoxyglucose suppresses inflammatory response in innate immune cells and experimental staphylococcal endophthalmitis. Exp Eye Res *197*, 108079.

Fulgione, A., Di Matteo, A., Contaldi, F., Manco, R., Ianniello, F., Incerti, G., De Seta, M., Esposito, N., Crasto, A., Iannelli, D.*, et al.* (2016). Epistatic interaction between MyD88 and TIRAP against *Helicobacter pylori*. FEBS Lett *590*, 2127-2137.

Funami, K., Matsumoto, M., Enokizono, Y., Ishii, N., Tatematsu, M., Oshiumi, H., Inagaki, F., and Seya, T. (2015). Identification of a Regulatory Acidic Motif as the Determinant of Membrane Localization of TICAM-2. J Immunol *195*, 4456-4465.

Funami, K., Matsumoto, M., Oshiumi, H., Inagaki, F., and Seya, T. (2017). Functional interfaces between TICAM-2/TRAM and TICAM-1/TRIF in TLR4 signaling. Biochem Soc Trans *45*, 929-935.

Funami, K., Sasai, M., Ohba, Y., Oshiumi, H., Seya, T., and Matsumoto, M. (2007). Spatiotemporal mobilization of Toll/IL-1 receptor domain-containing adaptor molecule-1 in response to dsRNA. J Immunol *179*, 6867-6872.

Funami, K., Sasai, M., Oshiumi, H., Seya, T., and Matsumoto, M. (2008). Homo-oligomerization is essential for Toll/interleukin-1 receptor domain-containing adaptor molecule-1-mediated NF-kappaB and interferon regulatory factor-3 activation. J Biol Chem *283*, 18283-18291.

Ganesan, R., Hos, N.J., Gutierrez, S., Fischer, J., Stepek, J.M., Daglidu, E., Krönke, M., and Robinson, N. (2017). *Salmonella* Typhimurium disrupts Sirt1/AMPK checkpoint control of mTOR to impair autophagy. PLoS Pathog *13*, e1006227.

Garlanda, C., Anders, H.J., and Mantovani, A. (2009). TIR8/SIGIRR: an IL-1R/TLR family member with regulatory functions in inflammation and T cell polarization. Trends Immunol *30*, 439-446.

Garlanda, C., Riva, F., Bonavita, E., and Mantovani, A. (2013). Negative regulatory receptors of the IL-1 family. Semin Immunol *25*, 408-415.

Garrenton, L.S., Stefan, C.J., McMurray, M.A., Emr, S.D., and Thorner, J. (2010). Pheromone-induced anisotropy in yeast plasma membrane phosphatidylinositol-4,5-bisphosphate distribution is required for MAPK signaling. Proc Natl Acad Sci U S A *107*, 11805-11810.

Georg, I., Díaz-Barreiro, A., Morell, M., Pey, A.L., and Alarcón-Riquelme, M.E. (2019). BANK1 interacts with TRAF6 and MyD88 in innate immune signaling in B cells. Cell Mol Immunol.

George, J., Kubarenko, A.V., Rautanen, A., Mills, T.C., Colak, E., Kempf, T., Hill, A.V., Nieters, A., and Weber, A.N. (2010). MyD88 adaptor-like D96N is a naturally occurring loss-of-function variant of TIRAP. J Immunol *184*, 3025-3032.

George, J., Motshwene, P.G., Wang, H., Kubarenko, A.V., Rautanen, A., Mills, T.C., Hill, A.V., Gay, N.J., and Weber, A.N. (2011). Two human MYD88 variants, S34Y and R98C, interfere with MyD88-IRAK4-myddosome assembly. J Biol Chem *286*, 1341-1353.

Gerdts, J., Summers, D.W., Sasaki, Y., DiAntonio, A., and Milbrandt, J. (2013). Sarm1-mediated axon degeneration requires both SAM and TIR interactions. J Neurosci *33*, 13569-13580.

Giersch, R.M., and Finnigan, G.C. (2017). Yeast Still a Beast: Diverse Applications of CRISPR/Cas Editing Technology in *S. cerevisiae*. Yale J Biol Med *90*, 643-651.

Głowacka, P., Żakowska, D., Naylor, K., Niemcewicz, M., and Bielawska-Drózd, A. (2018). *Brucella* - Virulence Factors, Pathogenesis and Treatment. Pol J Microbiol *67*, 151-161.

Goffeau, A., Barrell, B.G., Bussey, H., Davis, R.W., Dujon, B., Feldmann, H., Galibert, F., Hoheisel, J.D., Jacq, C., Johnston, M.*, et al.* (1996). Life with 6000 genes. Science *274*, 546, 563-547.

Gomes, A.P., Price, N.L., Ling, A.J., Moslehi, J.J., Montgomery, M.K., Rajman, L., White, J.P., Teodoro, J.S., Wrann, C.D., Hubbard, B.P.*, et al.* (2013). Declining NAD(+) induces a pseudohypoxic state disrupting nuclear-mitochondrial communication during aging. Cell *155*, 1624-1638.

Gong, J., Wei, T., Stark, R.W., Jamitzky, F., Heckl, W.M., Anders, H.J., Lech, M., and Rössle, S.C. (2010). Inhibition of Toll-like receptors TLR4 and 7 signaling pathways by SIGIRR: A computational approach. Journal of Structural Biology *169*, 323-330.

Gray, P., Dunne, A., Brikos, C., Jefferies, C.A., Doyle, S.L., and O'Neill, L.A. (2006). MyD88 adapter-like (Mal) is phosphorylated by Bruton's tyrosine kinase during TLR2 and TLR4 signal transduction. J Biol Chem *281*, 10489-10495.

Grohmann, E., Christie, P.J., Waksman, G., and Backert, S. (2018). Type IV secretion in Gram-negative and Gram-positive bacteria. Mol Microbiol *107*, 455-471.

Guidolin, L.S., Arce-Gorvel, V., Ciocchini, A.E., Comerci, D.J., and Gorvel, J.P. (2018). Cyclic β-glucans at the bacteria-host cells interphase: One sugar ring to rule them all. Cell Microbiol *20*, e12850.

Gurung, P., Fan, G., Lukens, J.R., Vogel, P., Tonks, N.K., and Kanneganti, T.D. (2017). Tyrosine Kinase SYK Licenses MyD88 Adaptor Protein to Instigate IL-1α-Mediated Inflammatory Disease. Immunity *46*, 635-648.

Guven-Maiorov, E., Keskin, O., Gursoy, A., VanWaes, C., Chen, Z., Tsai, C.J., and Nussinov, R. (2015). The Architecture of the TIR Domain Signalosome in the Toll-like Receptor-4 Signaling Pathway. Sci Rep *5*, 13128.

Ha, H.J., Chun, H.L., and Park, H.H. (2020). Assembly of platforms for signal transduction in the new era: dimerization, helical filament assembly, and beyond. Exp Mol Med, 10.1038/s12276-12020-10391-12273.

Halabi, S., Sekine, E., Verstak, B., Gay, N.J., and Moncrieffe, M.C. (2017). Structure of the Toll/Interleukin-1 Receptor (TIR) Domain of the B-cell Adaptor That Links Phosphoinositide Metabolism with the Negative Regulation of the Toll-like Receptor (TLR) Signalosome. J Biol Chem *292*, 652-660.

Hammond, G.R. (2016). Does PtdIns(4,5)P2 concentrate so it can multi-task? Biochem Soc Trans *44*, 228-233.

Han, C., Jin, J., Xu, S., Liu, H., Li, N., and Cao, X. (2010). Integrin CD11b negatively regulates TLR-triggered inflammatory responses by activating Syk and promoting degradation of MyD88 and TRIF via Cbl-b. Nat Immunol *11*, 734-742.

Harrison, J.C., Bardes, E.S., Ohya, Y., and Lew, D.J. (2001). A role for the Pkc1p/Mpk1p kinase cascade in the morphogenesis checkpoint. Nat Cell Biol *3*, 417-420.

Hartwell, L.H. (1974). *Saccharomyces cerevisiae* cell cycle. Bacteriol Rev *38*, 164-198.

Hasan, U., Chaffois, C., Gaillard, C., Saulnier, V., Merck, E., Tancredi, S., Guiet, C., Brière, F., Vlach, J., Lebecque, S.*, et al.* (2005). Human TLR10 is a functional receptor, expressed by B cells and plasmacytoid dendritic cells, which activates gene transcription through MyD88. J Immunol *174*, 2942-2950.

Hawn, T.R., Dunstan, S.J., Thwaites, G.E., Simmons, C.P., Thuong, N.T., Lan, N.T.N., Quy, H.T., Chau, T.T.H., Hieu, N.T., Rodrigues, S.*, et al.* (2006). A polymorphism in Toll-interleukin 1 receptor domain containing adaptor protein is associated with susceptibility to meningeal tuberculosis. J Infect Dis *194*, 1127-1134.

Henrick, B.M., Yao, X.-D., Zahoor, M.A., Abimiku, A.l., Osawe, S., and Rosenthal, K.L. (2019). TLR10 Senses HIV-1 Proteins and Significantly Enhances HIV-1 Infection. Front Immunol *10*, 482-482.

Herskowitz, I. (1988). Life cycle of the budding yeast *Saccharomyces cerevisiae*. Microbiol Rev *52*, 536-553.

Hibino, T., Loza-Coll, M., Messier, C., Majeske, A.J., Cohen, A.H., Terwilliger, D.P., Buckley, K.M., Brockton, V., Nair, S.V., Berney, K.*, et al.* (2006). The immune gene repertoire encoded in the purple sea urchin genome. Dev Biol *300*, 349-365.

References

Honda, K., Yanai, H., Mizutani, T., Negishi, H., Shimada, N., Suzuki, N., Ohba, Y., Takaoka, A., Yeh, W.-C., and Taniguchi, T. (2004). Role of a transductional-transcriptional processor complex involving MyD88 and IRF-7 in Toll-like receptor signaling. Proc Natl Acad Sci U S A *101*, 15416-15421.

Hong, L., Wang, S., Guo, J., Yin, X., Yu, Q., Yang, M., Wang, Y., Ke, Y., and Li, W. (2019). Bacterial TIR domain-derived peptides inhibit innate immune signaling and catabolic responses in chondrocyte. Mol Biol Rep *46*, 2493-2504.

Hornbeck, P.V., Zhang, B., Murray, B., Kornhauser, J.M., Latham, V., and Skrzypek, E. (2015). PhosphoSitePlus, 2014: mutations, PTMs and recalibrations. Nucleic Acids Res *43*, D512-520.

Horng, T., Barton, G.M., Flavell, R.A., and Medzhitov, R. (2002). The adaptor molecule TIRAP provides signalling specificity for Toll-like receptors. Nature *420*, 329-333.

Horng, T., Barton, G.M., and Medzhitov, R. (2001). TIRAP: an adapter molecule in the Toll signaling pathway. Nat Immunol *2*, 835-841.

Horsefield, S., Burdett, H., Zhang, X., Manik, M.K., Shi, Y., Chen, J., Qi, T., Gilley, J., Lai, J.S., Rank, M.X., *et al.* (2019). NAD(+) cleavage activity by animal and plant TIR domains in cell death pathways. Science *365*, 793-799.

Hsieh, C.L., Hsieh, S.Y., Huang, H.M., Lu, S.L., Omori, H., Zheng, P.X., Ho, Y.N., Cheng, Y.L., Lin, Y.S., Chiang-Ni, C., *et al.* (2020). Nicotinamide Increases Intracellular NAD(+) Content to Enhance Autophagy-Mediated Group A Streptococcal Clearance in Endothelial Cells. Front Microbiol *11*, 117.

Hu, M.M., Xie, X.Q., Yang, Q., Liao, C.Y., Ye, W., Lin, H., and Shu, H.B. (2015). TRIM38 Negatively Regulates TLR3/4-Mediated Innate Immune and Inflammatory Responses by Two Sequential and Distinct Mechanisms. J Immunol *195*, 4415-4425.

Huai, W., Song, H., Wang, L., Li, B., Zhao, J., Han, L., Gao, C., Jiang, G., Zhang, L., and Zhao, W. (2015). Phosphatase PTPN4 preferentially inhibits TRIF-dependent TLR4 pathway by dephosphorylating TRAM. J Immunol *194*, 4458-4465.

Huang, H., Arighi, C.N., Ross, K.E., Ren, J., Li, G., Chen, S.-C., Wang, Q., Cowart, J., Vijay-Shanker, K., and Wu, C.H. (2017). iPTMnet: an integrated resource for protein post-translational modification network discovery. Nucleic Acids Research *46*, D542-D550.

Huang, J., Lesser, C.F., and Lory, S. (2008). The essential role of the CopN protein in *Chlamydia pneumoniae* intracellular growth. Nature *456*, 112-115.

Hughes, M.M., Lavrencic, P., Coll, R.C., Ve, T., Ryan, D.G., Williams, N.C., Menon, D., Mansell, A., Board, P.G., Mobli, M., *et al.* (2017). Solution structure of the TLR adaptor MAL/TIRAP reveals an intact BB loop and supports MAL Cys91 glutathionylation for signaling. Proc Natl Acad Sci U S A *114*, E6480-e6489.

Hyun, K.G., Lee, Y., Yoon, J., Yi, H., and Song, J.J. (2016). Crystal structure of *Arabidopsis thaliana* SNC1 TIR domain. Biochem Biophys Res Commun *481*, 146-152.

Imbert, P.R., Louche, A., Luizet, J.B., Grandjean, T., Bigot, S., Wood, T.E., Gagné, S., Blanco, A., Wunderley, L., Terradot, L., *et al.* (2017). A *Pseudomonas aeruginosa* TIR effector mediates immune evasion by targeting UBAP1 and TLR adaptors. Embo j *36*, 1869-1887.

Ishii, A., Kawasaki, M., Matsumoto, M., Tochinai, S., and Seya, T. (2007). Phylogenetic and expression analysis of amphibian *Xenopus* Toll-like receptors. Immunogenetics *59*, 281-293.

Jakka, P., Bhargavi, B., Namani, S., Murugan, S., Splitter, G., and Radhakrishnan, G. (2018). Cytoplasmic Linker Protein CLIP170 Negatively Regulates TLR4 Signaling by Targeting the TLR Adaptor Protein TIRAP. J Immunol *200*, 704-714.

Jakka, P., Namani, S., Murugan, S., Rai, N., and Radhakrishnan, G. (2017). The *Brucella* effector protein TcpB induces degradation of inflammatory caspases and thereby subverts non-canonical inflammasome activation in macrophages. J Biol Chem *292*, 20613-20627.

Jang, T.H., and Park, H.H. (2014). Crystal structure of TIR domain of TLR6 reveals novel dimeric interface of TIR-TIR interaction for toll-like receptor signaling pathway. J Mol Biol *426*, 3305-3313.

Janssens, S., Burns, K., Tschopp, J., and Beyaert, R. (2002). Regulation of Interleukin-1- and Lipopolysaccharide-Induced NF-κB Activation by Alternative Splicing of MyD88. Current Biology *12*, 467-471.

Jault, C., Pichon, L., and Chluba, J. (2004). Toll-like receptor gene family and TIR-domain adapters in *Danio rerio*. Mol Immunol *40*, 759-771.

Jaý, M., Girault, G., Perrot, L., Taunay, B., Vuilmet, T., Rossignol, F., Pitel, P.-H., Picard, E., Ponsart, C., and Mick, V. (2018). Phenotypic and Molecular Characterization of *Brucella microti*-Like Bacteria From a Domestic Marsh Frog (*Pelophylax ridibundus*). Frontiers in Veterinary Science *5*.

Jenkins, K.A., and Mansell, A. (2010). TIR-containing adaptors in Toll-like receptor signalling. Cytokine *49*, 237-244.

Jiménez-Gutiérrez, E., Alegría-Carrasco, E., Sellers-Moya, Á., Molina, M., and Martín, H. (2020). Not just the wall: the other ways to turn the yeast CWI pathway on. Int Microbiol *23*, 107-119.

Ka, D., Oh, H., Park, E., Kim, J.H., and Bae, E. (2020). Structural and functional evidence of bacterial antiphage protection by Thoeris defense system via NAD(+) degradation. Nat Commun *11*, 2816.

Kachroo, A.H., Laurent, J.M., Yellman, C.M., Meyer, A.G., Wilke, C.O., and Marcotte, E.M. (2015). Evolution. Systematic humanization of yeast genes reveals conserved functions and genetic modularity. Science *348*, 921-925.

Kagan, J.C., Magupalli, V.G., and Wu, H. (2014). SMOCs: supramolecular organizing centres that control innate immunity. Nat Rev Immunol *14*, 821-826.

Kagan, J.C., and Medzhitov, R. (2006). Phosphoinositide-Mediated Adaptor Recruitment Controls Toll-like Receptor Signaling. Cell *125*, 943-955.

Kagan, J.C., Su, T., Horng, T., Chow, A., Akira, S., and Medzhitov, R. (2008). TRAM couples endocytosis of Toll-like receptor 4 to the induction of interferon-beta. Nat Immunol *9*, 361-368.

Kaplan-Türköz, B., Koelblen, T., Felix, C., Candusso, M.P., O'Callaghan, D., Vergunst, A.C., and Terradot, L. (2013). Structure of the Toll/interleukin 1 receptor (TIR) domain of the immunosuppressive *Brucella* effector BtpA/Btp1/TcpB. FEBS Lett *587*, 3412-3416.

Karody, V.R., Le, M., Nelson, S., Meskin, K., Klemm, S., Simpson, P., Hines, R., and Sampath, V. (2013). A TIR domain receptor-associated protein (TIRAP) variant SNP (rs8177374) confers protection against premature birth. J Perinatol *33*, 341-346.

Kawai, T., and Akira, S. (2007). Signaling to NF-kappaB by Toll-like receptors. Trends Mol Med *13*, 460-469.

Ke, Y., Li, W., Wang, Y., Yang, M., Guo, J., Zhan, S., Du, X., Wang, Z., Yang, M., Li, J.*, et al.* (2016). Inhibition of TLR4 signaling by *Brucella* TIR-containing protein TcpB-derived decoy peptides. Int J Med Microbiol *306*, 391-400.

Ke, Y., Wang, Y., Li, W., and Chen, Z. (2015). Type IV secretion system of *Brucella* spp. and its effectors. Front Cell Infect Microbiol *5*, 72.

Keestra, A.M., de Zoete, M.R., Bouwman, L.I., Vaezirad, M.M., and van Putten, J.P. (2013). Unique features of chicken Toll-like receptors. Dev Comp Immunol *41*, 316-323.

Kelly, B., and O'Neill, L.A. (2015). Metabolic reprogramming in macrophages and dendritic cells in innate immunity. Cell Res *25*, 771-784.

Khan, J.A., Brint, E.K., O'Neill, L.A., and Tong, L. (2004). Crystal structure of the Toll/interleukin-1 receptor domain of human IL-1RAPL. J Biol Chem *279*, 31664-31670.

Khor, C.C., Chapman, S.J., Vannberg, F.O., Dunne, A., Murphy, C., Ling, E.Y., Frodsham, A.J., Walley, A.J., Kyrieleis, O., Khan, A.*, et al.* (2007). A Mal functional variant is associated with protection against invasive pneumococcal disease, bacteremia, malaria and tuberculosis. Nat Genet *39*, 523-528.

Khurana, V., and Lindquist, S. (2010). Modelling neurodegeneration in *Saccharomyces cerevisiae*: why cook with baker's yeast? Nat Rev Neurosci *11*, 436-449.

Kim, S., Park, J., Kim, T., and Lee, J.S. (2020). The functional study of human proteins using humanized yeast. J Microbiol *58*, 343-349.

Krogh, A., Larsson, B., von Heijne, G., and Sonnhammer, E.L. (2001). Predicting transmembrane protein topology with a hidden Markov model: application to complete genomes. J Mol Biol *305*, 567-580.

Krumm, B., Xiang, Y., and Deng, J. (2014). Structural biology of the IL-1 superfamily: key cytokines in the regulation of immune and inflammatory responses. Protein Sci *23*, 526-538.

References

Kubo-Murai, M., Hazeki, K., Sukenobu, N., Yoshikawa, K., Nigorikawa, K., Inoue, K., Yamamoto, T., Matsumoto, M., Seya, T., Inoue, N.*, et al.* (2007). Protein kinase Cdelta binds TIRAP/Mal to participate in TLR signaling. Mol Immunol *44*, 2257-2264.

Lacerda, T.L., Salcedo, S.P., and Gorvel, J.P. (2013). *Brucella* T4SS: the VIP pass inside host cells. Curr Opin Microbiol *16*, 45-51.

Latty, S.L., Sakai, J., Hopkins, L., Verstak, B., Paramo, T., Berglund, N.A., Cammarota, E., Cicuta, P., Gay, N.J., Bond, P.J.*, et al.* (2018). Activation of Toll-like receptors nucleates assembly of the MyDDosome signaling hub. Elife *7*.

Lauenstein, J.U., Scherm, M.J., Udgata, A., Moncrieffe, M.C., Fisher, D.I., and Gay, N.J. (2020). Negative Regulation of TLR Signaling by BCAP Requires Dimerization of Its DBB Domain. J Immunol *204*, 2269-2276.

Laurent, J.M., Young, J.H., Kachroo, A.H., and Marcotte, E.M. (2016). Efforts to make and apply humanized yeast. Brief Funct Genomics *15*, 155-163.

Lee, A.H., Bastedo, D.P., Youn, J.Y., Lo, T., Middleton, M.A., Kireeva, I., Lee, J.Y., Sharifpoor, S., Baryshnikova, A., Zhang, J.*, et al.* (2019). Identifying *Pseudomonas syringae* Type III Secreted Effector Function via a Yeast Genomic Screen. G3 (Bethesda) *9*, 535-547.

Lee, B.C., Miyata, M., Lim, J.H., and Li, J.D. (2016). Deubiquitinase CYLD acts as a negative regulator for bacterium NTHi-induced inflammation by suppressing K63-linked ubiquitination of MyD88. Proc Natl Acad Sci U S A *113*, E165-171.

Lee, M.E., DeLoache, W.C., Cervantes, B., and Dueber, J.E. (2015). A Highly Characterized Yeast Toolkit for Modular, Multipart Assembly. ACS Synthetic Biology *4*, 975-986.

Lee, Y.S., Park, J.S., Kim, J.H., Jung, S.M., Lee, J.Y., Kim, S.J., and Park, S.H. (2011). Smad6-specific recruitment of Smurf E3 ligases mediates TGF-β1-induced degradation of MyD88 in TLR4 signalling. Nat Commun *2*, 460.

Lemaitre, B., Nicolas, E., Michaut, L., Reichhart, J.M., and Hoffmann, J.A. (1996). The dorsoventral regulatory gene cassette spätzle/Toll/cactus controls the potent antifungal response in *Drosophila* adults. Cell *86*, 973-983.

Li, K., and Zhong, B. (2018). Regulation of Cellular Antiviral Signaling by Modifications of Ubiquitin and Ubiquitin-like Molecules. Immune Netw *18*, e4.

Li, W., Ke, Y., Wang, Y., Yang, M., Gao, J., Zhan, S., Xinying, D., Huang, L., Li, W., Chen, Z.*, et al.* (2016). *Brucella* TIR-like protein TcpB/Btp1 specifically targets the host adaptor protein MAL/TIRAP to promote infection. Biochem Biophys Res Commun *477*, 509-514.

Lin, S.-C., Lo, Y.-C., and Wu, H. (2010). Helical assembly in the MyD88-IRAK4-IRAK2 complex in TLR/IL-1R signalling. Nature *465*, 885-890.

Lin, Z., Lu, J., Zhou, W., and Shen, Y. (2012). Structural insights into TIR domain specificity of the bridging adaptor Mal in TLR4 signaling. PLoS One *7*, e34202.

Lindquist, S. (1997). Mad cows meet psi-chotic yeast: the expansion of the prion hypothesis. Cell *89*, 495-498.

Liu, H., and Naismith, J.H. (2008). An efficient one-step site-directed deletion, insertion, single and multiple-site plasmid mutagenesis protocol. BMC Biotechnol *8*, 91.

Liu, S., Cai, X., Wu, J., Cong, Q., Chen, X., Li, T., Du, F., Ren, J., Wu, Y.T., Grishin, N.V.*, et al.* (2015a). Phosphorylation of innate immune adaptor proteins MAVS, STING, and TRIF induces IRF3 activation. Science *347*, aaa2630.

Liu, W., Xie, Y., Ma, J., Luo, X., Nie, P., Zuo, Z., Lahrmann, U., Zhao, Q., Zheng, Y., Zhao, Y.*, et al.* (2015b). IBS: an illustrator for the presentation and visualization of biological sequences. Bioinformatics *31*, 3359-3361.

Lu, Y.-C., Yeh, W.-C., and Ohashi, P.S. (2008). LPS/TLR4 signal transduction pathway. Cytokine *42*, 145-151.

Luizet, J.-B., Raymond, J., Lacerda, T.L.S., Bonici, M., Lembo, F., Willemart, K., Borg, J.-P., Gorvel, J.-P., and Salcedo, S.P. (2019). *Brucella* effector hijacks endoplasmic reticulum quality control machinery to prevent premature egress. bioRxiv, 699330.

Luo, L., Lucas, R.M., Liu, L., and Stow, J.L. (2019). Signalling, sorting and scaffolding adaptors for Toll-like receptors. J Cell Sci *133*.

Mahita, J., and Sowdhamini, R. (2017). Integrative modelling of TIR domain-containing adaptor molecule inducing interferon-β (TRIF) provides insights into its autoinhibited state. Biol Direct *12*, 9.

Mahita, J., and Sowdhamini, R. (2018a). Investigating the effect of key mutations on the conformational dynamics of toll-like receptor dimers through molecular dynamics simulations and protein structure networks. Proteins *86*, 475-490.

Mahita, J., and Sowdhamini, R. (2018b). Probing subtle conformational changes induced by phosphorylation and point mutations in the TIR domains of TLR2 and TLR3. Proteins *86*, 524-535.

Manning, B.D., and Toker, A. (2017). AKT/PKB Signaling: Navigating the Network. Cell *169*, 381-405.

Mansell, A., Brint, E., Gould, J.A., O'Neill, L.A., and Hertzog, P.J. (2004). Mal interacts with tumor necrosis factor receptor-associated factor (TRAF)-6 to mediate NF-kappaB activation by toll-like receptor (TLR)-2 and TLR4. J Biol Chem *279*, 37227-37230.

Mansell, A., Smith, R., Doyle, S.L., Gray, P., Fenner, J.E., Crack, P.J., Nicholson, S.E., Hilton, D.J., O'Neill, L.A., and Hertzog, P.J. (2006). Suppressor of cytokine signaling 1 negatively regulates Toll-like receptor signaling by mediating Mal degradation. Nat Immunol *7*, 148-155.

Marchesini, M.I., Herrmann, C.K., Salcedo, S.P., Gorvel, J.P., and Comerci, D.J. (2011). In search of *Brucella abortus* type IV secretion substrates: screening and identification of four proteins translocated into host cells through VirB system. Cell Microbiol *13*, 1261-1274.

Marchesini, M.I., Morrone Seijo, S.M., Guaimas, F.F., and Comerci, D.J. (2016). A T4SS Effector Targets Host Cell Alpha-Enolase Contributing to *Brucella abortus* Intracellular Lifestyle. Front Cell Infect Microbiol *6*, 153.

Marongiu, L., Gornati, L., Artuso, I., Zanoni, I., and Granucci, F. (2019). Below the surface: The inner lives of TLR4 and TLR9. J Leukoc Biol *106*, 147-160.

Martín, H., Arroyo, J., Sánchez, M., Molina, M., and Nombela, C. (1993). Activity of the yeast MAP kinase homologue Slt2 is critically required for cell integrity at 37 degrees C. Mol Gen Genet *241*, 177-184.

Martín, H., Rodríguez-Pachón, J.M., Ruiz, C., Nombela, C., and Molina, M. (2000). Regulatory mechanisms for modulation of signaling through the cell integrity Slt2-mediated pathway in *Saccharomyces cerevisiae*. J Biol Chem *275*, 1511-1519.

Matsumoto, M., Funami, K., Oshiumi, H., and Seya, T. (2013). Toll-IL-1-receptor-containing adaptor molecule-1: a signaling adaptor linking innate immunity to adaptive immunity. Prog Mol Biol Transl Sci *117*, 487-510.

Matsumura, T., Oyama, M., Kozuka-Hata, H., Ishikawa, K., Inoue, T., Muta, T., Semba, K., and Inoue, J. (2010). Identification of BCAP-(L) as a negative regulator of the TLR signaling-induced production of IL-6 and IL-10 in macrophages by tyrosine phosphoproteomics. Biochem Biophys Res Commun *400*, 265-270.

McGettrick, A.F., Brint, E.K., Palsson-McDermott, E.M., Rowe, D.C., Golenbock, D.T., Gay, N.J., Fitzgerald, K.A., and O'Neill, L.A. (2006). Trif-related adapter molecule is phosphorylated by PKC{epsilon} during Toll-like receptor 4 signaling. Proc Natl Acad Sci U S A *103*, 9196-9201.

Medzhitov, R., and Janeway, C., Jr. (2000). Innate immunity. N Engl J Med *343*, 338-344.

Medzhitov, R., Preston-Hurlburt, P., and Janeway, C.A., Jr. (1997). A human homologue of the *Drosophila* Toll protein signals activation of adaptive immunity. Nature *388*, 394-397.

Mekonnen, E., Bekele, E., and Stein, C.M. (2018). Novel polymorphisms in TICAM2 and NOD1 associated with tuberculosis progression phenotypes in Ethiopian populations. Glob Health Epidemiol Genom *3*, e1.

Mesquita, I., Varela, P., Belinha, A., Gaifem, J., Laforge, M., Vergnes, B., Estaquier, J., and Silvestre, R. (2016). Exploring NAD+ metabolism in host-pathogen interactions. Cell Mol Life Sci *73*, 1225-1236.

Miggin, S.M., Pålsson-McDermott, E., Dunne, A., Jefferies, C., Pinteaux, E., Banahan, K., Murphy, C., Moynagh, P., Yamamoto, M., Akira, S*., et al.* (2007). NF-kappaB activation by the Toll-IL-1

receptor domain protein MyD88 adapter-like is regulated by caspase-1. Proc Natl Acad Sci U S A *104*, 3372-3377.

Miller, C.N., Smith, E.P., Cundiff, J.A., Knodler, L.A., Bailey Blackburn, J., Lupashin, V., and Celli, J. (2017). A *Brucella* Type IV Effector Targets the COG Tethering Complex to Remodel Host Secretory Traffic and Promote Intracellular Replication. Cell Host Microbe *22*, 317-329.e317.

Mink, M., Fogelgren, B., Olszewski, K., Maroy, P., and Csiszar, K. (2001). A Novel Human Gene (SARM) at Chromosome 17q11 Encodes a Protein with a SAM Motif and Structural Similarity to Armadillo/β-Catenin That Is Conserved in Mouse, *Drosophila*, and *Caenorhabditis elegans*. Genomics *74*, 234-244.

Misch, E.A., and Hawn, T.R. (2008). Toll-like receptor polymorphisms and susceptibility to human disease. Clin Sci (Lond) *114*, 347-360.

Mitchell, D.A., Marshall, T.K., and Deschenes, R.J. (1993). Vectors for the inducible overexpression of glutathione S-transferase fusion proteins in yeast. Yeast *9*, 715-722.

Mitchell, S., Vargas, J., and Hoffmann, A. (2016). Signaling via the NFκB system. Wiley Interdiscip Rev Syst Biol Med *8*, 227-241.

Mol, J.P., Costa, E.A., Carvalho, A.F., Sun, Y.H., Tsolis, R.M., Paixão, T.A., and Santos, R.L. (2014). Early transcriptional responses of bovine chorioallantoic membrane explants to wild type, ΔvirB2 or ΔbtpB *Brucella abortus* infection. PLoS One *9*, e108606.

Moncrieffe, M.C., Bollschweiler, D., Li, B., Penczek, P.A., Hopkins, L., Bryant, C.E., Klenerman, D., and Gay, N.J. (2020). MyD88 Death-Domain Oligomerization Determines Myddosome Architecture: Implications for Toll-like Receptor Signaling. Structure *28*, 281-289.e283.

Murata, H., Khine, C.C., Nishikawa, A., Yamamoto, K.I., Kinoshita, R., and Sakaguchi, M. (2018). c-Jun N-terminal kinase (JNK)-mediated phosphorylation of SARM1 regulates NAD(+) cleavage activity to inhibit mitochondrial respiration. J Biol Chem *293*, 18933-18943.

Myeni, S., Child, R., Ng, T.W., Kupko, J.J., 3rd, Wehrly, T.D., Porcella, S.F., Knodler, L.A., and Celli, J. (2013). *Brucella* modulates secretory trafficking via multiple type IV secretion effector proteins. PLoS Pathog *9*, e1003556.

Nagpal, K., Plantinga, T.S., Wong, J., Monks, B.G., Gay, N.J., Netea, M.G., Fitzgerald, K.A., and Golenbock, D.T. (2009). A TIR domain variant of MyD88 adapter-like (Mal)/TIRAP results in loss of MyD88 binding and reduced TLR2/TLR4 signaling. J Biol Chem *284*, 25742-25748.

Naiki, Y., Michelsen, K.S., Zhang, W., Chen, S., Doherty, T.M., and Arditi, M. (2005). Transforming growth factor-beta differentially inhibits MyD88-dependent, but not TRAM- and TRIF-dependent, lipopolysaccharide-induced TLR4 signaling. J Biol Chem *280*, 5491-5495.

Nanson, J.D., Kobe, B., and Ve, T. (2019). Death, TIR, and RHIM: Self-assembling domains involved in innate immunity and cell-death signaling. J Leukoc Biol *105*, 363-375.

Newman, R.M., Salunkhe, P., Godzik, A., and Reed, J.C. (2006). Identification and characterization of a novel bacterial virulence factor that shares homology with mammalian Toll/interleukin-1 receptor family proteins. Infect Immun *74*, 594-601.

Ngo, V.N., Young, R.M., Schmitz, R., Jhavar, S., Xiao, W., Lim, K.H., Kohlhammer, H., Xu, W., Yang, Y., Zhao, H.*, et al.* (2011). Oncogenically active MYD88 mutations in human lymphoma. Nature *470*, 115-119.

Nimma, S., Ve, T., Williams, S.J., and Kobe, B. (2017). Towards the structure of the TIR-domain signalosome. Curr Opin Struct Biol *43*, 122-130.

Nobel-Assembly (2001). 2001 Nobel Prize in Physiology or Medicine jointly awarded to Leland H. Hartwell, R. Timothy (Tim) Hunt and Paul M. Nurse for their discoveries of “key regulators of the cell cycle”.

Nobel-Assembly (2011). 2011 Nobel Prize in Physiology or Medicine shall be divided, with one half jointly to Bruce A. Beutler and Jules A. Hoffmann for their discoveries concerning the activation of innate immunity and the other half to Ralph M. Steinman for his discovery of the dendritic cell and its role in adaptive immunity (Nobel Media AB 2020).

Nobel-Assembly (2013). 2013 Nobel Prize in Physiology or Medicine awarded jointly to James E. Rothman, Randy W. Schekman and Thomas C. Südhof for their discoveries of machinery regulating vesicle traffic, a major transport system in our cells.

Nobel-Assembly (2016). 2016 Nobel Prize in Physiology or Medicine to Yoshinori Ohsumi for his discoveries of mechanisms for autophagy.

Novick, P., and Schekman, R. (1979). Secretion and cell-surface growth are blocked in a temperature-sensitive mutant of *Saccharomyces cerevisiae*. Proc Natl Acad Sci U S A *76*, 1858-1862.

Nyman, T., Stenmark, P., Flodin, S., Johansson, I., Hammarstrom, M., and Nordlund, P. (2008). The crystal structure of the human toll-like receptor 10 cytoplasmic domain reveals a putative signaling dimer. J Biol Chem *283*, 11861-11865.

O'Carroll, A., Chauvin, B., Brown, J.W.P., Meagher, A., Coyle, J., Schill, J., Bhumkhar, A., Hunter, D.J.B., Ve, T., Kobe, B.*, et al.* (2018). Pathological mutations differentially affect the self-assembly and polymerisation of the innate immune system signalling adaptor molecule MyD88. BMC Biol *16*, 149.

Ohashi, K., Kawai, S., and Murata, K. (2013). Secretion of quinolinic acid, an intermediate in the kynurenine pathway, for utilization in NAD+ biosynthesis in the yeast *Saccharomyces cerevisiae*. Eukaryot Cell *12*, 648-653.

Ohnishi, H., Tochio, H., Kato, Z., Kawamoto, N., Kimura, T., Kubota, K., Yamamoto, T., Funasaka, T., Nakano, H., Wong, R.W.*, et al.* (2012). TRAM is involved in IL-18 signaling and functions as a sorting adaptor for MyD88. PLoS One *7*, e38423.

Ohnishi, H., Tochio, H., Kato, Z., Orii, K.E., Li, A., Kimura, T., Hiroaki, H., Kondo, N., and Shirakawa, M. (2009). Structural basis for the multiple interactions of the MyD88 TIR domain in TLR4 signaling. Proc Natl Acad Sci U S A *106*, 10260-10265.

Ohto, U., Shibata, T., Tanji, H., Ishida, H., Krayukhina, E., Uchiyama, S., Miyake, K., and Shimizu, T. (2015). Structural basis of CpG and inhibitory DNA recognition by Toll-like receptor 9. Nature *520*, 702-705.

Oliver, M.D., Fernández-Acero, T., Luna, S., Rodríguez-Escudero, I., Molina, M., Pulido, R., and Cid, V.J. (2017). Insights into the pathological mechanisms of p85α mutations using a yeast-based phosphatidylinositol 3-kinase model. Biosci Rep *37*.

Orchard, R.C., and Alto, N.M. (2012). Mimicking GEFs: a common theme for bacterial pathogens. Cellular microbiology *14*, 10-18.

Oshiumi, H., Sasai, M., Shida, K., Fujita, T., Matsumoto, M., and Seya, T. (2003). TIR-containing adapter molecule (TICAM)-2, a bridging adapter recruiting to toll-like receptor 4 TICAM-1 that induces interferon-beta. J Biol Chem *278*, 49751-49762.

Osterloh, J.M., Yang, J., Rooney, T.M., Fox, A.N., Adalbert, R., Powell, E.H., Sheehan, A.E., Avery, M.A., Hackett, R., Logan, M.A.*, et al.* (2012). dSarm/Sarm1 is required for activation of an injury-induced axon death pathway. Science *337*, 481-484.

Otero, J.M., Cimini, D., Patil, K.R., Poulsen, S.G., Olsson, L., and Nielsen, J. (2013). Industrial systems biology of *Saccharomyces cerevisiae* enables novel succinic acid cell factory. PLoS One *8*, e54144-e54144.

Oughtred, R., Stark, C., Breitkreutz, B.J., Rust, J., Boucher, L., Chang, C., Kolas, N., O'Donnell, L., Leung, G., McAdam, R.*, et al.* (2019). The BioGRID interaction database: 2019 update. Nucleic Acids Res *47*, D529-d541.

Ovsyannikova, I.G., Haralambieva, I.H., Vierkant, R.A., Pankratz, V.S., Jacobson, R.M., and Poland, G.A. (2011). The role of polymorphisms in Toll-like receptors and their associated intracellular signaling genes in measles vaccine immunity. Hum Genet *130*, 547-561.

Paiano, A., Margiotta, A., De Luca, M., and Bucci, C. (2019). Yeast Two-Hybrid Assay to Identify Interacting Proteins. Curr Protoc Protein Sci *95*, e70.

Pajuelo, D., Gonzalez-Juarbe, N., and Niederweis, M. (2020). NAD hydrolysis by the tuberculosis necrotizing toxin induces lethal oxidative stress in macrophages. Cell Microbiol *22*, e13115.

References

Pajuelo, D., Gonzalez-Juarbe, N., Tak, U., Sun, J., Orihuela, C.J., and Niederweis, M. (2018). NAD(+) Depletion Triggers Macrophage Necroptosis, a Cell Death Pathway Exploited by *Mycobacterium tuberculosis*. Cell Rep *24*, 429-440.

Palsson-McDermott, E.M., Doyle, S.L., McGettrick, A.F., Hardy, M., Husebye, H., Banahan, K., Gong, M., Golenbock, D., Espevik, T., and O'Neill, L.A. (2009). TAG, a splice variant of the adaptor TRAM, negatively regulates the adaptor MyD88-independent TLR4 pathway. Nat Immunol *10*, 579-586.

Pappas, G., Panagopoulou, P., Christou, L., and Akritidis, N. (2006). *Brucella* as a biological weapon. Cell Mol Life Sci *63*, 2229-2236.

Paracha, R.Z., Ali, A., Ahmad, J., Hussain, R., Niazi, U., and Muhammad, S.A. (2014). Structural evaluation of BTK and PKCδ mediated phosphorylation of MAL at positions Tyr86 and Tyr106. Comput Biol Chem *51*, 22-35.

Park, B.S., Song, D.H., Kim, H.M., Choi, B.-S., Lee, H., and Lee, J.-O. (2009). The structural basis of lipopolysaccharide recognition by the TLR4-MD-2 complex. Nature *458*, 1191-1195.

Patot, S., Imbert, P.R., Baude, J., Martins Simões, P., Campergue, J.B., Louche, A., Nijland, R., Bès, M., Tristan, A., Laurent, F.*, et al.* (2017). Correction: The TIR Homologue Lies near Resistance Genes in *Staphylococcus aureus*, Coupling Modulation of Virulence and Antimicrobial Susceptibility. PLoS Pathog *13*, e1006291.

Patra, M.C., and Choi, S. (2018). Insight into Phosphatidylinositol-Dependent Membrane Localization of the Innate Immune Adaptor Protein Toll/Interleukin 1 Receptor Domain-Containing Adaptor Protein. Front Immunol *9*, 75.

Patterson, N.J., and Werling, D. (2013). To con protection: TIR-domain containing proteins (Tcp) and innate immune evasion. Vet Immunol Immunopathol *155*, 147-154.

Peng, J., Yuan, Q., Lin, B., Panneerselvam, P., Wang, X., Luan, X.L., Lim, S.K., Leung, B.P., Ho, B., and Ding, J.L. (2010). SARM inhibits both TRIF- and MyD88-mediated AP-1 activation. Eur J Immunol *40*, 1738-1747.

Piao, W., Song, C., Chen, H., Wahl, L.M., Fitzgerald, K.A., O'Neill, L.A., and Medvedev, A.E. (2008). Tyrosine phosphorylation of MyD88 adapter-like (Mal) is critical for signal transduction and blocked in endotoxin tolerance. J Biol Chem *283*, 3109-3119.

Pidugu, V.K., Pidugu, H.B., Wu, M.-M., Liu, C.-J., and Lee, T.-C. (2019). Emerging Functions of Human IFIT Proteins in Cancer. Front Mol Biosci *6*, 148-148.

Płóciennikowska, A., Hromada-Judycka, A., Borzęcka, K., and Kwiatkowska, K. (2015a). Co-operation of TLR4 and raft proteins in LPS-induced pro-inflammatory signaling. Cell Mol Life Sci *72*, 557-581.

Płóciennikowska, A., Zdioruk, M.I., Traczyk, G., Świątkowska, A., and Kwiatkowska, K. (2015b). LPS-induced clustering of CD14 triggers generation of PI(4,5)P2. J Cell Sci *128*, 4096-4111.

Poltorak, A., He, X., Smirnova, I., Liu, M.Y., Van Huffel, C., Du, X., Birdwell, D., Alejos, E., Silva, M., Galanos, C.*, et al.* (1998). Defective LPS signaling in C3H/HeJ and C57BL/10ScCr mice: mutations in Tlr4 gene. Science *282*, 2085-2088.

Poole, A.Z., and Weis, V.M. (2014). TIR-domain-containing protein repertoire of nine anthozoan species reveals coral-specific expansions and uncharacterized proteins. Dev Comp Immunol *46*, 480-488.

Popa, C., Coll, N.S., Valls, M., and Sessa, G. (2016). Yeast as a Heterologous Model System to Uncover Type III Effector Function. PLoS Pathog *12*, e1005360.

Radhakrishnan, G.K., Harms, J.S., and Splitter, G.A. (2011). Modulation of microtubule dynamics by a TIR domain protein from the intracellular pathogen *Brucella melitensis*. Biochem J *439*, 79-83.

Radhakrishnan, G.K., Yu, Q., Harms, J.S., and Splitter, G.A. (2009). *Brucella* TIR Domain-containing Protein Mimics Properties of the Toll-like Receptor Adaptor Protein TIRAP. J Biol Chem *284*, 9892-9898.

Rana, R.R., Zhang, M., Spear, A.M., Atkins, H.S., and Byrne, B. (2013). Bacterial TIR-containing proteins and host innate immune system evasion. Med Microbiol Immunol *202*, 1-10.

Randez-Gil, F., Prieto, J.A., and Sanz, P. (1995). The expression of a specific 2-deoxyglucose-6P phosphatase prevents catabolite repression mediated by 2-deoxyglucose in yeast. Current Genetics *28*, 101-107.

Rangel, L.T., Marden, J., Colston, S., Setubal, J.C., Graf, J., and Gogarten, J.P. (2019). Identification and characterization of putative *Aeromonas* spp. T3SS effectors. PLoS One *14*, e0214035.

Robert, X., and Gouet, P. (2014). Deciphering key features in protein structures with the new ENDscript server. Nucleic Acids Research *42*, W320-W324.

Rodríguez-Escudero, I., Andrés-Pons, A., Pulido, R., Molina, M., and Cid, V.J. (2009). Phosphatidylinositol 3-kinase-dependent activation of mammalian protein kinase B/Akt in *Saccharomyces cerevisiae*, an *in vivo* model for the functional study of Akt mutations. J Biol Chem *284*, 13373-13383.

Rodríguez-Escudero, I., Fernández-Acero, T., Bravo, I., Leslie, N.R., Pulido, R., Molina, M., and Cid, V.J. (2015). Yeast-based methods to assess PTEN phosphoinositide phosphatase activity *in vivo*. Methods *77-78*, 172-179.

Rodríguez-Escudero, I., Ferrer, N.L., Rotger, R., Cid, V.J., and Molina, M. (2011). Interaction of the *Salmonella* Typhimurium effector protein SopB with host cell Cdc42 is involved in intracellular replication. Mol Microbiol *80*, 1220-1240.

Rodríguez-Escudero, I., Hardwidge, P.R., Nombela, C., Cid, V.J., Finlay, B.B., and Molina, M. (2005a). Enteropathogenic *Escherichia coli* type III effectors alter cytoskeletal function and signalling in *Saccharomyces cerevisiae*. Microbiology *151*, 2933-2945.

Rodríguez-Escudero, I., Roelants, F.M., Thorner, J., Nombela, C., Molina, M., and Cid, V.J. (2005b). Reconstitution of the mammalian PI3K/PTEN/Akt pathway in yeast. Biochem J *390*, 613-623.

Rodríguez-Escudero, I., Rotger, R., Cid, V.J., and Molina, M. (2006). Inhibition of Cdc42-dependent signalling in *Saccharomyces cerevisiae* by phosphatase-dead SigD/SopB from *Salmonella* Typhimurium. Microbiology *152*, 3437-3452.

Rodríguez-Escudero, M., Cid, V.J., Molina, M., Schulze-Luehrmann, J., Lührmann, A., and Rodríguez-Escudero, I. (2016). Studying *Coxiella burnetii* Type IV Substrates in the Yeast *Saccharomyces cerevisiae*: Focus on Subcellular Localization and Protein Aggregation. PLoS One *11*, e0148032.

Rodríguez-Pachón, J.M., Martín, H., North, G., Rotger, R., Nombela, C., and Molina, M. (2002). A novel connection between the yeast Cdc42 GTPase and the Slt2-mediated cell integrity pathway identified through the effect of secreted *Salmonella* GTPase modulators. J Biol Chem *277*, 27094-27102.

Rosadini, C.V., and Kagan, J.C. (2015). Microbial strategies for antagonizing Toll-like-receptor signal transduction. Current opinion in immunology *32*, 61-70.

Rowe, D.C., McGettrick, A.F., Latz, E., Monks, B.G., Gay, N.J., Yamamoto, M., Akira, S., O'Neill, L.A., Fitzgerald, K.A., and Golenbock, D.T. (2006). The myristoylation of TRIF-related adaptor molecule is essential for Toll-like receptor 4 signal transduction. Proceedings of the National Academy of Sciences *103*, 6299.

Ruysschaert, J.-M., and Lonez, C. (2015). Role of lipid microdomains in TLR-mediated signalling. Biochim Biophys Acta *1848*, 1860-1867.

Salcedo, S.P., Marchesini, M.I., Degos, C., Terwagne, M., Von Bargen, K., Lepidi, H., Herrmann, C.K., Santos Lacerda, T.L., Imbert, P.R., Pierre, P.*, et al.* (2013). BtpB, a novel *Brucella* TIR-containing effector protein with immune modulatory functions. Front Cell Infect Microbiol *3*, 28.

Salcedo, S.P., Marchesini, M.I., Lelouard, H., Fugier, E., Jolly, G., Balor, S., Muller, A., Lapaque, N., Demaria, O., Alexopoulou, L.*, et al.* (2008). *Brucella* control of dendritic cell maturation is dependent on the TIR-containing protein Btp1. PLoS Pathog *4*, e21.

Sambrook, J., and Russell, D.W. (2001). Molecular cloning : a laboratory manual (Cold Spring Harbor, N.Y.: Cold Spring Harbor Laboratory Press).

Sambrook, J., and Russell, D.W. (2006). The inoue method for preparation and transformation of competent *E. coli*: "ultra-competent" cells. CSH Protoc *2006*.

Sancho-Shimizu, V., Pérez de Diego, R., Lorenzo, L., Halwani, R., Alangari, A., Israelsson, E., Fabrega, S., Cardon, A., Maluenda, J., Tatematsu, M.*, et al.* (2011). Herpes simplex encephalitis in children with autosomal recessive and dominant TRIF deficiency. J Clin Invest *121*, 4889-4902.

Saqib, U., and Baig, M.S. (2019). Scaffolding role of TcpB in disrupting TLR4-Mal interactions: Three to tango. J Cell Biochem *120*, 3455-3458.

Sasai, M., Tatematsu, M., Oshiumi, H., Funami, K., Matsumoto, M., Hatakeyama, S., and Seya, T. (2010). Direct binding of TRAF2 and TRAF6 to TICAM-1/TRIF adaptor participates in activation of the Toll-like receptor 3/4 pathway. Mol Immunol *47*, 1283-1291.

Schindelin, J., Arganda-Carreras, I., Frise, E., Kaynig, V., Longair, M., Pietzsch, T., Preibisch, S., Rueden, C., Saalfeld, S., Schmid, B.*, et al.* (2012). Fiji: an open-source platform for biological-image analysis. Nature Methods *9*, 676-682.

Schrödinger, L. (2020). The PyMOL Molecular Graphics System.

Schroeder, R.Y., Zhu, A., Eubel, H., Dahncke, K., and Witte, C.-P. (2018). The ribokinases of *Arabidopsis thaliana* and *Saccharomyces cerevisiae* are required for ribose recycling from nucleotide catabolism, which in plants is not essential to survive prolonged dark stress. New Phytologist *217*, 233-244.

Sechi, S., and Chait, B.T. (1998). Modification of cysteine residues by alkylation. A tool in peptide mapping and protein identification. Anal Chem *70*, 5150-5158.

Sengupta, D., Koblansky, A., Gaines, J., Brown, T., West, A.P., Zhang, D., Nishikawa, T., Park, S.-G., Roop, R.M., and Ghosh, S. (2010). Subversion of Innate Immune Responses by *Brucella* through the Targeted Degradation of the TLR Signaling Adapter, MAL. The Journal of Immunology *184*, 956.

Shao, Z.Q., Xue, J.Y., Wu, P., Zhang, Y.M., Wu, Y., Hang, Y.Y., Wang, B., and Chen, J.Q. (2016). Large-Scale Analyses of Angiosperm Nucleotide-Binding Site-Leucine-Rich Repeat Genes Reveal Three Anciently Diverged Classes with Distinct Evolutionary Patterns. Plant Physiol *170*, 2095-2109.

Sheedy, F.J., and O'Neill, L.A. (2007). The Troll in Toll: Mal and Tram as bridges for TLR2 and TLR4 signaling. J Leukoc Biol *82*, 196-203.

Shevlin, E., and Miggin, S.M. (2014). The TIR-domain containing adaptor TRAM is required for TLR7 mediated RANTES production. PLoS One *9*, e107141.

Shim, J.H., Xiao, C., Paschal, A.E., Bailey, S.T., Rao, P., Hayden, M.S., Lee, K.Y., Bussey, C., Steckel, M., Tanaka, N.*, et al.* (2005). TAK1, but not TAB1 or TAB2, plays an essential role in multiple signaling pathways *in vivo*. Genes Dev *19*, 2668-2681.

Shirey, K.A., Lai, W., Brown, L.J., Blanco, J.C.G., Beadenkopf, R., Wang, Y., Vogel, S.N., and Snyder, G.A. (2020). Select targeting of intracellular Toll-interleukin-1 receptor resistance domains for protection against influenza-induced disease. Innate Immun *26*, 26-34.

Sievers, F., Wilm, A., Dineen, D., Gibson, T.J., Karplus, K., Li, W., Lopez, R., McWilliam, H., Remmert, M., Söding, J.*, et al.* (2011). Fast, scalable generation of high-quality protein multiple sequence alignments using Clustal Omega. Molecular Systems Biology *7*, 539.

Siggers, K.A., and Lesser, C.F. (2008). The Yeast *Saccharomyces cerevisiae*: a versatile model system for the identification and characterization of bacterial virulence proteins. Cell Host Microbe *4*, 8-15.

Sikorski, R.S., and Hieter, P. (1989). A system of shuttle vectors and yeast host strains designed for efficient manipulation of DNA in *Saccharomyces cerevisiae*. Genetics *122*, 19-27.

Singh, M.D., Ni, M., Sullivan, J.M., Hamerman, J.A., and Campbell, D.J. (2018). B cell adaptor for PI3-kinase (BCAP) modulates CD8(+) effector and memory T cell differentiation. J Exp Med *215*, 2429-2443.

Singhal, A., and Cheng, C.Y. (2019). Host NAD+ metabolism and infections: therapeutic implications. Int Immunol *31*, 59-67.

Smith, E.P., Cotto-Rosario, A., Borghesan, E., Held, K., Miller, C.N., and Celli, J. (2020). Epistatic Interplay between Type IV Secretion Effectors Engages the Small GTPase Rab2 in the *Brucella* Intracellular Cycle. mBio *11*.

Smith, J.A., Khan, M., Magnani, D.D., Harms, J.S., Durward, M., Radhakrishnan, G.K., Liu, Y.P., and Splitter, G.A. (2013). *Brucella* induces an unfolded protein response via TcpB that supports intracellular replication in macrophages. PLoS Pathog *9*, e1003785.

Smith, M.G., and Snyder, M. (2006). Yeast as a model for human disease. Curr Protoc Hum Genet *Chapter 15*, Unit 15.16.

Snyder, G.A., Cirl, C., Jiang, J., Chen, K., Waldhuber, A., Smith, P., Römmler, F., Snyder, N., Fresquez, T., Dürr, S.*, et al.* (2013). Molecular mechanisms for the subversion of MyD88 signaling by TcpC from virulent uropathogenic *Escherichia coli*. Proc Natl Acad Sci U S A *110*, 6985-6990.

Snyder, G.A., Deredge, D., Waldhuber, A., Fresquez, T., Wilkins, D.Z., Smith, P.T., Durr, S., Cirl, C., Jiang, J., Jennings, W.*, et al.* (2014). Crystal structures of the Toll/Interleukin-1 receptor (TIR) domains

from the *Brucella* protein TcpB and host adaptor TIRAP reveal mechanisms of molecular mimicry. J Biol Chem *289*, 669-679.

Song, C., Ye, M., Liu, Z., Cheng, H., Jiang, X., Han, G., Songyang, Z., Tan, Y., Wang, H., Ren, J.*, et al.* (2012). Systematic analysis of protein phosphorylation networks from phosphoproteomic data. Molecular & Cellular Proteomics, mcp.M111.012625.

Spear, A.M., Loman, N.J., Atkins, H.S., and Pallen, M.J. (2009). Microbial TIR domains: not necessarily agents of subversion? Trends Microbiol *17*, 393-398.

Sporny, M., Guez-Haddad, J., Lebendiker, M., Ulisse, V., Volf, A., Mim, C., Isupov, M.N., and Opatowsky, Y. (2019). Structural Evidence for an Octameric Ring Arrangement of SARM1. J Mol Biol *431*, 3591-3605.

Sporty, J.L., Kabir, M.M., Turteltaub, K.W., Ognibene, T., Lin, S.J., and Bench, G. (2008). Single sample extraction protocol for the quantification of NAD and NADH redox states in *Saccharomyces cerevisiae*. J Sep Sci *31*, 3202-3211.

Stack, J., Doyle, S.L., Connolly, D.J., Reinert, L.S., O'Keeffe, K.M., McLoughlin, R.M., Paludan, S.R., and Bowie, A.G. (2014). TRAM is required for TLR2 endosomal signaling to type I IFN induction. J Immunol *193*, 6090-6102.

Stefan, C.J., Audhya, A., and Emr, S.D. (2002). The yeast synaptojanin-like proteins control the cellular distribution of phosphatidylinositol (4,5)-bisphosphate. Mol Biol Cell *13*, 542-557.

Storey, D., McNally, A., Åstrand, M., Sa-Pessoa Graca Santos, J., Rodriguez-Escudero, I., Elmore, B., Palacios, L., Marshall, H., Hobley, L., Molina, M.*, et al.* (2020). *Klebsiella pneumoniae* type VI secretion system-mediated microbial competition is PhoPQ controlled and reactive oxygen species dependent. PLoS Pathog *16*, e1007969.

Stottmeier, B., and Dick, T.P. (2016). Redox sensitivity of the MyD88 immune signaling adapter. Free Radic Biol Med *101*, 93-101.

Strickson, S., Emmerich, C.H., Goh, E.T.H., Zhang, J., Kelsall, I.R., Macartney, T., Hastie, C.J., Knebel, A., Peggie, M., Marchesi, F.*, et al.* (2017). Roles of the TRAF6 and Pellino E3 ligases in MyD88 and RANKL signaling. Proc Natl Acad Sci U S A *114*, E3481-e3489.

Summers, D.W., Gibson, D.A., DiAntonio, A., and Milbrandt, J. (2016). SARM1-specific motifs in the TIR domain enable NAD+ loss and regulate injury-induced SARM1 activation. Proc Natl Acad Sci U S A *113*, E6271-e6280.

Takeda, K., and Akira, S. (2015). Toll-like receptors. Curr Protoc Immunol *109*, 14.12.11-14.12.10.

Takeshige, K., Baba, M., Tsuboi, S., Noda, T., and Ohsumi, Y. (1992). Autophagy in yeast demonstrated with proteinase-deficient mutants and conditions for its induction. J Cell Biol *119*, 301-311.

Tan, Y., and Kagan, J.C. (2019). Innate Immune Signaling Organelles Display Natural and Programmable Signaling Flexibility. Cell *177*, 384-398.e311.

Tao, X., Xu, Y., Zheng, Y., Beg, A.A., and Tong, L. (2002). An extensively associated dimer in the structure of the C713S mutant of the TIR domain of human TLR2. Biochem Biophys Res Commun *299*, 216-221.

Tatematsu, M., Ishii, A., Oshiumi, H., Horiuchi, M., Inagaki, F., Seya, T., and Matsumoto, M. (2010). A molecular mechanism for Toll-IL-1 receptor domain-containing adaptor molecule-1-mediated IRF-3 activation. J Biol Chem *285*, 20128-20136.

Tenor, J.L., and Aballay, A. (2008). A conserved Toll-like receptor is required for *Caenorhabditis elegans* innate immunity. EMBO reports *9*, 103-109.

Thomas, B.J., and Rothstein, R. (1989). Elevated recombination rates in transcriptionally active DNA. Cell *56*, 619-630.

Toshchakov, V.Y., and Javmen, A. (2020). Targeting the TLR signalosome with TIR domain-derived cell-permeable decoy peptides: the current state and perspectives. Innate Immun *26*, 35-47.

Toshchakov, V.Y., and Neuwald, A.F. (2020). A survey of TIR domain sequence and structure divergence. Immunogenetics *72*, 181-203.

Treusch, S., Hamamichi, S., Goodman, J.L., Matlack, K.E., Chung, C.Y., Baru, V., Shulman, J.M., Parrado, A., Bevis, B.J., Valastyan, J.S.*, et al.* (2011). Functional links between Aβ toxicity, endocytic trafficking, and Alzheimer's disease risk factors in yeast. Science *334*, 1241-1245.

References

Troutman, T.D., Hu, W., Fulenchek, S., Yamazaki, T., Kurosaki, T., Bazan, J.F., and Pasare, C. (2012). Role for B-cell adapter for PI3K (BCAP) as a signaling adapter linking Toll-like receptors (TLRs) to serine/threonine kinases PI3K/Akt. Proc Natl Acad Sci U S A *109*, 273-278.

Tuon, F.F., Gondolfo, R.B., and Cerchiari, N. (2017). Human-to-human transmission of *Brucella* - a systematic review. Trop Med Int Health *22*, 539-546.

Udenwobele, D.I., Su, R.-C., Good, S.V., Ball, T.B., Varma Shrivastav, S., and Shrivastav, A. (2017). Myristoylation: An Important Protein Modification in the Immune Response. Front Immunol *8*.

Ullah, M.O., Sweet, M.J., Mansell, A., Kellie, S., and Kobe, B. (2016). TRIF-dependent TLR signaling, its functions in host defense and inflammation, and its potential as a therapeutic target. J Leukoc Biol *100*, 27-45.

Ullah, M.O., Valkov, E., Ve, T., Williams, S., Mas, C., Mansell, A., and Kobe, B. (2015). Recombinant production of functional full-length and truncated human TRAM/TICAM-2 adaptor protein involved in Toll-like receptor and interferon signaling. Protein Expr Purif *106*, 31-40.

Ullah, M.O., Ve, T., Mangan, M., Alaidarous, M., Sweet, M.J., Mansell, A., and Kobe, B. (2013). The TLR signalling adaptor TRIF/TICAM-1 has an N-terminal helical domain with structural similarity to IFIT proteins. Acta Crystallogr D Biol Crystallogr *69*, 2420-2430.

Ulrichts, P., Bovijn, C., Lievens, S., Beyaert, R., Tavernier, J., and Peelman, F. (2010). Caspase-1 targets the TLR adaptor Mal at a crucial TIR-domain interaction site. J Cell Sci *123*, 256-265.

Valanne, S., Wang, J.H., and Rämet, M. (2011). The *Drosophila* Toll signaling pathway. J Immunol *186*, 649-656.

Valkov, E., Stamp, A., Dimaio, F., Baker, D., Verstak, B., Roversi, P., Kellie, S., Sweet, M.J., Mansell, A., Gay, N.J.*, et al.* (2011). Crystal structure of Toll-like receptor adaptor MAL/TIRAP reveals the molecular basis for signal transduction and disease protection. Proc Natl Acad Sci U S A *108*, 14879-14884.

van Teijlingen Bakker, N., and Pearce, E.J. (2020). Cell-intrinsic metabolic regulation of mononuclear phagocyte activation: Findings from the tip of the iceberg. Immunol Rev *295*, 54-67.

Ve, T., Vajjhala, P.R., Hedger, A., Croll, T., DiMaio, F., Horsefield, S., Yu, X., Lavrencic, P., Hassan, Z., Morgan, G.P.*, et al.* (2017). Structural basis of TIR-domain-assembly formation in MAL- and MyD88-dependent TLR4 signaling. Nat Struct Mol Biol *24*, 743-751.

Ve, T., Williams, S.J., and Kobe, B. (2015). Structure and function of Toll/interleukin-1 receptor/resistance protein (TIR) domains. Apoptosis *20*, 250-261.

Venter, G., Oerlemans, F.T., Wijers, M., Willemse, M., Fransen, J.A., and Wieringa, B. (2014a). Glucose controls morphodynamics of LPS-stimulated macrophages. PLoS One *9*, e96786.

Venter, G., Oerlemans, F.T., Willemse, M., Wijers, M., Fransen, J.A., and Wieringa, B. (2014b). NAMPT-mediated salvage synthesis of NAD+ controls morphofunctional changes of macrophages. PLoS One *9*, e97378.

Verstak, B., Nagpal, K., Bottomley, S.P., Golenbock, D.T., Hertzog, P.J., and Mansell, A. (2009). MyD88 adapter-like (Mal)/TIRAP interaction with TRAF6 is critical for TLR2- and TLR4-mediated NF-kappaB proinflammatory responses. J Biol Chem *284*, 24192-24203.

Verstak, B., Stack, J., Ve, T., Mangan, M., Hjerrild, K., Jeon, J., Stahl, R., Latz, E., Gay, N., Kobe, B.*, et al.* (2014). The TLR signaling adaptor TRAM interacts with TRAF6 to mediate activation of the inflammatory response by TLR4. J Leukoc Biol *96*, 427-436.

Vida, T.A., and Emr, S.D. (1995). A new vital stain for visualizing vacuolar membrane dynamics and endocytosis in yeast. J Cell Biol *128*, 779-792.

von Bernuth, H., Picard, C., Jin, Z., Pankla, R., Xiao, H., Ku, C.-L., Chrabieh, M., Mustapha, I.B., Ghandil, P., Camcioglu, Y.*, et al.* (2008). Pyogenic bacterial infections in humans with MyD88 deficiency. Science (New York, NY) *321*, 691-696.

Vyncke, L., Bovijn, C., Pauwels, E., Van Acker, T., Ruyssinck, E., Burg, E., Tavernier, J., and Peelman, F. (2016). Reconstructing the TIR Side of the Myddosome: a Paradigm for TIR-TIR Interactions. Structure *24*, 437-447.

Wagner, T.M., Janice, J., Paganelli, F.L., Willems, R.J., Askarian, F., Pedersen, T., Top, J., de Haas, C., van Strijp, J.A., Johannessen, M.*, et al.* (2018). *Enterococcus faecium* TIR-Domain Genes Are Part of a Gene Cluster Which Promotes Bacterial Survival in Blood. Int J Microbiol *2018*, 1435820.

Waldhuber, A., Puthia, M., Wieser, A., Cirl, C., Dürr, S., Neumann-Pfeifer, S., Albrecht, S., Römmler, F., Müller, T., Zheng, Y.*, et al.* (2016). Uropathogenic *Escherichia coli* strain CFT073 disrupts NLRP3 inflammasome activation. J Clin Invest *126*, 2425-2436.

Walsh, M.C., Lee, J., and Choi, Y. (2015). Tumor necrosis factor receptor- associated factor 6 (TRAF6) regulation of development, function, and homeostasis of the immune system. Immunol Rev *266*, 72-92.

Wan, L., Essuman, K., Anderson, R.G., Sasaki, Y., Monteiro, F., Chung, E.H., Osborne Nishimura, E., DiAntonio, A., Milbrandt, J., Dangl, J.L.*, et al.* (2019). TIR domains of plant immune receptors are NAD(+)-cleaving enzymes that promote cell death. Science *365*, 799-803.

Wang, C., Chen, T., Zhang, J., Yang, M., Li, N., Xu, X., and Cao, X. (2009). The E3 ubiquitin ligase Nrdp1 'preferentially' promotes TLR-mediated production of type I interferon. Nat Immunol *10*, 744-752.

Wang, W., Feng, B., Zhou, J.-M., and Tang, D. (2020). Plant immune signaling: Advancing on two frontiers. Journal of Integrative Plant Biology *62*, 2-24.

Wang, W., and Malcolm, B.A. (1999). Two-stage PCR protocol allowing introduction of multiple mutations, deletions and insertions using QuikChange Site-Directed Mutagenesis. Biotechniques *26*, 680-682.

Williams, S.J., Sohn, K.H., Wan, L., Bernoux, M., Sarris, P.F., Segonzac, C., Ve, T., Ma, Y., Saucet, S.B., Ericsson, D.J.*, et al.* (2014). Structural basis for assembly and function of a heterodimeric plant immune receptor. Science *344*, 299-303.

Williams, S.J., Yin, L., Foley, G., Casey, L.W., Outram, M.A., Ericsson, D.J., Lu, J., Boden, M., Dry, I.B., and Kobe, B. (2016). Structure and Function of the TIR Domain from the Grape NLR Protein RPV1. Front Plant Sci *7*, 1850.

Xie, L., Liu, C., Wang, L., Gunawardena, H.P., Yu, Y., Du, R., Taxman, D.J., Dai, P., Yan, Z., Yu, J.*, et al.* (2013). Protein phosphatase 2A catalytic subunit α plays a MyD88-dependent, central role in the gene-specific regulation of endotoxin tolerance. Cell Rep *3*, 678-688.

Xu, Y., Tao, X., Shen, B., Horng, T., Medzhitov, R., Manley, J.L., and Tong, L. (2000). Structural basis for signal transduction by the Toll/interleukin-1 receptor domains. Nature *408*, 111-115.

Yadav, M., Zhang, J., Fischer, H., Huang, W., Lutay, N., Cirl, C., Lum, J., Miethke, T., and Svanborg, C. (2010). Inhibition of TIR domain signaling by TcpC: MyD88-dependent and independent effects on *Escherichia coli* virulence. PLoS Pathog *6*, e1001120.

Yamamoto, M., Sato, S., Hemmi, H., Sanjo, H., Uematsu, S., Kaisho, T., Hoshino, K., Takeuchi, O., Kobayashi, M., Fujita, T.*, et al.* (2002). Essential role for TIRAP in activation of the signalling cascade shared by TLR2 and TLR4. Nature *420*, 324-329.

Yamamoto, M., Sato, S., Hemmi, H., Uematsu, S., Hoshino, K., Kaisho, T., Takeuchi, O., Takeda, K., and Akira, S. (2003). TRAM is specifically involved in the Toll-like receptor 4-mediated MyD88-independent signaling pathway. Nat Immunol *4*, 1144-1150.

Yan, F., Guan, J., Peng, Y., and Zheng, X. (2017). MyD88 NEDDylation negatively regulates MyD88-dependent NF-κB signaling through antagonizing its ubiquitination. Biochem Biophys Res Commun *482*, 632-637.

Yang, Y., Liao, B., Wang, S., Yan, B., Jin, Y., Shu, H.B., and Wang, Y.Y. (2013). E3 ligase WWP2 negatively regulates TLR3-mediated innate immune response by targeting TRIF for ubiquitination and degradation. Proc Natl Acad Sci U S A *110*, 5115-5120.

Yates, A.D., Achuthan, P., Akanni, W., Allen, J., Allen, J., Alvarez-Jarreta, J., Amode, M.R., Armean, I.M., Azov, A.G., Bennett, R.*, et al.* (2019). Ensembl 2020. Nucleic Acids Research *48*, D682-D688.

Yoneyama, M., Kikuchi, M., Matsumoto, K., Imaizumi, T., Miyagishi, M., Taira, K., Foy, E., Loo, Y.M., Gale, M., Jr., Akira, S.*, et al.* (2005). Shared and unique functions of the DExD/H-box helicases RIG-I, MDA5, and LGP2 in antiviral innate immunity. J Immunol *175*, 2851-2858.

References

Zanoni, I., Ostuni, R., Marek, Lorri R., Barresi, S., Barbalat, R., Barton, Gregory M., Granucci, F., and Kagan, Jonathan C. (2011). CD14 Controls the LPS-Induced Endocytosis of Toll-like Receptor 4. Cell *147*, 868-880.

Zhan, C., Qi, R., Wei, G., Guven-Maiorov, E., Nussinov, R., and Ma, B. (2016). Conformational dynamics of cancer-associated MyD88-TIR domain mutant L252P (L265P) allosterically tilts the landscape toward homo-dimerization. Protein Eng Des Sel *29*, 347-354.

Zhang, J., Kong, X., Zhou, C., Li, L., Nie, G., and Li, X. (2014). Toll-like receptor recognition of bacteria in fish: Ligand specificity and signal pathways. Fish & Shellfish Immunology *41*, 380-388.

Zhang, J., Li, M., Li, Z., Shi, J., Zhang, Y., Deng, X., Liu, L., Wang, Z., Qi, Y., and Zhang, H. (2019a). Deletion of the Type IV Secretion System Effector VceA Promotes Autophagy and Inhibits Apoptosis in *Brucella*-Infected Human Trophoblast Cells. Curr Microbiol *76*, 510-519.

Zhang, J., Ou, J., and Wan, X. (2019b). LRRC62 attenuates Toll-like receptor signaling by deubiquitinating TAK1 via CYLD. Exp Cell Res *383*, 111497.

Zhang, Q., Zmasek, C.M., Cai, X., and Godzik, A. (2011). TIR domain-containing adaptor SARM is a late addition to the ongoing microbe-host dialog. Dev Comp Immunol *35*, 461-468.

Zhang, X., Bernoux, M., Bentham, A.R., Newman, T.E., Ve, T., Casey, L.W., Raaymakers, T.M., Hu, J., Croll, T.I., Schreiber, K.J.*, et al.* (2017a). Multiple functional self-association interfaces in plant TIR domains. Proc Natl Acad Sci U S A *114*, E2046-e2052.

Zhang, Z.M., Ma, K.W., Gao, L., Hu, Z., Schwizer, S., Ma, W., and Song, J. (2017b). Mechanism of host substrate acetylation by a YopJ family effector. Nat Plants *3*, 17115.

Zhao, B., Shu, C., Gao, X., Sankaran, B., Du, F., Shelton, C.L., Herr, A.B., Ji, J.Y., and Li, P. (2016). Structural basis for concerted recruitment and activation of IRF-3 by innate immune adaptor proteins. Proc Natl Acad Sci U S A *113*, E3403-3412.

Zhao, X., Xiong, W., Xiao, S., Tang, T.X., Ellena, J.F., Armstrong, G.S., Finkielstein, C.V., and Capelluto, D.G. (2017). Membrane targeting of TIRAP is negatively regulated by phosphorylation in its phosphoinositide-binding motif. Sci Rep *7*, 43043.

Zhi, F., Zhou, D., Bai, F., Li, J., Xiang, C., Zhang, G., Jin, Y., and Wang, A. (2019). VceC Mediated IRE1 Pathway and Inhibited CHOP-induced Apoptosis to Support *Brucella* Replication in Goat Trophoblast Cells. Int J Mol Sci *20*.

Annexes

Annexes

Directly related publications

- Coronas-Serna JM, Louche A, Rodríguez-Escudero M, Roussin M, Imbert PRC, Rodríguez-Escudero I, Terradot L, Molina M, Gorvel JP, Cid VJ, Salcedo SP. The TIR-domain containing effectors BtpA and BtpB from *Brucella abortus* impact NAD metabolism. PLoS Pathog. 2020 Apr 16;16(4):e1007979. doi: 10.1371/journal.ppat.1007979. PMID: 32298382; PMCID: PMC7188309.

Other publications produced during this Thesis

- Barnett KC, Coronas-Serna JM, Zhou W, Ernandes MJ, Cao A, Kranzusch PJ, Kagan JC. Phosphoinositide Interactions Position cGAS at the Plasma Membrane to Ensure Efficient Distinction between Self- and Viral DNA. Cell. 2019 Mar 7;176(6):1432-1446.e11. doi: 10.1016/j.cell.2019.01.049. Epub 2019 Feb 28. PMID: 30827685; PMCID: PMC6697112.

- Coronas-Serna JM, Valenti M, Del Val E, Fernández-Acero T, Rodríguez-Escudero I, Mingo J, Luna S, Torices L, Pulido R, Molina M, Cid VJ. Modeling human disease in yeast: recreating the PI3K-PTEN-Akt signaling pathway in *Saccharomyces cerevisiae*. Int Microbiol. 2020 Jan;23(1):75-87. doi: 10.1007/s10123-019-00082-4. Epub 2019 Jun 19. PMID: 31218536.

- Coronas-Serna JM, Fernández-Acero T, Molina M, Cid VJ. A humanized yeast-based toolkit for monitoring phosphatidylinositol 3-kinase activity at both single cell and population levels. Microb Cell. 2018 Nov 12;5(12):545-554. doi: 10.15698/mic2018.12.660. PMID: 30533419; PMCID: PMC6282018.